NIST Internal Report
NISTIR 8581

Applied and Computational Mathematics Division

Summary of Activities for Fiscal Year 2024

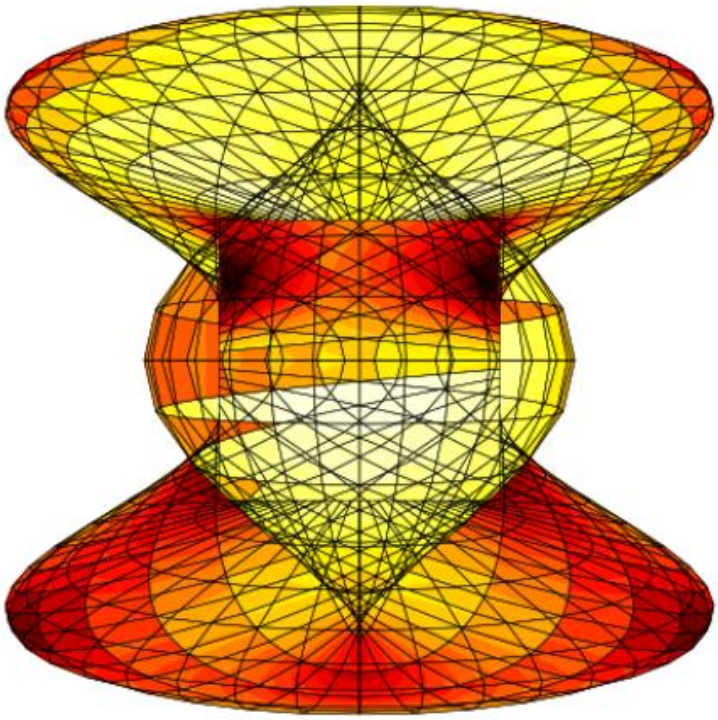

This publication is available free of charge from:
https://doi.org/10.6028/NIST.IR.8581

NIST NATIONAL INSTITUTE OF STANDARDS AND TECHNOLOGY
U.S. DEPARTMENT OF COMMERCE

NIST Internal Report
NISTIR 8581

Applied and Computational Mathematics Division

Summary of Activities for Fiscal Year 2024

Ronald F. Boisvert, Editor
Andrew Dienstfrey, Editor
Applied and Computational Mathematics Division
Information Technology Laboratory

This publication is available free of charge from:
https://doi.org/10.6028/NIST.IR.8581

July 2025

U.S. Department of Commerce
Howard Lutnick, Secretary

National Institute of Standards and Technology
Craig Burkhardt, Acting Under Secretary of Commerce for Standards and Technology and Acting NIST Director

NISTIR 8581
July 2025

Certain equipment, instruments, software, or materials, commercial or non-commercial, are identified in this paper in order to specify the experimental procedure adequately. Such identification does not imply recommendation or endorsement of any product or service by NIST, nor does it imply that the materials or equipment identified are necessarily the best available for the purpose.

Publication History
Approved by the NIST Editorial Review Board on 2025-07-10.

How to Cite this NIST Technical Series Publication
Ronald F. Boisvert (2025) Applied and Computational Mathematics Division, Summary of Activities for Fiscal Year 2024. (National Institute of Standards and Technology, Gaithersburg, MD), NIST Series NISTIR 8581. https://doi.org/10.6028/NIST.IR.8581

NIST Author ORCID iD
Ronald F. Boisvert: 0000-0002-4445-1044
Andrew Dienstfrey: 0000-0002-5461-8741

Contact Information
- Ronald F. Boisvert, 100 Bureau Drive, Mail Stop 8910, NIST, Gaithersburg, MD 20899-8910
  email boisvert@nist.gov
- Andrew Dienstfrey, NIST, Mail Stop 891.00, 325 Broadway, Boulder, CO 80305
  email andrew.dienstfrey@nist.gov
- See the Division's Web site at https://www.nist.gov/itl/math/

Abstract

This report summarizes recent technical work of the Applied and Computational Mathematics Division of the Information Technology Laboratory at the National Institute of Standards and Technology (NIST). Part I (Overview) provides a high-level overview of the Division's activities, including highlights of technical accomplishments during the previous year. Part II (Features) provides further details on projects of particular note this year. This is followed in Part III (Project Summaries) by brief synopses of all technical projects active during the past year. Part IV (Activity Data) provides listings of publications, technical talks, and other professional activities in which Division staff members have participated. The reporting period covered by this document is October 2023 through December 2024.

Keywords

applied mathematics; computational science and engineering; high-performance computing; materials modeling and simulation; mathematical knowledge management; mathematical modeling; mathematics of biotechnology; mathematics of metrology; scientific visualization; quantum information science.

Cover Visualization

Output from the OOF system for finite element modeling of materials. See page 34.

Acknowledgements

Thanks to Lochi Orr who contributed to the compiling of Part IV. Thanks also to Brian Cloteaux and Justyna Zwolak who read the manuscript and offered corrections and suggestions for improvement. The "word cloud," which is found at the start of each Part of this document was created using the Wordle word cloud app, with the text of this document as input.

Table of Contents

Part I

Overview

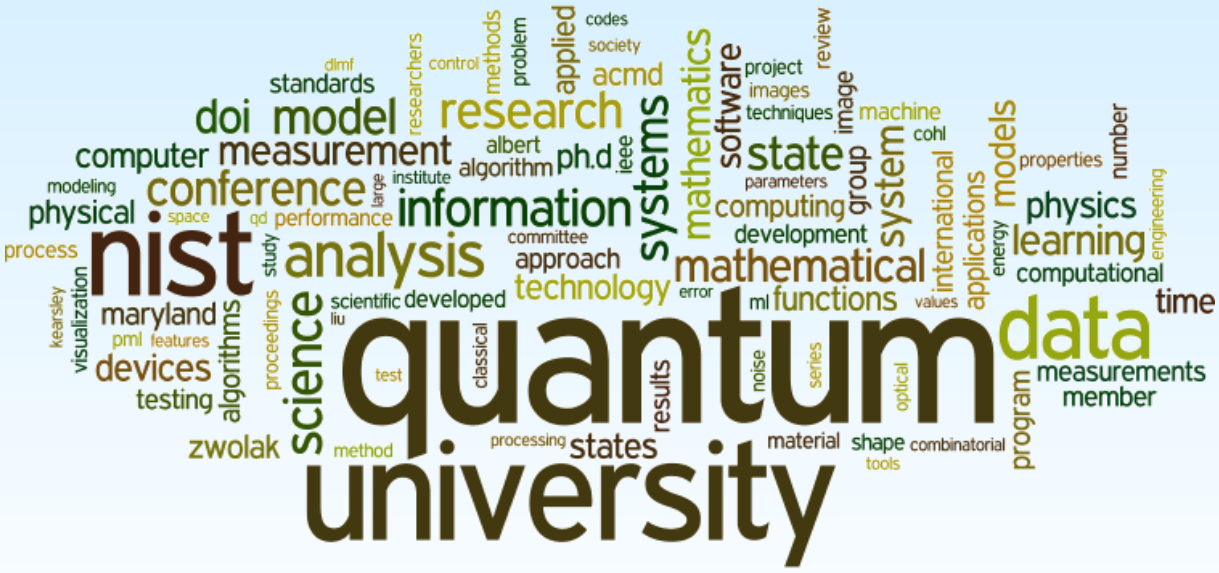

Introduction

Founded in 1901, the National Institute of Standards and Technology (NIST) is a non-regulatory federal agency within the U.S. Department of Commerce. Its mission is to promote U.S. innovation and industrial competitiveness by advancing measurement science, standards, and technology in ways that enhance economic security and improve our quality of life. The technical disciplines represented in the NIST Laboratories include physics, electrical engineering, nanotechnology, materials science, chemistry, biotechnology, manufacturing and construction engineering, fire research, information technology, mathematics, and statistics. The two main NIST laboratory sites are located in Gaithersburg, MD, (headquarters—234 hectare/578-acre campus) and Boulder, CO (84 hectare/208-acre campus). NIST employs about 3400 scientists, engineers, technicians, and support personnel, and hosts about 3500 associates from academia, industry, and other government agencies, who collaborate with NIST staff and access its facilities.

The Information Technology Laboratory (ITL) is one of six major units that comprise the NIST Labs. ITL's singular purpose is to cultivate trust in information technology and metrology. This is done through the development of measurements, standards, tests, and guidance to support innovation in and deployment of information technology by industry and government, as well as through the application of advanced mathematics, statistics, and computer science to help ensure the quality of measurement science.

The Applied and Computational Mathematics Division (ACMD) is one of six technical Divisions in ITL. At its core, ACMD's purpose is to nurture trust in metrology and scientific computing. To do so, ACMD provides leadership within NIST in the use of applied and computational mathematics to solve technical problems arising in measurement science and related applications. In that role staff members

- perform research in applied mathematics and computational science and engineering, including analytical and numerical methods, high-performance computing, and visualization,
- perform applied research in computer science and engineering for future computing and communications technologies,
- engage in peer-to-peer collaborations to apply mathematical and computational techniques and tools to NIST problems,
- develop and disseminate mathematical reference data, software, and related tools, and
- work with internal and external groups to develop standards, tests, reference implementations, and other measurement technologies for current and future scientific computing systems.

Division staff is organized into four groups:

- Mathematical Analysis and Modeling Group (*Bradley Alpert, Leader*). Performs research and maintains expertise in applied mathematics, mathematical modeling, and numerical analysis for application to measurement science.
- Mathematical Software Group (*Bonita Saunders, Leader*). Performs research and maintains expertise in the methodology and application of mathematical algorithms and software in support of computational science within NIST as well as in industry and academia.
- High Performance Computing and Visualization Group (*Judith Terrill, Leader*). Performs research and maintains expertise in the methodologies and tools of high-performance scientific computing and visualization for use in measurement science.
- Quantum Information Group[1] (*Ronald Boisvert, Acting Leader; Oliver Slattery, Project Leader*). Performs research and maintains expertise in fundamental mathematics, physics, and measurement science necessary to enable the exploitation of quantum phenomena for information processing tasks.

The technical work of the Division is organized into six thematic areas; these are described in the sidebar. Project descriptions in Part III of this document are organized according to these broad themes.

[1] Note: The Computing and Communications Theory Group was renamed as The Quantum Information Group in late 2024.

Division Thematic Areas

Broad Areas

Mathematics of Metrology. Mathematics plays an important role in measurement science. Mathematical models are needed to understand how to design effective measurement systems and to analyze the results they produce. Mathematical techniques are used to develop and analyze idealized models of physical phenomena to be measured, and mathematical algorithms are necessary to find optimal system parameters. Mathematical and statistical techniques are needed to transform measured data into useful information. We develop fundamental mathematical methods and tools necessary for NIST to remain a world-class metrology institute, and to apply these to measurement science problems.

High Performance Computing and Visualization. Computational capability continues to advance rapidly, enabling modeling and simulation to be done with greatly increased fidelity. Doing so often requires computing resources well beyond what is available on the desktop. Developing software that makes effective use of such high-performance computing platforms remains very challenging, requiring expertise that application scientists rarely have. We maintain such expertise for application to NIST problems. Such computations, as well as modern experiments, typically produce large volumes of data, which cannot be readily comprehended. We are developing the infrastructure necessary for advanced interactive, quantitative visualization and analysis of scientific data, including the use of 3D immersive environments, and applying the resulting tools to NIST problems.

Current Focus Areas

Mathematics of Biotechnology. As proof-of-concept academic work in engineering biology meets the market realities of bringing lab science to product initiation, there are needs to compare biological products, measure whether desired outcomes are realized, and optimize biological systems for desired behaviors. NIST is working to deliver tools and standards to measure such biological technologies, outputs, and processes from healthcare to manufacturing and beyond. We support this effort with the development and deployment of innovative mathematical modeling and data analysis techniques and tools.

Quantum Information Science. An emerging discipline at the intersection of physics and computer science, quantum information science is likely to revolutionize 21st century science and technology in the same way that lasers, electronics, and computers did in the 20th century. By encoding information into quantum states of matter, one can, in theory, enable phenomenal increases in information storage and processing capability. At the same time, such computers would threaten the public-key infrastructure that secures all of electronic commerce. Although many of the necessary physical manipulations of quantum states have been demonstrated experimentally, scaling these up to enable fully capable quantum computers and networks remains a grand challenge. We engage in (a) theoretical studies to understand the power of quantum computing, (b) collaborative efforts with the multi-laboratory experimental quantum science program at NIST to characterize and benchmark specific physical realizations of quantum information processing, and (c) demonstration and assessment of technologies for quantum networking.

Foundations of Measurement Science for Information Systems. ITL assumes primary responsibility within NIST for the development of measurement science infrastructure and related standards for IT and its applications. ACMD develops the mathematical foundations for such work. This can be very challenging. For example, many large-scale information-centric systems can be characterized as an interconnection of many independently operating components (e.g., software systems, communication networks, the power grid, transportation systems, financial systems). Exactly how the structure of such large-scale interconnected systems and the local dynamics of its components leads to system-level behavior is only weakly understood. This inability to predict the systemic risk inherent in system design leaves us open to unrealized potential to improve systems or to avoid potentially devastating failures.

Mathematical Knowledge Management. We work with researchers in academia and industry to develop technologies, tools, and standards for representation, exchange, and use of mathematical data. Of particular concern are semantic-based representations which can provide the basis for interoperability of mathematical information processing systems. We apply these representations to the development and dissemination of reference data for applied mathematics. The centerpiece of this effort is the Digital Library of Mathematical Functions, a freely available interactive and richly linked online resource, providing essential information on the properties of the special functions of applied mathematics, the foundation of mathematical modeling in all of science and engineering.

Highlights

In this section we identify some of the major accomplishments of the Division during the past year. We also provide news related to ACMD staff.

Recent Technical Highlights

ACMD has made significant technical progress on many fronts during the past year. Here we highlight a few notable technical accomplishments.

- Mathematical modeling and uncertainty quantification were critical contributions of ACMD staff members Michael Donahue and Mark-Alexander Henn of ACMD to the Thermal MagIC project, a five-year effort supported by the NIST Director's Office's Innovations in Measurement Science program, which concluded this year. The PML/MML/ITL team developed a non-contact thermal imaging technology capable of precise temperature measurement at any point within the bulk of a material. They synthesized magnetic nanoparticles and used them in novel three-dimensional magnetic imaging to achieve a precision of 25 millikelvin at a spatial resolution of 100 μm), exceeding all known thermal three-dimensional imaging capabilities. This technology has applications in thermal sensing of biological environments, advanced packaging for semiconductors, ballistic impact of materials, and additive manufacturing. See page 32.
- Shawn Geller, Scott Glancy, and Emanuel Knill of ACMD were part of a PML/ITL team that performed one of the most convincing demonstrations of quantum advantage to date, i.e., a computation for which classical computer is too inefficient to realistically accomplish. Instead of using a purely photonic system as in previous demonstrations, the team performed boson sampling in a system of ultracold atoms in a two-dimensional optical lattice of intersecting laser beams. In the experiment, 180 atoms were engaged to perform "quantum walks" over the 1015 lattice sites. Not only was this the largest boson sampling experiment to date, but its error rate was the lowest of any boson sampling demonstration. An account of the accomplishment was published in *Nature*. See page 81.
- Arrays of gate-defined semiconductor quantum dots are among the leading candidates for building scalable quantum processors. High-fidelity initialization, control, and readout of spin qubit registers require exquisite and targeted control. However capacitive crosstalk between gates makes tuning large collections of quantum dots impossible to do "by hand." Justyna Zwolak and collaborators at the University of Maryland have developed a general and modular framework that utilizes machine learning and physics-based models to autonomously construct a complete stack of virtual gates in real time. Using their techniques, colleagues in the Netherlands were able to successfully demonstrate accurate virtualization of a dense two-dimensional array comprising ten quantum dots, the largest such system successfully tuned to date. See page 70.
- ACMD's expertise in mathematical modeling and optimization have provided key insights in the design of microfluidics devices at NIST. For example, Paul Patrone and Anthony Kearsley, working with colleagues Gregory Cooksey and Matthew DiSalvo in PML have created the world's most sensitive microfluidic flowmeter, able to accurately measure flows in the nanoliter per minute range. Recently a company, Lumos NanoLabs, was created to commercialize this NIST-developed technology. See page 40.
- Implementation of metropolitan-scale quantum networks transmitting quantum information via single photons through deployed optical fibers spanning several tens of kilometers. Major challenges include compensation for polarization fluctuation, high-precision clock synchronization, and compensation for cumulative transmission time fluctuations. One approach addressing these challenges is to co-propagate classical probe signals in the same fiber as the quantum signal, allowing both signals to experience the same conditions, which can therefore be monitored and compensated for.

ACMD's quantum networking team, working with collaborators in PML and CTL, have used this technique to demonstrate high-fidelity entanglement distribution between nodes separated by 100 km of optical fiber. This advancement is a significant step towards the practical implementation of robust and efficient metropolitan-scale quantum networks. See page 95.

Technology Transfer and Community Engagement

The volume of technical output of ACMD remains high. During the last 15 months, Division staff members were (co-)authors of 41 articles appearing in peer-reviewed journals, 21 papers in conference proceedings, and 14 published in other venues. Fifteen additional papers were accepted for publication, while 47 others are undergoing review. Division staff gave 64 invited technical talks and presented 39 others in conferences and workshops. Staff members were co-inventors on two patents; three others are under review.

ACMD continues to maintain an active website with a variety of information and services, most notably the Digital Library of Mathematical Functions. Legacy services that are no longer actively developed, like the Guide to Available Mathematical Software, the Matrix Market, and the SciMark Java benchmark still see significant use. Another indication of the successful transfer of our technology is references to our software in refereed journal articles. For example, our software system for nano-magnetic modeling (OOMMF) was cited in 153 such papers published in CY 2024 alone.

Members of the Division are also active in professional circles. Staff members hold a total of 13 editorial positions in peer-reviewed journals. Staff members are also active in conference organization, serving on 26 organizing/steering/program committees.

Service within professional societies is also prevalent among our staff. For example, Bonita Saunders is a member of the Board of Trustees of the Society for Industrial and Applied Mathematics (SIAM). Staff members are also active in a variety of working groups. Andrew Dienstfrey is Chair of the International Federation for Information Processing (IFIP) Working Group 2.5 on Numerical Software, Donald Porter is a member of the Tcl Core Team, Bruce Miller is a member of W3C's Math Working Group, and Sandy Ressler is a member of the W3C Advisory Committee. Further details can be found in Part IV of this report.

Staff News

Once again, ACMD experienced a large number of staffing changes during this period. We welcomed one new NRC Postdoctoral Associate (a federal appointment), while bidding farewell to six postdocs and three permanent Federal employees. We continue to host a large number of non-federal guest researchers (i.e., students, postdocs, and senior researchers), who are collectively known as NIST associates. We hosted a total of 81 associates during this period, many of whom work alongside us on one of the NIST campuses, with the rest being off-site collaborators. Of these associates, 34 were student interns (17 graduate students, 15 undergraduate students, and 2 high school students). See Table 3 and Table 4 on pages 134 and 135 for a list of our interns.

Of note this year, two of our federal staff members and one associate received Ph.D. degrees based on research work performed at NIST. Alex Kwiatkowski and Shawn Geller received Ph.D.'s in physics from the University of Colorado in Boulder advised by ACMD staff member Manny Knill. Katjana Ladic received a Ph.D. in electrical engineering and computing from the University of Zagreb advised by ACMD staff member Kamran Sayrafian.

Further details on our staff changes and awards are provided below.

Arrivals

Figure 2. *Anthony Brady* (Photo courtesy of A. Brady)

Anthony Brady joined ACMD as a NIST/NRC Postdoctoral Associate on July 1, 2024. He received a B.S. in physics from the University of North Georgia in 2016, and a Ph.D. in physics from Louisiana State University in 2021. Since then, he has held postdoctoral positions at the University of Arizona and at USC. His research involves exploring quantum sensing technologies for fundamental problems in physics (e.g., entangled sensor arrays for futuristic, entanglement-enhanced dark matter searches) and designing bosonic quantum error correcting codes. At NIST he will work with his adviser, Victor Albert, on bosonic quantum information and control at the NIST/UMD Joint Center for Quantum Information and Computer Science (QuICS) in College Park, Maryland.

At NIST, all staff members who are not Federal employees are termed associates. These include student interns, postdocs, and visiting senior researchers. Many associates work on one of the NIST campuses, and others are remote collaborators. ACMD hosts many such associates. During the current 15-month period, for example, we brought on or renewed the appointments of 76 different associates, 35 of whom were students, and six of whom were postdocs. Senior researchers who began new appointments during this period include the following:

- **Hilma Macedo De Vasconcelos**, Associate Professor of Teleinformatics Engineering at Universidade Federal do Ceará (Brazil) spent a month in early 2024 visiting the NIST Labs in Boulder, where she worked with Scott Glancy on theory and application of quantum optical measurements.
- **Changhoon Park** of the Korean Institute of Science and Technology (KIST) began a year-long stay in ACMD in Gaithersburg to work with Lijun Ma on the development and testing of quantum memory technologies.
- **Luca Argenti**, Associate Professor of Physics at the University of Central Florida, spent two months in Gaithersburg working with William Earwood on computational methods for the interaction of electromagnetic radiation with polyatomic molecules.

Departures

In December 2023, **Danielle Middlebrooks,** who had been a postdoctoral researcher in ACMD since 2020 left NIST to begin an appointment within the U.S. Department of Defense**.** At NIST, she worked with Paul Patrone on the analysis of cytometry systems and with Justyna Zwolak on the use of AI for the tuning of quantum dots.

Timothy Burns, Leader of the Mathematical Analysis and Modeling Group, retired from NIST in December 2023 after 37 years of service. Tim began his tenure at NIST in 1986 as a staff member of the Scientific Computing Division in the Computing and Applied Mathematics Laboratory. Tim applied his expertise in nonlinear dynamics to the mathematical modeling of the mechanical properties of materials. Over the years he had extensive collaborations with the NIST Engineering Lab modeling aspects of high-speed machine tools, as well as pulse-heated Kolsky bar measurements of high strain rate flow stress. The NIST publications database lists 45 technical papers on these and other topics. In 2004, Tim was a member of a multi-OU team which won the prestigious Allen Astin Measurement Science Award. The team was cited

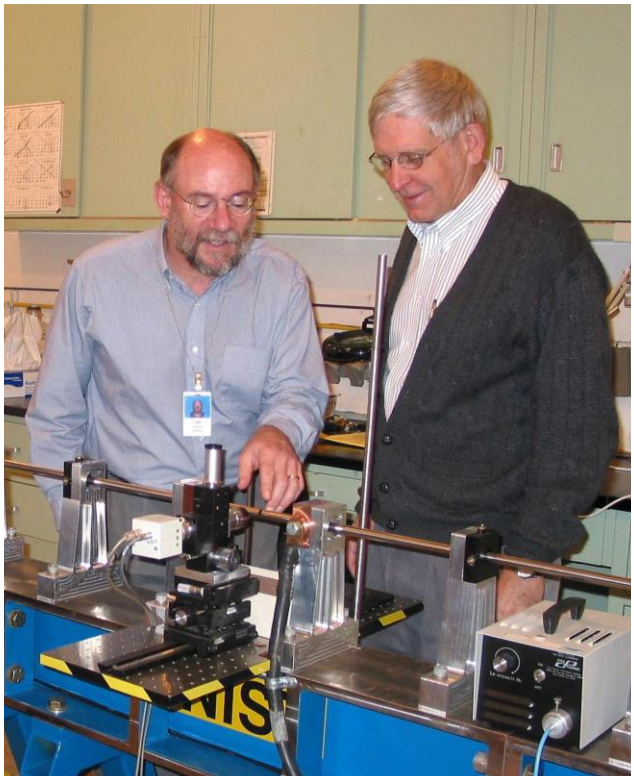

Figure 3. *Timothy Burns (left) working with Richard Rhorer on the Kolsky bar.* (Photo credit: NIST)

for outstanding advancements in measurement science for dynamic material properties, leading to the first ever measurement of the stress-strain relationship of a material under high strain-rate and heating-rate conditions prior to temperature-induced transformation.

Anne Talkington joined ACMD as a NIST/NRC Postdoctoral Associate in December 2023. She received a B.S. in mathematics and a B.A. in biology from Duke in 2016, an M.S. in applied mathematics from the University of North Carolina (UNC) in 2019, and a Ph.D. in bioinformatics and computational biology from UNC in 2021. Before joining NIST she was a postdoctoral researcher at the University of Virginia where she worked on modeling intercellular communication in melanoma tumors. In ACMD she worked with adviser Tony Kearsley on optimization of immunotherapeutic strategies in tumor microenvironments. In December of 2024 she began a tenure-track position in the Department of Pharmaceutical Sciences at the University of Buffalo.

Roldan Pozo retired on May 31, 2024, after nearly 30 years of Federal service. An expert in high-performance mathematical software, Roldan was the principal designer of several C++ numerical linear algebra libraries, including Lapack++, SparseLib++, MV++, IML++, and the Template Numerical Toolkit (TNT). He was also coauthor of the book, *Templates for the Solution of Linear Systems: Building Blocks for Iterative Methods*, and one of the developers of Matrix Market. He also created the SciMark benchmark for Java numerical computing and was co-author of the Jama linear algebra package. In recent years he turned his attention to the development and computation of metrics for characterizing very large-scale graphs. Roldan was a recipient of the Presidential Early Career Award for Science and Engineering (PECASE) and a NIST Bronze Medal. Roldan returned to NIST in 2024 to work part-time as a re-employed annuitant.

Figure 4. *Roldan Pozo with a bottle of port which he purchased the year he started work at NIST.* (Photo courtesy of R. Boisvert)

Camilo Montoya, a NIST-NRC postdoctoral associate in ACMD, completed his two-year appointment on June 20, 2024. At NIST, Camilo worked with adviser Howard Cohl on double summation addition theorems for Jacobi functions of the first and second kind. He also worked on Segre varieties and their intersections, also known as polarizations, of real hypersurfaces in C^n.

NIST-NRC postdoctoral associate **Deborah McGlynn** left ACMD on July 5, 2024, to take a postdoctoral position at the Environmental Protection Agency in Research Triangle Park, NC. That location houses the EPA's major center for research on air, climate, and energy. At NIST she worked with adviser Tony Kearsley on improved discrimination of mass spectral isomers using the high dimensional consensus mass spectral similarity algorithm. She also had a fruitful collaboration with the NIST Biomolecular Measurement Division, Mass Spectrometry Data Center (MSDC) in MML and UC Berkeley on improved identification of complex mass spectral datasets using atmospherically collected wildfire data.

William Earwood ended his two-year NRC Postdoctoral Associateship in ACMD in December 2024. At NIST, where he was advised by Barry Schneider and Luca Argenti, he developed PRISM (Polycentric Routines for Ionization and Scattering in Molecules), an advanced library of computational tools built from the ground up. PRISM has since become a critical component of ASTRA, a cutting-edge software for polyatomic scattering and photoionization research. In late 2024 he rejoined ACMD to work on a CHIPS-funded project to develop novel methods to measure and replace environmentally hazardous PFAS chemicals. There he will work on the computation of electron-molecule scattering data for large molecular targets.

Also departing NIST in December 2024 was **Stephen Sorokanich**, an NRC Postdoctoral Associate. At NIST he worked on the modeling of Bose-Einstein Condensates and fluxonium qubits for quantum computers.

Recognition

ACMD staff members were recognized with a variety of awards this year, including the following.

Thomas Gerrits of ACMD, along with colleagues in PML and MML, was recognized with a 2023 Department of Commerce Bronze Medal for developing precision measurement techniques for molecular absorption of photon pairs that resulted in the refutation of controversial published claims about quantum-enhanced microscopy.

Thomas Gerrits of ACMD, along with colleagues in PML, was recognized with a 2024 Department of Commerce Gold Medal for the development of high-efficiency, low-noise, superconducting transition-edge sensors able to count single photons for photonic quantum computers.

Anthony Kearsley and **Paul Patrone** of ACMD, along with colleagues Gregory Cooksey and Matthew DiSalvo of NIST PML received a 2023 Department of Commerce Gold Medal for the invention of serial cytometry, which will enable early cancer identification and tracking of residual disease via rare-cell detection. Their achievements enable rigorous, single-cell measurements in cytometry, removing a longstanding hindrance to robust medical diagnostics and providing the first ever real-time dynamic measurements of cellular functions. The advance is the result of a NIST Innovations in Measurement Science project led by ACMD. The same team received the 2023 Department of Commerce Ron Brown Award for Excellence in Innovation.

Figure 5. *ACMD mathematician (center) received multiple distinctions this year, including a Presidential Early Career Award in Science and Engineering (PECASE), an Excellence in Research in Mathematics Award from the Washington Academy of Sciences, and a Department of Commerce Bronze Medal. Here she receives congratulations from ACMD Division Chief Ronald Boisvert (left) and ITL Director Kevin Stine (right).* (Photo courtesy of James St. Pierre.)

Four Department of Commerce Bronze Medals were awarded to ACMD staff in 2024:

Justyna Zwolak, for pioneering the application of machine learning to the control of systems at the frontiers of quantum science and technology. (Joint with PML staff)

Bruce Miller, for enabling newfound access to technical documents by those with visual impairments.

Michael Donahue, for the development of three-dimensional, high-resolution, temperature measurement and imaging of materials using embedded magnetic nanoparticles. (Joint with PML and MML staff)

Thomas Gerrits, Paulina Kuo, and Oliver Slattery, for the development of a dictionary of standardized terms and metrics to enable a fair comparison of competing single-photon technologies. (Joint with PML staff)

Justyna Zwolak was named the 2024 winner of the Washington Academy of Science Excellence in Research in Applied Mathematics Award in recognition of her outstanding contributions in the application of machine learning to the control of systems at the frontiers of quantum science and technology. In early 2025 we were notified that **Justyna Zwolak** was a winner of the Presidential Early Career Award for Scientists and Engineers (PECASE).

In 2024 ACMD captured six of the 11 awards given out in the annual ITL Awards program. The ACMD winners were:

Prajakta Bedekar
Outstanding Associate
For excellence in mathematical modeling for biometrology and for outstanding contributions to the research environment of ITL.

Matthew Coudron
Outstanding Conference Paper
For "Quantum Algorithms and the Power of Forgetting" presented at the 14th Innovations in Theoretical Computer Science Conference in January 2023.

Justyna Zwolak
Outstanding Journal Paper
For the paper "Colloquium: Advances in Automation of Quantum Dot Devices Control" published in *Reviews of Modern Physics* in February 2023.

Anthony Kearsley
Outstanding Mentorship
For outstanding mentorship of research trainees within NIST and beyond.

Thomas Gerrits, Paulina Kuo, and Oliver Slattery
Outstanding Standards Document
For outstanding initiative enabling fair comparison of competing single-photon sources and detectors.

Bruce Miller
Outstanding Technology Transfer
For enabling newfound access to technical documents by those with visual impairments.

Sesha Challa, a NIST Associate in ACMD, was selected for the American Vacuum Society (AVS) Nanoscale Science and Technology Division Early Career Award. The award, which highlights and celebrates exceptional researchers working on the frontiers of nanoscience, was presented at the AVS 69th International Symposium and Exhibition held in Portland, OR in November 2023. He was cited for his work on process development for fabrication of low-loss thin-film lithium niobate waveguides.

In Memoriam

Barry Schneider, a physicist in ACMD, passed away at home in Sterling, VA, on July 3, 2024. He was 83. Barry was an undisputed giant in the field of computational physics. While he had struggled with several medical issues for several years, his passing was nevertheless a shock, as he was an active and vibrant staff member right until the end, taking meetings from his hospital bed and working hard to meet deadlines.

Barry originally came to NIST in 2014 to serve as general editor of the NIST Digital Library of Mathematical Functions[2], the 21st century successor to NIST's biggest-selling publication of all time: *The*

[2] https://dlmf.nist.gov/

Handbook of Mathematical Functions. But Barry had two full careers before starting at NIST. From 1972 to 1991 he was a staff member in the Theoretical Division at Los Alamos National Laboratory, where he worked in the field of atomic, molecular, and optical (AMO) physics, which is the study of matter-matter and light-matter interactions at the scale of one or a few atoms.

Figure 6. *Barry Schneider* (Photo courtesy of Heman Gharibnejad)

It was at Los Alamos that he foresaw the sea change that high-performance computing could bring to physics. He developed new computational approaches to electron-molecule scattering and photoionization that are still in use today. Seeking to make an even larger impact on the application of high-performance computing to AMO physics, in 1992 Barry became a program manager at the National Science Foundation's Physics Division and later in NSF's Office of Advanced Cyberinfrastructure. He was instrumental in the development and management of several innovative NSF programs, such as Physics at the Information Frontier and the eXtreme Science and Engineering Discovery Environment (XSEDE) program.

While still at NSF, Barry got his first taste of NIST as a guest researcher in Charles Clark's Electron and Optical Physics Division, where, among other things, Barry worked on the modeling of solitons and vortices in Bose-Einstein condensates. One of Barry's papers about this research has been cited 1,680 times.

While he came to NIST on a more permanent basis in 2014 to work on the Digital Library of Mathematical Functions project, he also continued his work in computational physics, focusing on computational techniques for modeling polyatomic molecules exposed to attosecond radiation. "Atto" is the scientific prefix that represents 10^{-18}, which is a decimal point followed by 17 zeroes and a 1. So, a flash of light lasting an attosecond, or 0.000000000000000001 of a second, is an extremely short pulse of light. Of note: The 2023 Nobel Prize in physics was given for the creation of extremely short pulses of light used to capture and study rapid processes inside atoms. It's just these processes that Barry was studying. In fact, a paper Barry co-authored just before coming to NIST is cited in the technical document describing the Nobel prize-winning work.

While the contributions mentioned above were outstanding, two other things he did while at NIST stand out. Barry was dismayed that, in contrast to other areas of physics, researchers in the world's AMO research community did not have a culture of sharing research software. He felt, and rightly so, that this impeded scientific progress. To help change this, Barry became the driving force[3] behind what is now the AMOS Gateway[4], a portal for research and education in atomic, molecular and optical science. Among other things, this site hosts research codes, i.e., mathematical models of how atoms and molecules behave, that anyone can easily utilize for free in carrying out AMO research. This is a great boon to young researchers trying to break into the field of AMO physics.

The second area that will contribute to Barry's legacy within NIST stems from his interest in high-performance computing. When Barry got here, he was surprised at the lack of formal institutional support for scientific computing and worked hard to help change that. He led a task force that provided a new vision for scientific computing at NIST, which led to major changes in NIST support for such tools. His many connections with the nation's leading figures in high-performance computing centers were extremely beneficial as NIST worked to reimagine its computing infrastructure. Future generations of NIST researchers will find a much more conducive environment for computational science thanks in large part to Barry's efforts.

[3] https://www.nist.gov/blogs/taking-measure/amo-all-how-online-portals-are-democratizing-field-atomic-molecular-and-optical
[4] https://amosgateway.org/

Barry was the author of some 140 refereed publications during his long career. He also found time to serve the profession in other ways. From 2004 to 2005 he served as chair of the American Physical Society's Division of Computational Physics. From 2018 to 2020, he was co-chair of the Networking and Information Technology Research and Development (NITRD) Program's High-Performance Computing Working Group, and he was recently co-chair of the U.S. Fast Track Action Committee that was tasked with updating the U.S. strategic computing plan. For many years he served as Associate Editor-in-Chief for the journal *IEEE Computing in Science and Engineering* and as a specialist editor for the journal *Computer Physics Communications*.

His work resulted in numerous accolades, including the Poste Rouge of the French government's National Centre for Scientific Research (1980), being named an American Physical Society Fellow (1982), receiving the Humboldt Research Award from the German government (1987-88), and receiving the Department of Commerce Bronze Medal (2020).

On a personal level, Barry was extremely outgoing. He loved people and loved to talk. (Getting the last word in an email back-and-forth with Barry was simply impossible.) He was generous in sharing stories from his long career. He loved music and actually led a rock-blues band all through college. He claimed not to be a very good musician, but he admitted that he sang well. He admired good guitar players, like Chet Atkins and Danny Gatton. But Barry also loved opera and shared many happy conversations with fellow opera lovers at NIST. The Italian tenor Franco Corelli was one of his favorites. Barry was also a serious runner before a heart condition forced him to discontinue that kind of exercise. His father had passed away in his 50s of heart problems, so Barry worked hard through dieting and exercise to keep healthy.

Barry also was a great mentor. At NIST he supervised two postdocs, a graduate student, and several undergraduates, all of whom were very successful. Barry was also generous with his time. Whenever someone was needed to perform some special tasks for the lab or the division, Barry was there. We don't know how he had the time to do everything he did. But he loved his work and loved NIST and kept working productively up to a few days before his passing.

We are grateful for that and are grateful for what he has given us. He was an undisputed giant in the field of computational physics. Barry's passing has left a big gap, but his legacy is everywhere.

Part II

Features

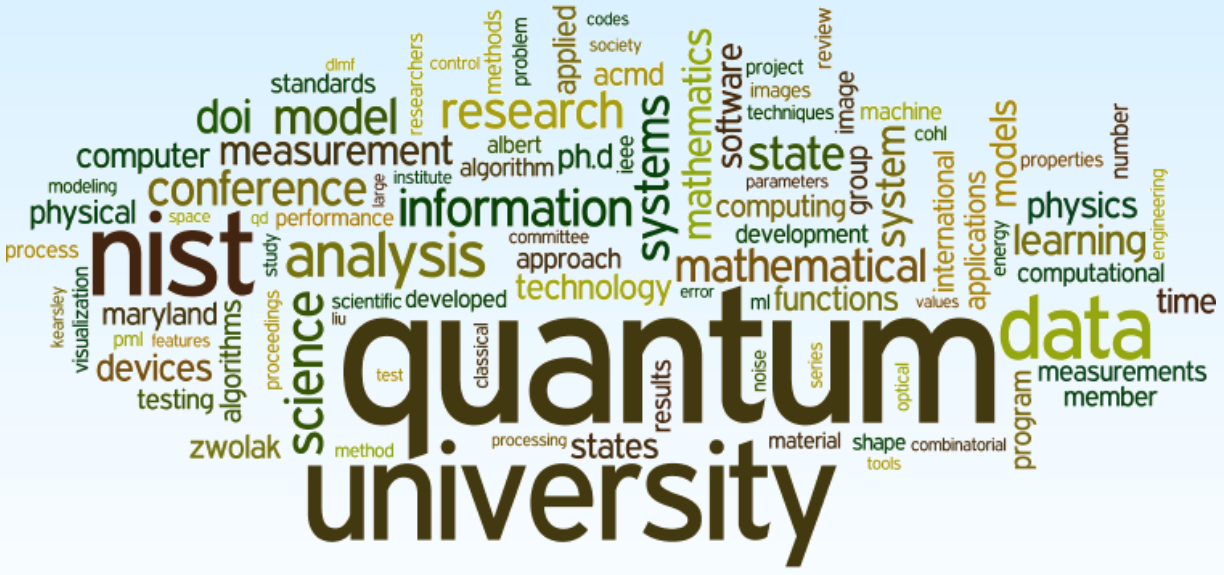

Algorithms to Enable Materials Research with Imaging

Our team has developed computational algorithms to support experts' analysis and inference in materials research. Our sustained efforts are motivated by the goal of improving the quality of solid material microscopy. To do this we develop metrological tools for analyzing material microstructure imagery. This metrology enables principled and quantitative analysis of the produced images.

Gunay Doğan
Zachary Grey

The macroscale behavior of a solid material, e.g., its strength, ductility, or conductivity, is not determined entirely by chemical composition, but fundamentally by its microstructure, an intricate geometric tiling of organized atomic constituents measured at the microscopic level. Thus, measurements enabling quantitative characterization of the imaged microstructure are key to designing and manufacturing next generation materials that will perform as intended in various scientific and engineering applications. Improving these technologies is a key facet of the evolving US economy. Example scenarios for applying this technology include:

- Question: If my industrial measurement device is noisy or has gaps in the data, how can I smooth or "in-paint" the image to better predict the microstructure and the subsequent physical properties?
- Question: If material from supplier "A" admits specific microstructure which is "trusted", but I want to switch to supplier "B" for economic reasons, does the microstructure of material produced from supplier B match what I previously trusted from supplier A? If not, is it better or worse in some quantifiable way?
- Question: If I process an image with one method but then I apply or generate an image (perhaps using AI or a physics-informed model) with another method, are the microstructures the same or different? If they are different, why?

Several material types that underpin a healthy US economy, such as metals, ceramics, mineral formations, (rocks), are polycrystals, i.e., they are comprised of many crystallites or grains [1]. A grain is a region of material constituents in a highly organized lattice structure. Hence, a grain and the locations in a grain, have an orientation with respect to a lab frame, and the orientation can be measured to aid in characterizing the microstructure of a material. As the union of the grains compose

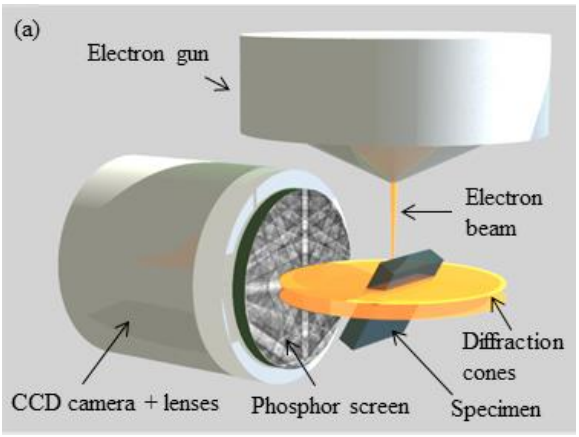

Figure 7. *Illustration of a typical EBSD imaging hardware configuration.* (Illustration by Stefano Vespucci et al., https://dx.doi.org/10.1103/PhysRevB.92.205301, CC BY-SA 3.0, https://commons.wikimedia.org/w/index.php?curid=129474938)

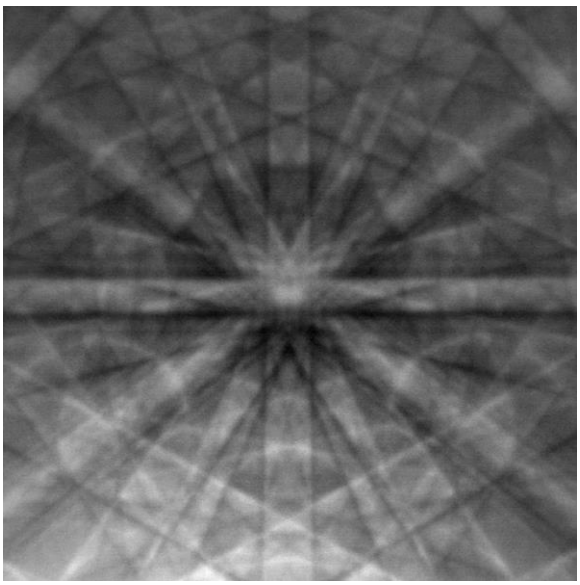

Figure 8. *An example of the Kikuchi pattern produced by the scattered electrons from one probed location on the material sample during EBSD imaging.*
(Image by Ben Britton, Own work, CC BY-SA 3.0, https://commons.wikimedia.org/w/index.php?curid=5316267)

the polycrystalline material, the orientations of the grains constitute the texture of the material. To analyze the microstructure of a polycrystalline material sample, scientists study the sizes, shapes and locations of the grains and their boundaries in addition to statistics of orientation and texture [2].

This measurement exercise involves mapping grain orientations to form an image obtained with scanning electron microscopy (SEM). In this microscopy, each

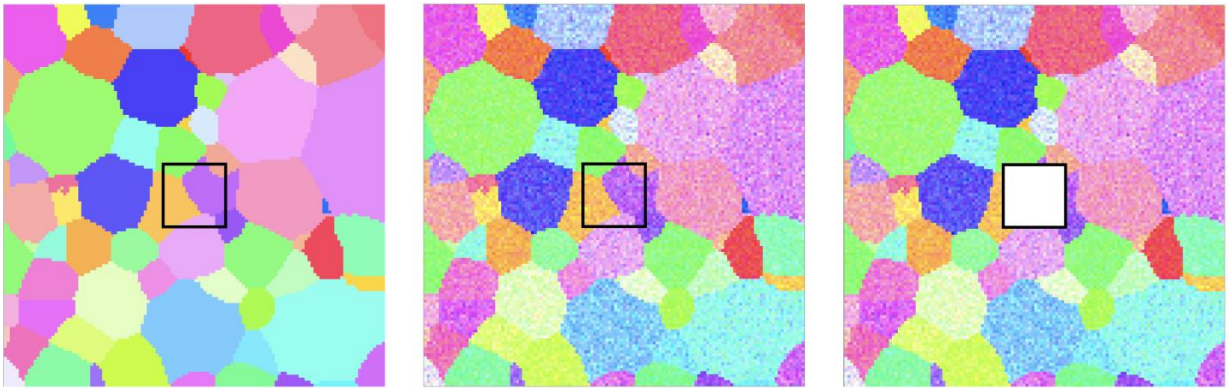

(a) (b) (c)

Figure 9. *Clean, noisy EBSD maps, and missing region used for demonstration. (a) IPF-z map of clean EBSD map generated using the Dream.3D software. (b) IPF-z map of original noisy EBSD map with de la Vallée Poussin noise of b = 4 (c) missing region of size 20 × 20 represented as a white block. The goal of inpainting algorithms is to take the map in (c) as an input and obtain an inpainting result as close as possible to the map in (b).*

pixel location in the image contains orientation information, usually in the form of three Euler angles (as opposed to RGB values for color images), that encode the volumetric orientation of the corresponding physical location. This produces an orientation map of the material sample which can be loaded into simulation software, such as OOF [3], to model the measured sample. For this analysis, OOF generates a finite element mesh matching the grains and their boundaries in the orientation map, and the user can then solve physics-based equations, modeling such things as elasticity or heat transfer, on the mesh representing the material sample (see the entry *OOF: Finite Element Analysis of Material Microstructures* on page 34 of this document for more information). It is important to note, however, that the accuracy of such an analysis is predicated on the accuracy of the measured orientation map.

Another central role of orientation maps in materials research and development is to reveal the intrinsic geometry and patterns of microstructure to a researcher, enabling them to relate macroscopic material behavior to the underlying microstructure. The governing features of these maps include grain sizes, shapes, topology, and texture in the microstructure. Materials scientists would like to understand what features in a given orientation map imply an observed macroscopic behavior. Once a rigorous relationship or hypothesis has been established, they would like to leverage this knowledge to create better materials through design and manufacturing by manipulating the distributions and contents of these intrinsic microscopic features. The manufactured outcomes are expected to achieve more desirable macroscopic behavior and performance; for example, improved grain features will imply lighter, but stronger, steel for automobile manufacturing. However, the massive array of orientation angles in the map is not, independently, very informative and does not immediately elucidate critical structures or features informing improved manufactured materials. We need algorithms to detect and extract such structures and features, and more importantly, to guide analyses governed by the underlying microscopic patterns. Developing these algorithms is the central focus of this project. These imaging algorithms include: i) orientation map reconstruction, ii) statistical assessments of extracted shapes and tools to identify persistent patterns, and iii) generation of informed summaries and interpretations based on the distribution of extracted features. This concert of algorithms facilitates explicit and interpretable comparison between imaged microstructures to address each of the hypothetical questions posed above.

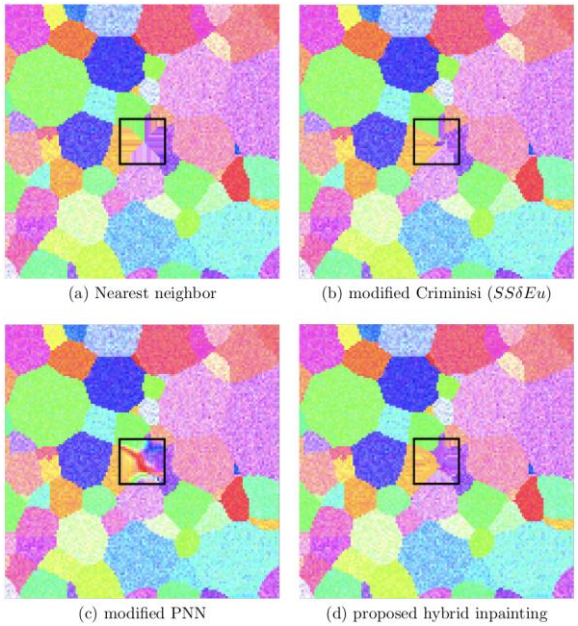

Figure 10. *IPF-z maps of the inpainting results for the EBSD map shown in* Figure 9. *(a) using the Dream.3D neighborhood filling filter, (b) results with modified Criminisi algorithm, (c) using the modified PNN algorithm, (d) using the proposed hybrid algorithm.*

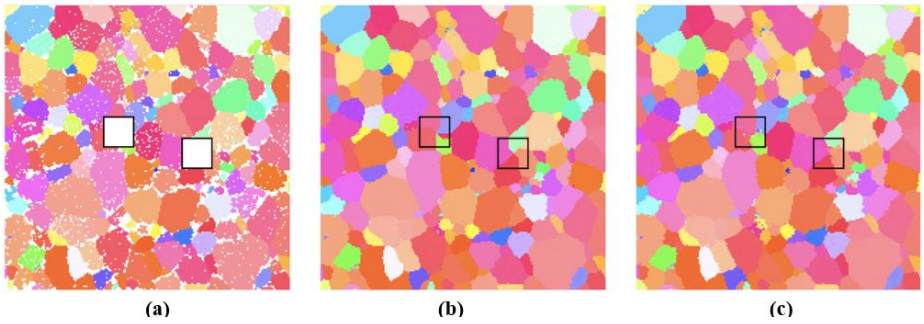

Figure 11. *IPF-z maps for the (a) real EBSD data (courtesy of Adam Creuziger, MML/NIST) with 20 × 20 sized missing blocks introduced, (b) inpainting result using the nearest neighbor inpainting from Dream.3D software, (c) inpainting using the proposed hybrid method.*

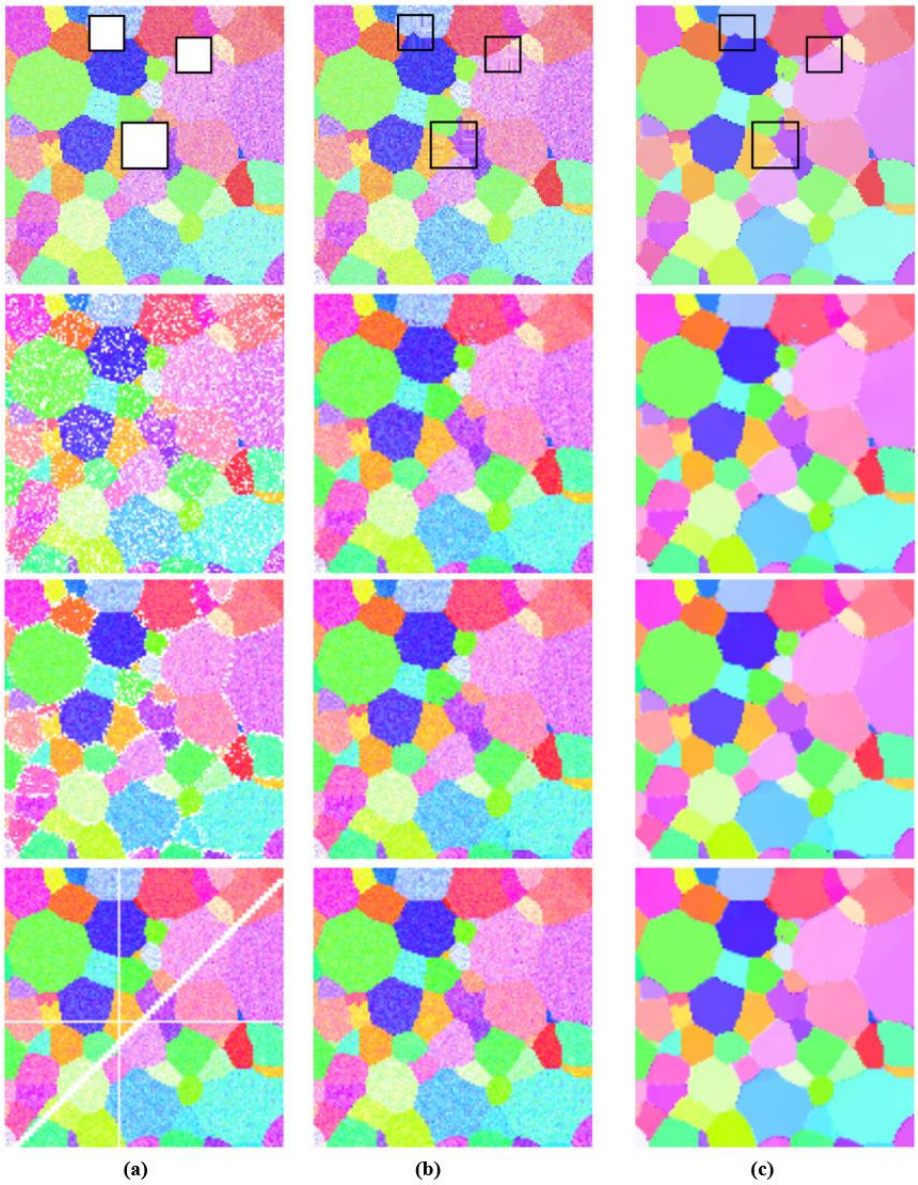

Figure 12. *IPF-z maps of the (a) given noisy EBSD maps with various patterns of missing regions, (b) inpainting result using the proposed hybrid algorithm, (c) result of the denoising algorithm proposed in Atindama et al. [4]. Compare the restored map in (c) with the original clean EBSD map in* Figure 9.

We utilize electron backscatter diffraction (EBSD) as a specialized SEM measurement technique that can generate a map of grains and orientations. EBSD uses a focused electron beam to probe a material sample one point at a time. To obtain a complete map, either the electron gun or the tilted sample is moved in a systematic pattern so that each location on the sample can be probed. (See Figure 7 for an illustration of a typical EBSD setup). When the electron beam hits the sample, the electrons are backscattered from the lattice layers, and as the backscattered electrons interact with the atoms of the sample they are diffracted and lose energy. The scattered electrons leave the sample at different angles and hit a phosphor screen, where they form the so-called Kikuchi patterns (see Figure 8). In principle, a Kikuchi pattern can be indexed to infer the orientation at the probed location. However, in practice, errors and ambiguities can creep in due to various factors in the physical setup, including some impulse noise due to large errors at isolated points, and in the measurement's indexing algorithm. Additionally, the orientation information at some locations of the map might be missing when the indexing algorithm fails to estimate the orientation from the corresponding Kikuchi pattern. Thus, the acquired measurement of

Table 1. *Per pixel reconstruction errors (in radians) using various inpainting algorithms for input noise with half-width parameters: 0, 2, 4, 6, and 8. The empirically best denoising error is boldfaced, while the error with the empirically second-best method is in italicized. The stars indicate the p-value for the statistically best performance compared with the second-best method. The p-values reported are for the paired t-test between the best methods and its closest competitor. * p < 0.1, ** p < 0.01, *** p < 0.001.*

half-width (b)	nearest neighbor	modified Criminisi	modified PNN	proposed hybrid	p-values
0	0.783	0.756	0.607	**0.528 ****	.005
2	0.453	0.429	0.447	**0.230 *****	< .001
4	0.790	0.739	0.559	**0.386 *****	< .001
6	0.613	0.570	0.466	**0.345 *****	< .001
8	0.608	0.582	0.515	**0.408 *****	< .001

the full microstructure orientation map may require further processing to mitigate these effects.

Off-the-shelf image processing algorithms are sometimes used to clean up and restore EBSD maps. However, their performance on EBSD maps is usually subpar compared to natural images, as these algorithms are typically designed to work on RGB-valued pixels of color images and do not take into account the equivalence of certain orientations due to crystal symmetries. In FY 2023, members of our team developed a customized denoising algorithm that was highly effective in restoring EBSD images [4]. This algorithm was based on the total variation partial differential equation (PDE) which can be used to smooth noisy measurements without destroying important geometric features, like grain boundaries and triple junctions. The denoising method included special preprocessing steps to preserve the angle space structure and crystal symmetry. An illustration of the denoising algorithm [4] on synthetic EBSD examples is given in Figure 12. However, denoising algorithms alone do not reconcile voids in the data. So, in FY 2024, we developed a solution for restoration of the missing orientation values in the EBSD maps [5].

Depending on measurement values and uncertainties, the mapping algorithm of the microscope can fail to estimate and assign orientation values in some locations of the EBSD map. Then the output from the microscope is an EBSD map with missing regions (of orientation values), as shown in Figure 10. These missing regions prevent us from segmenting the EBSD maps correctly which is a critical step to extract the grains and their boundaries for statistical analysis and inference on the material microstructure. An effective algorithm for EBSD inpainting is required to fill in the missing regions with accurately estimated orientation values. Estimating orientation values can be challenging depending on how much information is available in the immediate neighborhood. For a large missing region, the estimation problem is particularly ill-posed in the interior of the region as there is no nearby orientation to inform the estimation. Commonly used algorithms like nearest neighbor inpainting can fill in the missing regions resulting in an unnatural look that does not match the expected appearance of a polycrystal microstructure. See Figure 10(a), the result of nearest neighbor inpainting, and contrast with Figure 10(d), the result of our hybrid inpainting algorithm.

Various inpainting algorithms to fill in missing pixels in images have been proposed in the image processing literature. Two successful examples using complementary approaches are the exemplar-based inpainting algorithm of Criminisi et al. [6], and the partial convolution neural network (PNN) algorithm of Liu et al. [7]. These two algorithms work well for natural images, but not as well for EBSD maps (see Figure 10(b)(c)), as their contents, orientations and grains, are very different from RGB images of natural scenes for which these algorithms are designed and trained. However, we were able to adopt and build on these algorithms to create an effective EBSD inpainting algorithm.

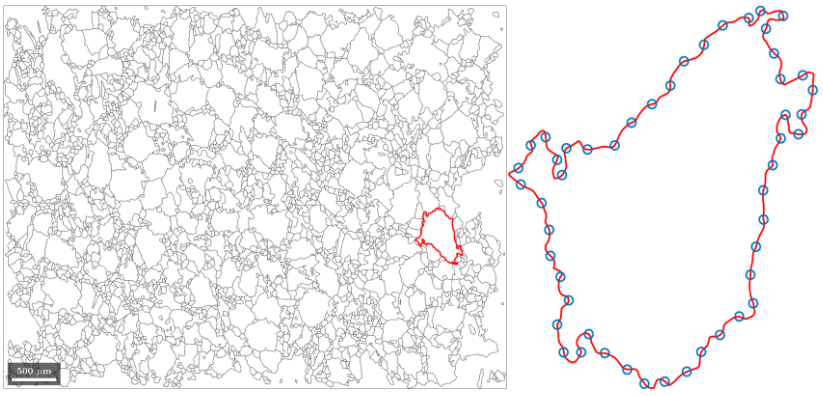

Figure 13. *An ensemble of thousands of grain boundaries from an EBSD image [14] (left) and an example segmented grain boundary (right) with arc-length reparametrization landmarks (blue circles) generated by an interpolating curve (red).*

The Criminisi inpainting algorithm [6] keeps track of most similar image patches to the missing image patch and uses these similar patches to inform the estimation of the missing pixels. This estimation process is executed by propagating the estimates inwards from the boundary of the missing region by prioritizing the locations for which the most amount of information is available. In its

original form, the Criminisi algorithm does not work well for EBSD maps, so we modified it to prioritize closer EBSD patches and to compare orientations using disorientation metrics rather than pixel-based metrics. The improvement in results from the modified Criminisi algorithm can be seen in Figure 10(b), compared to Figure 10(a) from the nearest neighbor inpainting.

Although the modified Criminisi algorithm performed better than the commonly used nearest neighbor algorithm, the grain boundary geometry in the completed regions still did not appear as those observed in real EBSD maps. This led us to adopt more flexible algorithms that can learn complex nonlinear relationships from data, namely, neural network algorithms. We modified the PNN algorithm of Liu et al. [7] and its loss function to work for EBSD maps. The success of a neural network solution, such as PNN, depends very much on the availability of a comprehensive training dataset that covers the range of examples that it is expected to process. This is a challenge in material science, because unlike in usual computer vision settings, it is very hard, and often infeasible, to create large training datasets with enough variety in material samples. To circumvent this, we relied on synthetic training examples to generate a large enough dataset using the Dream.3D software [8] (see Figure 9). The training dataset did not only include a large collection of microstructures, but also a variety of missing data patterns (see Figure 12). Once trained on this synthetic dataset, our modified PNN inpainting algorithm started showing satisfactory performance.

The best inpainting results, namely those with the natural appearance observed in real microstructures, were obtained

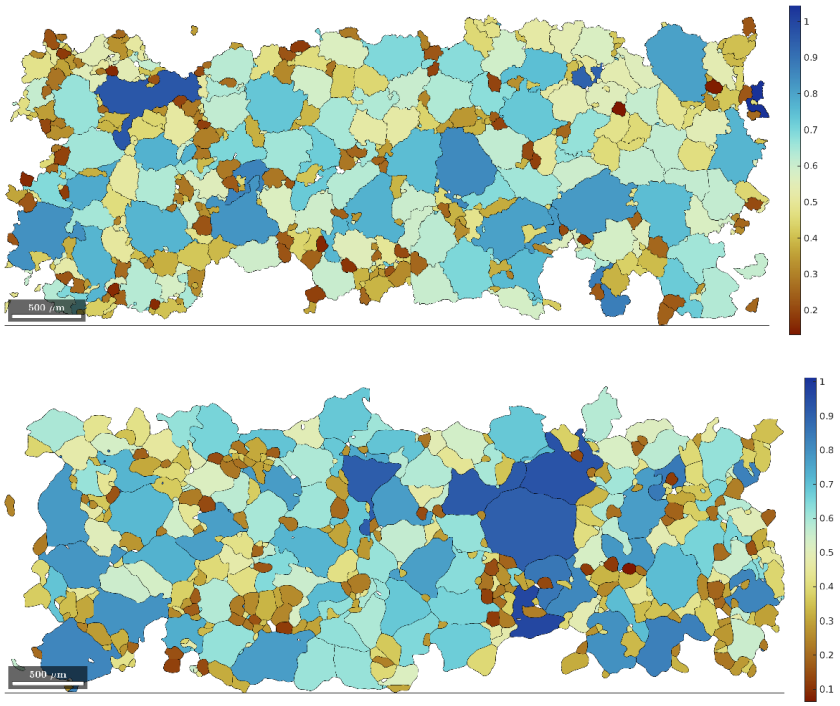

Figure 14. *Comparison of two locally partitioned subsets of a larger EBSD image from a common ice sample [14] (PIL184) with N = 933 total curves and n = 500 landmarks per curve. No shapes or boundaries are duplicated between the partition. However, using a simple moving average in the MTEX 'smooth' routine [9], the upper partition (top image) is not smoothed while the bottom is smoothed to some extent. Magnifying the top image, it is possible to see small differences in the nonlinear deformations of shapes along the grain boundaries. The difference is nearly visually indistinguishable. Yet, the approximate inferences enabled by our explainable binary classification framework [11] suggest differences in undulations and common scales. When the top image is smooth in a consistent way, the explanation is resolved, and the two distributions are considered equivalent in both undulation and scale.*

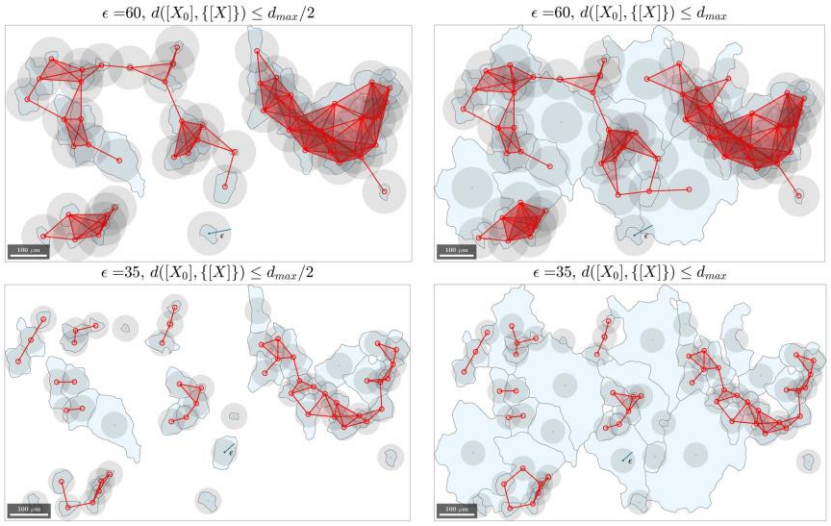

Figure 15. *Examples of simplices forming Rips-Vietoris complexes defining a filtration taken over a sub-region in a larger EBSD image for topological data analysis. Two filtrations are formed as columns by connecting grain centroids across changing ϵ over rows. Grains with shape distance less than half the maximum distance define the left-column filtration while all grains in the sub-region of the EBSD image define the right-column filtration. Grains are filled with a light blue to help visually distinguish preshapes from unfilled regions.*

with our hybrid inpainting algorithm that leveraged both the modified Criminisi algorithm and the modified PNN algorithm (see [5] for details). Some representative results are shown in Figure 9, Figure 10, and Figure 11. We evaluated the hybrid algorithm rigorously against nearest neighbors, modified Criminisi, and modified PNN algorithms, and tried to see how accurately each algorithm restored the missing values of known ground-truth maps. Our hybrid inpainting algorithm outperformed the alternatives by a significant margin. Visual comparisons are shown in Figure 10, and a table of actual restoration errors are given in Table 1. When we finally used the inpainting and the denoising algorithms together, as shown in Figure 11, we were able to obtain high-quality restorations of EBSD maps without any noise or missing values, very suitable for segmentation algorithms, such as those available in MTEX toolbox [9], used for processing EBSD maps.

In parallel to our efforts for restoration of EBSD maps, members of our team worked on principled approaches for analysis and inference on material microstructure images, using higher level features, such as grain boundaries, extracted from these images (see Figure 13). Traditional methods for comparing EBSD scans of microstructures include the assessment of key parameters such as relative size of the grains, which is linked to the strength of the material, and largest observed grain, as this can correlate with a manufactured part's failure. Volume content in the material of an inclusion or second matter phase, and spatial arrangement (topology) of the shapes are also relevant for properties of strength, elongation, and failure.

Existing standards for EBSD maps are defined by quantifying intuitive characteristics of shapes, which limit their applicability to a wider range of shapes and topologies of grains. While many of these hand-picked features have been linked to key properties of materials, there is no evidence to suggest that they are comprehensive or representative, and summary statistics that compare them can be misleading, i.e., a phenomenon akin to Anscombe's quartet. In computer assisted analysis of microstructures, additional metrics of shape are often considered beyond what is listed in documentary standards. A wide variety of software is available for these, e.g., see the list of "Shape Parameters" from MTEX [9]. However, a variety of distinct implementations, oversimplification of shape representations (e.g., fitting a circle or ellipse), and emphasis on a single metric (such as area or perimeter) limit comparisons of microstructures and the development of standards.

On the other hand, shape-based metrics, proposed to capture invariances over specific curve transformations, are well-suited for precise measurement of highly varied and complex morphologies found in EBSD maps, in particular, the grains, and their boundaries. Separable shape tensors (SST) proposed in [10] are an effective representation and basis to compute such shape-based metrics. SST separates linear and nonlinear geometric features of interest augmented by a data-driven framework for learning a submanifold of shapes informing statistical assessments. This process is efficient, promotes a regularization of shape representations against noisy segmentation, and offers clear theoretical interpretations of learned features in contrast with the outcomes of machine learning approaches that are hard to interpret.

In [11], we demonstrated how kernel metrics over learned SST features could inform an explainable binary classification of shape ensembles (e.g., representing collections of grain boundaries in EBSD maps; see Figure 13) capable of effectively distinguishing pairs of images like those in Figure 14. The central question to be answered in explainable binary classification is: *"Is this shape ensemble the same as the other shape ensemble?"* and will often include the follow-up question to explain the discrepancy: *"If they are different, why?"* We should emphasize that the notion of 'difference' in this context is *statistical*, given the stochastic nature by which material grains form and evolve. In other words, a naive deterministic perspective that assesses if ensembles of shapes in different EBSD maps are identical with respect to some point-wise metric/distance is uninformative, since no two sampled micrographs are ever the same, leading to limited conclusions in this presumed stochastic materials application. This is why we employed a stochastic notion of difference based on maximum mean discrepancy (MMD), leading to the more relevant question: *Are the approximated distributions of representative shape features over the ensemble in one EBSD map statistically significant from the ensemble in another?* To answer this question, we first (i) represented grain shapes as SSTs, separating important distinguishing features, 'generalized scale' and 'undulation,' then (ii) discretized to approximate feature distributions of the shapes from both EBSD maps with higher order quadratures, and finally, (iii) tested for statistically significant discrepancies in distributions between two EBSD ensembles using MMD. This corresponds to statistically comparing thousands of shapes in two ensembles given two EBSD images (see Figure 14 for an example of a comparison).

It is important to note that shape is only one significant piece of the quite literal puzzle in Figure 13. The explainable binary classification approach ignores the role of textures intrinsic to the tiling, i.e., the spatial arrangement of the shapes, and instead treats the ensemble of shapes as independent realizations from some generating distribution. Still, visual inspection can also reveal that two given microstructures exhibit very different spatial patterns of shapes. This motivated us to augment our analysis by quantifying the inherit topological structure to explore patterns in the spatial arrangement conditioned on similarities (distances) of individual shapes over the submanifold of SST. In contrast to shape

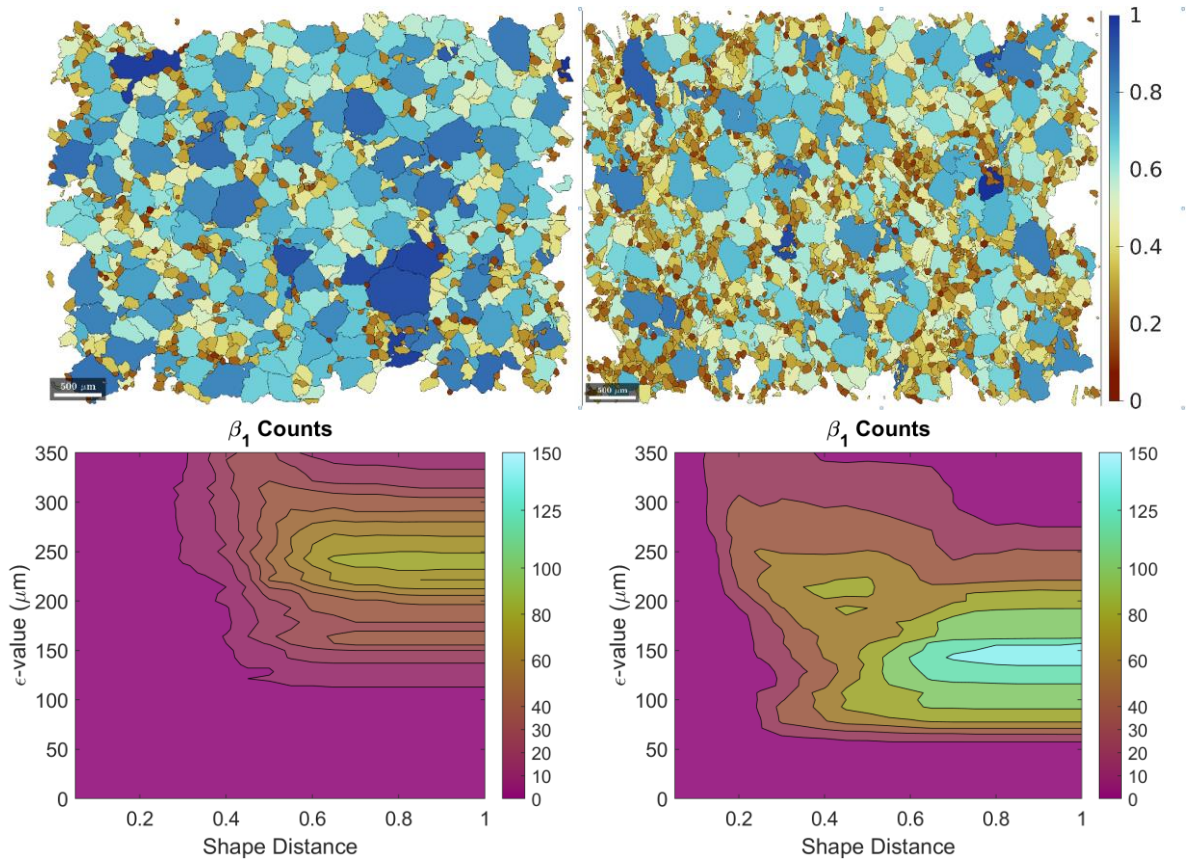

Figure 16. *Microstructures of two ice samples PIL184 (left) and PIL185 (right) from [14] shown at the top row. Grains are colored according to the (normalized) product submanifold shape distance of reparametrized grain boundary landmarks from the approximated origin. The corresponding bifiltration filled contour images created for topological data analysis are shown at the bottom row. Just like the grid of simplicial complexes in Figure 9, the vertical axes represent ϵ values defining a Rip's complex constructed over grain centroids less than a shape distance level set in the horizontal axis. Persistent homology is calculated using the open-source software Javaplex [2] with grain centroids as point cloud data. The contours represent β_1 and, thus, PIL185 admits a very different topology with many more loops.*

representation and statistical ensembles, topological descriptions focus on the global connectivity of a dataset, offering an abstract view of its structure that is independent of precise geometry. Topological data analysis (TDA) captures global characteristics answering questions such as: "*How many distinct pieces (connected components) exist in the data?*" "*How many loops or cycles does the structure form?*" and "*Are there voids or enclosed spaces within the data?*" Thus, a TDA can encode global characteristics of pattern in complicated spatial morphologies to complement individual shape representations.

Pursuing this aspect of the problem, we proposed a novel framework in [12] merging TDA with shape analysis by combining topological persistence with shape distances, e.g., SST product submanifold distances. This framework leverages biparameter persistence analysis of a spatial TDA filtration parameter conditioned on shape distances from an intrinsic, archetypal (origin) shape. The dual-parameter approach not only considers the persistence of topological features across different scales but also evaluates features' geometric similarity (see Figure 15). The result is a more nuanced understanding of "texture" in imaging data, which refers to the spatial arrangement and quantitative representation of shapes forming patterns. In practical terms, this allows scientists to ask not only "*Are these two random ensembles of shapes from the image the same?*" but also "*How are they arranged, and what global patterns emerge from their arrangement?*" The resulting visualization of a bifiltration analysis example is shown in Figure 16.

This richer analysis is particularly important in fields like materials science, where understanding more comprehensive notions of texture in a material's microstructure can be crucial for determining subsequent macroscopic properties and performance. The tools that we developed in this work facilitate key pattern recognition tasks with methods to augment existing standards in materials science. Broadly, they also motivate novel, holistic quantification of coherent patterns in scientific imaging. The transparent and principled nature of our approach complements those leveraging artificial intelligence to accomplish similar tasks, replacing ambiguous latent spaces that can be difficult to interpret

and explain. Thus, our approach offers a clear path to systemically explaining which patterns are intrinsic and significant in given scientific images.

References

[1] S. Zaefferer. A Critical Review of Orientation Microscopy in SEM and TEM. *Crystal Research Technology* **46**:6 (2011), 607–628. DOI: 10.1002/crat.201100125

[2] A. Creuziger and M. Vaudin. Report on VAMAS Round Robin of ISO 13067: Microbeam Analysis - Electron Backscatter Diffraction - Measurement of Average Grain Size. NISTIR 7814, National Institute of Standards and Technology, 2011. DOI: 10.6028/NIST.IR.7814

[3] S. A. Langer, E. R. Fuller, and W. C. Carter. OOF: An Image-Based Finite-Element Analysis of Material Microstructures. *Computing in Science and Engineering* **3**:3 (2001), 15–23. DOI: 10.1109/5992.919261

[4] E. Atindama, P. Lef, G. Doğan, and P. Athavale. Restoration of Noisy Orientation Maps from Electron Backscatter Diffraction Imaging. *Integrating Materials and Manufacturing Innovation* **12** (2023), 251–266. DOI: 10.1007/s40192-023-00304-8

[5] E. Atindama, C. Miller-Lynch, H. Wilhite, C. Mattice, G. Doğan, and P. Athavale. Hybrid Algorithm for Filling in Missing Data in Electron Backscatter Diffraction Maps. In process.

[6] A. Criminisi, P. Perez, and K. Toyama. Region Filling and Object Removal by Exemplar-Based Image Inpainting. *IEEE Transactions on Image Processing* **9** (2004), 1200–1212. DOI: 10.1109/TIP.2004.833105

[7] G. Liu, F.A. Reda, K.J. Shih, T. Wang, A. Tao, and B. Catanzaro. Image Inpainting for Irregular Holes Using Partial Convolutions. Preprint arXiv:1804.07723, 2018. DOI: 10.48550/arXiv.1804.07723

[8] Dream.3D. http://dream3d.bluequartz.net/. Online, accessed January 1, 2025.

[9] F. Bachmann, R. Hielscher, and H. Schaeben. Texture Analysis with MTEX–free and Open Source Software Toolbox. *Solid State Phenomena* **160** (2010), 63–68.

[10] Z. J. Grey, O. A. Doronina, and A. Glaws. Separable Shape Tensors for Aerodynamic Design. *Journal of Computational Design and Engineering* **10**:1 (2023), 468–487.

[11] Z. Grey, N. Fisher, A. Glaws, and G. Doğan. Explainable Binary Classification of Separable Shape Ensembles. arXiv:2410.12994, 2024. DOI: 10.48550/arXiv.2410.12994

[12] J. Schreiber, Z. J. Grey, and A. Ceuziger. Topology of Shape and Data in Material Microstructures. In process.

[13] H. Adams, A. Tausz, and M. Vejdemo-Johansson. Javaplex: A Research Software Package for Persistent (Co) Homology. In *Mathematical Software–ICMS 2014: 4th International Congress*, Seoul, South Korea, August 5-9, 2014. Proceedings 4, 129–136. Springer, 2014.

[14] S. Fan, D. J. Prior, A. J. Cross, D. L. Goldsby, T. Hager, M. Negrini, and C. Qi. EBSD Data for Synthetic Polycrystalline Pure Water Ice Samples Deformed at High Homologous Temperatures. FigShare, 2020.

Participants

Günay Doğan, Zachary Grey (ACMD); Prashant Athavale, Emmanuel Atindama, Connor Miller-Lynch (Clarkson University); Adam Creuziger (MML/NIST); Nicholas Fisher (Portland State University); Andrew Glaws (National Renewable Energy Lab); Cody Mattice (Middlebury College); Jeanie Schreiber (George Mason University); Huston Wilhite (University of Michigan, Ann Arbor)

SiC-based Integrated Quantum Device Efforts

Silicon carbide (SiC) has emerged as a promising material for integrated quantum devices due to its compatibility with complementary metal-oxide-semiconductor (CMOS) technology, coupled with favorable mechanical, electrical, thermal, and photonic properties. SiC's unique attributes, such as its wide bandgap, high thermal conductivity, and robust optical characteristics, make it an ideal candidate for high-performance quantum applications. To benefit from these advantages, we have collaborated with researchers at Carnegie Mellon University to develop and characterize a prototype entangled photon source based on a SiC micro-ring resonator.

Lijun Ma
Anouar Rahmouni

We are developing an entangled photon source built on a 4H-silicon-carbide-on-insulator (4H-SiCOI) platform, where a silicon dioxide (SiO_2) layer provides isolation from the silicon substrate. A compact 36-µm-radius SiC micro-ring resonator is used to generate photon pairs by way of the nonlinear spontaneous four-wave mixing (SFWM) process. Advanced nanofabrication techniques have enabled the realization of micro-ring resonators with an optical quality factor (Q factor) exceeding 1 million, which is critical for efficient photon pair generation.

In our pioneering work, we demonstrated, for the first time, an entangled photon source integrated into the SiC platform. Specifically, we used a compact micro-ring resonator fabricated on a 4H-SiCOI platform to achieve efficient generation of strongly correlated photon pairs. These pairs are generated through the nonlinear process of SFWM at the telecom C-band wavelength (around 1550 nm), a wavelength regime that is particularly important for quantum communication and fiber-optic applications. A schematic of this integrated source is shown in Figure 17.

Our results show that the maximum coincidence-to-accidental ratio (CAR) exceeds 600, corresponding to a pair generation rate of 9×10^3 pairs per second. This high CAR indicates excellent entanglement quality and low background noise, which are critical for practical quantum information processing. Furthermore, we demonstrated energy-time entanglement between the signal and idler photons, with two-photon interference fringes exhibiting a visibility greater than 99 %, as shown in Figure 18. This high visibility is a hallmark of strong quantum correlation between the photon pairs and is a key indicator of the source's potential for quantum communication and sensing applications.

We also characterized the heralded single-photon properties of the source, measuring the second-order correlation function $g^{(2)}(0)$ on the order of 10^{-3}, which confirms the strong antibunching of the heralded photons (Figure 19). Such antibunching is a clear signature of quantum behavior and further underscores the suitability of SiC as an ideal material for single-photon sources. The ability to generate heralded single photons with such low $g^{(2)}(0)$ values enables applications in quantum communication and quantum networks.

This work positions SiC as a fully integrated, CMOS-compatible platform for generating entangled

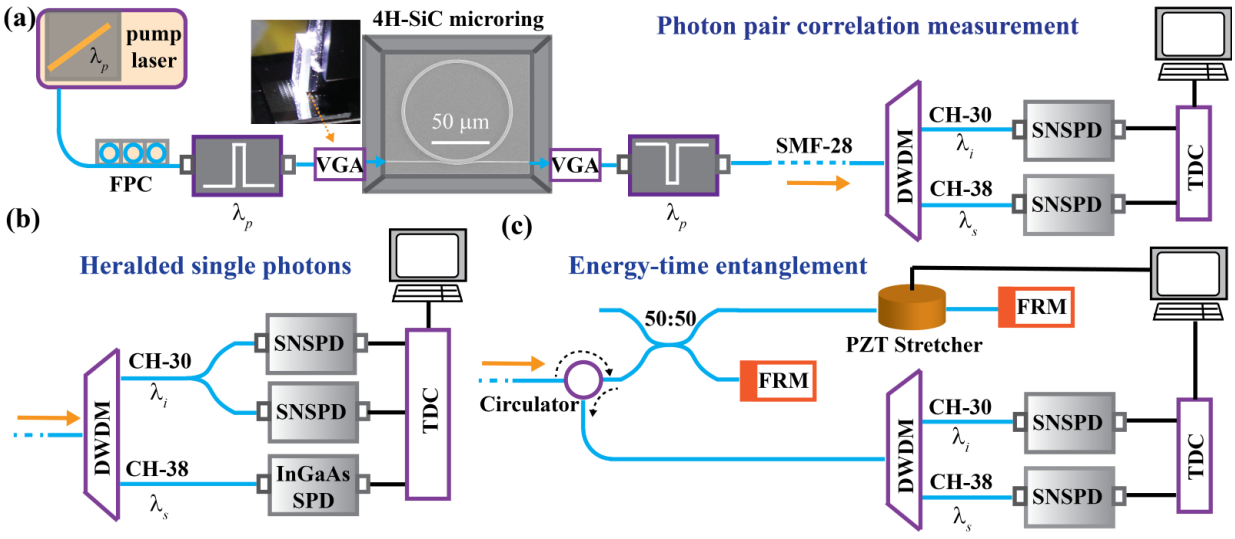

Figure 17. *The SiC-based entangled photon source and the experimental set-up for characterization.*

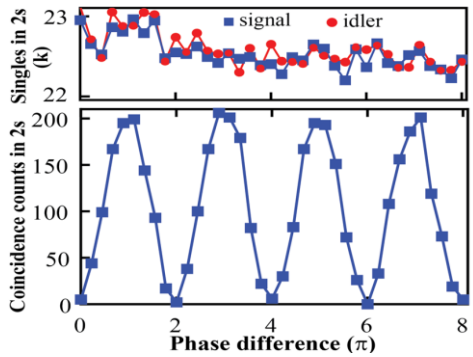

Figure 18. *Two-photon interference fringe using an unbalanced Franson interferometer configuration.*

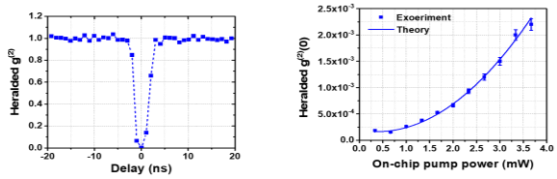

Figure 19. *Measured heralded $g^{(2)}(0)$ is on the order of 10^{-3} indicating strong antibunching.*

photon pairs, which is an essential building block for quantum networks and other quantum technologies. Notably, we achieved precise wavelength alignment between the signal and idler photons and the Dense Wavelength Division Multiplexing (DWDM) ITU-grade channels, which are commonly used in telecommunication systems. This alignment ensures that the generated photon pairs are directly compatible with existing optical networking infrastructure, thereby facilitating the integration of SiC-based entangled photon sources into real-world quantum communication networks.

In addition to demonstrating the basic functionality of the SiC-based entangled photon source, we anticipate that further engineering refinements will enable the scalability and practical deployment of these devices. With continued development, SiC-based sources could play a crucial role in the emerging quantum industry, offering robust, scalable, and cost-effective solutions for quantum networks, sensing, and metrology. We are also working towards integrating these sources into the NIST Gaithersburg and DC-QNet quantum network testbeds which will serve as an important proof-of-concept for real-world applications and demonstrate their potential impact on the quantum industry.

In summary, our work highlights the potential of SiC as a key material for advancing quantum technologies, and with further development, SiC-based entangled photon sources could become a cornerstone of the quantum communication and networking infrastructure of the future. The results have been published in *Light: Science and Application* [1] and presented at the Single Photon Workshop [2].

References

[1] Rahmouni, R. Wang, J. Li, X. Tang, T. Gerrits, O. Slattery, Q. Li, and L. Ma. Entangled Photon Pair Generation in an Integrated SiC Platform. *Light: Science & Applications* **13**:1 2024), 110. DOI: 10.1038/s41377-024-01443-z

[2] Rahmouni, R. Wang, J. Li, X. Tang, T. Gerrits, O. Slattery, Q. Li, and L. Ma. "Entangled Photon Pair Generation in an Integrated SiC Platform." *Single Photon Workshop*, Edinburgh, November 2024.

Participants

Lijun Ma, Anouar Rahmouni, Oliver Slattery, Thomas Gerrits, Xiao Tang (ACMD); Qing Li, Ruixuan Wang, Jingwei Li (CMU); Michael Spencer (MSU)

Part III

Project Summaries

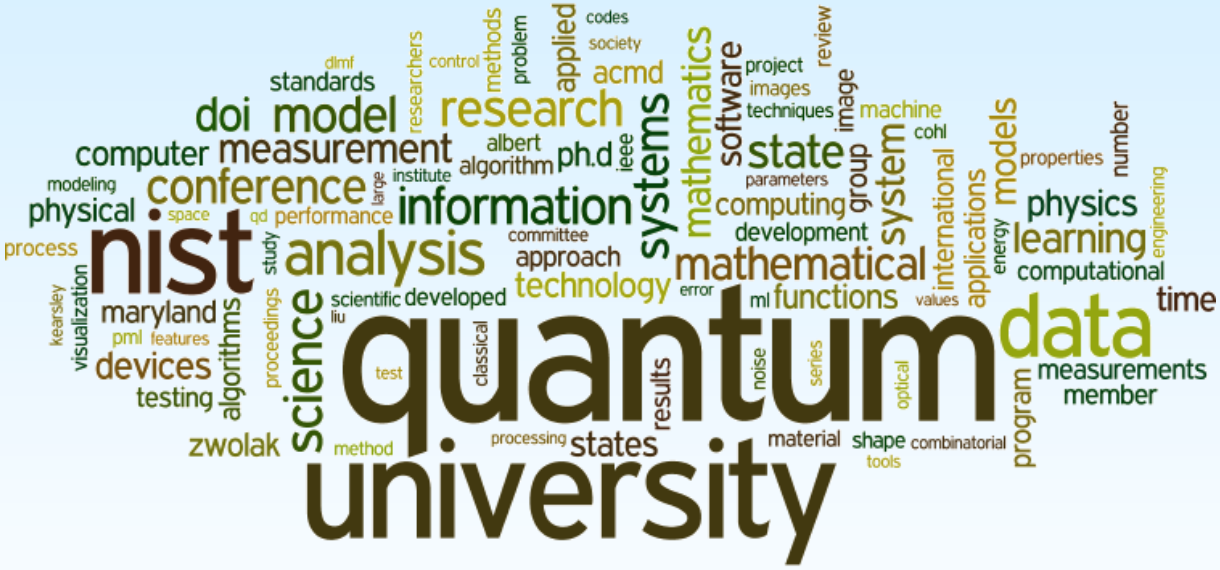

Mathematics of Metrology

Mathematics plays an important role in measurement science. Mathematical models are needed to understand how to design effective measurement systems and to analyze the results they produce. Mathematical techniques are used to develop and analyze idealized models of physical phenomena to be measured, and mathematical algorithms are necessary to find optimal system parameters. Mathematical and statistical techniques are needed to transform measured data into useful information. We develop fundamental mathematical methods and tools necessary for NIST to remain a world-class metrology institute, and to apply these to measurement science problems

True Becquerel: A New Paradigm for 21st Century Radioactivity Measurements

Bradley Alpert
Ryan Fitzgerald (NIST PML)
Denis Bergeron (NIST PML)
Richard Essex (NIST PML)
Svetlana Nour (NIST PML)
Galen O'Neil (NIST PML)
Daniel Schmidt (NIST PML)
Gordon Shaw (NIST PML)
Mike Verkouteren (NIST MML)
Kelsey Morgan (NIST PML)
Daniel Swetz (NIST PML)
Joel Ullom, et al. (NIST PML)

Expanding applications of radioactivity in medicine, energy, and security demand quantification of complex mixtures at uncertainty levels that are currently unachievable. This project is enabling measurement of absolute activity (Bq) of radionuclide mixtures, avoiding chemical separation, by analysis of the decay heat signature of gravimetric samples embedded within microcalorimeter detectors. This capability consolidates multiple measurements into one, reducing cost and uncertainty. Success is creating a primary realization of the Bq for direct assay of real-world samples at NIST and beyond, resulting in faster clinical trials of new radiopharmaceuticals and a faster, expanded nuclear forensics "fingerprinting" method for improved decision making.

The project enters its fifth (and last) year of NIST Innovations in Measurement Science funding, having demonstrated success in preparation, deposition, weighing, and energy spectrometry of milligram samples containing one or a few radionuclides. Novel transition-edge-sensor (TES) designs have reduced prior uncertainty from nuclide decays outside of the microcalorimeter absorber and enabled dynamic reconfiguration through wire-bonding to accommodate different decay energy spectra. Spectrometry of Am-241 alpha decays and Am-241 with Am-243 alpha decays have been validated with standard methods involving liquid scintillation. Characterization of other radionuclide decays, including beta decays from daughter product Np-239, and other alpha decays, are now in process.

The analysis challenges include (1) characterization of detector dynamics, to enable determination of decay energies of events with poor temporal separation, limiting detector dead time, at an accuracy that reflects the exquisite precision of the TES detector, (2) characterization of the partial energy losses due to transport out of the absorber material of alpha, beta, and gamma rays, and (3) disambiguation of the spectrum into constituents, based on a library of radionuclide decays, with full quantification. Two new tools for detector dynamics characterization are (a) fabricated capability for electronic excitation of the detector with known energy depositions, and (b) algorithms for ordinary differential equation (ODE) parameter sensitivity, of much recent attention, to determine an ODE system from its input/output behavior. This machine learning (ML) technique will be combined with more conventional supervised ML for library-based disambiguation of spectra. The uncertainty, and risk, for both techniques is whether the stringent accuracy requirements of the project can be achieved.

[1] R. P. Fitzgerald, B. K. Alpert, D. T. Becker, D. E. Bergeron, R. M. Essex, K. Morgan, S. Nour, G. O'Neil, D. R. Schmidt, G. E. Shaw, D. Swetz, R. M. Verkouteren, and D. Yan. Toward a New Primary Standardization of Radionuclide Massic Activity Using Microcalorimetry and Quantitative Milligram-Scale Samples. *Journal of Research of the National Institute of Standards and Technology* **126** (2021), 126048. DOI: 10.6028/jres.126.048

[2] R. P. Fitzgerald, B. K. Alpert, D. E. Bergeron, M. B. Carlson, R. M. Essex, K. M. Morgan, S. Muramoto, S. Nour, G. C. O'Neil, D. R. Schmidt, G. A. Shaw, D. S. Swetz, and R. M. Verkouteren. Absolute Spectroscopic Activity Assay of Microliter Aliquots of Radioactive Solution Without Tracers or Calibrants. In review.

Overcoming Barriers: Nanoscale Interface Metrology and Electrical Characterization for Advanced Electronics

Bradley Alpert
Alexana Roshko (NIST PML)
Allison Mis (NIST PML)
Edwin Supple (NIST PML)

As devices become smaller, more complex, and more highly integrated, interfaces are increasingly important and limiting. The ability to accurately predict interface behavior is critical for accelerating device development times but requires atomic-scale knowledge of interface electric fields, which is currently unavailable. This CHIPS-funded project aims to develop standardized data collection and analysis protocols to enable nanoscale electric field determination from artifact free differential phase contrast four-dimensional scanning transmission electron microscopy (DPC 4D-STEM) data.

Existing theories (Schottky-Mott, Metal-Induced Gap State, Charge-Neutrality-Level and Interface Dipole Theory) are based on work functions measured for electrons passing from a pure bulk material into vacuum, which is an unrealistic model for two different materials in contact. Thus, in the absence of detailed knowledge of what happens at the interface, existing theoretical efforts are insufficient. True understanding and control of interfaces requires atomic scale knowledge of interface structure, composition, bonding, strain, and electric field. While the small probe size and high current density of aberration-corrected scanning transmission electron microscopes has enabled many of these measurements, determination of the electric field on the atomic scale remains problematic. DPC 4D-STEM using fast, pixelated electron detectors is a promising method for atomic scale measurement of electric field. The technique has been demonstrated in a few academic labs; however, it requires the capture, processing, and analysis of extremely large datasets and is rarely used. This project will provide critical, currently unavailable data on atomic-scale electric field distributions at a variety of interfaces pertinent for current and future devices. In addition, data collection and analysis protocols will be developed for a nascent measurement technique (DPC 4D-STEM) to make further atomic scale mapping of electric field accessible to the semiconductor industry.

Early-stage effort by Alpert involves opening the software communication protocol between the DPC 4D-STEM instrument and its controller. Protocol revisions will customize scanning and data collection to enable real-time experiment monitoring and specialization for material interface measurement. Later work will be aimed at developing parametrized models of electric fields at material interfaces to incorporate detailed nanoscale structural knowledge.

Elastic Shape Registration of Surfaces in 3-Dimensional Space

Javier Bernal
James Lawrence

The computation of the elastic shape registration of two surfaces in 3D space together with the elastic shape distance between them has applications in the study of geological terrains, surfaces of anatomical objects and structures such as facial surfaces.

In the context of shape analysis [3, 5, 8, 9], results were obtained and presented in [2] for computing the elastic shape registration of two simple surfaces in 3-dimensional space and the elastic shape distance between them. Those algorithms were based on a gradient descent approach for reparametrizing one of the surfaces similar to those by Kurtek, Jermyn, et al. [4, 6], and more recently by Riseth [7]. The rotation and reparameterization presented in [1] for reparametrizing one of the surfaces to obtain a partial elastic shape registration of the surfaces was used as the input initial solution to the algorithm. We note that the gradient descent approach used to obtain our results is a generalization to surfaces in 3-dimensional space of the gradient descent approach for reparametrizing one of two curves in the plane when computing the elastic shape distance between them presented in [8]. For the sake of completeness, in [2] we describe and justify the approach for curves as it is done in [8], and then present and justify its generalization to surfaces in 3-dimensional space. This generalization together with its justification was developed independently of similar work in [4, 6, 7].

[1] J. Bernal and J., Lawrence. Partial Elastic Shape Registration of 3D Surfaces using Dynamic Programming. NIST Technical Note 2274 (2023). DOI: 10.6028/NIST.TN.2274

[2] J. Bernal, J. Lawrence. Elastic Shape Registration of Surfaces in 3D Space with Gradient Descent and Dynamic Programming. NIST Technical Note 2310 (2024). DOI: 10.6028/NIST.TN.2310

[3] J. Bernal. Shape Analysis, Lebesgue Integration and Absolute Continuity Connections. NISTIR 8217 (2018). DOI: 10.6028/NIST.IR.8217

[4] H. Jermyn, S. Kurtek, E. Klassen, and A. Srivastava. Elastic Shape Matching of Parameterized Surfaces Using Square Root Normal Fields. In *Proceedings of the 12th European Conference on Computer Vision* (ECCV'12), Volume V, Springer, Berlin (2012), 804-817.

[5] S. H. Joshi, E. Klassen, A. Srivastava, and I. H. Jermyn. A Novel Representation for Riemannian Analysis of

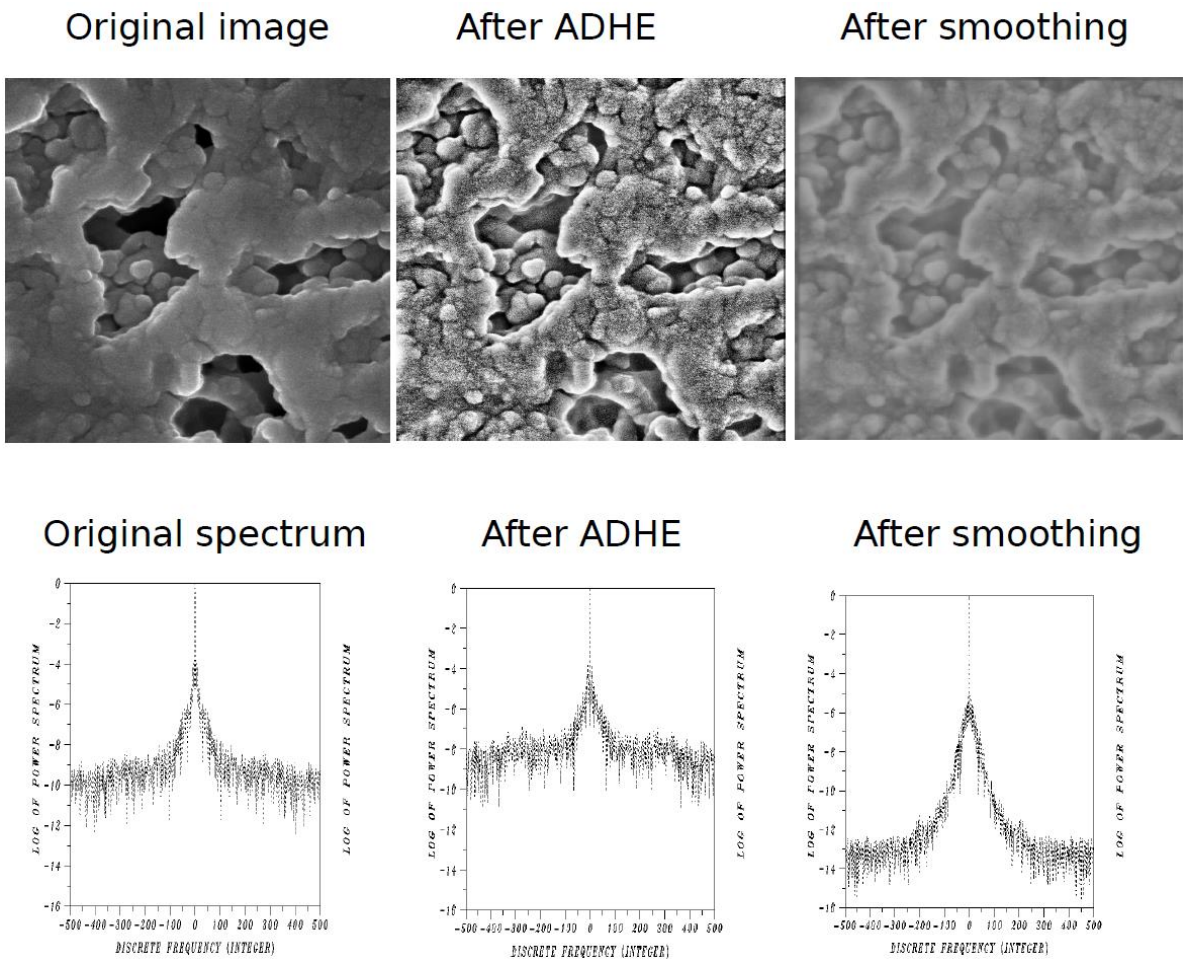

Figure 20. *Adaptive Histogram Equalization (ADHE) reveals valuable information while generating significant noise that must be smoothed out. This is reflected in the respective Fourier spectra.*

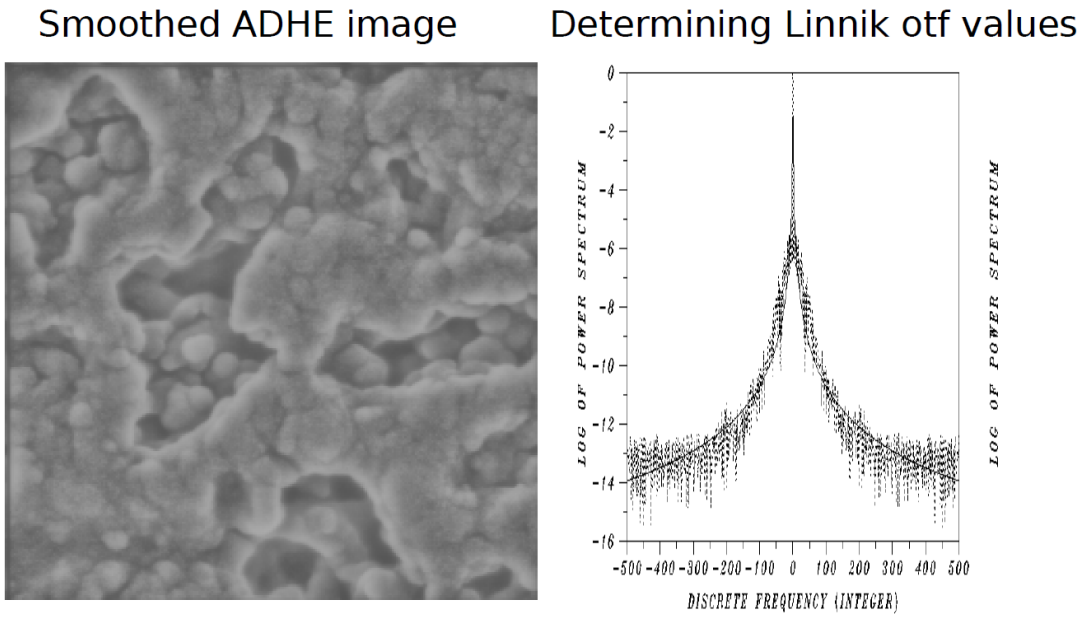

Figure 21. *In the smoothed ADHE image* $\boldsymbol{g(x,y)}$*, least squares fitting* $\boldsymbol{\log|\hat{g}(\xi,0)|}$ *with the expression* $\boldsymbol{-\lambda\log(1+4\pi^2\gamma\xi^2)-1.5}$*, leads to parameter values* $\boldsymbol{\lambda=0.696,\gamma=1.64}$*, for* $\boldsymbol{\hat{h}(\xi,\eta)}$*.*

Elastic Curves in Rⁿ. In *Proceedings of the IEEE Conference on Computer Vision and Pattern Recognition* (CVPR), Minneapolis, MN, June 2007.

[6] S. Kurtek, E. Klassen, Z. Ding, and A. Srivastava. A Novel Riemannian Framework for Shape Analysis of 3D Objects. In *Proceedings of the IEEE Conference on Computer Vision and Pattern Recognition* (CVPR), San Francisco, CA, June 2010.

[7] J. N. Riseth. Gradient Based Algorithms in Shape Analysis for Reparameterization of Parametric Curves and Surfaces. Norwegian University of Science and Technology, Department of Mathematical Sciences, 2021.

[8] A. Srivastava and E. P. Klassen. *Functional and Shape Data Analysis*. Springer, New York, 2016.

[9] A. Srivastava, E. P. Klassen, S. H. Joshi, and I. H. Jermyn. Shape Analysis of Elastic Curves in Euclidean Spaces. *IEEE Transactions on Pattern Analysis and Machine Intelligence* **33**:7 (2011), 1415-1428.

Explicit Computation of Unstable Time-Reversed Dissipative Equations

Alfred Carasso

The work discussed below is covered in greater detail in References [1-3].

Sharpening Electron Microscopy Images. Ill-posed deconvolution problems and related time-reversed dissipative evolution equations, pervade measurement science. In numerous scientific measurements, the instrument point spread function is a bell-shaped distribution that may be well-approximated by a Gaussian, or by a heavy-tailed infinitely divisible probability density, often with parameters that are only tentatively known. This is the case in important NIST work on engineered nanostructures, involving scanning electron microscopes (SEM), and Helium ion microscopes (HIM). Earlier NIST work on blind deconvolution of SEM and HIM images, discussed in [4-5], was based on postulated point spread functions in the form of low exponent Lévy stable densities, and implemented as time-reversed fractional diffusion equations. Most recently, previous blind deconvolution work on Hubble Space Telescope imagery, developed in [6], and based on time-reversed logarithmic diffusion equations, was found to produce superior results on SEM and HIM images, provided these images are suitably *preconditioned*. This preconditioning consists of adaptive histogram equalization (ADHE), followed by low exponent Lévy smoothing to remove the unwanted noise produced by ADHE. As was the case in [4-5], the new method is only applicable to a restricted class of blurred images $g(x,y)$, with Fourier transforms $\hat{g}(\xi,\eta)$ such that $\log \hat{g}(\xi,0)$ is globally monotone decreasing and convex. The method does not apply to defocus and motion blurs. A Linnik optical transfer function $\hat{h}(\xi,\eta)$ is postulated,

$$\hat{h}(\xi,\eta) = \left(1 + 4\pi^2\gamma(\xi^2+\eta^2)\right)^{-\lambda}$$

with the parameters γ, λ obtained by least squares fitting the Fourier transform of the preconditioned image $g(x,y)$. This process is illustrated in Figure 20 and Figure 21. It is useful to define $\hat{h}(\xi,\eta,t)$ for $0 \le t \le 1$ as

$$\hat{h}(\xi,\eta,t) = \left(1 + 4\pi^2\gamma(\xi^2+\eta^2)\right)^{-\lambda t}$$

In the Linnik blind deconvolution procedure discussed in [1], deconvolution unfolds as a backward in time marching procedure, in Fourier space, from $t = 1$ to $t = 0$, in a diffusion equation involving the *logarithm* of the identity plus the negative Laplacian, $w_t = -\lambda w \log\left(I + \gamma(-\Delta)\right)$, using the preconditioned microscopy image $g(x,y)$ as data at $t = 1$.

The *slow evolution* (SECB) constraint, previously developed in [7], is applied to stabilize the ill-posed backward computation. A complete discussion, given in [4], leads to the partially deblurred Linnik SECB Fourier image $\widehat{w}(\xi,\eta,t)$ defined as follows,

$$\widehat{w}(\xi,\eta,t) = \frac{\hat{h}(\xi,\eta,t)\hat{h}(\xi,\eta)\hat{g}(\xi,\eta)}{\hat{h}^2(\xi,\eta) + K^{-2}\left(1 - \hat{h}(\xi,\eta,s)\right)^2}$$

with suitably chosen positive constants s and K. Typical values for these constants might be $s = 0.001$ and $K = 100$. An inverse Fourier transform of the above leads to $w(x,y,t)$, the partial deconvolution at time t. A partial deconvolution at some positive time $\bar{t} < 1$, often provides better results than the total deconvolution at $t = 0$. The above blind deconvolution method requires familiarity with the algorithm, interactive search for optimal parameter values for s, K and $\bar{t}$, and knowledge of the type of microscopy image that needs sharpening. Above all, guidance from an experienced microscopist is vital. In [1], NIST co-author Andras Vladar's long experience in SEM imaging, as indicated in [8], was invaluable in arriving at the unexpected striking results shown in Figure 22, and in the several other images in [1].

Data Assimilation in 2D Incompressible Navier-Stokes Equations. Data assimilation is an important research topic in the geophysical sciences, as may be seen from the bibliographies in [2-3]. In a dissipative evolution system, hypothetical and poorly known non-smooth data are given at some time $T > 0$, and the object is to find initial values at time $t = 0$ that can evolve, through the dissipative system, into useful approximations to the given hypothetical data at time T. These hypothetical data *may not correspond* to an actual solution at time T, and it *may not be possible* to find useful initial values. This inverse problem is fundamentally different from the ill-posed backward recovery problems considered in

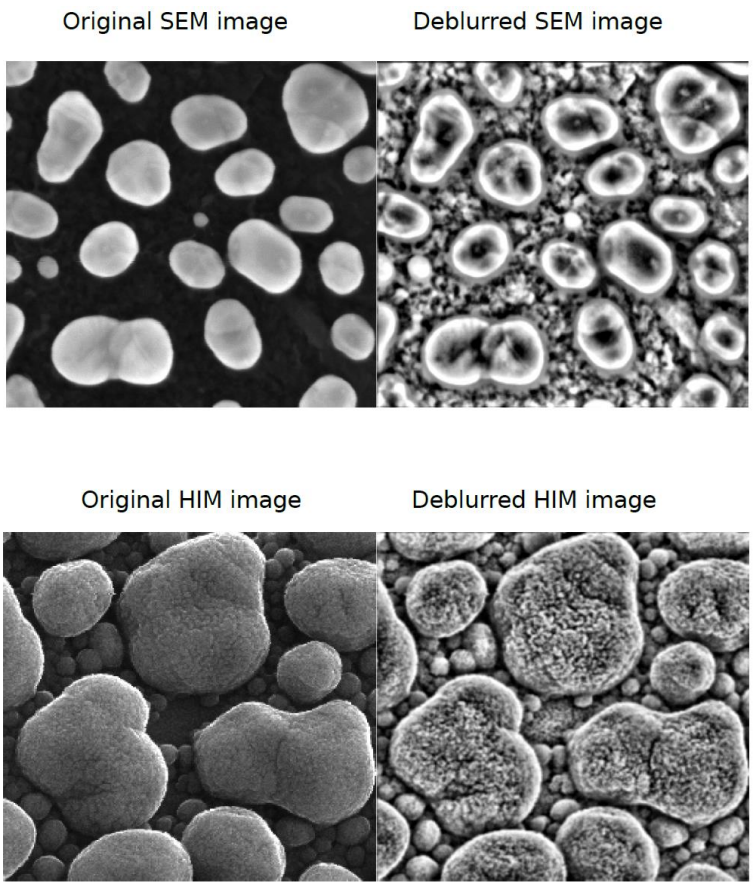

Figure 22. *Linnik blind deconvolution in SEM and HIM images. Original 0.7nm resolution secondary electron images of Au nanoparticles, shown on the left, reveal rich surface details after Linnik processing, shown on the right.*

[9-10], where the given noisy data at time $T > 0$ are relatively smooth and are known to approximate an actual solution at time T to within a *known small* $\delta > 0$ in the L^2 norm. In the present case, the hypothetical data at time T may differ from an actual solution by an *unknown, possibly large* $\delta > 0$ in the L^2 norm.

Nevertheless, as was the case in [9], it is possible to stabilize the backward marching leapfrog scheme by applying a compensating smoothing operator at each time step. This leads to a small error at each step, whose cumulative effects in the data assimilation problem remain negligible, provided T is sufficiently small. In [2], the 2D Navier-Stokes problem is considered in *stream function/vorticity* formulation on the unit square Ω, with stream functions that vanish, together with all their derivatives, on and near boundary of Ω. Computational data assimilation experiments are performed using 256×256 pixels gray-scale images of hurricanes. In the leftmost column of Figure 23, the same highly non-smooth image is postulated as hypothetical data at three distinct values of $T > 0$. Such non-smooth data cannot correspond to actual solutions of the Navier-Stokes system considered in [2]. The stabilized computations of the associated initial values are presented in the middle column in Figure 23, and the Navier-Stokes evolutions of these initial values form the rightmost column in Figure 23. Assimilation is successful if the rightmost image is a useful approximation to the leftmost image. This is the case if $T \leq 7.5 \times 10^{-4}$. It is noteworthy that such a value for T is significantly larger than would be expected at the present Reynolds number of 8500, based on the best-known uncertainty estimates given in [11].

Data Assimilation in 2D Coupled Sound and Heat Flow. In [3], a coupled nonlinear dissipative system is considered, involving a 2D wave equation and a 2D diffusion equation. With $u(x, y, t)$ denoting temperature, $v(x, y, t)$ denoting wave velocity, and $w(x, y, t)$ denoting wave displacement, this coupled system is posed in a quarter circle region in the unit square Ω in R^2, with vanishing u, v, w on and outside the boundary of the quarter circle region. As was the case in [10] backward marching explicit schemes can be stabilized by applying a compensating smoothing operator at every time step. In Figure 24, with $T = 1.6 \times 10^{-4}$, and with the hypothetical non-smooth data shown in the leftmost column, the stabilized explicit computation of the corresponding initial values is shown in the middle column. Evidently, the three images interact with each other as the evolution progresses. The evolution of the middle column initial data to time T, shown in the rightmost column, is a good approximation to the desired data. Clearly, data assimilation was successful in that example. However, in Figure 25, the value of T was chosen five times larger, and the Liz Taylor image was replaced with the USAF Resolution Chart image, in the hypothetical data at time T shown in the leftmost column. Now, as shown in the rightmost column, the computed initial values in the middle column did not evolve into a useful approximation to the leftmost column, and data assimilation was unsuccessful.

Concluding Remarks. Artificial intelligence methods, coupled with machine learning (AI/ML), are increasingly being used in image enhancement work in microscopy, as well as in data assimilation problems in the geophysical sciences. Direct methods such as are discussed in [1-3], may provide useful initial solutions that can be refined by such AI/ML methods. Additionally, such direct methods may be developed as stand-alone alternative procedures, ready to be used as needed, to validate unexpected results produced by AI/ML methods.

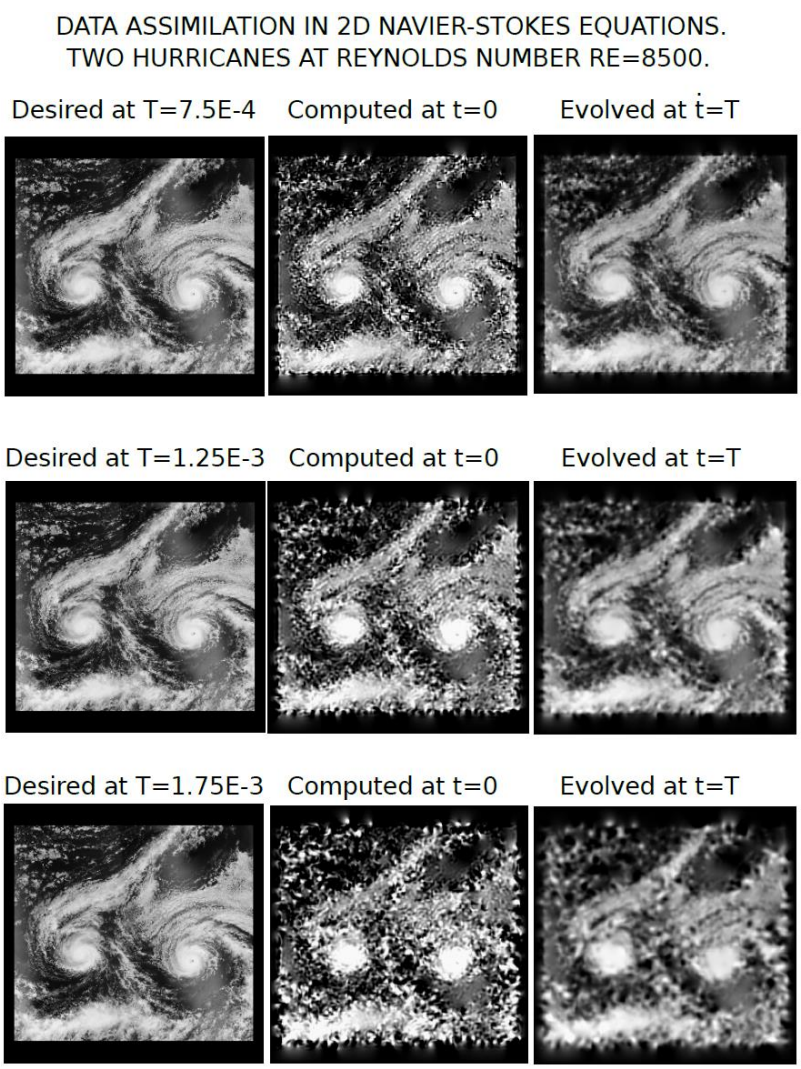

Figure 23. *Using the same hypothetical data at various times T > 0, the leftmost column features a NASA satellite image of two hurricanes approaching Hawaii. The middle column presents the corresponding initial values, obtained by solving the 2D Navier-Stokes equations backward in time. The rightmost column presents the forward evolution to time T of these initial values, obtained by solving the same equations forward in time. In each row, data assimilation is successful if the rightmost image is a useful approximation to the leftmost image. Here, this requires* $T \leq 7.5 \times 10^{-4}$. *At the present Reynolds number, that T value is significantly larger than expected, based on the best-known Navier-Stokes uncertainty estimates given in [11].*

[1] A. S. Carasso and A. E. Vladar. Linnik Point Spread Functions, Time-Reversed Logarithmic Diffusion Equations, and Blind Deconvolution of Electron Microscope Imagery. NIST TN 2324. DOI: 10.6028/NIST.TN.2324

[2] A. S. Carasso. Data Assimilation in 2D Incompressible Navier-Stokes Equations, using a Stabilized Explicit $O(\Delta t)^2$ Leapfrog Finite Difference Scheme Run Backward in Time. NIST TN 2299. DOI: 10.6028/NIST.TN.2299

[3] A. S. Carasso. Data Assimilation in 2D Nonlinear Coupled Sound and Heat Flow, using a Stabilized Explicit Finite Difference Scheme Run Backward in Time. NIST TN 2322. DOI: 10.6028/NIST.TN.2322

[4] A. S. Carasso. The APEX Method in Image Sharpening and the Use of Low Exponent Lévy Stable Laws. *SIAM Journal on Applied Mathematics* **63** (2002), 593-618.

[5] A. S. Carasso, D. S. Bright, and A. E. Vladar. APEX Method and Real-Time Blind Deconvolution of Scanning Electron Microscope Imagery. *Optical Engineering* **41** (2002), 2499-2514.

[6] A. S. Carasso. Bochner Subordination, Logarithmic Diffusion Equations, and Blind Deconvolution of Hubble Space Telescope Imagery and Other Scientific Data. *SIAM Journal on Imaging Sciences* **3** (2010), 954-980.

[7] A. S. Carasso. Overcoming Hölder Continuity in Ill-Posed Continuation Problems. *SIAM J. Numerical Analysis* **31** (1994), 1535-1557.

[8] E. Vladar and V. D. Hodoroaba. Characterization of Nanoparticles by Scanning Electron Microscopy. In *Characterization of Nanoparticles*, Elsevier, (2020), 7-27. DOI: 10.1016/B978-0-12-814182-3.00002-X

[9] A. S. Carasso. Stabilized Leapfrog Scheme Run Backward in Time, and the Explicit $O(\Delta t)^2$ Stepwise Computation of Ill-Posed Time-Reversed 2D Navier-Stokes Equations. *Inverse Problems in Science and Engineering* (2021). DOI: 10.1080/17415977.2021.1972997

[10] A. S. Carasso. Stabilized Backward in Time Explicit Marching Schemes in the Numerical Computation of Ill-Posed Time-Reversed Hyperbolic/Parabolic Systems. *Inverse Problems in Science and Engineering* **1** (2018), 1–32. DOI: 10.1080/17415977.2018.1446952

[11] R. J. Knops and L. E. Payne. On the Stability of Solutions of the Navier-Stokes Equations Backward in Time. *Archives Rational Mechanics Analysis* **29** (1968), 331–335.

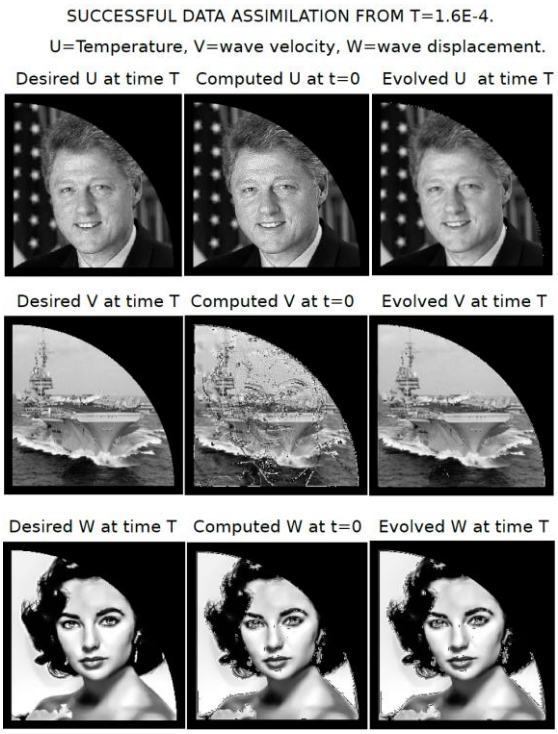

Figure 24. *Data assimilation is successful if the rightmost column is a useful approximation to the desired leftmost column. This is the case here, with $T = 1.6 \times 10^{-4}$. Interesting interactions among the three images are noticeable as the evolution progresses.*

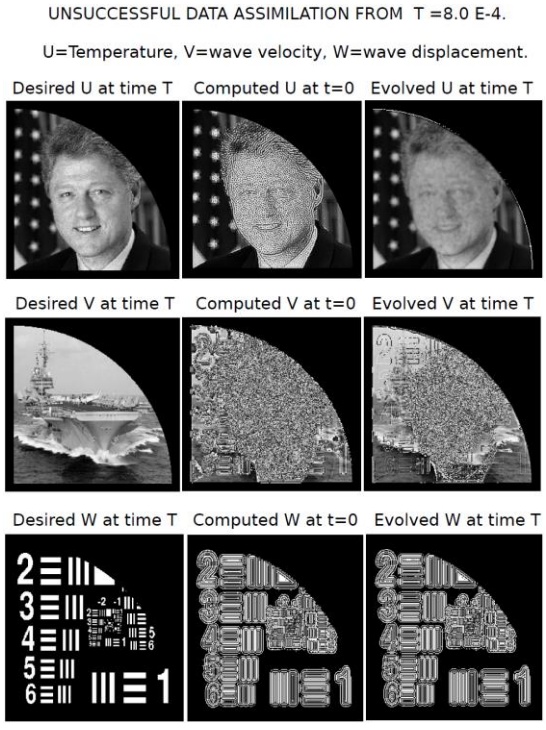

Figure 25. *Data assimilation is unsuccessful with $T = 8.0 \times 10^{-4}$, and a different hypothetical data set in the leftmost column.*

[5] https://github.com/fangohr/oommf

Micromagnetic Modeling

Michael Donahue
Donald Porter
Aman Rani
Mark-Alexander Henn
Cindi Dennis (NIST MML)
Jim Booth (NIST CTL)
Ron Goldfarb (NIST PML)
Pavel Kabos (NIST PML)

https://math.nist.gov/oommf/

Advances in magnetic devices such as field sensors, spin torque oscillators, magnetic nonvolatile memory (MRAM), and thermal sensors are dependent on an understanding of magnetization processes in magnetic materials at the nanometer level. Micromagnetics, a mathematical model used to simulate magnetic behavior, is needed to interpret measurements at this scale. ACMD is working with industrial and academic partners, as well as with colleagues in the NIST MML, CTL, and PML, to improve the state-of-the-art in micromagnetic modeling.

We have developed a public domain computer code for performing computational micromagnetics, the Object-Oriented Micromagnetic Modeling Framework (OOMMF). OOMMF serves as an open, well-documented environment in which algorithms can be evaluated on benchmark problems. OOMMF has a modular structure that allows independent developers to contribute extensions that add to its basic functionality. OOMMF also provides a fully functional micromagnetic modeling system, handling three-dimensional problems, with extensible input and output mechanisms. From October 2023 through December 2024, the software was downloaded 12500 times by more than 4300 distinct client machines. The software is also available to the public via GitHub[5] and nanoHUB[6]. There are 157 known peer-reviewed journal articles published from October 2023 to December 2024 that acknowledge the use of OOMMF. Total OOMMF citations now number more than 3 800. OOMMF has become an invaluable tool in the magnetics research community. Developments in the last year include:

- Released version 2.1a1 of OOMMF[7]:
  - Introduces an integer field file format and associated utilities.
  - Supports conversions to the SVG format for vector images.
  - Parallel execution of build scripts.
  - More expressive color maps in vector field display.

[6] https://nanohub.org/resources/oommf
[7] https://math.nist.gov/oommf/software-21.html

  - Support for Tcl/Tk versions 8.6 and 9.0, bridging the transition.
- Released updates to contributed OOMMF extension tuw_cvodeevolve, linking OOMMF to the well-known ODE solver.

In addition to the continuing development of OOMMF, the project also does collaborative research using OOMMF. M. Donahue and M.-A. Henn were team members on the nanothermometry project Thermal MagIC[8]. Addressing Thermal MagIC questions prompted the development of a "string method" thermal barrier calculation coupled with OOMMF simulations, and enhanced color maps for better visualization of reversal dynamics in magnetic nanoparticle chains. The tools developed for Thermal MagIC show promise to address fundamental questions in magnetic particle imaging, which has applications in biomedical diagnostic imaging. The Thermal MagIC team is to be recognized with a Department of Commerce Bronze Medal in January 2025[9]. Publications of Thermal MagIC continued to appear in 2024 and beyond [1-3].

The ACMD micromagnetic project also contributes to CHIPS-funded work. A multi-laboratory effort named "Metrology for Integration of New Magnetic Materials" is a partnership of J. Booth, P. Kabos, M. Donahue, and R. Goldfarb. Post-doc A. Rani (Ph.D. Mathematics, Texas Tech University, August 2024) has been hired on to the team, and consultations with Intel Corporation are in progress.

D. Porter serves on the Tcl Core Team, the managers of development on the open source Tcl and Tk libraries which are a foundation for OOMMF. Tcl/Tk 9.0.0 was released in September 2024[10], concluding a lengthy major release cycle, during which compatibility with OOMMF was successfully sustained.

M. Donahue served as a session chair at the 68th Annual Conference on Magnetism and Magnetic Materials (MMM2023)[11], and as the External Examiner on the Ph.D. Thesis Committee for Martin Lang at the University of Southampton (UK).

[1] J. Borchers, K. Krycka, B. Bosch-Santos, E. de Lima Correa, A. Sharma, H. Carlton, Y. Dang, M. Donahue, C. Grüttner, R. Ivkov and C. L. Dennis. Magnetic Anisotropy Dominates Over Physical and Magnetic Structure in Performance of Magnetic Nanoflowers. *Small Structures* **6**:2 (2025), 2400410. DOI: 10.1002/sstr.202400410

[2] F. M. Abel, E. L. Correa, T. Q. Bui, A. J. Biacchi, M. J. Donahue, M. T. Merritt, J. E. Seppala, S. I. Woods, A. R. Hight Walker, and C. L. Dennis. Strongly Interacting Nanoferrites for Magnetic Particle Imaging and Spatially Resolved Thermometry. *ACS Applied Materials & Interfaces* **16**:40 (2024), 54328. DOI: 10.1021/acsami.4c03076

[3] T. Q. Bui, S. D. Oberdick, F. M. Abel, M. J. Donahue, K. N. Quelhas, C. L. Dennis, T. Cleveland, Y. Liu, and S. I. Woods. Magnetodynamics of Few-nanoparticle Chains. In review.

OOF: Finite Element Analysis of Material Microstructures

Stephen A. Langer
Günay Doğan
Andrew C.E. Reid (NIST MML)
Shahriyar Keshavarz (NIST MML)

http://www.ctcms.nist.gov/oof/

The OOF Project, a collaboration between ACMD and MML, is developing software tools for analyzing real material microstructure. The microstructure of a material is the (usually) complex ensemble of polycrystalline grains, second phases, cracks, pores, and other features occurring on length scales large compared to atomic sizes. The goal of OOF is to use data from a micrograph of a real or simulated material to compute its macroscopic behavior via finite element analysis.

The OOF user loads images into the program, assigns material properties to the features of the image, generates a finite element mesh that matches the geometry of the features, chooses which physical properties to solve for, and performs virtual experiments to determine the effect of the microstructural geometry on the material. OOF is intended to be a general tool, applicable to a wide variety of microstructures in a wide variety of physical situations. OOF2 and OOF3D are used by educators and researchers in industry, academia, and government labs worldwide.

There are two versions of OOF, OOF2 and OOF3D, each freely available on the OOF website. OOF2 starts with two dimensional images of microstructures and solves associated two-dimensional differential equations, assuming that the material being simulated is either a thin freely suspended film or a slice from a larger volume that is unvarying in the third dimension (generalizations of plane stress and plane strain, respectively). OOF3D starts with three dimensional images and solves equations in three dimensions.

The OOF developers made progress on multiple fronts this year: adding image processing tools to OOF2, computing plastic deformation in OOF3D, and documenting and updating OOF2.

[8] https://www.nist.gov/programs-projects/thermal-magic-si-traceable-method-3d-thermal-magnetic-imaging-and-control

[9] https://www.nist.gov/nist-awards/2024-bronze-medal-award-adam-biacchi-thinh-bui-cindi-dennis-michael-donahue-angela-hight

[10] https://www.tcl-lang.org/software/tcltk/9.0.html

[11] https://2023.magnetism.org/

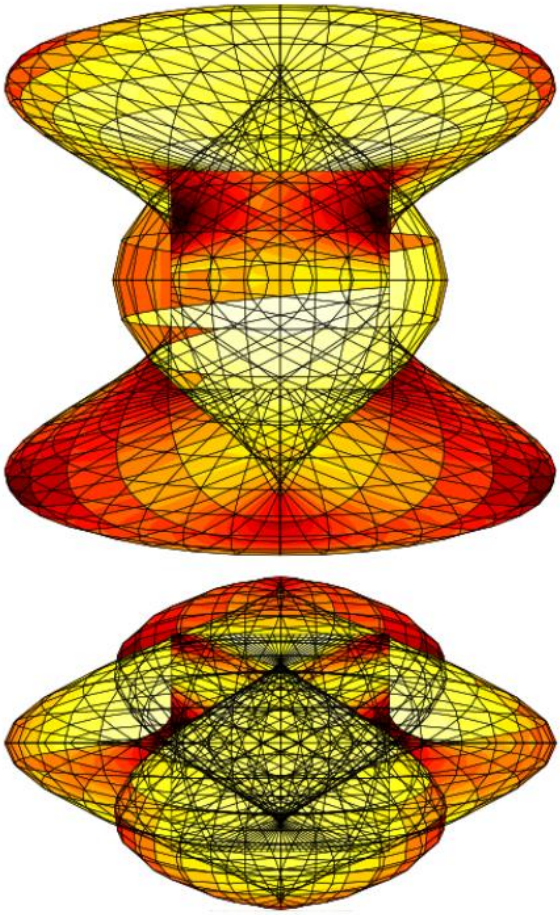

Figure 26. *Output from OOF2 obtained while updating the manual. In the old version, if a user were writing an extension that defined certain terms in a constitutive equation, it would be necessary to include a non-intuitive minus sign in some circumstances. To avoid having to explain the circumstances in the manual, the code was changed so that the minus sign was never required. These two plots are the result of solving an OOF2 test case with and without the minus sign. Neither is correct. The images ought to show a deformed square elastic material subject to a sinusoidal external force. The color corresponds to the magnitude of the geometric strain, which goes from black (zero) to yellow (unphysical)*

Two crucial steps of an OOF analysis are the preprocessing and segmentation of the input microstructure image. The preprocessing improves the quality of the input image using functions, such as median filtering or gaussian blurring for denoising, contrast enhancement, histogram equalization, etc. This makes it easier to subsequently segment the image, and to identify and label pixels belonging to different regions/phases/materials successfully. The segmentation, i.e. the labeled regions, then inform the mesh that will be created and used to compute the finite element solutions of the selected physics models. The correctness and accuracy of the segmentation (and the preprocessing that enables it) are critical to the correctness and accuracy to the OOF solution and analysis of the physics model.

Current and past versions of OOF have depended on the widely available ImageMagick package to provide image preprocessing functionality. ImageMagick is a C++ package that includes a wide variety of useful image processing functions and is thus a good match for much of an OOF user's needs. It is a large package, and for some users, it can be difficult to install and interface with OOF, which is mainly a Python tool. For this reason, we pursued mature Python-based alternatives in FY 2024 and found that Scikit-Image met and exceeded our needs. Scikit-Image is a highly developed open-source Python package with a wide variety of functions for preprocessing and segmenting images, supported by an active community of developers. In FY 2024, we were able to replace the ImageMagick preprocessing functions in OOF2 with matching and, in some cases, improved functions from Scikit-Image. We found that Scikit-Image functions often seemed to have more options and better performance as they were implementations of more recent algorithms. In FY 2025, we will continue to incorporate functionality from Scikit-Image, focusing on image segmentation functions, making it easier for users to segment images in an unsupervised and semi-supervised manner.

The plasticity project reached a milestone in proving the architecture of a software solution, including the required modularity and generalizability, in a test code with greater sophistication than the previous prototype code. This code was able to remain numerically stable for strains of up to 12 %, while retaining the object structure that makes new plastic constitutive models "pluggable." The principal breakthrough involved a change in strategy for how time-stepping is handled in this code.

The next step is integration into the OOF3D code, with the corresponding changes to the time-stepping scheme. A challenge for this effort is the departure from NIST of Shahriyar Keshavarz, who was the resident expert on solid mechanics. Finding sufficient time among the remaining personnel to move this forward will be difficult, but not impossible.

In the process of updating and improving the OOF2 manual[12], many problems were detected and repaired in the code. In particular, documenting the steps necessary to add extensions to OOF2 (such as new equations or physical properties) revealed that rewriting certain parts of the program would make it much easier for users to add extensions. This has delayed the completion of the manual but resulted in a more polished and easier to use

[12] The old manual can be found at https://www.ctcms.nist.gov/~langer/oof2man/. A draft of the new manual can be found at https://www.ctcms.nist.gov/~langer/oof2man-draft/ until it replaces the old version.

code base. After the manual is complete, the next step in the OOF maintenance project will be to update OOF3D similarly to the way OOF2 has been updated during the past few years.

The latest versions of OOF2, OOF3D, and OOFCanvas, the library OOF2 uses for graphical displays, are available as source code from the OOF2 website. OOF2 can also be used downloaded and installed on Macintosh computers via MacPorts[13]. Both OOF2 and OOF3D can run directly on the NSF nanoHUB facility[14]. At nanoHUB, OOF2 was used 3 600 times in FY23, and has been run 72 000 times since the first version was installed there in December 2007. OOF3D was run less often on nanoHUB, 170 times, which is not surprising, due to the relative scarcity of 3D images and the less developed state of the 3D code.

AI for Deep Ocean Energy

Zachary J. Grey
Ryan King (NREL)
Alireza Doostan (University of Colorado Boulder)
Gianluca Geraci (Sandia National Laboratory)
Andrew Glaws (NREL)

AI has recently (re)-emerged as a compelling universal computational framework for addressing several scientific, commercial, and economic challenges. Our basic thesis is to explore the use of AI for creating a cleaner and more secure energy future for the nation by utilizing novel physical infrastructure. This initiative, funded by the Department of Energy Wind Energy Technology Office, seeks to: (i) rigorously evaluate a use-case for trustworthy AI implementations to deliver on energy solutions, (ii) promote the application of AI to deliver on U.S. energy economy security, and (iii) an opportunity to demonstrate the efficacy of inter-agency and academic collaborations to these ends.

Our challenge is to supplement and facilitate tools for resilient commercial deployments considering interactions of (i) a complex ocean system ecology, (ii) local economies, and (iii) an incredibly volatile ocean environment fraught with uncertainty and extreme events. An extensive modeling, analysis, and measurement of these interactions must be trustworthy given inherent difficulties and expenses of accessing deep ocean sites. Overcoming these high-risk challenges will require technical innovations in design and measurement from modeling to manufacturing to monitoring.

In contrast to conventional AI/ML applications, which have enormous training data sets, deep ocean observational data are characteristically sparse, noisy, and multimodal. Further, they are often non-Euclidean (e.g., conical lidar slices of randomly evolving wave-shape surface conditions), which prohibits the straightforward application of existing AI/ML techniques developed for image processing. Domain-specific data representations, such as knowledge graph structures and improved shape representations, can reduce problem complexity and improve AI/ML predictive performance and interpretability. Finally, a rich modeling hierarchy exists for many ocean-based energy applications, but new multifidelity approaches to AI/ML model training and evaluation are necessary to make the best use of these model hierarchies to reduce computational burdens, address data limitations, and characterize AI/ML uncertainty.

The first year of the project has successfully delivered generative models capable of emulating wind-wave inflow conditions from sparse high-fidelity simulations. Results were presented in January 2025 AIAA SciTech conference proceedings. Additionally, a graph-based surrogate studying the forces imposed on floating offshore platforms was developed to explore the sensitivity of physical forcing on deep ocean structures. These results were also presented during AIAA SciTech.

Looking forward into 2025 promises to deliver new insights about the trustworthiness of generated in-flow conditions by investigating the intrinsic coherent structures and physical properties of generated flow fields. Moreover, surrogate models for the platform design will be evolved to incorporate dimension reduction and more sophisticated shape and truss-structure representations.

Computational Tools for Image Analysis

Günay Doğan
Stephen Lund (NIST ITL)
Prashant Athavale (Clarkson University)
Emmanuel Atindama (Clarkson University)
Connor Miller-Lynch (Clarkson University)
Selin Aslan (Koç University)
Doğa Gürsoy (Argonne National Laboratory)
Jiyoung Park (Texas A&M University)

The main goal of this project is to develop efficient and reliable computational tools to detect geometric structures, such as curves, regions and boundaries, from given direct and indirect measurements, e.g., microscope images or tomographic measurements, as well as to evaluate and compare these geometric structures or shapes in a quantitative manner. This is important in

[13] https://ports.macports.org/port/oof2/

[14] https://nanohub.org/resources/oof2 and https://nanohub.org/resources/oof3d

many areas of science and engineering, where practitioners obtain their data as images, and would like to detect and analyze objects in the data. Examples include microscopy images for cell biology or micro-CT (computed tomography) images of microstructures in material science, and shoeprint images in crime scenes for footwear forensics. In FY 2024, advances were made in various fronts on this project. Python implementations of solutions for problems in these areas were implemented, and documentation and examples were provided. In the following, we provide more details on the specific work carried out.

Image segmentation is the problem of finding distinct regions and their boundaries in given images. It is a necessary data analysis step for many problems in cell biology, forensics, and material science, as well as other fields in science and engineering. In FY 2024, G. Doğan and his collaborators continued to work on multiple strategies for image segmentation. This included preprocessing algorithms to improve segmentation and image analysis performance. Updates to segmentation algorithms were implemented and released as part of the scikit-shape Python package.[15]

Images obtained in different domains can have very different characteristics and can vary substantially in quality. Thus, domain-specific solutions are often required. An application domain of interest is material microstructures. Various imaging modalities provide imaging of material microstructures with the goal of quantitatively characterizing them and relating the microstructure geometry to the material's macroscopic behavior. Electron backscatter diffraction imaging (EBSD) is one such modality used to obtain orientation images of a material's crystal structure. EBSD images can sometimes be noisy and can have missing values or regions, which makes it hard to segment and analyze them. Doğan, Athavale, Atindama and Lef developed an EBSD denoising algorithm in FY 2023 [1], and Doğan and collaborators developed an additional EBSD inpainting algorithm to estimate and fill in missing values in EBSD images in FY 2024 [2]. This inpainting algorithm was a hybrid algorithm combining an exemplar-based approach with partial convolutional neural networks and showed remarkable performance on synthetic and real benchmark examples. More details on this work given in the entry entitled "Algorithms to Enable Materials Research with Imaging*"* on page 15 of this document.

A common task in image analysis is image alignment, the task of overlaying an object or region from one image to another in a different image. This is a crucial task for quantitative comparison of objects or features in images. In FY 2024, Doğan and Lund worked on a custom image alignment algorithm, applied to image features found in shoeprints, to enable trustworthy and quantitative comparisons for shoeprint forensics. They developed a versatile matching metric that performed well on pairs of images with very different characteristics and distributions of pixel values. They also implemented fast numerical methods for efficient computation of various components of the alignment algorithm. In FY 2025, they will finalize the implementation of the image alignment algorithm and release it for the forensics community.

In the image segmentation literature, many algorithms have been developed using a model-based approach, and more recently a learning-based approach. The advantages of the model-based approaches are their efficiency, interpretability and that they require no training data, whereas the advantages of learning-based approaches are their flexibility and superior performance if sufficiently large training datasets are available. In FY 2024, Doğan continued his work on model-based segmentation algorithms from the previous years but also explored learning-based segmentation solutions. One model-based algorithm that Abawonse and Doğan had previously implemented was the split-Bregman algorithm for two-phase image segmentation, which computes foreground-background segmentations for given approximately piecewise-constant images. They further improved the optimization procedure required by this algorithm in FY 2024 and submitted the paper describing this algorithm for review [3].

Meanwhile, Doğan, Aslan and Gürsoy investigated segmentation problems related to computed tomography. Computed tomography is a versatile technology used in medical imaging, material science and non-destructive testing for engineering. Typically, an image of a medium or component is reconstructed using computed tomography. Then regions or objects of interest are segmented out for further analysis. Doğan et al. formulated a new model to compute the segmentation directly from tomographic measurements bypassing the need for image reconstruction in FY 2023. They advanced the implementation of this model in FY 2024. Upon analysis of various components of this joint reconstruction-segmentation model, they were able to devise better algorithms for the subproblems that they needed to solve. In FY 2025, they plan to integrate the solutions of the subproblems into an effective solution for the full model.

Doğan worked on learning-based algorithms as well in FY 2024. A particular class of interest is deep learning algorithms, which learn both the right informative image features and an effective classifier and can produce impressive segmentation results. However, this performance is contingent on the availability of large representative training data sets. Unlike typical computer vision applications, creating large, annotated data

[15] http://scikit-shape.org

sets for scientific applications can be difficult, sometimes impractical. This can be a barrier to using deep learning algorithms. Doğan has been investigating hybrid approaches that can incorporate partial model information, such as regularity and invariances, to obtain more economical deep learning models. Doğan and J. Park, a Ph.D. student from Texas A&M University, have been researching and testing possible hybrid algorithms. One such algorithm was a modified version of the probabilistic U-Net algorithm [4, 5], in which they incorporated modules that induced spatial coherence of segmented objects. Doğan and Park showed that the modified algorithm outperformed the probabilistic U-Net algorithm. They described this new algorithm and their results in [6].

Most data analysis and machine learning algorithms rely on dissimilarity metrics or distances that quantify how dissimilar or far the data records (e.g. image, shape, text) in the analyzed data set are. The choice of the dissimilarity metric is central to achieving the data analysis and machine learning goals. On the other hand, using different data representations or different versions of the algorithms lead to different dissimilarity metrics, and this brings the question of which metric would perform best. In the previous years, Doğan and Fleisig (UC Berkeley) developed a Python program, VEMOS (Visual Explorer for Metrics of Similarity) that can be used to evaluate and compare multiple competing similarity/dissimilarity metrics. VEMOS can be used in a versatile manner to evaluate multiple alternative dissimilarity metrics for heterogeneous data sets, including images, shapes, point clouds and other data types. In FY 2024, Doğan continued to develop VEMOS, made bug fixes, and added new features. A report describing the capabilities of VEMOS is available in the NIST technical note [7], and the software is available for download.[16]

[1] E. Atindama, P. Lef, G. Doğan, and P. Athavale. Restoration of Noisy Orientation Maps from Electron Backscatter Diffraction Imaging. *Integrating Materials and Manufacturing Innovation* **12** (2023), 251–266. DOI: 10.1007/s40192-023-00304-8

[2] E. Atindama, C. Miller-Lynch, H. Wilhite, C. Mattice, G. Doğan, and P. Athavale. Hybrid Algorithm for Filling in Missing Data in Electron Backscatter Diffraction Maps. In process.

[3] O. Abawonse and G. Doğan. Image Segmentation using the Split Bregman Method. In review.

[4] O. Ronneberger, P. Fischer, and T. Brox. U-net: Convolutional Networks for Biomedical Image Segmentation. In *Proceedings of Medical Image Computing and Computer-Assisted Intervention–MICCAI*, Munich, Germany, October 5-9, 2015. Springer, 2015.

[5] S. Kohl, B. Romera-Paredes, C. Meyer, J. De Fauw, J. R. Ledsam, K. Maier-Hein, S. M. Eslami, D. Jimenez Rezende, and O. Ronneberger. A Probabilistic U-net for Segmentation of Ambiguous Images. *Advances in Neural Information Processing Systems* **31** (2018).

[6] J. Park and G. Doğan. Probabilistic U-net with Kendall Shape Spaces for Geometry-Aware Segmentations of Images. Preprint arXiv:2410.14017, 2024.

[7] E. Fleisig and G. Doğan. VEMOS: GUI for Evaluation of Similarity Metrics of Complex Data Sets. NIST Technical Note 2160, June 2021, 34 pages. DOI: 10.6028/NIST.TN.2160

[16] https://github.com/usnistgov/VEMOS

Provably "Overwhelming" Transformer Models with Tailored Input

Matthew Coudron
Lev Stambler (University of Maryland)
Seyed Sajjad Nezhadi (University of Maryland)

Our research program focuses on establishing the first algorithmically generated mathematical proofs of operationally relevant statements about trained AI models. We are now preparing the manuscript on the following result for submission in FY 2025.

In this work we exhibit an algorithm which, given a trained transformer model M as input, finds strings of tokens that, when included in the input, provably "overwhelm" the model M, making it insensitive to all other parts of the input. More precisely, given a trained transformer model, M, and an integer k, our algorithm can find a string of input tokens, OVERWHELM, with the property that the output of the model evaluated on this string plus additional content, M(OVERWHELM + CONTENT), is independent of the string of tokens CONTENT whenever length(CONTENT) < k.

When our algorithm outputs the string OVERWHELM, it also outputs a mathematical proof that that string has the desired property with respect to model M and integer k. An exhaustive proof of this statement would require time exponential in k, but our approach uses a carefully designed analysis of Lipschitz continuity, combined with convex relaxations to produce much smaller mathematical proofs in time and space $O(k^2)$. We have used our algorithm to successfully produce provably overwhelming inputs for several single layer transformer language models complete with Attention Head, LayerNorm, and MLP/ReLU layers as well as positional encoding.

Since the inception of practically useful neural network architectures, it has remained a widespread and elusive goal of many in the scientific community to develop a predictive theoretical understanding of these objects, especially at the level of proof-based mathematics. In this work we exhibit initial positive results from

a new approach to proving guarantees about AI models. Our approach is a trade-off, focusing on guarantees that are smaller in scope, applying only to limited behaviors of specific models, but, in exchange, offers an algorithm to check when our proof applies to any given model, as well as completely rigorous, operationally relevant guarantees for any model on which our algorithm succeeds.

The majority of theoretical attempts to understand neural network architectures thus far have focused either on results about training, or on expressability results. Theoretical attempts to analyze model training face the notorious difficulty of proving any meaningful statement about heuristic descent algorithms on high dimensional, non-convex optimization spaces. On the other hand, while theoretical results about expressability can establish rigorous limits on the capabilities of a given architecture, they must account for highly contrived and unnatural parameter settings, and thus often fail to capture model performance in practice. Therefore, we take a different approach to proving results about neural networks, focusing on the enormously popular transformer architecture, specifically the decoder-only GPT style architecture [1]. Rather than attempting mathematical proofs capturing all possible parameter settings of a model, we design an algorithm which produces provable guarantees about a specific trained transformer model, reminiscent of [2]. While our algorithm's guarantees are valid only for the transformer model on which it is run, the fact that the guarantees can be produced and checked in an automated manner means that they can potentially be re-established on new AI models just as fast as those models are produced.

As a concrete example, in this work we use our framework to generate proofs specifically about text inputs that "overwhelm" several different trained single-layer transformer models. We selected this application initially because it is the most concrete and has the simplest proofs, but we believe that the same framework will be useful in the future for establishing more sophisticated provable results, automatically tailored to specific, fixed, AI models. We also provide a roadmap for extending our results to multi-layer transformer models, which we expect to accomplish in follow-up work.

[1] S. Black, S. Biderman, E. Hallahan, Q. Anthony, L. Gao, L. Golding, H. He, C. Leahy, K. McDonell, J. Phang, M. Pieler, USVSN Sai Prashanth, S. Purohit, L. Reynolds, J. Tow, B. Wang, and S. Weinbach. Gpt-neox-20b: An Open-source Autoregressive Language Model. Preprint arXiv:2204.06745, 2022. DOI: 10.48550/arXiv.2204.06745

[2] J. Gross, R. Agrawal, T. Kwa, E. Ong, C. Hei Yip, A. Gibson, S. Noubir, and L. Chan. Compact Proofs of Model Performance Via Mechanistic Interpretability. In *ICML 2024 Workshop on Mechanistic Interpretability*, 38th Conference on Neural Information Processing Systems (NeurIPS 2024).

Mathematics of Biotechnology

As proof-of-concept academic work in engineering biology meets the market realities of bringing lab science to product initiation, there are questions in how to compare biological products, measure whether desired outcomes are realized, and optimize biological systems for desired behaviors. NIST is working to deliver tools and standards to measure such biological technologies, outputs, and processes from healthcare to manufacturing and beyond. We support this effort with the development and deployment of innovative mathematical modeling and data analysis techniques and tools.

Metrology for Cytometry and Microfluidics

Paul Patrone
Anthony Kearsley
Prajakta Bedekar
Amudhan Krishnaswamy-Usha
Matthew DiSalvo (NIST PML)
Megan Catterton (NIST PML)
Gregory Cooksey (NIST PML)
Nicholas Drachman (Brown University)
Graylen Chickering (Brown University)

For more than 30 years, flow cytometry, a technique used to measure characteristics of cells, has been a mainstay for cancer detection, drug development, and biomedical research. It has remained a primarily qualitative platform, however, because measurement uncertainties associated with this technique are so large. While exact economic figures are difficult to estimate, this has clearly had a significant impact on the roughly $200 billion of waste in the healthcare industry and contributed to the broader reproducibility crisis in biomedical research [1]. The challenge of making cytometry an accurate and precise metrological tool arises from the competing requirement that it have high throughput. Typical biological samples can have up to hundreds of millions of cells, which must be analyzed over a few hours.

To achieve the required throughput, cytometers direct cells through a microfluidic channel at high-speed, past an optical interrogation region that collects fluorescence light from antibodies attached to surface proteins. The total fluorescence collected from each cell should then, in principle, be proportional to the total number of markers on its surface. But in practice, this idealized picture is complicated by the cumulative effects of the physical phenomena involved: fluid-dynamic forces cause cells to move across streamlines and/or have unpredictable trajectories; optical geometric collection efficiencies depend on position in the interrogation region; and signal acquisition and processing tools introduce non-linear effects and measurement uncertainties through discrete sampling. These challenges, in addition to the complexity of exactly replicating the necessary measurement infrastructure at the micron scale, have made it virtually impossible to reproduce measurements on a single cell, a necessary first step in fully assessing and controlling uncertainties in cytometry.

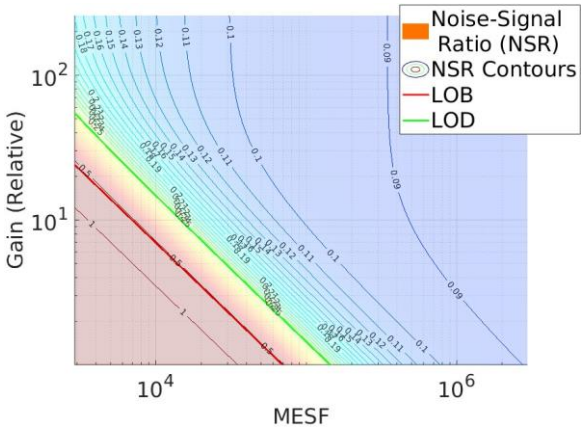

Figure 27. *Example of noise modeling for a cytometer. The contours and color scale illustrates the noise-to-signal ratio of a cytometer as a function of MESF (a dimensionless measure of brightness) and instrument gain. The limit of background (LOB) and limit of detection (LOD) are the solid red and green lines. For a sample with a characteristic MESF value, this figure indicates the set of gain values at which measurements can be run with low noise. Such plots also allow for direct comparison of instruments.*

In FY 2020, ACMD, PML, and MML staff were awarded a NIST Innovations in Measurement Science (IMS) award to develop a microfluidic-based cytometer, whose design explicitly allows control and study of repeated measurements of cells. Following on work in FY 2020 and FY 2021, in FY 2022 we derived a key result indicating that all cytometry events (e.g., for a fixed cell marker type) are identical up to a set of straightforward linear transformations that depend on physical parameters such as the cell size, speed, and number of biomarkers. Using optimization, we can determine these unknown parameters by mapping different signals onto one another. Critically, this also yields multiple, model based but distinct realizations of what a measurement would look like if it could be reproduced on the same measurand. When applied to large collections of signals, residuals not accounted for by the data collapse quantify

uncertainty in the shape of the time-series associated with each event [2].

In FY 2024 we continued this research in signals analysis, uncertainty quantification (UQ), and fundamental metrology for cytometry. In particular, we pursued a new set of projects to identify and measure the elasticity of deformable particles in a cytometer. Here the key idea is to recognize that as a particle traverses the interrogation region, its shape is convolved with the laser profile. Thus, a deformable particle should have a signal whose shape is distinguishable from a sphere, for example. Preliminary analysis using our data collapse algorithms indicates that the corresponding residuals for deformable particles cannot be explained by the UQ for rigid spheres, indicating that our instrument is likely sensitive enough to detect shape change. As a prototypical case, we also performed this "shapes analysis" on cells undergoing growth and division, showing that we can in fact distinguish between normal cells and those whose DNA has doubled in anticipation of mitotic division. A manuscript on this latter work is in preparation.

In a separate project, we also demonstrated that one can construct uncertainty models that distinguish instrument variability (e.g. shot noise, flow instability, and Johnson-Nyquist noise) from inherent population and biological variability in cells. By fitting this model to calibration data associated with standard reference beads commonly used in cytometry, one can not only identify dominant sources of uncertainty in the measurement process, but also identify optimal (i.e., minimum uncertainty) operating conditions. This analysis also allows one to directly compare cytometers on the basis of their signal-to-noise ratios, and it yields rigorous definitions of concepts such as *limit-of-detection, limit of background, and limit of quantification* [3, 4, 5]; see also [6] and Figure 27. Despite being a seemingly standard analysis in many metrology settings, such issues have never been addressed before in cytometry.

Work in cytometry has also led to new efforts in the broader field of microfluidics. Following on successes from FY 2018 – FY 2022, we participated in a FedTech incubator program whose goal is to start companies based on NIST inventions. As a result of this effort, a company (Lumos NanoLabs) was created to commercialize our microfluidic flowmeter. En route to realizing this technology in the field, we also recently solved the problem of quantifying the relaxation kinetics and time-dependent properties of our flowmeter in response to time-varying flow rates [7, 8].

[1] W. H. Shrank, T. L. Rogstad, and N. Parekh. Waste in the US Health Care System: Estimated Costs and Potential for Savings. *JAMA* **322**:15 (2019), 1501-1509.

[2] P. N. Patrone, M. DiSalvo, A. J. Kearsley, G. B. McFadden, and G. A. Cooksey. Reproducibility in Cytometry: Signals Analysis and its Connection to Uncertainty Quantification. *PLOS One* **18** (12), e0295502.

[3] P. N. Patrone, A. J. Kearsley, M. A. Catterton, and G. A. Cooksey. Uncertainty Quantification in Cytometry Part I: An Analytical Perspective Beyond Q and B. In review.

[4] M. A. Catterton, M. DiSalvo, P. N. Patrone, and G. A. Cooksey. Uncertainty Quantification for Cytometry Part II: Comparison of Serial and Traditional Cytometers. In review.

[5] P. Bedekar, M. A. Catterton, M. DiSalvo, G. A. Cooksey, A. J. Kearsley, and P. N. Patrone. Per-event Uncertainty Quantification for Flow Cytometry using Calibration Beads. In review.

[6] A. Krishnaswamy-Usha, G. A. Cooksey, and P. N. Patrone. Uncertainty Quantification in Flow Cytometry Using a Cell Sorter. In review.

[7] N. Drachman, P. N. Patrone, G. A. Cooksey. Relaxation Times and Dynamic Behavior of an Optofluidic Flow Meter in the Nanoliter Per Minute Regime. *Physics of Fluids* **36** (2024) 022029. DOI: 10.1063/5.0193599

[8] G. A. Cooksey, S. Iavarone-Garza, N. Drachman, P. N. Patrone. Accuracy and Dynamics of Flow Measurements to 1 NL/min using an Optofluidic Flow Meter. *Measurement: Sensors* (2024), 101548. DOI: 10.1016/j.measen.2024.101548

Modeling DNA Origami

Ryan M. Evans
Allison Carson
Jacob Majikes (NIST PML)
Rouhong Shi (NIST PML)
Arvind Balijepalli (NIST PML)
Anthony J. Kearsley

Our team is developing fast, accurate, inexpensive, and portable biosensors that may be used for point of care diagnostics, as well as pathogen detection, in food and water. Typical experiments involve chemical reactants diffusing through a solution and a chemical reactant confined to a nanostructure built out of DNA known as *DNA origami*, which acts as a signal amplifier. Once a chemical reactant in solution reaches the chemical reactant in the nanostructure, it actuates the upper arm of the clamshell to close. Since DNA is negatively charged, this induces capacitive changes at the surface that can be measured as a function of applied voltage, electrolyte concentrations, and time. It has been shown that DNA origami can amplify the signal by a factor of twenty thousand [2].

This leads to natural questions of optimal nanostructure design. It has been demonstrated experimentally that capacitance is a function of the nanostructure's shape. Different shapes lead to different capacitance curves, and we wish to choose the nanostructure that maximizes capacitance. To a limited extent this may be accomplished experimentally through trial and error, but this is an expensive and time-consuming process since it does not rely on a physically

informed mathematical model. With a model we can pose this question as an optimal control problem.

A complete model for this process involves coupling Maxwell's equations with mass conservation equations for electrolyte concentrations. We have shown that, to leading order, the magnetic field is zero and the electric field may be modeled as quasi-static, with changes driven only by the origami and electrolytes. Thus, to leading order, the dimensionless governing equations for the electrolytes C_i and the potential φ are [1, 3]

$$\frac{\partial C_i}{\partial t} = D_i \nabla \cdot (\nabla C_i + z_i \mathcal{V} C_i \nabla \varphi), \tag{1a}$$

$$\epsilon \Delta \varphi = -\sum_{i=1}^{N} z_i C_i. \tag{1b}$$

In the upper equation, D_i is the ratio of the diffusivity of species i to the average diffusivity, z_i is the integral valence associated with species i, and $\mathcal{V}$ is the ratio of the maximum applied voltage to the thermal voltage. In the lower equation, ϵ is the squared ratio of the Debeye length to characteristic length scale of the potential. For typical experiments $D_i \approx 1$, $\mathcal{V} \approx 15$, and $\epsilon \approx 0.2$. This system of equations holds on the domain $\boldsymbol{\Omega}$ shown in Figure 28.

This governing system is supplemented by appropriate initial and boundary conditions. The concentrations and potential are assumed to behave periodically on the left ($x = 0$) and right ($x = 1$) boundaries. Since electrolytes may pass permeably through the DNA, each of the C_i are continuous across the DNA's interface. On the other hand, there is a discontinuity in the potential's normal derivative owing to the fact that DNA is negatively charged:

$$\nabla \varphi_+ - \nabla \varphi_- = \Phi \mathbf{n} \tag{2}$$

Here Φ is a dimensionless parameter that characterizes the strength of the DNA's surface charge to the applied potential at the boundary; for typical experiments $\Phi \approx -75$ (the negative sign reflects DNA's negative charge). Since the potential is grounded at infinity, we have

$$\lim_{y \to \infty} \varphi(x, y, t) = 0.$$

In the far field the normal component of the species' flux vanishes:

$$\lim_{y \to \infty} \left(\frac{\partial C_i}{\partial y} + z_i \mathcal{V} C_i \frac{\partial \varphi}{\partial y} \right) = 0. \tag{3}$$

At the bottom boundary, there is no flux of electrolyte through the instrument's surface and the potential assumes an experimentally controlled prescribed value. At the start of the experiment the system is in equilibrium, so (1a) holds with the left-hand-side equal to zero together with (1b) and the boundary conditions described above. This constitutes a complete description of the electrolyte concentrations and potential, from which we may calculate capacitance of as a function of time.

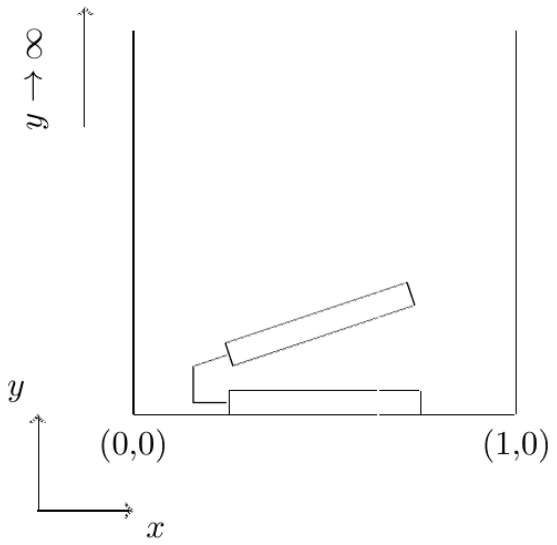

Figure 28. *Our domain* $\boldsymbol{\Omega}$*, featuring an idealized DNA nanostructure.*

This nonlinear system of partial differential equations (PDEs) naturally leads to numerical discretization, and we are presently discretizing this system with finite difference methods using overset grids. Overset grids are a natural way to accommodate the DNA nanostructure, especially in view of future work. During experiments, the DNA's upper arm can actuate in response to a chemical reactant in solution binding to a chemical reactant confined to the nanostructure. This process can be modeled with a stochastic differential equation. In this case, calculating capacitance from (1) involves solving a set of PDEs on a moving domain, something at which overset grids are adept. Solving these problems are important steps toward solving an optimal control problem in which the origami's shape is the design variable chosen to maximize capacitance.

[1] Brian J Kirby. *Micro- and Nanoscale Fluid Mechanics: Transport in Microfluidic Devices*. Cambridge University Press, 2010.

[2] J. M. Majikes, S. Choe, T. E. Cleveland, J. A. Liddle, and A. Balijepalli. Variable Gain DNA Nanostructure Charge Amplifiers for Biosensing. *Nanoscale* **16**:45 (2024), 2089-20902.

[3] Isaak Rubinstein. *Electro-Diffusion of Ions*. SIAM, 1990.

Topology and Geometry of Membranes

Leroy Jia
Xinyi Liu
Raymond Adkins (Yale University)
Joanna Robaszewski (Harvard University)
Seungwoo Shin (UC Santa Barbara)
Fridtjof Brauns (UC Santa Barbara)
Ayantika Khanra (Indian Inst. of Science, Bangalore)
Prerna Sharma (Indian Institute of Science, Bangalore)
Robert Pelcovits (Brown University)
Thomas Powers (Brown University)
Zvonimir Dogic (UC Santa Barbara)

Changes in shape and topology are a hallmark of biological processes, whether it is the division of cells during mitosis, the growth of thin epithelial tissues into three-dimensional organs throughout embryonic development, or the formation of lipid bilayer bridges and pores in membranes undergoing endo- or exocytosis. Despite the importance of these shapeshifting processes to the miracle of life, we know strikingly little about their dynamics, as their small time and length scales prohibit all but the most challenging experiments. Below, we report progress made over the last year in understanding the physics behind topological and geometric changes in one important class of biological material: membranes.

As part of a collaboration spanning half a dozen institutions across the world, ACMD participated in the modeling of the self-assembly and reorganization dynamics of large synthetic colloidosomes composed of rod-shaped viruses. These so-called "colloidal membranes" have properties that mimic those of lipid bilayers, including their topological transitions, but are an order of magnitude larger and are thus easier to experimentally control [1]. They are well described by a minimal model based on the Helfrich bending energy of a surface:

$$E = \int \left(\frac{\kappa}{2}(2H)^2 + \bar{\kappa}K\right) \mathrm{d}A + \gamma \int ds,$$

subject to the constraint of fixed area, which accounts for the relative inextensibility of membranes. Here, H and K are the mean and Gaussian curvatures of the surface, respectively, and κ and $\bar{\kappa}$ are material parameters. If the membrane is an open surface, then the line tension γ of its boundary also contributes to the energy. A quick calculation shows that for membranes with large areas, spherical vesicles are more energetically favorable than flat disks, and that the critical area for this transition is $A_c = \frac{4\pi(2\kappa+\bar{\kappa})^2}{\gamma^2}$. However, detailed images of the process by which such a membrane alters its topology when transitioning between these phases have, until now, remained elusive. An observed pathway of shapes is shown in Figure 29; the membrane first ruptures, generating a small metastable pore, and then the pore gradually expands with decreasing membrane surface area until the membrane becomes a flat sheet. The shapes in this transition closely match theoretical predictions obtained by minimizing the Helfrich energy. Alternate pathways in which two pores appear simultaneously and expand to create catenoid-like intermediate shapes are also observed. The unprecedented degree of experimental control offered by these colloidal membranes make them a promising avenue for studying other aspects of lipid bilayer membrane mechanics, as well as potential components in encapsulation and drug delivery systems. The manuscript describing this project was submitted in the fall of 2024 [2].

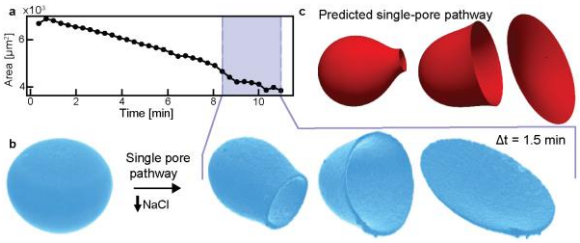

Figure 29. *The unwrapping of a vesicle into a disk [2]. a) Varying the salt concentration of the background fluid causes the membrane area to decrease over time. b) The observed pathway of shapes in which a single pore appears and gradually expands until the membrane flattens. c) The theoretical pathway corresponding to the shapes in b.*

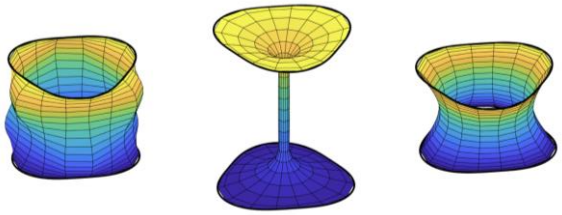

Figure 30. *A selection of spectrally accurate membrane shapes obtained by minimizing the Helfrich functional. The shapes exhibit (left) solid-like bucking, (center) tethering, and (right) fluid-like surface area minimization.*

Inspired by the rich physics of these bioinspired membranes, Liu and Jia also investigated a related mathematical question. The famous Plateau problem, named after the Belgian physicist Joseph Plateau, asks the following: given a boundary (possibly consisting of multiple curves), what is the surface of minimal area with the given boundary? Historically, this question kicked off the study of minimal surfaces, which have vanishing mean curvature and are realized in everyday life by fixed-tension soap films and other fluid interfaces. We propose a variation of this problem whose solutions are realized by membranes: what is the shape assumed by a fluid surface with a resistance to bending that has a given boundary? Mathematically, this entails minimizing the aforementioned Helfrich energy; here,

we focus on shapes with two boundary rings, akin to the classic catenoid. The critical surfaces of this functional can be understood as an amalgamation of the solutions to two classic problems in the calculus of variations [3]. In the case of $\bar{\kappa} = 0$, one can see that unconstrained shapes will tend to be minimal surfaces: $H = 0$, like for a soap film. However, the presence of external confining forces, combined with the area constraint, introduces the possibility of buckled solutions, analogous to how compressing the ends of a slender inextensible elastic rod gives rise to the Euler buckling instability. Consequently, our shapes can have both a maximal extension and an infinitely large solution space of buckled configurations (Figure 30). There is also the possibility of fluid tethers when the surface area exceeds the area spanned by the two boundary rings. Remarkably, a one-to-one correspondence maps the eigenvalues of our problem onto those of the minimal surface problem, enabling precise mechanical predictions without calculation. The case of $\bar{\kappa} \neq 0$ is particularly interesting, as it introduces singularities that both complicate the problem yet also must be present to stabilize a free-standing surface. Methods of singular perturbation theory have proven successful in dealing with the axisymmetric case [3], and a spectral solver to find general shapes has been written. A talk on this work was presented at the 77th Annual Meeting of the American Physical Society Division of Fluid Dynamics in November 2024.

Membranes are a simple physical model yet possess countless applications in biology, chemistry, and materials science. Essential to their ubiquity are the ease and robustness with which they change geometry and topology. By studying their phases, the transitions between them, and ways to control these transitions, we are building the foundation for innovations in regenerative medicine, bioinspired engineering, and metamaterials design.

[1] T. Gibaud, et al. Reconfigurable Self-Assembly through Chiral Control of Interfacial Tension. *Nature* **481** (2012), 348. DOI: 10.1038/nature10769

[2] R. Adkins, et al. Topology and Kinetic Pathways of Colloidosome Assembly and Disassembly. In review.

[3] L. L. Jia, S. Pei, R. A. Pelcovits, and T. R. Powers. Axisymmetric Membranes under External Force: Buckling, Minimal Surfaces, and Tethers. *Soft Matter* **17** (2021), 7268. DOI: 10.1039/D1SM00827G

Mechanics of Corkscrew Esophagus: Instability and Growth

Xinyi Liu
Leroy Jia
Sourav Halder (Northwestern University)
Walter Kou (Northwestern University)
Dustin Carlson (Northwestern University)
Peter Kahrilas (Northwestern University)
John Pandolfino (Northwestern University)
Neelesh Patankar (Northwestern University)

This research concerns corkscrew esophagus, a pathological condition characterized by abnormal spiral deformations of the esophagus, with a focus on the interplay between tissue hypertrophy, remodeling, and mechanical instability. The esophagus, a tubular organ connecting the mouth to the stomach, plays a critical role in swallowing. Disorders such as achalasia and distal esophageal spasm (DES) are often accompanied by muscle hypertrophy, where esophageal muscles grow in response to excessive contraction forces [1]. Corkscrew esophagus, which involves extreme tissue deformation, is usually observed in the context of growth in the esophageal wall. A comparable remodeling phenomenon is also observed in the airway, where airway wall thickness increases in response to chronic inflammation [2]. Thus, growth and mechanical forces are hypothesized to destabilize biological tissue, leading to dramatic shape transformations. On the other hand, clinical observations also demonstrate that corkscrew esophagus becomes more pronounced during swallowing, where atypical muscle contractions exacerbate the deformation. These observations indicate that the underlying mechanisms of the corkscrew phenomenon are multifaceted and cannot be fully accounted for by a single mechanical explanation. This lack of understanding of the fundamental cause of the deformation significantly complicates both diagnosis and treatment. Mathematical modeling plays a crucial role in quantifying the factors contributing to this instability.

To understand and simulate corkscrew esophagus, we use a mathematical framework based on continuum mechanics, which helps us describe how the esophageal tissue deforms and behaves under stress. Growth can be modeled by combining changes in mass and elastic deformations, as established in foundational works by Skalak and others [3, 4]. They framed growth as a mapping from an initial to a new reference configuration, enabling kinematic concepts like velocity and deformation gradients to describe a body's evolution and mechanical response. This culminates in a multiplicative decomposition of the deformation gradient $\boldsymbol{F}$ of the form

$$\boldsymbol{F} = \boldsymbol{F}_e \boldsymbol{F}_g$$

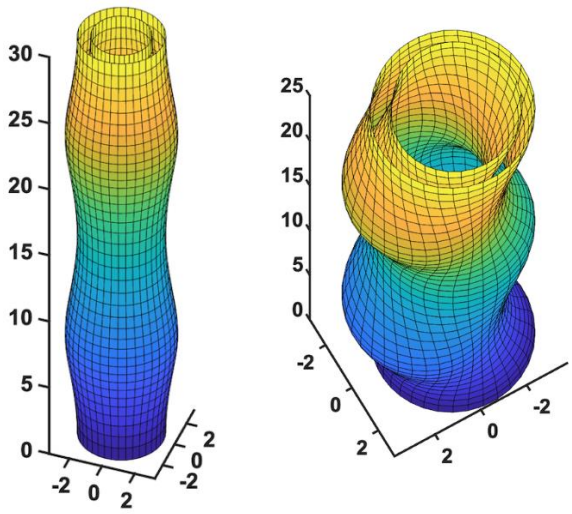

Figure 31. *Axisymmetric (left) and non-axisymmetric (right) shows the different deformation patterns an elastic tube under internal pressures can undergo in response to perturbations.*

where growth, represented by $\boldsymbol{F_g}$, adds material locally and elasticity, represented by $\boldsymbol{F_e}$, ensures compatibility and structural integrity [5]. The deformation gradient contains all the information about relative deformations of a body, and can be used to define secondary quantities, such as the left and right Cauchy-Green tensors, which contain information about the strain developed during a deformation. The governing equations of continuum mechanics are obtained by considering the balance of physical quantities. For example, the conservation of momentum gives the equilibrium condition $\nabla \cdot \sigma = 0$, where σ is the Cauchy stress. Once we specify the material, reference configuration, and boundary conditions, the deformations and stresses at equilibrium can be computed by solving a system of nonlinear partial differential equations.

The stability of the finite deformation solution can be probed by bifurcation theory. A bifurcation indicates the potential for instability, which can be explored by either studying the dynamics of the new solutions, or by examining the second variation of the energy, if applicable [4, 6]. To model this phenomenon and the underlying instability in this framework, we assume that the solution for the Cauchy stress and deformations is known for given boundary conditions and is controlled by several parameters. We refer to this solution as the base solution. Then, we apply a small non-axisymmetric perturbation to the base solution. By expanding all quantities to first order, we reduce the partial differential equation system to an ordinary differential equation system whose eigenvalues represent the critical dilation factor required for instability. Figure 31 shows simulation results for the perturbed shapes from a cylinder. Using the dilation factor, we identified critical pressures needed for the instability under different growth conditions. We find that for the axisymmetric case, the onset of instability is influenced by critical pressure, with variations in radial, circumferential, and axial growth altering the preferred instability patterns and wavelengths. This work was presented at the 77th Annual Meeting of the American Physical Society Division of Fluid Dynamics in November 2024.

Future efforts will focus on enhancing the resolution and complexity of the current model to better capture the structural and functional dynamics of the esophagus. The model incorporates three primary layers: the longitudinal muscle layer, circular muscle layer, and mucosa, each representing key structural and functional components. The longitudinal and circular muscle layers are responsible for esophageal motility, driving peristaltic waves that facilitate the transport of food, while the mucosa protects the lumen from mechanical stresses and acid from the stomach. For the muscle layers, we introduce a fiber component that includes a contraction parameter into the strain energy function to model active forces generated by muscular contraction. This three-layer model simplifies the complex anatomy while retaining the essential elements needed to study esophageal function and the cause of instability induced by contraction.

The significance of this project lies in addressing a fundamental challenge in tissue engineering and biomechanics: understanding how subtle changes in mechanical forces or tissue properties can lead to significant and sometimes pathological deformations. The corkscrew esophagus phenomenon exemplifies mechanical instability, a concept observed across biological systems. For example, in hypertrophic cardiomyopathy, abnormal thickening of the heart muscle leads to changes in mechanical loading and tissue deformation, which can be modeled using similar principles. Airway remodeling in asthma patients involves increased airway wall thickness and stiffness, often driven by chronic inflammation and altered mechanical forces, which significantly impair respiratory function. In each of these cases, mechanical instability plays a crucial role in the progression of the disease, making it essential to quantify the interactions between growth, remodeling, and mechanical forces. By analyzing the mechanics and dynamics of corkscrew esophagus, we aim to uncover universal principles of instability that could inform broader applications in tissue engineering and regenerative medicine. For instance, advanced mathematical models derived from this research could aid in designing patient-specific treatments, such as stents for aneurysms or bioengineered airway scaffolds, to restore structural stability and functionality in affected tissues. Furthermore, these principles could guide the development of more resilient engineered tissues for use in regenerative therapies.

[1] R. Mittal. Hypertrophy of the Muscularis Propria of the Lower Esophageal Sphincter and the Body of the Esophagus in Patients with Primary Motility Disorders of the

Esophagus. *The American Journal of Gastroenterology* **98** (2003), 1705–1712.

[2] L. James, P. D. Pare, and J. C. Hogg. The Mechanics of Airway Narrowing in Asthma. *The American Review of Respiratory Disease* **139**:1 (1989), 242–246.

[3] R. Skalak. Growth as a Finite Displacement Field. In *Proceedings of the IUTAM Symposium on Finite Elasticity*, (D. E. Carlson and R. T. Shield, ed.), 347–355, Springer, 1981.

[4] R. Skalak, G. Dasgupta, M. Moss, E. Otten, P. Dullemeijer, and H. Vilmann. Analytical Description of Growth. *Journal of Theoretical Biology* **94**:3 (1982), 555–577.

[5] E. K. Rodriguez, A. Hoger, and A. D. McCulloch. Stress-dependent Finite Growth in Soft Elastic Tissues. *Journal of Biomechanics* **27**:4 (1994), 455–467.

[6] R. Skalak. Growth as a Finite Displacement Field. In *Proceedings of the IUTAM Symposium on Finite Elasticity*, (D. E. Carlson and R. T. Shield, ed.), 347–355, Springer, 1981.

A Wearable Flexible Loop Antenna for In-Body Beamforming

Katjana Krhac
Kamran Sayrafian
Uzay Bengi (Boğaziçi University, Turkey)
Sema Dumanli (Boğaziçi University, Turkey)

Wearable and implantable medical devices will be playing a prominent role in the future healthcare system. They will enable major applications such as personal or remote health monitoring. Wearable antennas can be used to sense physical changes inside the human body both through their reflection and transmission coefficient parameters [1]. However, monitoring these parameters presents challenges due to the high attenuation of the propagation channel inside the human body. Designing efficient antennas is critical to achieve good performance with wearable monitoring devices. In addition, it is important to consider constraints such as biocompatibility, usability, accuracy, and robustness, as well as regulatory restrictions such as specific absorption rate (SAR).

A potential methodology to enhance in-body propagation is using on-body antenna arrays and beamforming. It is conceivable that through beamforming, the transmitted energy can be focused in a specific direction, leading to an increased distance in signal penetration or, equivalently, higher received signal power at a given distance. Compared to free space propagation, in-body beamforming is more challenging due to the non-homogenous human body environment. In this research, we propose and study an on-body coplanar waveguide-fed loop antenna operating in the MICS band (i.e., 401 to 406 MHz). At these frequencies, antenna miniaturization is often required to enhance usability.

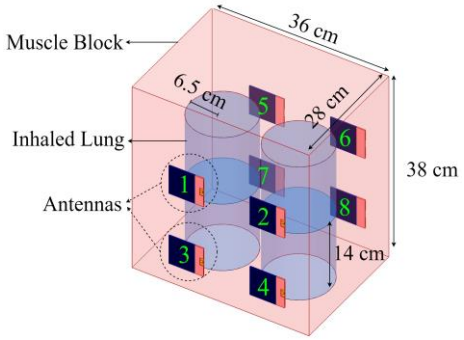

Figure 32. *The simulation setup: Four-element antenna array covering the lungs inside the torso model.*

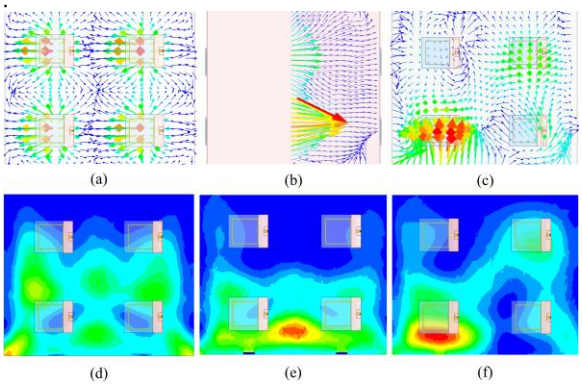

Figure 33. *In-body beamforming demonstrated by Poynting Vector and SAR plots: (a) & (d): No beamforming (front views), (b) & (e): Beamforming to lower lobes (PV side view, SAR front view), (c) & (f): Beamforming to right bottom lobe (front views).*

To achieve this, we propose utilizing a novel silicon-based flexible material as the antenna substrate. By doping RTV silicon with graphite, a substrate with a relative permittivity value of 11 can be fabricated. This high-permittivity flexible substrate (HPFS) allows us to achieve both reasonable antenna size and flexibility for the user's convenience

Figure 32 shows a simplified model of the human torso. The model consists of a rectangular block with dielectric properties of the human muscle and two cylinders representing the human lungs. Frequency-dependent characteristics of the tissues (i.e., muscle and lung) are considered in the numerical analysis. The dielectric properties of the lung tissue are chosen to correspond to the inhaled state. Copies of the antenna described earlier are placed on the anterior and posterior of the torso model in a 2×2 array configuration to realize beamforming towards a specific lobe of the lungs.

The in-body beamforming is illustrated through Poynting Vector and SAR plots as shown in Figure 33 [2]. Initially, no beamforming is performed as seen in Figure 33(a) and (d). Then, proper phase shifts are introduced to the transmit ports of the antennas to form and steer the beam towards the lower section (i.e., lower lobes of the lungs). This steering is observed in Figure

33(b) and Figure 33(e). Finally, the beam is steered towards the right bottom lobe as seen in Figure 33(c) and (f).

To the best of our knowledge, there is no prior work in the literature performing in-body beamforming with a microwave flexible antenna. Further studies using a higher number of antenna elements and a more detailed investigation of phase shift strategies to achieve optimal beamforming are planned in continuation of this research.

[1] K. Krhac, K. Sayrafian, U. Bengi, and S. Dumanli-Oktar. A Wearable Wireless Monitoring System for the Detection of Pulmonary Edema. In *IEEE Global Communications Conference* (GLOBECOM), Madrid, Spain, December 7-11, 2021. DOI: 10.1109/GLOBECOM46510.2021.9685118

[2] U. Bengi, K. Krhac, K. Sayrafian, and S. Dumanli. A Wearable Flexible Loop Antenna for In-Body Beamforming. In *IEEE International Symposium on Antennas and Propagation*, Florence, Italy, July 14-19, 2024. DOI: 10.1109/AP-S/INC-USNC-URSI52054.2024.10686699

An Immersive Visualization System to Study UWB Propagation Channel in Smart Pills Applications

Katjana Ladic
Kamran Sayrafian
Kamya Yekeh Yazdandoost (KDDI Research Inc, Japan)

Smart pills are a potentially revolutionary technology that allows physicians to easily evaluate the health of the human gastrointestinal (GI) tract. A smart pill is basically a wireless, ingestible capsule that can measure or sense a variety of health data including images or videos as it passes through the GI tract. It is also envisioned that small pills will be capable of delivering drugs to specific location(s) inside the GI tract. A Capsule Endoscope is a smart pill that offers an effective alternative procedure to traditional wired endoscopy. In capsule endoscopy, a tiny wireless camera embedded in a capsule is swallowed by the patient. As the capsule travels through the GI tract, the camera takes periodic photos and transmits them to on-body receivers that are typically located inside a belt worn by the patient. The operating frequency band of capsules available in the market today is typically within the 430 MHz to 440 MHz frequency range. To allow transmission of high-resolution images or videos of the GI tract, high data rate communication technologies such as Ultra-Wideband (UWB) could be used in the future.

Knowledge of the underlying propagation channel is critical during the design of any wireless system. More efficient and reliable communication can be achieved with an in-depth understanding of the propagation processes for the desired application. For wireless implants or ingestible sensors, acquiring channel information by conducting physical measurements in humans is nearly impossible. As a result, computational models, liquid phantoms, or animals are typically used by researchers to conduct channel measurements or related experiments. From the limited results available in the literature, it can be observed that conducting experiments using different approaches, experimental setup, antennas, and even measurement scenarios can lead to noticeable differences in the derived channel models or parameters. In [1], the potential impact of the locations of the measurement points and their distribution on the extracted parameters of the UWB implant channel model was highlighted through a series of matching simulation and experimental studies. It was shown that a judicious selection of measurement points could lead to a sample set that better represents the transmitter-receiver distances; and therefore, a more accurate statistical model for the propagation channel can be achieved.

In this research, a three-dimensional immersive system has been developed to study UWB propagation in smart pills applications. The block diagram of the system is shown in Figure 34.

To select the sample positions of the capsule antenna and conducting simulation, we first computed the centerline that goes through the entire small intestine of the computational body model. Mathematically, this line is the median of all paths through the intestine. It can be used to represent the forward trajectory of the capsule on average. If a set of uniformly spaced locations along the centerline is chosen as sample capsule positions (see Figure 35(a), the distribution of distances with the on-body receivers will be highly non-uniform. This distribution is shown in Figure 35(b). As observed, there are high concentrations of sample distances for certain ranges, but insufficient samples for low and higher distances. The intertwined path along the small intestine impacts the distribution of the distances between the transmitter-receiver pairs. Highly non-uniform distributions due to biased samples will reduce the accuracy of the data analysis that is used for statistical pathloss modeling. Therefore, an approach for judicious selection of the measurement points is needed. This approach can be potentially obtained by formulating and solving a complicated mathematical problem that can identify the proper set of capsule locations. However, in our system, using the immersive platform, we have developed a simple interactive procedure to find the proper set.

Initially, a set of positions along the centerline at specific distances (i.e., 5 cm to 25 cm) from the on-body receivers is computed. Then, using interactive probing and picking at the immersive platform, a new candidate position along the centerline is chosen. Using a *k*-nearest-neighbor algorithm, the closest matching

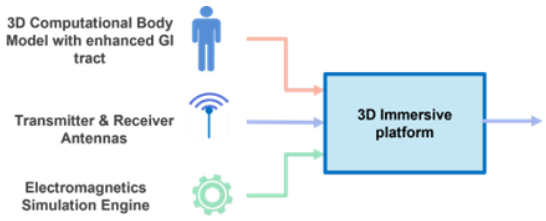

Figure 34. *Immersive system to study propagation channel in capsule endoscopy.*

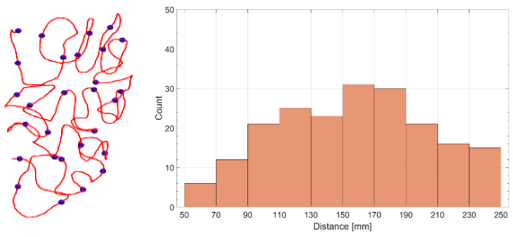

(a) (b)

Figure 35. *(a) uniformly spaced capsule positions along the centerline, (b) the resulting distribution of distances between the capsule and on-body receivers.*

(a) (b)

Figure 36. *(a) final capsule positions selected using the immersive platform, (b) resulting distribution of distances between the capsule and on-body receivers.*

precomputed position is found next, and at the same time a histogram of the communication channel distances is generated. The user in the immersive platform can immediately observe whether the set of the sample positions have an approximately uniform distribution within the range of 5 cm to 25 cm. The process of interactive adding or subtracting sample positions is continued until the desired distribution is achieved. Following this procedure inside the immersive platform, 20 candidate positions for the capsule antenna placement were carefully selected, see Figure 36(a). The final set of capsule positions resulted in a more uniform distance distribution from the on-body receivers. The distribution of these distances is shown in Figure 36(b).

The set of simulation scenarios identified after this procedure effectively captures the impact of various body tissues, distance distribution from the on-body receivers and antenna orientations [2]. Through numerical analysis, a statistical pathloss model for a capsule endoscope operating within the lower UWB spectrum (i.e., 3.1 GHz to 4.1 GHz) has been obtained using this set [3]. This model has been contributed to the Task Group 6ma (TG6ma) of the IEEE 802.15 working group for the UWB capsule endoscopy use-case. TG6ma is currently working on the revision of the wireless body area networks standard (IEEE 802.15.6-2012). Further studies on the minimum number and best locations of the on-body receivers are needed to ensure reliable communication from the capsule regardless of its position within the small intestine. The platform described above will also be used to study potential multipath nature of the UWB channel and investigate the applicability of a tapped-delay-line channel model in continuation of this research.

[1] S. Perez-Simbor, K. Krhac, C. Garcia-Pardo, K. Sayrafian, D. Simunic, and N. Cardona. Impact of Measurement Points Distribution on the Parameters of UWB Implant Channel Model. In *IEEE Conference on Standards for Communications and Networking*, Paris, France, October 29-31, 2018.

[2] K. Ladic, K. Sayrafian, and K. Y. Yazdandoost. An Immersive Visualization System to Study UWB Propagation Channel in Smart Pills Applications. In *IEEE Conference on Standards for Communications and Networking*, Belgrade, Serbia, November 25-27, 2024

[3] K. Ladic, K. Sayrafian, D. Simunic, and K. Y. Yazdandoost. Wireless Channel Characterization for UWB Communication in Capsule Endoscopy. *IEEE Access* **11** (2023), 95858 – 95873.

Evaluation of LoRaWAN for Remote Health Monitoring

Brian Cloteaux
Kamran Sayrafian
Konstantinos Katzis (European Univ. Cyprus, Cyprus)
Nina Evetovic (University of Novi Sad, Serbia)
Dragana Bajić (University of Novi Sad, Serbia)

Wearable and personal medical devices are becoming an integral part of the healthcare system, fundamentally changing and enhancing the ways we perceive, monitor, and manage our health. These devices have the potential to become indispensable tools for individuals and healthcare professionals, therefore revolutionizing healthcare delivery. Furthermore, the mobility, convenience, and low-cost features, make such devices attractive solutions for providing continuous health monitoring of patients in remote areas. Continuous monitoring transcends traditional healthcare boundaries and enables real-time data sharing with healthcare providers. It will also lead to more personalized care for individuals with chronic diseases. In addition, the collected data

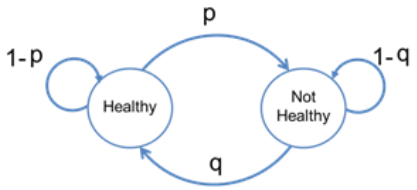

Figure 37. *Two-state Markov model for Remote Home Monitoring Scenario.*

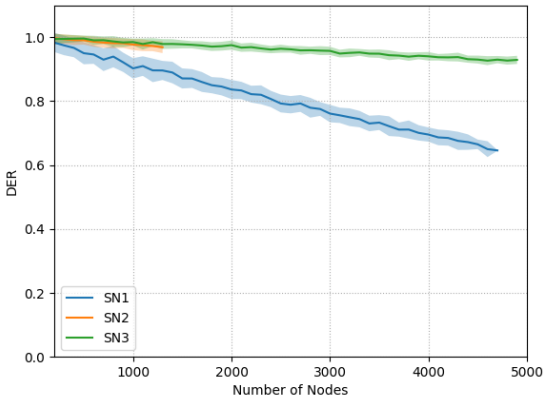

Figure 38. *Remote home monitoring results.*

could help pharmaceutical industry to better assess the efficacy of certain medications. Hospitals can also benefit from the integration of wearable devices to allow seamless observation and monitoring of the patients' vital signs and other relevant physiological signals.

Monitoring health data from patients that are hospitalized or reside in their own home involves transmitting the measured data at fixed or random intervals over a wireless communication network. As the measurements typically consists of small packets of data and don't require constant or high-bandwidth connectivity, Low Power Wide Area Network (LPWAN) technology is a good candidate to support data generated from such wearable or personal devices. These networks also don't require expensive spectrum licenses as they typically operate within unlicensed frequency bands. Long Range Wide Area Networks (LoRaWAN) is a low power wide area networking protocol that has been designed to wirelessly connect battery operated devices to the Internet in regional, national or global networks. It also provides bi-directional communication capability, end-to-end security, mobility and localization services. Because of its simple architecture, LoRaWAN is relatively easy, effective and inexpensive to deploy at scale. It can specially support low power applications such as smart home devices.

LoRaWAN can address challenges facing connectivity through Bluetooth or WiFi by eliminating the need for intermediate devices and fees associated with cellular networks. It can provide long-distance and reliable communication through its gateways. Depending on the application, both indoor and outdoor LoRaWAN gateways can be utilized to facilitate seamless data collection. This project provides a preliminary evaluation on how mass deployment of healthcare devices can affect the overall performance of the LoRaWAN in a hospital-based environment and remote home monitoring of patients. Two types of traffic models are proposed to simulate the traffic generated for these two scenarios.

In a hospital environment, vital signs of patients hospitalized in the general wards are typically measured every four hours. In some post operative cases, vital signs must be measured on an hourly basis for a few hours before switching to a four-hour monitoring pattern. For remote health monitoring of patients at their homes, there are no empirical statistical models that can comprehensively describe the traffic from their devices. Developing such models is a complicated task as it depends on many factors such as type and number of the devices that a given person might use, the frequency of usage, and size of the measurement data, etc. Empirical data to generate such models will become more available as the adoption of personal health monitoring devices accelerates. In our preliminary analysis, we propose a simple model based on a pattern that is likely followed by people who use personal health monitoring devices. We consider a Markov model that describes the general health of a person in two states i.e., healthy and not-healthy states (see Figure 37).

The healthy state corresponds to the normal physical condition of a person which results in routine daily measurements of his/her target physiological indicators or vitals. The not-healthy state describes the occurrence of possible health issues. For example, for people with chronic conditions, the not-healthy state might correspond to the flare-up periods of their specific conditions. The transition probabilities between these states depends on the many factors and could vary across individuals with different conditions. For simplicity, we consider a fixed transition probabilities (i.e., p and q) across all individuals in our analysis. At each state, the individual conducts self-monitoring using personal devices; however, the frequency of measurement is different depending on the patient health condition. This frequency is naturally higher in the not-healthy state. As the time of home measurements in each state doesn't follow a periodic pattern, we propose considering two Poisson processes to model the health data transmission times. In the healthy state, the measurements are less frequent, so a Poisson process with a low rate may effectively capture the packet transmission times. On the other hand, in the not-healthy state, the individual at home is likely to conduct measurement more often to closely monitor his/her condition. This may also be represented by a Poisson process with a higher rate.

In this project, we investigated the performance of a single cell LoRaWAN network under different monitoring scenarios. In particular, the impact of the number

of health monitoring devices on the Data Extraction Rate (DER) is evaluated. DER which is defined as the ratio of the received to transmitted messages over a period of time is used as an indicator of the quality of service. LoRaSIM is a discrete-event simulator based on SimPy that is used for simulating collisions in LoRa networks and analyzing its scalability [1]. We have used LoRaSIM in our simulation study with custom modifications to incorporate our proposed traffic patterns. We also considered three sets of simulation parameters (SN1, SN2 and SN3) in this study. These parameter sets include transmission power, spreading factor, coding rate, pathloss exponent, number of transmitted bytes and simulation time. These sets emulate the slowest and fastest data rates for packet transmission.

Figure 38 shows the simulation results for remote patient monitoring under different parameter sets. As observed, under SN1, up to 1200 monitoring devices can be used while maintaining a DER above 90%. However, under SN3, the DER remains above 90% even when the number of devices increases to 4800. The low spreading factor under SN2 imposes limitation on the distance of the devices to the gateway. Considering the spatial distribution used in LoRaSIM, this implies a limit on the number of devices that can be considered in the simulation. This is the reason that Figure 38 shows only a maximum of 1300 devices under SN2 with DER > 90%. In this case, more gateways will be required in order to accommodate a greater number of devices.

The preliminary results in our study show that LoRaWAN can be used to reliably deliver non-real-time data in hospitals and from homes. In particular, the results show that in both scenarios a significant number of nodes (Hospitals = 500, Remote home monitoring = 4800) can be accommodated while maintaining a high DER >90%. In continuation of this study, we plan to extend the traffic models by considering different types of data from various monitoring devices and conduct simulation with more traffic features and mixed types of sources. In addition, we plan to consider multiple LoRaWAN clusters and the impact of various indoor propagation conditions as well as the interference between the clusters. Further details and results of this project can be found in [2].

[1] M. C. Bor, U. Roedig, T. Voigt, and J. M. Alonso. Do LoRa Low-Power Wide-Area Networks Scale? In *Proceedings of the 19th ACM International Conference on Modeling, Analysis and Simulation of Wireless and Mobile Systems*, New York, USA, November 2016.

[2] K. Katzis, N. Evetovic, B. Cloteaux, K. Sayrafian, and D. Bajić. Evaluation of LoRaWAN for Remote Health Monitoring: A Preliminary Study. In *IEEE Conference on Standards for Communications and Networking*, Belgrade, Serbia, November 25-27, 2024.

Time-dependent Multiclass Antibody Kinetics

Prajakta Bedekar
Rayanne Luke
Anthony Kearsley

The world's response to the severe acute respiratory syndrome coronavirus 2 (SARS-CoV-2) pandemic raised questions about antibody kinetics, pushing them to the forefront of scientific research, especially in the context of public health and serosurveillance. Comprehensive study of such questions remains valuable as the lessons learned from this pandemic will help tackle future emergent diseases.

We developed a new fundamental mathematical framework [1] built on optimal decision theory that leveraged seroprevalence to efficiently classify samples into immune-naïve and previously infected. We extended this framework to accommodate multiple classes such as immune-naïve, infected, and vaccinated [2]. In parallel, we extended the binary framework to the time-

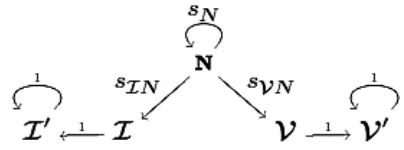

Figure 39. *Graph describing the allowable movements between states. Here, N is naïve, I is newly infected, I' is previously infected, V is newly vaccinated, and V' is previously vaccinated. Double subscripts on s denote the transition probability from the second state to the first.*

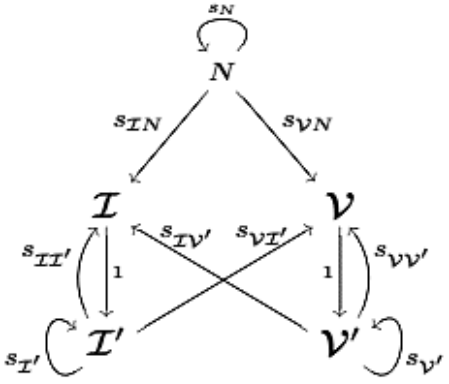

Figure 40. *Graph describing the allowable movements between states for the more general model, including reinfections, revaccinations, and cross effects. Here, N is naïve, I is newly infected, I' is previously infected, V is newly vaccinated, and V' is previously vaccinated. Double subscripts on s denote the transition probability from the second state to the first.*

dependent setting [3]. The latter work led to the interesting observation that an antibody measurement can be viewed as a convolution of the personal antibody response with the absolute timeline of the pandemic as measured by the incidence rates.

This framework provides valuable insights but can become unwieldy in a multiclass time-dependent setting. Personal immune responses to infection and vaccination may differ from eachother and their incidence rates will also be different in the absolute timeline. Furthermore, as a disease becomes endemic, personal trajectories of immune events for individuals can become longer and more intricate. Considering reinfection, revaccination, and cross effects is crucial. How these effects combine is an area of active theoretical and experimental research, as they can influence policy pertaining to timing vaccination and booster inoculations.

To generalize the existing work to enumerate the different personal trajectories, we developed an improved framework using time-inhomogeneous Markov chains. We model the probability of transition from one state to another using incidence rates of infection and vaccination within the population, capturing how the disease has progressed through the population. We then construct personal response models to probabilistically identify how individuals might respond to infection or vaccination. These personal response and time-inhomogeneous transition matrices describe the total probability of obtaining an antibody measurement.

Recent work [4] assumes that individuals may become either infected or vaccinated and remain in that state. This was exactly the case in January of 2021 with SARS-CoV-2, when very few people were infected or vaccinated more than once. We present a probabilistic model as an extension of previous works and prove that using time-inhomogeneous Markov chains (Figure 39) provides an equivalent approach. We use synthetic data for SARS-CoV-2 to demonstrate the equivalence numerically.

The next steps involve modeling a more general scenario, where reinfections and revaccinations are common. For this, we consider a more connected graph (Figure 40). Modeling the addition of personal responses of multiple events to mimic the effects of immunological memory remains an important and challenging consideration.

[1] P. N. Patrone and A. J. Kearsley. Classification Under Uncertainty: Data Analysis for Diagnostic Antibody Testing. *Mathematical Medicine and Biology: A Journal of the IMA* **38**:3 (2021), 396–416. DOI: 10.1093/imammb/dqab007

[2] R. A. Luke, A. J. Kearsley, and P. N. Patrone. Optimal Classification and Generalized Prevalence Estimates for Diagnostic Settings with More Than Two Classes. *Mathematical Biosciences* **358** (2023), 108982. DOI: 10.1016/j.mbs.2023.108982

[3] P. Bedekar, A. J. Kearsley, and P. N. Patrone. Prevalence Estimation and Optimal Classification Methods to Account for Time Dependence in Antibody Levels. *Journal of Theoretical Biology* **559** (2023), 111375. DOI: 10.1016/j.jtbi.2022.111375

[4] P. Bedekar, R. A. Luke, and A. J. Kearsley. Prevalence Estimation Methods for Time-Dependent Antibody Kinetics of Infected and Vaccinated Individuals: A Markov Chain Approach. *Bulletin of Mathematical Biology* (2025). DOI: 10.1007/s11538-024-01402-0

A Mathematica l Model of Penetration of Zona Pellucida

Daniel Anderson
Prajakta Bedekar
Zachary Goecker (NIST MML)
Anthony Kearsley

Fertilization of an ovum by a spermatozoon is a multistep process with vast implications on in-vitro fertilization, contraceptive development, food, and dairy industry to name a few. Fertilization consists of spermatozoa motion towards an oocyte, followed by acrosome reaction, tethering and penetration of zona pellucida (the outer layer of an ovum), and fusion. Many experimental, computational, and mathematical modeling studies have been performed on various aspects of fertilization (see [1] for a review), however the penetration of zona pellucida by spermatozoa is not very well understood. Biological experiments in this realm in the past have mostly comprised of gene-knockout studies paired with statistical analysis of percentage of successful fertilization, which doesn't address the dynamics of the process. As a result, the data for fitting these models is far from abundant and typically mathematical models in this arena use statistical aggregate quantities for building solely statistical aggregate or time-dependent models.

We study sperm-egg interaction by modeling the concentrations involved in penetration of zona pellucida by chemicals within the acrosome. We build a reaction-diffusion-decay model for the process under an assumption of second order reversible reaction between the chemicals involved. As ZP is an extracellular matrix, we assume it does not diffuse. This model can yield in-silico insight into underlying competing physiological factors leading to successful fertilization. and displays desirable properties such as positivity and boundedness. Numerical solution to the model system at different times with nominal diffusion, no decay is demonstrated in Figure 41. Initially, acrosin is concentrated at the right side of the space domain, ZP on the left, and the product is zero everywhere. As time passes, we see that the product slowly drifts into the ZP, thereby facilitating passage of the genetic material from the spermatozoan into the ovum, as expected.

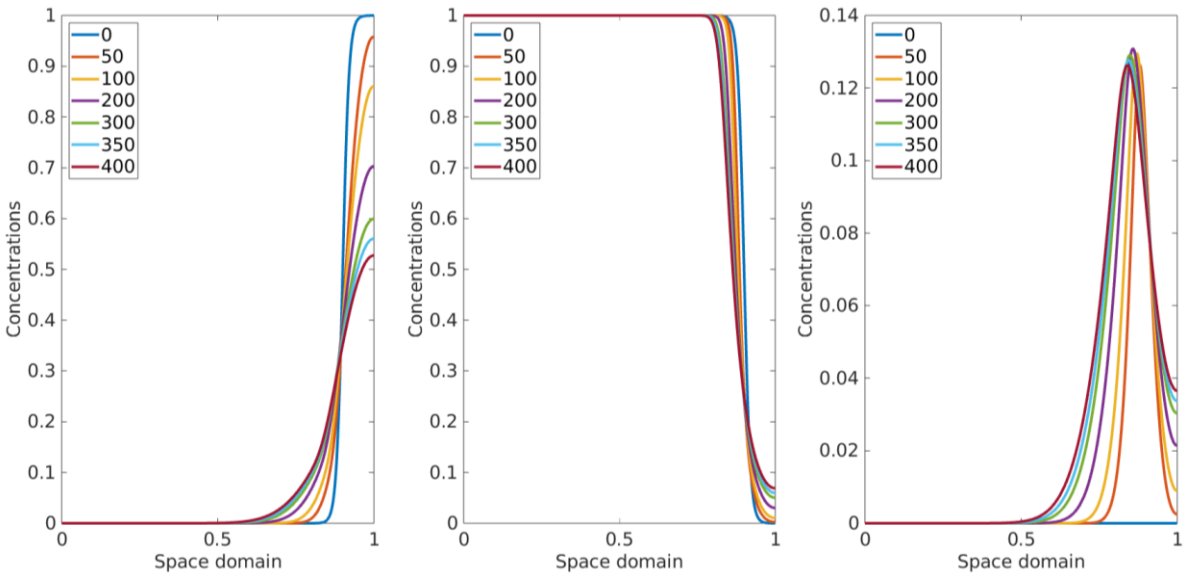

Figure 41. *Numerical solution to the model system at different times with nominal diffusion, no decay. Left to right: acrosin, zona pellucida, and the product of their reaction. Initially, acrosin is concentrated at the right side of the space domain, ZP on the left, and the product is zero everywhere. As time passes, we see that the product slowly drifts into the ZP, thereby facilitating passage of the genetic material from the spermatozoan into the ovum.*

This model remains general enough to accommodate a myriad of possible reaction mechanisms for the underlying chemicals. To illustrate this, we have compared model predictions for second order reversible reaction against the frequently employed, Michelis Menten model. This study demonstrates that more intricate reaction mechanisms paired with space-time diffusion-based models provide a valuable sandbox to examine competing biological hypothesis in-silico. Our approach yields insights used to define new experimental paradigms which will be investigated in collaboration with biologists at the Material Measurement Laboratory (MML) at NIST. This research serves to provide the crucial link to a fuller understanding of fertilization, opening the door to future investigation.

[1] L. J. Fauci, and R. Dillon. Biofluidmechanics of Reproduction. *Annual Review of Fluid Mechanics* **38**:1 (2006), 371-394.

Topological Data Analysis of the NIST Monoclonal Antibody

Melinda Kleczynski
Christina Bergonzo (NIST MML)
Anthony Kearsley

Many new medical treatments utilize monoclonal antibodies, a class of artificially produced antibodies. To inform analysis methods for large proteins including monoclonal antibodies, NIST provides the NIST Monoclonal Antibody (NISTmAb) as a reference material [1]. NIST researchers have worked to provide information about this benchmark molecule's structure and composition; see, for example, [2].

Antibodies are dynamic objects, with a range of possible conformations. A single structure is not sufficient to characterize an antibody. Rather, a complete description would quantify the variability in its structure. Potential configurations can be explored using molecular dynamics simulations; see, for example, [3]. These simulations produce different arrangements of atoms in the antibody. Some of these arrangements are visually different. Mathematical analysis allows us to quantify differences in structure rather than relying on qualitative determinations.

We are exploring different organizations of atoms using techniques from topological data analysis (TDA). TDA is a relatively new field which generates features orthogonal to those produced by classical analysis methods. Traditional network analysis represents objects as nodes and connections between pairs of objects as edges. TDA extends this framework by allowing connections between arbitrary numbers of objects in a generalization of a network called a simplicial complex.

Criteria for constructing simplicial complexes ensure that their structural features can be detected using tools from linear algebra. Therefore, once the appropriate simplicial complexes are defined, their subsequent quantification is automated and efficient. Additionally, TDA reveals hierarchical structure and requires few parameter choices. Using these techniques, we can measure a range of features in an antibody. This allows for classification of structures which emerge across different portions of molecular dynamics simulations. It

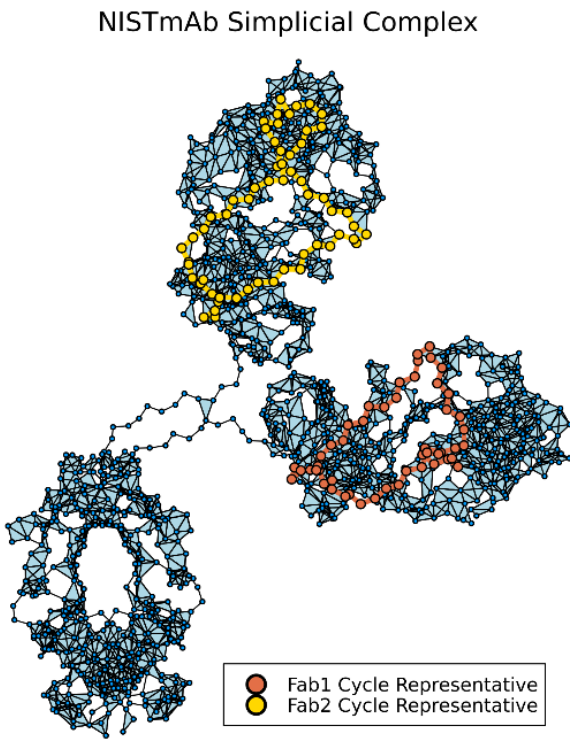

Figure 42. *NIST mAb simplicial complex.*

also provides a tool for comparing different types of antibodies. We have developed TDA matrix summaries which yield good classification of simulated glycosylated versus aglycosylated conformations of the NISTmAb Fc domain [4]. We expect this work to result in a better understanding of the NISTmAb as well as guidelines for other researchers interested in biomolecular feature extraction using TDA.

[1] National Institute of Standards and Technology (NIST). NIST Monoclonal Antibody Reference Material 8671. https://www.nist.gov/programs-projects/nist-monoclonal-antibody-reference-material-8671, 2023. Accessed 10/31/2023.

[2] C. Bergonzo and D. Travis Gallagher. Atomic Model Structure of the NIST Monoclonal Antibody (NISTmAb) Reference Material, 7 2021.

[3] C. Bergonzo, J. T. Hoopes, Z. Kelman, and D. T. Gallagher. Effects of Glycans and Hinge on Dynamics in the IgG1 Fc. *Journal of Biomolecular Structure and Dynamics* **42**:22 (2024), 12571-12579.

[4] M. Kleczynski, C. Bergonzo, and A. J. Kearsley. Spatial and Sequential Topological Analysis of Molecular Dynamics Simulations of IgG1 Fc Domains. *Journal of Chemical Theory and Computation*, to appear.

High Performance Computing and Visualization

Computational capability continues to advance rapidly, enabling modeling and simulation to be done with greatly increased fidelity. Doing so often requires computing resources well beyond what is available on the desktop. Developing software that makes effective use of such high-performance computing platforms remains very challenging, requiring expertise that application scientists rarely have. We maintain such expertise for application to NIST problems. Such computations, as well as modern experiments, typically produce large volumes of data, which cannot be readily comprehended. We are developing the infrastructure necessary for advanced interactive, quantitative visualization and analysis of scientific data, including the use of 3D immersive environments, and applying the resulting tools to NIST problems.

High Precision Calculations of Fundamental Properties of Few-Electron Atomic Systems

James Sims
Maria Ruiz (University of Erlangen, Germany)
Bholanath Padhy (Khallikote College, India)

https://www.nist.gov/itl/math/computation-atomic-properties-hy-ci-method

NIST has long been involved in supplying critically evaluated data on atomic and molecular properties such as the atomic properties of the elements contained in the Periodic Table and vibrational and electronic energy level data for neutral and ionic molecules contained in the NIST Chemistry WebBook. Fundamental to this work is the ability to predict, theoretically, a property more precisely than even the best experiments. It is our goal to be able to accomplish this for few-electron atomic systems.

While impressive advances have been made over the years in the study of atomic structure in both experiment and theory, the scarcity of information on atomic energy levels is acute, especially for highly ionized atoms. The availability of high precision results tails off as the state of ionization increases, not to mention higher angular momentum states. In addition, atomic anions have more diffuse electronic distributions, representing more challenging computational targets than the corresponding ground states.

In the past two decades, there have been breathtaking improvements in computer hardware and innovations in mathematical formulations and algorithms, leading to "virtual experiments" becoming a more and more cost effective and reliable way to investigate chemical and physical phenomena. Our contribution in this arena has been undertaking the theoretical development of our hybrid Hylleraas-CI (Hy-CI) wave function method to bring sub-chemical precision to atomic systems with more than two electrons.

Hy-CI has from its inception been an attempt to extend the success of the Hylleraas (Hy) method to systems with more than three electrons and hence is an attempt to solve not just the three-body problem but the more general N-body problem [1]. Fundamental to the method is the restriction of one r_{ij} per configuration state function (CSF). (For atomic systems with greater than four electrons, all relatively precise calculations nowadays adopt the Hy-CI methodology of one r_{ij} term per CSF.) In the case of three electron lithium systems, we have computed four excited states of the lithium atom to two orders of magnitude greater than has ever been done before [2]. At the four-electron level, to get truly precise chemical properties like familiar chemical electron affinities and ionization energies, it is important to get close to the nanohartree level we achieved for the three-electron atom, a significantly more difficult problem for four electrons than for three. By investigating more flexible atomic orbital basis sets and better configuration state function filtering techniques to control expansion lengths, we have been able to successfully tackle the four-electron case.

Progress to date has included computing the non-relativistic ground state energy of not only beryllium, but also many members of its isoelectronic sequence to eight significant digit precision. With the results from our calculations and a least-squares fit of the calculated energies, we have been able to compute the entire beryllium ground state isoelectronic sequence for Z = 4 through Z = 113 [3]. Li^- (with Z=3), nominally the first member of this series, has a decidedly different electronic structure and was not included in those calculations and subsequent discussions, but that omission has been corrected and we have subsequently carried out a large, comparable calculation for the Li^- ground state [4].

The first member of the Be isoelectronic ground state sequence, the negative Li^- ion, is also a four- electron system in which correlation plays a very important part in the binding. However, due to the reduced nuclear charge, it is a more diffuse system in which one of its outer two L shell electrons moves at a greater distance from the nucleus than the other; hence its nodal structure is different from that of a coupled L shell with an identical pair of electrons. The ground state of the singlet S

state of Li^- is the same type of problem as the first excited state of Be; it is like Be(2s3s), not Be(2s2s). Completing this calculation has provided the necessary insight to enable the calculation of the Be first excited state of singlet S symmetry, Be(2s3s), to an order of magnitude better than previous calculations. Armed with this result, we have been able to continue this level of precision to the Be(2s4s) excited state and have calculated the higher, more diffuse Be(2s5s) through Be(2s7s) states as well, and in the process have demonstrated that Hy-CI can calculate the higher, more diffuse Rydberg states with more complicated nodal structures to the same level of precision as the less excited states [5].

While our work has demonstrated the efficacy of Hy-CI as a solution to the N-body problem for four or more electrons, this work has also shown the presence of a "double cusp" $r_{12}r_{34}$ term type slow convergence problem at the nanohartree precision level which is ultimately built into Hy-CI for four or more electrons. We have investigated a generalization of the Hy-CI method to an exponentially correlated Hy-CI (E-Hy-CI) method in which the single r_{ij} of an Hy-CI wave function is generalized to a form which pairs an exponential r_{ij} factor with linear r_{ij}, producing a correlation factor which has the right behavior in the vicinity of the r_{ij} cusp, and also as r_{ij} goes to infinity. While this was proposed in 2012 and there have been several papers on E-Hy-CI integrals, there were no computational tests until our calculations. Not only has the E-Hy part (the part that differs from conventional Hy-CI) been tested, but E-Hy-CI calculations have been done for spherically symmetrical and non-symmetrical orbitals as well.

The purpose of this research has been to determine how effective exponential correlation factors can be. By comparing convergence of the E-Hy-CI wave function expansion to that of the Hy-CI wave function without exponential factors, both convergence acceleration and an improvement in the precision for the same basis are demonstrated. This makes the application of the E-Hy-CI method to systems with N > 4, for which this formalism with at most a single exponentially correlated and linear r_{ij} factor leads to solvable integrals, very promising. The ground 1 singlet S state non-relativistic energy of He is computed to be -2.9037 2437 7034 1195 9831 1084 hartrees (Ha) for the best expansion [6].

We followed the success on the ground state of the He atom with calculations on the ground 1 singlet S and the 2 singlet S through 6 singlet S excited S states of the Li^+ ion with the same technique, with results comparable to the He atom. This demonstrates the utility of the Hy-CI approach for not only ground but also excited states of S symmetry as well [7]. For a review of high precision studies of both Hy-CI and E-Hy-CI studies of atomic and molecular properties, see [8].

Our interest here is not just the wave functions and energies computed variationally with them, but also ultimately in the computation of atomic properties which the wave functions enable. When the energies are so phenomenally accurate, why not use the wave functions produced to determine important fundamental properties as well? Which brought us to the subject of the third paper in the E-Hy-CI series, computing oscillator strengths for the resonance transition of the helium isoelectronic sequence. To do that, we needed not just wave functions (and energies) for states of ^1S symmetry, but wave functions for states of ^1P symmetry as well.

In contrast to the closed shell $1s^2\ ^1S$ states, the ^1P states are open shell 1s2p ^1P states with the two electrons having different symmetries. The two different orbital exponent basis sets for ^1P are chosen to be representative of the two different electrons; in this case pairing an exponential r_{ij} factor with linear r_{ij} may have an enhanced role to play in providing the right behavior in the vicinity of the r_{ij} cusp and also the right behavior as r_{ij} goes to infinity. This resulted in E-Hy-CI wave functions for both the ^1S and ^1P lowest energy states for the Helium isoelectronic sequence first row (through the O^{+6} ion) which were accurate to 16-20 decimal places and for the ^1P states, the energies were the best ever computed.

The high-precision wave functions were used to compute oscillator strengths (also known as f values and transition probabilities) along with rigorous quantum mechanical upper and lower bounds in order to assess the quality of physical properties computed with these high precision wave functions. Interpolation techniques were used to carry out a graphical study of the oscillator strengths for $1s^2\ ^1S$ to 1s2p ^1P He isoelectronic sequence with rigorous non-relativistic quantum mechanical upper and lower bounds of (0.001 to 0.003) percent and probable precision less than or equal to 0.0000003, the best precision ever achieved. The significance of this work was recognized by the journal *Atoms* making this paper the cover story for the July 2023 issue [9].

Work is presently in progress (at the suggestion of Eli Pollak of the Weizmann Institute of Science, Israel) to compute lower bounds to energies. These are traditionally done by computing matrix elements of the square of the Hamiltonian (H^2), which present formidable mathematical difficulties when dealing with wave functions which have both exponential and linear r_{ij} terms. The Pollak-Martinazzo lower-bound theory [10] is intended to obviate this difficulty by computing variances using only data from the Hamiltonian matrix. However, it turns out that the quality of the ground state lower bound strongly depends not just on the ground state but also on the first excited state (and, to a lesser extent on higher states). Consequently, we intend to use E-Hy-CI wave functions to calculate the five lowest ^1S states of He I all in one wave function and the five lowest ^1P states of He I all in one wave function.

These wave functions will be used to calculate lower bounds to the energies both by calculating matrix elements of H^2 and by using the Pollak-Martinazzo lower-bound theory; they will also be used to calculate oscillator strengths, including upper and lower bounds, for the 25 lines arising from allowed transitions among these five ^1S and five ^1P states. The results of this study will be not only an assessment of the lower bound results but also oscillator strengths for the n $^1S \rightarrow$ m ^1P transitions (n = 1 to 5, m = 2 to 6) with rigorous upper and lower bounds.

Progress to date has been (1) to develop computer codes for calculating the new radial integrals which occur in calculating matrix elements of the required H^2 operator for Configuration-Interaction (CI) wave functions, (2) to construct a wave function which simultaneously yields high precision non-relativistic energies for the ground state and the first four ^1S excited states of He I, and (3) to obtain lower bounds for wave functions containing CI terms in the expansion. Once the necessary integrals are worked out for E-Hy-CI wave functions containing both linear and exponential r_{12} factors, the goal of determining how accurately lower bounds to non-relativistic energies can be obtained by (1) the traditional path of computing H^2 matrix elements and (2) by utilizing Pollak-Martinazzo lower-bound theory will be realized.

[1] J. S. Sims and S. A. Hagstrom. Combined Configuration Interaction – Hylleraas Type Wave Function Study of the Ground State of the Beryllium Atom. *Physical Review A* **4**:3 (1971), 908. DOI: 10.1103/PhysRevA.4.908

[2] J. S. Sims and S. A. Hagstrom. Hylleraas-Configuration Interaction Study of the 2 ^2S Ground State of Neutral Lithium and the First Five Excited ^2S States. *Physical Review A* **80** (2009), 052507. DOI: 10.1103/PhysRevA.80.052507

[3] J. S. Sims and S. A. Hagstrom. Hylleraas-Configuration Interaction Nonrelativistic Energies for the ^1S Ground States of the Beryllium Isoelectronic Series up Through Z = 113. *Journal of Chemical Physics* **140** (2014), 224312. DOI: 10.1063/1.4881639

[4] J. S. Sims. Hylleraas-Configuration Interaction Study of the ^1S Ground State of the Negative Li Ion. *Journal of Physics B: Atomic, Molecular and Optical Physics* **50** (2017), 245003. DOI: 10.1088/1361-6455/aa961e

[5] J. S. Sims. Hylleraas-Configuration Interaction (Hy-CI) Non-Relativistic Energies for the 3 ^1S, 4 ^1S, 5 ^1S, 6 ^1S and 7 ^1S States of the Beryllium Atom. *Journal of Research of the National Institute of Standards and Technology* **125** (2020), 125006. DOI: 10.6028/jres.125.00625.006

[6] J. S. Sims, B. Padhy and M. B. Ruiz. Exponentially Correlated Hylleraas-Configuration Interaction (E-Hy-CI) Non-Relativistic Energy of the 1 ^1S Ground State of the Helium Atom. *International Journal of Quantum Chemistry* **121**:4 (2020), e26470. DOI: 10.1002/qua.26470

[7] J. S. Sims, B. Padhy, and M. B. Ruiz. Exponentially Correlated Hylleraas-Configuration Interaction (E-Hy-CI) Studies of Atomic Systems. II. Non-relativistic Energies of the 1 ^1S through 6 ^1S States of the Li^+ Ion. *International Journal of Quantum Chemistry* **122**:1 (2021), e26823. DOI: 10.1002/qua.26823

[8] M. B. Ruiz, J. S. Sims, and B. Padhy. High-precision Hy-CI and E-Hy-CI Studies of Atomic and Molecular Properties. *Advances in Quantum Chemistry* **83** (2021), 171-208. DOI: 10.1016/bs.aiq.2021.05.010

[9] J. S. Sims, B. Padhy, and M. B. Ruiz. Exponentially Correlated Hylleraas-Configuration Interaction (E-Hy-CI) Studies of Atomic Systems. III. Upper and Lower Bounds to He-Sequence Oscillator Strengths for the Resonance Singlet S to Singlet P Transition. *Atoms* **11**:7 (2023), 107. DOI: 10.3390/atoms11070107

[10] E. Pollak and R. Marinazzo. Lower Bounds for Coulombic Systems. *Journal of Chemical Theory and Computation* **17:3** (2021), 1535-1547. DOI: 10.1021/acs.jctc.0c01301

Simulation of Dense Suspensions: Cementitious Materials

William George
Nicos Martys (NIST EL)
Jeffery Bullard (Texas A&M University)
William Sherman
Simon Su
Steven Satterfield
Judith Terrill
Luke Hawranick (West Virginia University)

A suspension is a collection of solid inclusions embedded in a fluid matrix. Suspensions play an important role in a wide variety of applications including paints, cement-based materials, slurries, and drilling fluids. Understanding the flow properties of a suspension is necessary in many such applications. However, measuring and predicting flow properties of suspensions remains challenging.

Suspensions can be quite complex, as the suspended inclusions may have a wide range of shapes and a broad size distribution. Further complicating matters is that different matrix fluids may have quite disparate flow behavior. While the simplest type of matrix fluid is Newtonian, where the local stress is proportional to the shear rate, matrix fluid can also be non-Newtonian, exhibiting complex behavior including shear thinning (viscosity decreases with shear rate), shear thickening (viscosity increases with shear rate), viscoelasticity (exhibiting both viscous and elastic properties), or even have a time dependent viscosity (thixotropic).

The dense suspension simulation code, QDPD (a Dissipative Particle Dynamics (DPD) and Smoothed Particle Hydrodynamics (SPH) code which uses Quaternions to track the tumbling of the suspended inclusions), that we have developed is generic in that it can be applied not only to cement, mortar, and concrete, but also

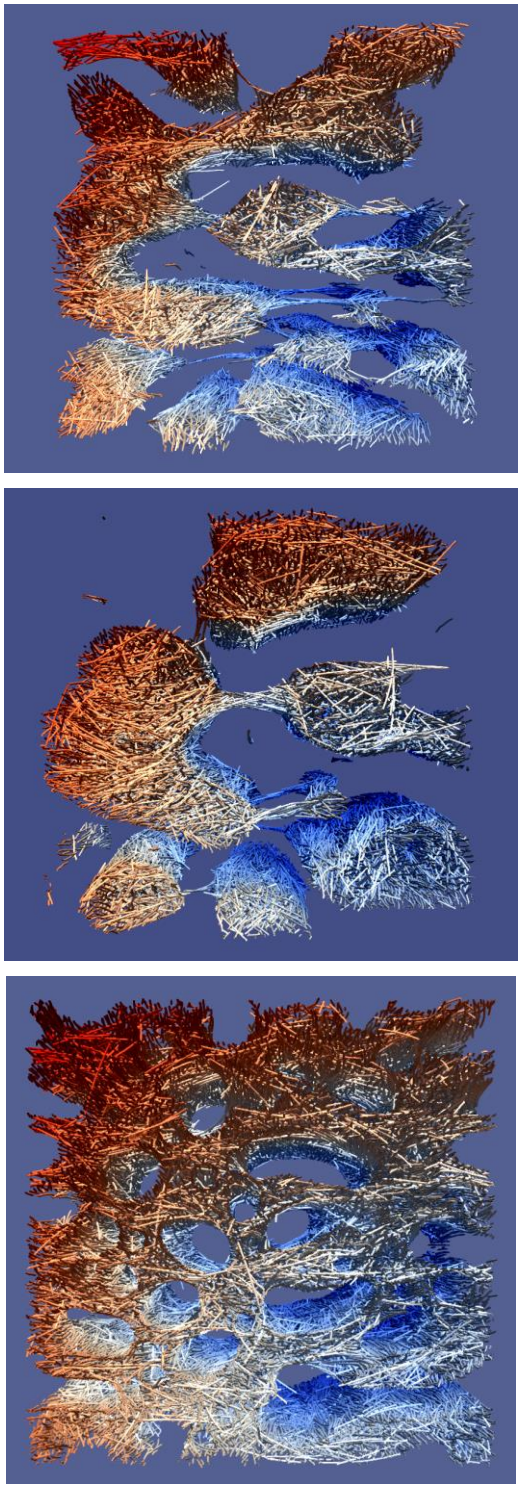

Figure 43. *Top: Late-stage phase separation of non-wetting fibers. The volume fraction of fibers is 10 %. Color indicates the velocity of the particles in the material. Middle: Same non-wetting fiber simulation as in top image, but after it was further strained. Bottom: Later stage phase separation of non-wetting fibers that are very stiff. The volume fraction of fibers in this system is 20 %. Note that at late stages there is the development of tube-like structures built of fibers.*

to any dense suspension of interest including pharmaceuticals such as suspensions of monoclonal antibodies or industrial such as paints and drilling fluids. Although some modification to the code may be needed in each case, QDPD is fully parameterized to handle a wide range of dense suspensions from rocks suspended in a mortar to proteins suspended in a fluid.

Our focus this year has been on studying the rheological properties of High-Performance Concrete (UHPC). These materials are of great interest because of their increased compressive and flexural strength as well as improved toughness and durability. This work is part of a U.S. Army Corps of Engineers project in collaboration with Professor Jeffrey Bullard of the Department of Materials Science and Engineering at Texas A&M University, and Nicos Martys of NIST EL. To simulate the specific UHPC materials of interest to the U.S. Army Corps of Engineers, we have enhanced the capabilities of QDPD to simulate both suspended flexible fibers (with stretching, bending, and twisting) and "stiff" steel fibers (no stretching, bending or twisting). For this study, we are modeling the flow of such fibers in a Newtonian fluid and also in a non-Newtonian shear thinning paste that is similar to materials that are used in UHPC. The computational approach is based on a Smoothed Particle presence of fibers. We are investigating the influence of the wetting properties of the fibers in the fluid medium as well as the effect of stiff angular steel fibers, straight steel fibers, and flexible fibers. When the fibers are non-wetting, they tend to phase separate from the fluid as it is not energetically favorable to be in contact with the fluid. Wetting fibers do exhibit this phase separation behavior. Images from several simulations showing phase separation are shown in Figure 43.

In the last year we completed the simulation of more than 100 different systems of suspended fibers with varying properties, such as volume fraction of fibers, fiber wetting properties, fiber stiffness, and shearing velocity. Early results from these simulations have been presented [1]. A complete report has been written and will be recorded in a NIST Internal Report in 2025. A more focused paper on these results will also be submitted.

Associated with this research, with the help of Luke Hawranick, a 2023 SURF (NIST Summer Undergraduate Research Fellowship) participant, we investigated some performance aspects of the QDPD code, specifically focusing on the inter-process communication used in this highly parallel program. One promising result from this investigation is the possibility of improving the performance of QDPD by re-ordering some of its operations to overlap inter-process communication with computations.

[1] J. Bullard, N. Martys, and W. George. "Rheology of High Performance Cement-Based Materials for Use in Additive Manufacturing." 8th Pacific Rim Conference on Rheology, University of British Columbia, Point Grey Campus, May 15-19, 2023.

HydratiCA: Simulating the Hydration of Cement

William George
Jeffery Bullard (Texas A&M University)
Judith Terrill
Morgan Ko

HydratiCA, a simulator developed at NIST, implements a stochastic reaction-diffusion model of cement hydration [1]. The term hydration refers to the set of chemical processes that occur when cement powder is mixed with water. This mixture subsequently transforms from a fluid suspension (cement paste) into a hardened solid. This process involves complex chemical and microstructural changes. Developing a deep understanding of this process, which would allow accurate prediction of the rates of these changes, is a longstanding goal.

The modeling of cement hydration is challenging due to the many coupled nonlinear rate equations, which describe the chemical reactions that take place over time, all of which must be solved in a highly irregular three-dimensional spatial domain. HydratiCA addresses these challenges with a computational model that has several advantages over others. Parallelization of the model and visualization of the output are important components of this project. With parallelization we can simulate systems that are large enough to be realistic, avoid finite size effects, and complete the simulations in a reasonable amount of time. Visualization of the data produced by HydratiCA is important both for validation and for understanding of the results.

This year we began a collaboration with J. Bullard, of Texas A&M University, along with NIST Guest Researcher M. Ko, to further develop HydratiCA for use on current HPC architectures. Currently this simulator has been shown to efficiently run on several hundred processors of a CPU-based HPC system, i.e. without the use of accelerators such as GPUs. Our goal is to extend the parallelism to utilize GPUs and other accelerators to improve the performance of HydratiCA and reduce the time to solution for materials of interest.

We have also focused on the visualization of these simulations using the ParaView visualization tool which we are extending to work in our CAVE and with head-mounted displays.

This project, which is a re-boot of this research, began in the summer of 2024 and is in its early stages. The code base has been updated to compile and run on NIST's computer cluster, Raritan, and a suite of test and verification runs have been completed as a baseline for this effort.

[1] J. W. Bullard, E. Enjolras, W. L. George, S. G. Satterfield and J. E. Terrill. A Parallel Reaction-Transport Model Applied to Cement Hydration and Microstructure Development, Modeling and Simulation. *Materials Science and Engineering* **18** (2010), 025007.

Standards in Visualization

William Sherman
Sandy Ressler
Simon Su
Judith Terrill

ACMD staff participate in working groups of The Khronos Group related to immersive interfaces (OpenXR), advanced rendering (ANARI), and 3D Formats. As members of these working groups, we participate in weekly meetings and raise issues and offer solutions to help advance the progress of those standards. We also write example software implementations that make use of these standards to provide a template upon which newcomers to the API can learn and extend.

This past year the ANARI specification 1.0 was approved by the Khronos Board of Directors, and the OpenXR 1.1 specification is nearing approval. We also participated in two sub-groups within the OpenXR working group: namely, the OpenXR tutorial development committee, and the Monado open-source development committee.

As part of our commitment to advancing standards in immersive technologies and advanced rendering, we also worked on software that adheres to these standards. We worked with Kitware Inc. to ensure that their VTK and ParaView products both make use of the OpenXR standard, and we performed tests to confirm the operation, and to suggest further improvements. Likewise, we worked with Kitware to add ANARI's rendering SDK as part of the VTK platform. We conducted tests that combined the ANARI and OpenXR standards using VTK and can confirm that these standards work well together. Development will continue on the ParaView project to incorporate ANARI as one of its rendering options. Separately, we continue to develop and test example programs that enable ANARI rendering in the NIST CAVE visualization system though the FreeVR open-source tool.

The 3D Formats Group is responsible for the continued evolution of glTF, a 3D graphics format becoming the "jpeg of 3D." The 3D Formats Group is actively involved in a variety of extensions to glTF. Primarily concerned with achieving high quality and high performance, taking advantage of GPU hardware is a signature overarching goal of the group. glTF is becoming more popular as a representation of 3D objects. Our participation ensures that it is aligned to our, and the public's needs, and keeps us on the leading edge of 3D format developments. glTF is now a formal ISO standard [1].

The NIST ACMD HPCVG team has also worked to promote these standards. We co-hosted a BOF at the SIGGRAPH conference on computer graphics and interaction which included promotion of the ANARI

standard (among other topics). Later, at the Supercomputing conference, we co-hosted a BOF specifically to present accomplishments thus-far and to advocate further adoption of ANARI. We presented the proposed standard at the annual DoE Computer Graphics Forum (DOE-CGF). We also promoted the use of tools that make use of these standards through a tutorial presented at the International Symposium on Visual Computing.

We recently expanded our participation in formal standards development. We were responsible for arranging for NIST membership in the Metaverse Standards Forum (MSF). The MSF has only existed for about two years, yet it already has approximately 2400 institutional members. Although not a formal standards development organization, the MSF is playing a key role in ensuring that many institutions involved with the actual standards development of the metaverse, talk to each other in a productive manner. We actively participate in the 3D Asset Interoperability Group. We participate in the IEEE Metaverse initiative steering committee.

In addition to glTF, the Universal Scene Description (USD) format is also experiencing significant growth. USD has been selected by Nvidia, Apple and Adobe as the main file format for the "metaverse." The MSF is expending significant effort to ensure a high degree of interoperability between glTF and USD. USD is being developed under the auspices of the OUSD (Open USD) organization part of the ASWF (Academy Software Foundation), which is part of the Linux Foundation. USD is under the care of an organization with a history of successful ISO standards development, and we continue to advocate for high degrees of interoperability.

HPCVG serves as an "Outreach Coordinator" for the 3D Formats and 3D Commerce groups of The Khronos Group. They publish on average three posts each week on LinkedIn and are receiving between 2000 to 10000 views for each post. It is raising the visibility of these groups for The Khronos Group significantly.

[1] ISO/IEC 12113:2022, Information Technology, Runtime 3D Asset Delivery Format, Khronos glTF 2.0.

[2] S. Su. "Future XR Technologies, Wearable Devices, and Content Authoring Tools for Immersive Collaborative Learning." The Learning Multiverse: Immersive Technologies (IM-TECH) in Training and Education, George Mason University, September 7, 2023.

[3] W. Sherman and J. Amstutz. "An Overview of ANARI 1.0: The Industry's First Open Standard, Cross-platform 3D Rendering Engine API." SIGGRAPH 2023, Khronos Developer-Day Birds of a Feather, August 9, 2023. URL: https://www.youtube.com/watch?v=PAJYWvRdgaU

[4] W. Sherman. "Portable and Scalable 3D Rendering using ANARI." DoE Computer Graphics Forum 2023, Idaho Falls, ID, April 26, 2023.

[5] W. Sherman and S. Su. "Immersive Visualization with the ParaView Open-Source Tool: A Tutorial." International Symposium on Visual Computing (ISVC), South Tahoe, NV, October 16, 2023.

[6] S. Ressler. "Virtual Reality the Metaverse and All that Reality Stuff." USPTO Patent Examiner Training, Online, May 9, 2023. URL: https://slides.com/d/xYg-nkEk/live

Transition to Open-Source Visualization Software

Michael Bailey
William George
Terence Griffin
Sandy Ressler
Steven Satterfield
William Sherman
Simon Su
Judith Terrill
Cory Quammen (Kitware)
Scott Wittenburg (Kitware)

As part of our research on immersive measurements and analysis, the ACMD High Performance Computing and Visualization Group (HPCVG) operates a fully immersive visualization environment (IVE) and has developed high end visualization (HEV) software to run it. We started developing software for our IVE more than two decades ago. During this time, we have upgraded and rewritten this software as our understanding of scientific visualization in an IVE developed and as outside innovations in hardware appeared. However, there were many limitations to our software. For example, it could only run on one specially configured operating system, and it had not kept up with recent advances in hardware visualization capabilities.

Our IVE is on a critical path for the success of collaborations with several NIST research groups and is used at every stage of these collaborations. These projects are wide ranging and span applications from nanotechnology to medical to materials, and often contribute to standard reference data and materials. For example, the IVE was essential in the success of NIST's development of standard reference materials (SRMs) for the measurement of the flow of cement paste, mortar, and concrete.

To take advantage of recent advances in visualization hardware, we are moving our IVE to ParaView, a fully open-source software environment. The ParaView software system is complex. Internally it uses a pipelined and proxy-based framework. The software consists of a Qt interface, which uses over 2000 VTK C++ classes to produce visualizations. It runs in an IVE as well as on Windows, Mac OS X, Linux, IBM Blue Gene, Cray and various Unix workstations, clusters, and supercomputers. It supports rendering shaders. It has a new real-time path-tracing back end using NVIDIA RTX technology. Thus, ParaView extends the environments

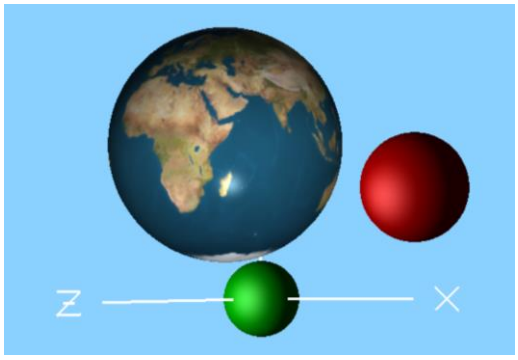

Figure 44. *Three examples of the pixel based "fatpoints graphics" shader.*

that the HPCVG HEV can work in, as well as provides access to real time ray tracing and global illumination made possible with modern GPUs. Access to high-end GPU rendering will continue to grow as ParaView adopts the ANARI rendering standard from the Khronos Group.

For the past two years we worked closely with Kitware, which maintains ParaView, on the ParaView Desktop, CAVE Interaction Plugin, and XR Interface Plugin's Collaboration mode. We completed the functionality of the CAVE Interaction Python Interaction Style, which is sufficiently powerful to be used by all analysis tasks.

Another new feature added this year is the ability to collaborate between HMD and CAVE-style immersive display systems as proposed in our ITL Building-the-Future project proposal. This feature is now in the prototype stage, and refinements continue to be implemented as we prepare for a public release. In addition, we enhanced the ability to read object representations in glTF (an emerging standard for models) and enhanced the usability features of the existing "Macro" feature of ParaView. As always, these now operational features have been added into the publicly available ParaView software download.

We also enhanced our ability to develop graphics shaders by installing the "*glman*" development environment from Oregon State University. This enables us to work on graphics shaders independent of other environments. We also programmed new "*fatpoints shaders*" which create pixel-based spheres with normal vectors from data points and include many options for customizing the spheres based on data. See Figure 44 for some examples. Other shaders programmed include an oval noise shader, "*fatline shader*", and a "*fatrocket shader*".

Additional open-source software that we continue to explore as part of an expanded suite of available tools for immersive visualization include the ANARI advanced rendering SDK, the VMD molecular visualization tool, and the Vrui suite of immersive visualization tools.

In the coming year we will increase the functionality of the CAVE-Interaction plugin, add a scenegraph capability to ParaView, enhance support for using graphics shaders in the ParaView ecosystem, and add support for interfacing ParaView to modern artificial intelligence (AI) systems.

[1] W. Sherman and S. Simon. "Advances to the ParaView Immersive Interface." Immersive Visualization Laboratories Workshop, IEEE VR, Orlando FL, March 17, 2024.

[2] W. Sherman. "Considerations on Preserving VR Experiences (ideas collected over 30 years)." Archiving VR Workshop, IEEE VR, Orlando FL, March 17, 2024.

[3] W. Sherman. Immersive Visualization with ParaView for HMDs & CAVE VR Systems. Sandia Annual XR Conference, Online, July 24, 2024.

[4] W. Sherman and S. Su. ParaView's Immersive Interface for CAVE and HMD, CAAV Conference, Madison WI, November 14, 2024.

[5] W. Sherman. Integrating ANARI into Virtual Reality. Birds-of-a-Feather Session on ANARI, The International Conference for High Performance Computing, Networking, Storage, and Analysis (SC24), Atlanta GA, November 19, 2024.

[6] W. Sherman, S. Su, and J. E. Terrill, contributors. ParaView 5.13.0. https://www.paraview.org/

[7] W. Sherman, S. Su, S. Wittenburg, S. Satterfield, T. Griffin, and J. E. Terrill. CAVE Interaction Plugin and XR Interface. ParaView Version 5.13.0.

[8] J. Stone, K. Griffin, W. Sherman, and V. Mateevitsi. Organizers: Birds of a Feather: ANARI Open Rendering Standard, The International Conference for High Performance Computing, Networking, Storage, and Analysis (SC24), Atlanta GA, November 19, 2024.

[9] W. Sherman. The Ins and Outs of Fixed-Screen Immersive Displays (aka CAVE-style VR). Tutorial, IEEE VR, Orlando FL, March 17, 2024.

[10] S. Su and W. Sherman. Co-Organizers. Workshop on Immersive Visualization Laboratory – Past, Present and Future, IEEE VR, Orlando FL, March 2024.

[11] W. Sherman and S. Su, editors. Introduction to the Presence Special Edition on Immersive Visualization Laboratories. *PRESENCE: Virtual and Augmented Reality* **33**:1 (2024).

[12] S. Su. "Immersive ParaView for Scientific Visualization." Poolesville High School, Poolesville, MD, October 2, 2024.

Transportable VR System

William Sherman
Simon Su
Judith Terrill

Our transportable VR system (aka "IQ-Station") has proven to be very robust and our enhancements with Immersive ParaView have enabled the use of the setup for

Figure 46. *Students identify geographical features using Immersive ParaView on an IQ-station brought to their classroom.*

Figure 47. *IQ-Station (along with head-mounted displays) being demonstrated at the Supercomputing 24 Conference in Atlanta*.

ad hoc immersive visualization. Collaborating with Poolesville High School (Poolesville MD), we were able to setup the transportable VR system to study the usability of our immersive scientific data visualization and exploration tool suite by the students in the classroom. Using the binary downloaded from ParaView website[17], we were able to use "CAVE Interaction Plugin" to support 3D immersive visualization and interaction of the visualization pipeline setup in ParaView by students as shown in Figure 46. The same ParaView binary is also available for use by the larger scientific community.

The system was also demonstrated at the Supercomputing 2024 conference in Atlanta, GA; see Figure 47. There we showcased use of collaborative features we recently developed in collaboration with Kitware, enabling joint visualization of immersive ParaView across XR Interface and CAVE Interaction plugins.

WebXR Graphics and Standards

Sandy Ressler

"XR" is a term that covers VR (virtual reality), AR (augmented reality) and MR (mixed reality). "WebXR" is a version of XR that is intimately connected to the Web. You go to a web page, click on the appropriate link and you become immersed into the application. You remain in the browser, but you are interacting with the application while wearing a headset that presents stereo imagery. Interaction is usually accomplished via specialized controllers or your hands but not the keyboard. The ability to use web pages with XR content with or without VR hardware makes these pages more widely useful as they do not depend on what is still exotic hardware. Simply put, 3D content utilizing XR standards can be made useful whether or not you have immersive hardware. Another related effort is OpenXR which is a formal standards effort led by the Khronos Group working to standardize the interface to headsets, position trackers and controllers.

In the case of AR, you remain in the real world because you still see the real world, with the graphics as an overlay. If you look at the real world, say via the camera of a cell phone, you might get a popup giving you directions with an arrow overlay for where to turn if walking, for example. AR will undoubtedly become the dominant form of virtual graphics when the form factor for displays are modified glasses which can be worn all day.

DLMF Explorer. The Digital Library of Mathematical Functions (DLMF)[18] is a long-standing project that continues to impact the physical sciences by providing essential reference data on the properties of commonly used functions. We are providing new interfaces to the graphics portion of the DLMF primarily as a way to illustrate the large variety of surfaces represented in the DLMF and as an eye grabbing educational tool.

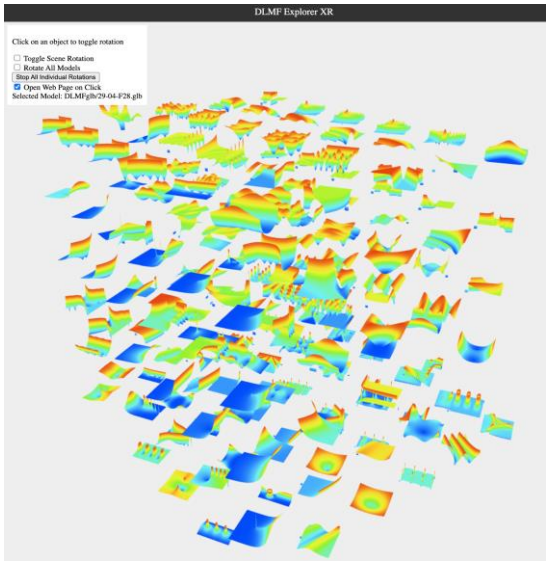

Figure 45. *Screenshot of the DLMF Explorer interface to all the DLMF surfaces.* See https://sandyressler.com/dlmf/threejs/dlmfGridWindow.html

[17] https://www.paraview.org/

[18] https://dlmf.nist.gov/

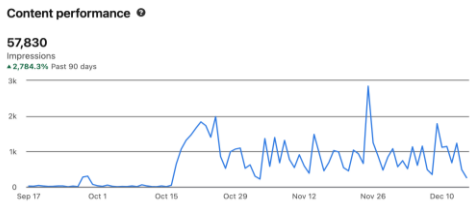

Figure 48. *Analytics of outreach LinkedIn posts for Khronos Group.*

3D Object Input and Capture. Viewing a 3D object on a web site first requires the object itself. Historically we have obtained our objects either from CAD systems or by visualization data. Missing from that set of objects are representations of "real" objects, artifacts that actually exist in real life. Photogrammetry hardware is becoming widely available. Your smartphone can take high quality images, and some phones have LIDAR hardware as well to capture 3D point cloud data. As hardware costs for capturing the shape and texture of real objects has plummeted, 3D object capture is becoming democratized. We have worked in this area as well.

3D Standards Participation. We are also involved with standards efforts run by the Khronos Group. One working group within Khronos is the 3D Formats Group, and is responsible for the continued evolution of glTF, a 3D graphics format becoming the "jpeg of 3D". The "3D Formats Group" is actively involved in a variety of extensions to glTF. Primarily concerned with achieving high quality and high performance, taking advantage of GPU hardware is a signature overarching goal of the group. glTF is becoming more popular as a representation of 3D objects. Our participation ensures that it is aligned to our, and the public's needs, and keeps us on the leading edge of 3D format developments. The Khronos Group is an industry-led consortium, and the participants are a highly skilled collection of technologists focused on real world practical problems. glTF is now a formal ISO standard, *ISO/IEC 12113:2022 Information technology, Runtime 3D asset delivery format, Khronos glTF 2.0*. For the 2nd half of FY 2024 Ressler was elected as the "outreach officer" for the 3D Interoperability and 3D Commerce groups of Khronos. This has primarily resulted in the creation of posts on LinkedIn to highlight a variety of work by the Khronos group. Many of these posts get approximately two to three thousand views, and we've heard positive comments from numerous sources. In addition, Ressler is a member of the IEEE Metaverse Advisory group. This year he published an article for their inaugural newsletter, "Have I got some metaverse standards for you." [19]

We continue to participate with the Metaverse Standards Forum (MSF). The MSF has only existed for about two and a half years yet already has approximately 2500 institutional members. Although not a formal standards development organization, the MSF is playing a key role ensuring that many institutions involved with the actual standards development of the metaverse, talk to each other in a productive manner. We actively participate in the "3D Asset Interoperability" group.

[19] https://metaversereality.ieee.org/publications/newsletter/have-i-got-some-metaverse-standards-for-you

2D to 3D Visualization and Analysis of Mathematical Model of Infectious Diseases

Simon Su
Dachollom Sambo
Kei Yoshida
Richard Huang
William Sherman
Judith Terrill

Data visualization plays a crucial role in managing and understanding infectious diseases. Here it is primarily used for deductive reasoning and as a communication tool after the modeling work has been completed, such as exploring disease transmission rates and geographic spread, making it easier to identify patterns and trends. Visualization also enhances communication between the simulation researcher and the stakeholders. Visualizations help to convey important information to the public, policymakers, and healthcare professionals, facilitating better decision-making and buy-in. Additionally, it enables real-time monitoring and response, tracking of disease spread, and assessment of intervention effectiveness. Visualization also supports public awareness, research, and global collaboration by standardizing data presentation and promoting data sharing. It aids in analyzing historical trends and making future predictions.

Infectious disease simulations are highly multivariate models which generally also incorporate intricate multivariable interactions. These variables, such as transmission rates, geographic spread, control parameters, demographic factors, etc., need to be visualized wholistically for improved understanding, representation, and presentation of the simulation and the results. Unfortunately, the traditional 2D-visualition and presentation techniques (which are mostly 2D line graphs and charts) of these models do not clearly represent or present multivariate results in ways that facilitate understanding to the policymakers or/and stakeholders who are often the target audience, the ones who are meant to benefit from the disease research.

3D visualizations of the output from mathematical models of infectious disease offer great advantages. Adding the third dimension to visualizations provide better harmonization and integration of multivariate parameters to be concurrently visualized. It also enhances spatial understanding, insight into data interaction, and clearer communication of complex data such as demographical changes, geographical effects, and the effect of control parameters due to temporal changes – controls that can be affected through an immersive (virtual reality) interface. Thus, there is a need to demonstrate to bioscientists how they can benefit from this paradigm shift from 2D to 3D of data presentation and interactions.

This particular research focuses on developing innovative and interactive 3D simulation algorithms and templates for the analysis, simulation, and visualization of infectious disease models by leveraging the advanced capabilities of the Trame[20] and ParaView[21] open-source visualization tools. The multivariate 2D simulations in the mathematical model of [1] have been used as a testbed for the development and validation of our innovative 3D simulation algorithms.

This project is ongoing, with current efforts now focused on advancing/transitioning from simulations based on discrete datasets to continuous, interactive 3D simulations algorithm of time-based infectious disease models. This advancement involves integrating the simulation algorithm into the existing 2D discrete simulation framework and utilizing the capabilities of ParaView to achieve continuous interactive 3D simulation algorithms. This innovation enables dynamic, real-time visualizations, offering deeper insights and improved understanding of infectious disease dynamics.

[1] S. Dachollom and C. Emilian Madubueze. Mathematical Model of The Transmission Dynamics of Lassa Fever Infection with Controls. *Mathematical Modelling and Applications* **5**:2 (2020), 65-86. DOI: 10.11648/j.mma.20200502.13

Explainable Scientific Image Data Analysis: Studies in Condensed Matter

Justyna P. Zwolak
Daniel Schug (University of Maryland)
Craig Greenberg (NIST ITL)
Ian Spielman (NIST PML)
Michael Dorris (University of Maryland)

Machine learning (ML) has become widely utilized in various scientific fields. However, challenges arise when human experts try to better understand the underlying relationships governing the decision-making of the ML model. Yet, in many applications, it is important that the model behaves consistently with expert assessment.

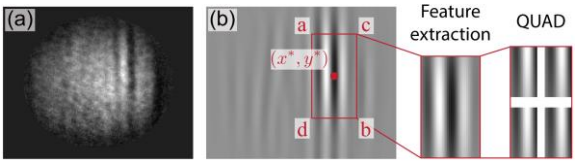

Figure 49. *(a) Sample soliton image dataset. (b)optimal Gabor filter corresponding to (a) annotated with the quadrant feature extraction.*

Image data poses a unique challenge with respect to interpretability, in part due to complex relationships that manifest with increased dimension. The past 20 years have seen a rapid growth of highly accurate computer vision models based on deep neural networks (DNN), demonstrating near-human and superhuman performance for specific tasks. While many such models have found extensive use in science, their black-box nature limits their utility in applications of consequence or exploration, as the models' inner workings are often hidden, obfuscating attempts to understand or verify the reasoning.

We seek to mitigate these challenges for scientific image data, opting away from DNN-type models in favor of explainable boosting machines (EBMs), a cutting-edge family of models capable of delivering superior interpretability without appreciable loss of performance [1]. EBMs enable users to interpret the model's reasoning both globally applying to all decisions and for each local decision. However, these models require tabular input, with each column having a well-defined meaning. To overcome this limitation, we are developing vectorization routines that retain the important information while remaining parsimonious enough to be interpreted by human experts.

In our previous work, we demonstrated the application of this image vectorization for the task of classifying solitonic excitations: solitary waves propagating through Bose-Einstein Condensate (BEC) [2]. The task was to classify images into longitudinal, partial, and vortex classes representing various asymmetries in the resulting wave. The nature of data used in this study poses numerous challenges, both due to the significant class imbalance, as well as the relative similarity of boundary cases. We employed a Gabor wavelet transform (GWT) based vectorization, which was able to capture the discriminative information while remaining openly interpretable, see Figure 49. The resulting features were then used to train an EBM, achieving comparable performance to state-of-the-art DNN techniques.

Building on this work, we now further explore the potential of EBMs in training interpretable models using

[20] https://www.kitware.com/trame

[21] https://www.paraview.org/

a wider variety of vectorization approaches. In addition to the methods initially demonstrated in the conference proceedings [2], we are developing two new methods, where we explore the spectrum of techniques leveraging domain knowledge. The first of these is based on phenomenological modeling [3], a recently introduced method for vectorizing image data. This approach still requires some degree of manual representation design in the form of selecting an adequate model. On the opposite end, we also explore the utility of principal component analysis (PCA) based techniques, which we call EigenSolitons, analogous to work done in facial recognition known as EigenFaces [4]. This approach requires minimal data-specific feature extraction. Both methods will add to the breadth of options afforded by EBM practitioners focusing their efforts on image data.

Revisiting the Soliton dataset, we seek to demonstrate the utility of phenomenological modeling in the context of interpretable classification, enabling useful, trustworthy models that can help scientists learn about the underlying patterns in vast scientific datasets. The techniques and algorithms developed may extend beyond condensed matter physics, allowing their use in other areas of science that benefit from enhanced interpretability.

[1] Y. Lou, R. Caruana, J. Gehrke, and G. Hooker. Accurate Intelligible Models with Pairwise Interactions. In *Proceedings of the 19th ACM SIGKDD International Conference on Knowledge Discovery and Data Mining*, 2013, 623–631.

[2] Daniel Schug, Sai Yerramreddy, Rich Caruana, Craig Greenberg, and Justyna P Zwolak. Extending Explainable Boosting Machines to Scientific Image Data. In *Proceedings of the XAI4Sci: Explainable Machine Learning for Sciences Workshop* (AAAI 2024), Vancouver, Canada, 2024, 1-6.

[3] D. Schug, T. J. Kovach, M. A. Wolfe, J. Benson, S. Park, J. P. Dodson, J. Corrigan, M. A. Eriksson, and J. P. Zwolak. Automation of Quantum Dot Measurement Analysis via Explainable Machine Learning. *Machine Learning: Science and Technology* **6** (2025), 015006.

[4] M. A. Turk and A. P. Pentland. Face recognition using eigenfaces. In *Proceeding: 1991 IEEE Computer Society Conference on Computer Vision and Pattern Recognition*, Maui, HI, 1991, 586-591

Automated Dark Soliton Detection in Bose-Einstein Condensates

Justyna P. Zwolak
Michael Dorris (University of Maryland)
Ian B. Spielman (NIST PML)

Harnessing the power of quantum systems ultimately hinges on measurement: the desired information must first be transferred from a quantum system to a classical measurement system, where the useful quantities in that measurement can then be extracted. Most data in quantum-gas experiments comes from direct images. Absorption imaging—by far the most popular technique—provides information about the atoms' spatial distribution, number, and temperature. While the analysis of such data is sophisticated, features are still detected and located using conventional fitting techniques, which are constrained by our limited ability to anticipate patterns in visual data. Machine learning (ML) techniques have enabled autonomous parameter exploration and optimization in various experiments. However, the use of ML in cold-atom systems remains nascent. Our work aims to fill this gap.

Using cold-atom Bose-Einstein condensates (BECs), we focus on solitonic excitations, robust solitary waves that retain their size, shape, and speed as they travel. These properties arise from an interplay between nonlinearity and dispersion that is present in many physical systems. Since their first observation in water channels, solitons have been found in rivers and seas, BECs, optical fibers, astronomical plasmas, and even human blood vesicles. Due to their inherent stability, solitons in optical fibers have found commercial applications in long-distance, high-speed transmission lines.

While the natural environment does not allow for the controlled study of quantum solitons, BECs are an ideal medium where individual or multiple solitons can be created on demand, with all their properties, such as position and velocity, tuned as necessary [1, 2]. Most measurements in BEC experiments produce raw data in the form of images that, in our context, provide information about the excitations' positions within the BEC.

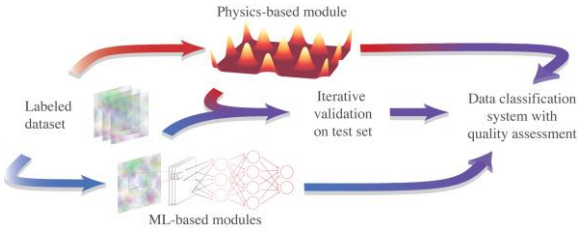

Figure 50. *Framework overview. The colored arrows link the preparation, validation, and application phases of the framework. The red path represents the preparation and implementation of the physics-based module while the blue path represents the ML modules. Adapted from [3].*

The challenge is to identify the number, type, and the exact location of excitations efficiently and reliably. Prior to this work, such information was obtained starting with traditional fits that were then manually validated and corrected [1], inhibiting the automated analysis of large datasets, which is crucial for solitonic dynamics studies.

Dark solitons appear as local depletions in BEC density; thus, visual inspection of the data is often sufficient to determine the number and position of solitons in BEC. Experiments involving solitons' dynamics, however, hinge on large datasets, and human-driven analysis is both tedious and error-prone. Semi-scripted protocols can process the data, but the final decision about the number and position of the solitons within BECs still must be validated manually [1].

In our previous work, we revised the hybrid soliton detection framework that integrates ML techniques with a science-driven analysis, as shown in Figure 50, to include the ability to identify the precise position of solitons along with a model that further refined the classification of the images [3]. This revision also added the ability to determine the quality of the detected solitons. The analysis of the images begins with a ConvNet classifier, followed by an ML object detector (OD) to automatically localize the features of interest (i.e., all solitonic excitations within the BEC). A physics-informed excitation (PIE) classifier then provides a fine-grained classification of individual solitonic excitations into physically motivated categories, such as clear longitudinal solitons, or solitonic vortices. Finally, a quality estimator is applied to the longitudinal solitons class to ascertain if the one-dimensional profile of a given excitation has parameters in the range expected for a well-formed solitonic excitation. This eliminates images of solitons that are faint, or malformed, leaving only well-formed solitons for further analysis.

Our previous work also established and curated a dataset of over 16 000 experimental images of BECs with and without solitonic excitations [4, 5]. The dataset consists of images manually labeled into the three predefined categories (i.e., no excitations, a lone excitation, other excitations; 33 % of the data) and unlabeled data. The lone excitation class is, in addition, tagged with the excitation position, PIE class, and quality score. The remaining 67 % of the data is automatically labeled using the SolDet package. This dataset is available via the MIDAS system at NIST and at data.gov [5] to provide an opportunity for the data science community to develop more sophisticated analysis tools and to further understand nonlinear many-body physics.

The latest iteration of SolDet shifted the ML framework from TensorFlow to PyTorch. Along with this, the file handling and user interface were updated to better support data from multiple sources, and the framework no longer requires a specific group and dataset structure when importing new content from HDF data files. Additionally, the overall structure of the framework has been updated to facilitate modularity of its feature set, as well as supporting user defined functionality to replace or enhance its different modules. Since it has been previously noted in [3] that the quality estimator can be unreliable when two or more solitonic excitations appear close together, changes were made to the physics-informed algorithm to better support multiple excitations in an image.

Our ongoing work in the short term aims to release the revised SolDet and, in the long term, to continue to extend the capabilities of the library. One of these extensions involves adding support for 2D vortex-like excitation identification and tracking, inspired by Ref. [6]. The second extension involves improving the reliability of the PIE classifier. The original iteration of the PIE classifier included physics-informed cuts that were manually derived from the BEC data coming from an experiment located at NIST. To ensure the compatibility of SolDet package with data coming from different experimental groups, we want to refine these cuts using a wider range of datasets on BEC images. These updates will make SolDet a more flexible and useful tool for data analysis for other groups working on BEC experiments.

The autonomous extraction of information from images is a first step toward the demonstration of a holistic approach: combining ML, physics-based simulations, and experiments to enable full automation of quantum technologies. Our next steps include autonomous extraction of the relevant magneto-optic trap (MOT) parameters, optimization of the pulses used to load MOTs, and autonomous optimization and operation of cold-atom experiments.

[1] A. R. Fritsch, Mingwu Lu, G. H. Reid, A. M. Piñeiro, and I. B. Spielman. Creating Solitons with Controllable and Near-Zero Velocity in Bose-Einstein Condensates. *Physical Review A* **101** (2020), 053629.

[2] L. M. Aycock, H. M. Hurst, D. K. Efimkin, D. Genkina, H-I Lu, V. M. Galitski, and I. B. Spielman. Soliton Diffusion in Bose–Einstein Condensates. *Proceedings of the National Academy of Sciences* **114** (2017), 2503-2508.

[3] S. Guo, S. M. Koh, A. R. Fritsch, I. B. Spielman, and J. P. Zwolak. Combining Machine Learning with Physics: A Framework for Tracking and Sorting Multiple Dark Solitons. *Physical Review Research* **4** (2022), 023163.

[4] Dark Solitons in BECs Database. NIST, 2022. DOI: 10.18434/mds2-2363

[5] A. R. Fritsch, S. Guo, S. M. Koh, I. B. Spielman, and J. P. Zwolak. Dark Solitons in Bose–Einstein Condensates: A Dataset for Many-Body Physics Research. *Machine Learning: Science and Technology* **3** (2022), 047001.

[6] F. Metz, J. Polo, N. Weber, and T. Busch. Deep Learning Based Quantum Vortex Detection in Atomic Bose-Einstein Condensates. *Machine Learning: Science and Technology* **2** (2021), 035019.

Machine Learning Applications in Laser Cooling and Trapping Atoms

Michael Doris (University of Maryland)
Justyna P. Zwolak
Ian Spielman (NIST PML)

Successful trapping and cooling of atoms requires the coordination of many pieces of equipment which must follow a specific sequence of events. A typical sequence could be described by hundreds of parameters, which can make optimization attempts challenging and time-consuming. These sequences are composed of human written stages, which constrains the searchable space for optimization efforts and could prevent a more optimum configuration from being discovered. A proposed solution to this is the use of machine learning (ML) to produce a compressed representation of experimental sequences that forms the parameter space to be optimized. The output of configurations in this space can then be used to generate new sequences that are not necessarily limited by some predefined timeline of events.

Currently, we are using neural networks (NN) to learn a representation of a typical cold atom sequence and produce a latent space whose dimensionality is reduced. This is done by collecting the command signals sent to the devices that take part in a laser cooling and trapping sequence and training an ML model to reproduce them. Once a compressed representation is obtained, this space can be modified to produce altered signals, which can be sent to the control software [1].

A basic interface has been written to integrate these models into control software and enable external optimizers to modify the compressed representation they produce. A typical optimization run would then involve capturing the command data from the equipment after an experimental shot is completed, encoding this into a compressed representation we will call a latent vector, feeding this vector into an optimizer to update the parameters, and decoding this back into a valid control signal to be sent to the experimental apparatus for evaluation.

For the following discussion, we define accuracy in terms of the mean-squared error (MSE) between the output of the model and the original input sequence. Given some input to an encoder and no modification of the resulting latent vector, the model is expected to reproduce the input as closely as possible. Models that have a lower MSE score across all sequences are categorized as good and are then rated on their ability to generate new sequences. Any new sequences that result from modifications of the latent vector are expected to not produce drastically different output. A model is determined to perform better by achieving a lower MSE while also generating well-behaved output.

Initially, several ML model architectures and data processing techniques were tested to reproduce a single

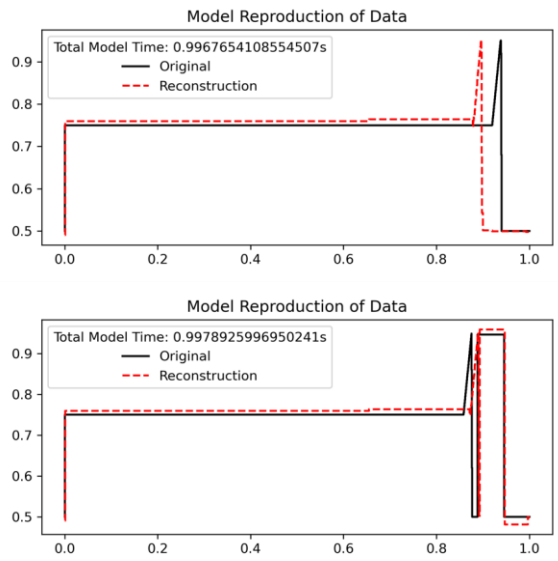

Figure 51. *Output from the transformer model of two command signals. The model can reproduce sequences that are converted into data the control software understands. The model gets close to the actual output, but still occasionally commands inputs shifted in time.*

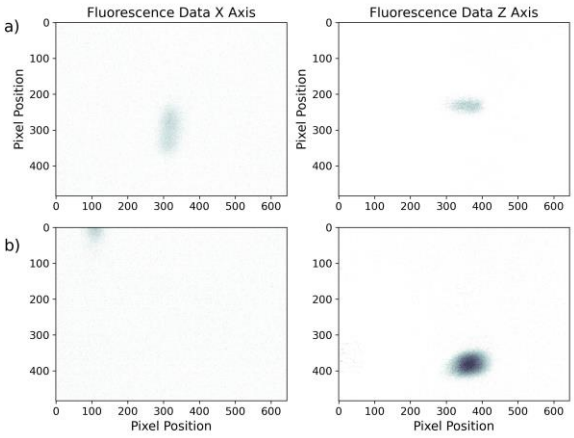

Figure 52. *Example of outputs from runs that successfully generated a trapped cloud of atoms. In (a) the model was able to generate a cloud somewhat central in the trapping region, but the resulting trap was weak with a smaller number of atoms. In (b) the model generated a stronger trap with more atoms, but this was translated away from the center of the trapping region.*

command signal whose latent space can be modified and sent to the control system. The most successful model was a fully connected encoder-decoder network based on the Transformer architecture [2], which produced well-behaved latent spaces and signal commands with a small error, see Figure 51.

Once single signal performance was demonstrated, we moved on to creating models that could output an arbitrary number of device sequences. This task required exploring model architectures better suited for this data. The best-performing model so far has been a combination of recurrent neural networks (RNN) with attention

mechanisms in an encoder-decoder architecture. This model uses the PyTorch implementation of the attention mechanism from the Transformer architecture and the PyTorch implementation of the Gated Recurrent Unit [3]. Although the output has not been as accurate as the single signal models, this multi-signal model has successfully generated a trapped cloud of atoms, see Figure 52. Data collection methods also required adjustment to support the multi-signal objective, and a good amount of time was spent improving the collection methods, preprocessing, and augmentation of the data to be used by the models. We now have a robust module that can be employed in multiple labs to collect large amounts of data for training and validation.

Despite this success, many latent vectors do not produce output that is sufficient to produce valid trapping sequences. Additionally, as the number of devices and the length of the sequences increase, training these models becomes more time-consuming and challenging. Our next course of action is to improve the amount of information compressed into the latent vectors by the model's encoder and improve the regularization of this space. We are also continuing to test different combinations of neural network topologies to improve reproducibility and training time. Once more consistent output is achieved, we will begin the optimization process, compare its performance to more traditional methods, and search for novel sequences during cooling and trapping.

[1] P. T. Starkey, C. J. Billington, S. P. Johnstone, M. Jasperse, K. Helmerson, L. D. Turner, and R. P. Anderson. A Scripted Control System for Autonomous Hardware Timed Experiments. *Review of Scientific Instruments* **84** (2013), 085111.

[2] A. Vaswani, N. Shazeer, N. Parmar, J. Uszkoreit, L. Jones, A. N. Gomez, L. Kaiser, and I. Polosukhin. Attention Is All You Need. *Advances in Neural Information Processing Systems (NeurIPS)* **30** (2017).

[3] J. Ansel, et al. PyTorch 2: Faster Machine Learning Through Dynamic Python Bytecode Transformation and Graph Compilation. In *Proceedings of the 29th ACM International Conference on Architectural Support for Programming Languages and Operating Systems* (ASPLOS '24), Vol. 2, 929–947.

Nondestructive Characterization of Laser-Cooled Atoms Using Machine Learning and its Applications

Justyna P. Zwolak
Guilherme de Sousa (University of Maryland)
Michael Doris (University of Maryland)
Dario D'Amato (University of Maryland)
Brady Egleston (University of Maryland)
Ian Spielman (NIST PML)

The past decade has witnessed a rapid adoption of machine learning (ML) techniques in the physical sciences [1]. ML tools have demonstrated the ability to identify and learn relevant information based on both simulated and experimental data.

Adding to this body of work, we study the use of ML to estimate the internal properties of laser-cooled atoms – their temperature and atom number – from purely non-destructive fluorescence images, where only scattered light intrinsic to the cooling process is observed. Traditionally, estimation of these properties relied on absorption imaging, a destructive measurement technique, where the trapped atoms are released from the trap and imaged after a period of free expansion, giving access to the velocity distribution [2].

As a proof of concept, we trained several ML models with differing levels of complexity to predict the temperature and number of atoms using two fluorescence images taken at the same time in two different orientations (imaging the $xy-$plane and $yz-$plane), see Figure 53(a). The three ML models we consider are a single-layer linear model, a fully connected neural network (FNN), and a convolution neural network (CNN).

The simplest model, which is the most straightforward to implement, is also the least precise. The FNN can learn the non-linear correlations when the dataset has enough spatial correlation between the fluorescence images. The more complex CNN model builds in translational invariance, which is desirable since the locations of the cloud in the image vary between measurements. The typical error we observed with all models is 5 % to 20 %. For the most accurate CNN models, the error ranges from 3 % to 8 % for temperature and atom number, depending on the specific data preprocessing. This is an ongoing effort, and we expect to see further improvement in the error rate.

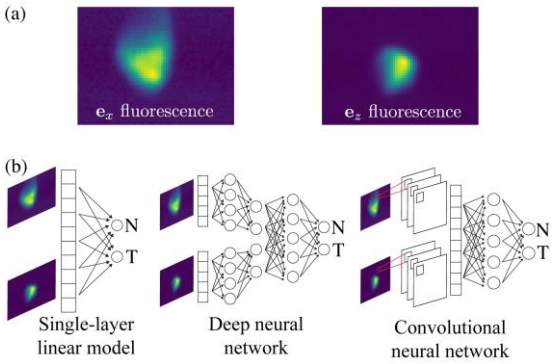

Figure 53. *(a) Sample fluorescence images. (b) The three neural network architectures we use for regression.*

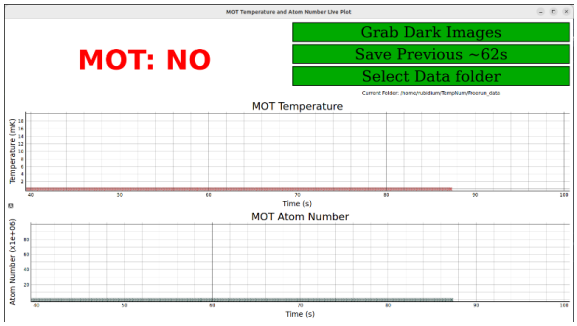

Figure 54. *A draft for the display for the CNN outputs.*

ML models that rely only on non-invasive measurements can be implemented as part of experiments, allowing one to estimate parameters of interest in real time and use that information to guide the evolution of the experiment. One immediate application of the ML models of this work is to use fluorescence images of the cloud to estimate temperature and verify in real time if the cooling techniques are being used efficiently. Closed-loop feedback can be implemented in response to the ML prediction. Using fast and non-invasive measurements, like the fluorescence image, one can estimate physical parameters that can be used to decide which next step to apply or correct and stabilize the system around a particular state. The typical evaluation time for all models is from 0.03 ms to 0.07 ms, which is fast enough within the experimental timescale. A manuscript reporting this work is currently being prepared [3].

Work is also being done to prepare a prototype for a laboratory instrument that performs the real-time estimation described above. Using a lightweight single-board computer (SBC), we downloaded one of the CNNs we had trained for estimating temperature and atom number and hooked up the SBC to computers in our laboratory. We have been able to use the CNN to provide live output of the temperature and atom number (to an attached monitor, see Figure 54) based on two incoming live streams of the possible cloud, currently at about 15 frames per second. A manuscript on this instrument is being prepared as well [4].

The final result of this project will deploy modern, state-of-the-art ML models and tools to speed up and increase the accuracy of cold atom experiments. ML techniques designed to learn complex patterns from output signals and images can also benefit studying quantum phenomena in cold atom systems. Further questions to be answered include an in-depth investigation of the prediction accuracy of the models for different stages of the BEC formation.

[1] S. Das Sarma, D. L. Deng, and L. M. Duan. Machine Learning Meets Quantum Physics. *Physics Today* **72** (2019), 48–54.

[2] P. D. Lett, R. N. Watts, C. I. Westbrook, W. D. Phillips, P. L. Gould, and H. J. Metcalf. Observation of Atoms Laser Cooled below the Doppler Limit. *Physical Review Letters* **61** (1988), 169.

[3] G. De Sousa, M. Doris, D. D'Amato, B. Egleston, J. P. Zwolak, and I. B. Spielman. Nondestructive Characterization of Laser-Cooled Atoms Using Machine Learning. In preparation.

[4] B. Egleston, G. De Sousa, D. D'Amato, M. Doris, I. B. Spielman, and J. P. Zwolak. MOTCOM: An Automated Instrument for Monitoring a Magneto-Optical Trap Cloud In-Situ. In preparation.

A Bayesian Approach to Analyzing Ramsey Data

Donovan Buterakos (University of Maryland)
Justyna P. Zwolak

An important problem in nuclear magnetic resonance (NMR) and related fields is determining the frequency of an unknown oscillatory function using a limited number of measurements [1]. Because measurements can be costly, it is desirable to know the most efficient method for determining the frequency as accurately as possible while requiring the fewest possible measurements.

A simple approach to solving this problem might involve taking some number of measurements uniformly over a given time interval and fitting the result to a sinusoidal function. However, not all data points contain the same amount of information on the frequency of the sine wave. This suggests that the sampling and fitting procedure could potentially be improved by quantifying the expected information gain and optimizing which points are chosen for measurements.

To this end, we develop a Bayesian framework for analyzing Ramsey data and determining at which points additional measurements should be taken. We consider a system where the underlying measurement probability is given by an exponentially decaying sine function as follows:

$$P_{\uparrow}(t) = A\, e^{-(t/\tau)^{\gamma}} \sin(2\pi\omega t + \phi) + b \qquad (1)$$

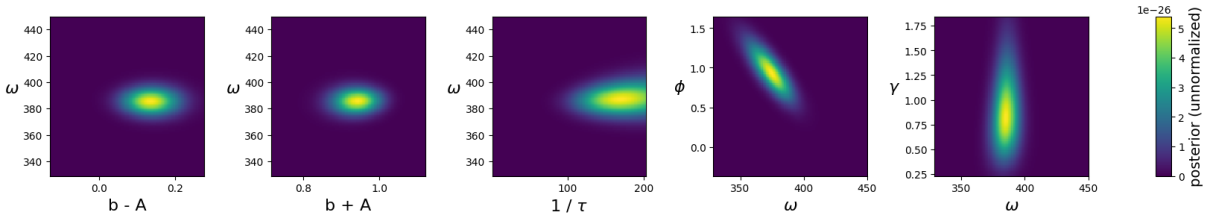

Figure 56. *2D slices of the posterior for a simulated dataset containing 30 t-points, with 10 measurements per point. Note that the only variable significantly correlated to ω is ϕ, as evidenced by the diagonal ellipse in the 4th panel.*

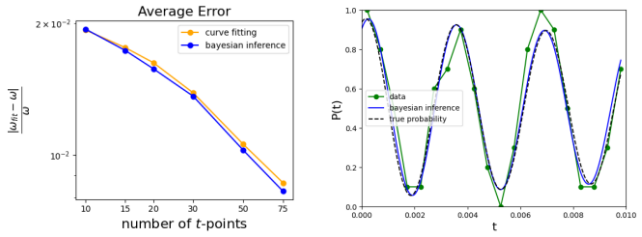

Figure 55. *(Left) Sample dataset, underlying probability function, and Bayesian inference result. (Right) Error, averaged over 1000 datasets, of Bayesian inference and standard curve-fitting. Bayesian Inference seems to perform roughly 3% better.*

where ω is the frequency that we wish to determine, ϕ is the phase offset, and the parameters *A*, *b*, τ, and γ define the wave envelope. Our default approach to analyzing Ramsey data is to make several (in this case, 10) measurements at evenly spaced points *t*, count the proportion of measurements at each *t* that yield spin up, and fit the resulting data to Eq. (1) using a least-squares fit. This serves as a benchmark against which we can compare the Bayesian approach.

The Bayesian approach involves the posterior distribution for the parameters **θ**, given a dataset *D*, as follows:

$$P(\boldsymbol{\theta}|D) \propto P(\boldsymbol{\theta}) * \prod_{(t,y)\in D} P(y|\boldsymbol{\theta}, t) \qquad (2)$$

where $P(\boldsymbol{\theta})$ is the prior knowledge about the parameters (e.g., what intervals they are bounded by), and $P(y|\boldsymbol{\theta}, t)$ is the probability of obtaining an outcome *y*, at a given time *t* with a choice of parameters **θ**, which is given by Eq. (1) for $y = \uparrow$. After defining the posterior, an optimization algorithm is used to find the peak of the posterior, that is, the most likely value of **θ** given the dataset *D*.

We calculate and plot the posterior for simulated datasets, generated by randomly choosing **θ** and then randomly deciding measurement outcomes at various times *t* according to Eq. (1). An example of such a plot is shown in Figure 55. We find that of the five other parameters, only ϕ is significantly correlated to ω. This means that, as long as reasonably accurate choices are made for the envelope parameters, the data can be fit only to ω and ϕ, keeping the envelope constant.

To benchmark our framework, we generate 1000 datasets and fit them with both Bayesian inference and traditional curve-fitting techniques. We compare the inferred value of ω to the value used to generate the dataset and calculate the relative error in each case. We find that both techniques perform similarly well, with the Bayesian approach having roughly 3 % less error. In addition to a minor improvement in accuracy, this Bayesian framework sets the groundwork for future, more complex, Bayesian-informed sampling protocols.

[1] S. Asaad, V. Mourik, B. Joecker, M. Johnson, A. Baczewski, H. Firgau, M. Mądzik, V. Schmitt, J. Pla, F. Hudson, K. Itoh, J. McCallum, A. Dzurak, A. Laucht, and A. Morello. Coherent Electrical Control of a Single High-Spin Nucleus in Silicon. *Nature* **579** (2020), 205–209.

Towards Robust Bootstrapping of Quantum Dot Devices

Justyna P. Zwolak
Danielle J. Middlebrooks
Anton Zubchenko (University of Copenhagen)
Torbjørn Raasø Rasmussen (Univ. of Copenhagen)
Anasua Chatterjee (University of Copenhagen)

Quantum computing is a type of computation whose operations can harness the phenomena of quantum mechanics performed on quantum computers. Most models of quantum computation are based on the quantum bit, or *qubit*, which is analogous to the bit in classical computation. One qubit realization is through quantum dots (QDs). The tuning and management of QD qubits is a large and complex task. To properly form QDs, electrons have to be finely confined in a 3D space. This is achieved through tuning metallic gate electrodes producing electric fields that repel or attract electrons, see Figure 57. Tuning is typically done by human operators and requires hours of work. The more QDs (and gates) one tries to tune, the harder it is to tune them all simultaneously to get qubits that work together properly.

The tuning process – an essential yet repetitive step for the initialization of QD-based qubits [1] – can be divided into a sequence of distinct phases: bootstrapping,

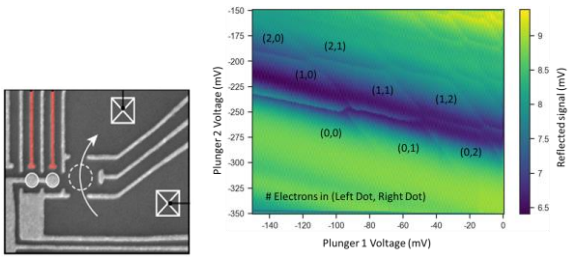

Figure 57. *Device layout (left) and the double quantum dot (DQD) regime (right). The dashed circle represents the region where the sensor QD is formed. Due to its capacitive coupling to the DQD region (marked by two solid line circles), charge sensing can be performed by measuring current or reflected off the sensor QD rf-signal supplied at resonant frequency via the ohmics (represented by crossed squares). The plunger (colored) gates are used to control the quantity of electrons localized in the DQD.*

coarse tuning, charge state tuning, and fine-tuning. Depending on the setup, an additional establishing controllability phase may be carried out after the charge state tuning phase to enable targeted gate control. In this work, we are focusing on the bootstrapping and coarse tuning steps specifically aimed at double QD (DQD) devices with charge sensing capabilities. DQDs host the singlet-triplet realization of qubits, which are currently being investigated as a possible quantum computing platform across the world.

The tools used for automated tuning schemes vary from simple fittings to heuristically defined algorithms to traditional computer vision techniques. A host of machine learning (ML)-based techniques have also been utilized. Most of the tuning efforts focused on the more advanced phases of tuning, assuming that the device is already pre-tuned, with a properly calibrated charge sensor, and that the safety regimes for all gates are already known. However, the initial bootstrapping phase of tuning is still nearly always done heuristically, requiring a highly trained researcher to be responsible for the subsequent decisions on how to adjust the relevant parameters.

Adding to the tuning toolbox, we have developed an automated routine to bridge the gap between the initial device cool-down and a voltage configuration in which other, previously developed automation schemes can take over for a GaAs QD device. One important step of the initial bootstrapping phase is to check which gates are functioning properly and which gates are not. To test this, our algorithm applies a decreasing voltage to each gate, with the aim of confining the electron path and eventually cutting it off entirely, and current is measured through the device. It then invokes a fitting procedure to automatically analyses the curves and extract features relevant for classification and voltages necessary for subsequent tuning stages.

After learning gate-specific parameters, such as voltages at which current saturates and pinches off, the tuning routine proceeds to form a sensor QD that will serve as a detector of the electron transitions taking place between the pair of QDs used to form a qubit. In general, forming a sensor QD is a time-consuming and labor-intensive task as it requires taking a multitude of two-dimensional scans and identification of the Coulomb blockade region by a trained specialist. Our automation facilitates the ray-based detection of the oscillatory behavior – a critical aspect of the Coulomb blockade – thus significantly reducing the task's time complexity [2]. Automation of this process provides an opportunity to quickly diagnose issues with the device, as well as, to efficiently retune the sensor. The formation of a high-quality sensor is a task of paramount importance for quantum computation, as it is essential for a fast qubit readout.

Recently, we have changed the measurement scheme to reflectometry (rf)-based charge sensing that allows the algorithm to see the very first electrons of each QD, something that is typically not possible in current measurements. With the sensor in place, the protocol utilizes a neural network in conjunction with the previously mentioned gate-specific parameters to establish a double QD region. This is achieved by algorithmic control of the plunger gates of each QD to adjust electron occupancy, as well as calibration of the barrier gate to regulate tunneling between the QDs. The results of this project have recently been published in *Physical Review Applied* [3].

The result of this autotuning procedure provides a sufficient starting point for the wide-ranging set of tasks for controlling QD qubits. With this approach, we can expand the applicability of automated tuning schemes to non-ideal devices by requiring a few predetermined assumptions about them. This is especially important when considering future, large-scale QD devices.

[1] J. P. Zwolak and J. M. Taylor. *Colloquium*: Advances in Automation of Quantum Dot Devices Control. *Reviews of Modern Physics* **95** (2023), 011006.

[2] J. P. Zwolak, T. McJunkin, S. S. Kalantre, S. F. Neyens, E. R. MacQuarrie, M. A. Eriksson, and J. M. Taylor. Ray-Based Framework for State Identification in Quantum Dot Devices. *PRX Quantum* **2** (2021), 020335.

[3] A. Zubchenko, D. Middlebrooks, T. Rasmussen, L. Lausen, F. Kuemmeth, A. Chatterjee, and J. P. Zwolak. Autonomous Bootstrapping of Quantum Dot Devices. *Physical Review Applied* **23** (2025), 014072.

MAViS: Modular Autonomous Virtualization System for 2D Semiconductor Quantum Dot Arrays

Justyna P. Zwolak
Anantha Rao (University of Maryland)
Donovan Buterakos (University of Maryland)
Barnaby van Straaten (Delft University of Technology)
Valentin John (Delft University of Technology)
Giordano Scappucci (Delft University of Technology)
Menno Veldhorst (Delft University of Technology)
Francesco Borsoi (Delft University of Technology)

Quantum dots (QDs) are a promising platform for developing quantum information technologies; however, tuning quantum dot devices is a time-consuming and challenging problem. We developed MAViS: Modular Autonomous Virtualization System for Two-Dimensional Semiconductor Quantum Dot Arrays [1], a modular software stack that automates the process of virtualizing the gates of a device. Specifically, it uses a mix of machine learning (ML) and classical image-recognition techniques to analyze charge stability diagrams (CSDs) and calculate the crosstalk between pairs of gates as well as the necessary correction coefficients to apply to neighboring gates. Visually, the crosstalk between plunger gates manifests itself through the honeycomb shapes of the charge state in the CSD; see Figure 58. For barrier, it is indicated through a shift of the charge state within a CSD as the barrier gate is modified; see Figure 59.

The first step of the tuning protocol is to virtualize the sensors, which is straightforward using standard techniques and does not require analyzing CSDs. After the sensors are calibrated, the next goal is to determine the plunger-plunger compensation coefficients. This is done by measuring CSDs for each pair of nearest-neighbor or next-nearest-neighbor dots and analyzing them to highlight horizontal or vertical transitions, as desired. CSDs are processed using an ensemble of convolutional neural network (CNN) pixel classifiers which label each pixel in the image as belonging to one of five classes: horizontal, vertical, interdot, or single-dot transitions, or no transitions. Of these classes, the first three are relevant to MAViS.

A Hough transform is then applied to the identified pixels, and the peaks of the Hough transform correspond to transition lines; see Figure 58. This allows the slopes of the transition lines to be found, from which the compensation coefficients can be calculated. Similarly, the Hough transform also encodes the spacing between transition lines. This spacing, along with the slopes of the transition lines, allows a linear transformation of the plunger voltages to be defined which, when applied to CSDs, orthogonalizes and normalizes the transitions.

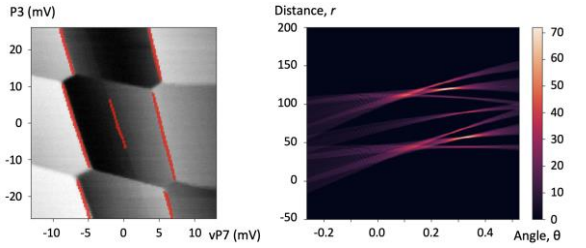

Figure 58. *Left: Pixels classified as vertical transitions by the CNN (plotted in red) overlayed onto the initial charge stability diagram (greyscale). Right: The Hough transform of the red pixels in the left image.*

Finally, the barrier gates must also be virtualized against the (now virtualized) plunger gates. This is done by measuring a series of charge-stability diagrams as a given barrier voltage is adjusted; see Figure 59. For each CSD, the coordinates of the interdot transitions are obtained, and the average change in coordinate values is compared with the change in barrier voltage between each diagram. The ratios of these quantities are used to correct for crosstalk on the barrier gates. This process is then repeated for all barrier-plunger pairs. While linear corrections are sufficient for most gates, in the high-coupling regime additional corrections are needed for neighboring gates. Therefore, after applying the initial correction, a more fine-tuned scan is performed, and quadratic corrections are found.

MAViS was tested on a state-of-the-art, 10-dot QD device in planar germanium [3], showing a great improvement in the tuning time compared to manual calibration. After applying the corrections obtained with MAViS, shifts of the charge states due to crosstalk were greatly reduced or eliminated; see Figure 59. Due to the increasing complexity of QD processors, a full integration of autonomous tuning software will be necessary for industry-scale devices. MAViS represents a significant step towards scalable quantum hardware and is useful for streamlining the tuning process of current experimental devices.

[1] A. Rao, D. Buterakos, B. van Straaten, V. John, C. Yu, S. Oosterhout, L. Stehouwer, G. Scappucci, M. Veldhorst, F. Borsoi, and J. Zwolak. MAViS: Modular Autonomous Virtualization System for Two-Dimensional Semiconductor Quantum Dot Arrays. Preprint arXiv:2411.12516, (2024).

[2] J. Ziegler, F. Luthi, M. Ramsey, G. Zheng, and J. Zwolak. Automated Extraction of Capacitive Coupling for Quantum Dot Systems. *Physical Review Applied* **19** (2023), 054077.

[3] L. Stehouwer, C. Yu, B. van Straaten, A. Tosato, V. John, D. Esposti, A. Elsayed, D. Costa, S. Oosterhout, N. Hendrickx, M. Veldhorst, F. Borsoi, and G. Scappucci. Exploiting Epitaxial Strained Germanium for Scaling Low Noise Spin Qubits at the Micron-Scale. Preprint arXiv:2411.11526, (2024).

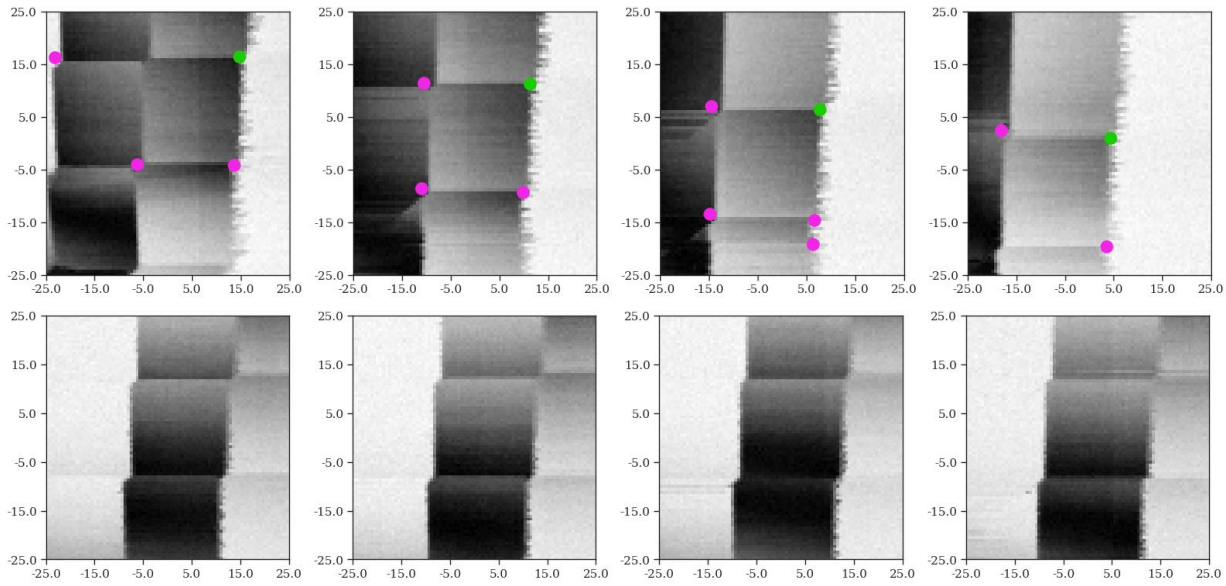

Figure 59. *Top: A sequence of charge-stability diagrams obtained by sweeping a barrier gate from -7.1 to 10 meV. Interdot transitions identified by the pixel-classifier are marked (one specific transition marked in green, all others in pink). Bottom: Charge stability diagrams measured from the same set of gates after corrections obtained by MAViS are applied. Note that there is now basically no shift in the locations of the charge state transitions.*

Introducing BATIS: Bootstrapping, Autonomous Testing, and Initialization System for Quantum Dot Devices

Justyna P. Zwolak
Daniel Schug (University of Maryland)
Tyler Kovach (University of Wisconsin)
Patrick J. Walsh (University of Wisconsin)
Jared Benson (University of Wisconsin)
Mark Friesen (University of Wisconsin)
M. A. Eriksson (University of Wisconsin)

Several promising platforms have been developed to devise scalable qubits for quantum computing, each with corresponding advantages and disadvantages [1]. In our work, we focus on the gate-defined quantum dot (QD) devices with the overlapping gates architecture. One of the big challenges with this platform is the complexity of the device control parameter space: there are many gates that need to be precisely configured, each affecting multiple neighboring gates. A false-color scanning electron microscopy (SEM) image in the top panel in Figure 60 demonstrates the problem. This quad-QD device has 29 connections for an up to 4-qubit architecture.

The QD device tuning and controllability problem is not new, and many community members have been actively researching ways to automate various tune-up tasks [2]. In addition, a more global issue for almost all physical qubit platforms is connecting the abstract qubit to physical experimental devices losslessly at scale while removing scientists from the control loop [3].

In QD tuning, numerous strategies have been employed to enable automated initialization and control of QD devices, many utilizing ML-based methods. However, due to the unique challenges posed by Si/SiGe devices, successful automation has been limited to later tuning steps, such as coarse and charge tuning, with the assumption that device initialization has been performed manually. Bootstrap, on the other hand, requires tuning at significantly higher temperatures and starting with fewer assumptions about device functionality. Although this step involves almost exclusively classical physics, it is vital in the process of initial screening and characterization of QD devices.

The *bootstrapping, autonomous testing, and initialization system* (BATIS) that we developed provides a compact, heuristic approach to automated tuning, focusing on the specific physical steps required to tune arbitrary linear arrays of QDs [4]. BATIS consists of six distinct physical phases: the leakage test, global accumulation, the accumulated leakage test, screening and reservoir gate characterization, forming 1D current channels, and finger gate characterization. Arranged with robust control logic, the resulting algorithm, shown schematically in bottom panel in Figure 60, can automatically determine the functionality and fully characterize the QD device. BATIS is constructed to handle error avoidance in an adaptive manner, curtailing and streamlining the process of debugging and avoiding experimental errors. What makes BATIS fundamentally different from past approaches is that it remains modular and eliminates most device architecture specificity.

BATIS has been experimentally demonstrated in a live environment at a relatively warm temperature of

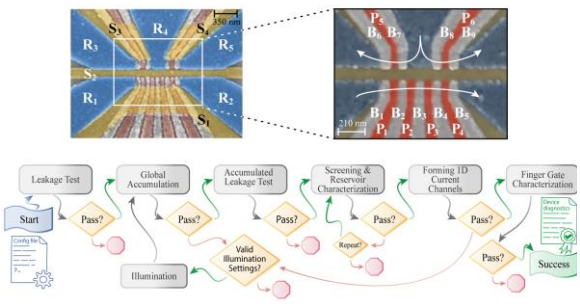

Figure 60. *(Top) A false-color scanning electron microscopy (SEM) image of the quad-QD device highlighting the different types of gates. (Bottom) The flow of BATIS. The algorithm is initialized with a minimal configuration file and returns device characterization and initialization information. BATIS extensively checks the functional status of the device and has a robust loop for handling and responding to error modes.*

1.3 K, eliminating the need to perform a full cooldown to verify the device's functional status. Furthermore, the routine is entirely device agnostic within the class of linear 1D arrays, enabling scientists to quickly validate and test new device architectures in an automated fashion.

In addition to filling an important role in QD tuning, the design and construction of BATIS have led to a more general implementation of QD tuning algorithms. Specifically, due to the modular construction and encoding of universal control logic, the software framework underlying BATIS can be easily adapted to many other tuning tasks. Towards this end, we are developing a more holistic framework designed to accommodate these needs and serve as a community-driven platform for QD auto-tuning. This framework will enable more open development of tuning algorithms and foster new discussions and collaboration in the effort to develop faster, more robust routines for tuning QD devices.

By providing push-of-button convenience for device initialization and testing, BATIS allows scientists to spend time where most needed, setting up devices with minimal involvement. It links between scientists and the bare metal QD gates to act as a tool, probing qubits and other abstract concepts. In the future, BATIS could extend beyond the bounds of traditional software and be reimplemented in hardware to reduce latency or placed on-chip to aid with scalable control, leading towards fully automatic, scalable tuning of QD devices.

[1] S. Resch, U. R. Karpuzcu. Quantum Computing: An Overview Across the System Stack. Preprint arXiv:1905.07240v3, (2019)

[2] J. P. Zwolak and J. M. Taylor. *Colloquium*: Advances in Automation of Quantum Dot Devices Control. *Reviews of Modern Physics* **95** (2023), 011006.

[3] L. M. K. Vandersypen, H. Bluhm, J. S. Clarke, *et al.* Interfacing spin qubits in quantum dots and donors—hot, dense, and coherent. *npj Quantum Information* **3** (2017), 34.

[4] T. J. Kovach, D. Schug, M. A. Wolfe, E. R. MacQuarrie, P. J. Walsh, J. Benson, M. Friesen, M. A. Eriksson, and J. P. Zwolak, BATIS: Bootstrapping, Autonomous Testing, and Initialization System for Quantum Dot Devices. Preprint arXiv:2412.07676.

Optimizing High-Fidelity Readout Using Reinforcement Learning Methods

Justyna P. Zwolak
Harry S. Chalfin (University of Maryland)
M.D. Stewart, Jr. (NIST PML)
Michael Gullans (NIST PML)

Quantum dot (QD) devices are a promising candidate to realize quantum computing platforms. In our work, we focus on silicon spin qubit systems, in which individual electrons can be isolated, manipulated, and measured in a spin readout process [1]. The goal of this project is to develop software tools for automated tuning of high-fidelity readout and control of silicon spin qubits to complement the existing suite of tools for initialization, calibration, and control of QD devices [2].

While we focus on the well-established case of the Elzerman readout [3], the resulting optimization blueprint will be easily adaptable to other measurement schemes. The Elzerman spin readout relies on the coupling of the spin state of a charge state to a current state. The presence or absence of a current signal can then be interpreted as a spin-up or spin-down measurement. However, as the readout becomes noisier, the corresponding fidelity begins to degrade. The chief aim of our work is to investigate whether the redesigning of the control circuit board can improve measurement fidelity, using the max-point method to distinguish signal from noise in the readout phase. The max-point method predicts a spin-up electron if the maximum current signal during the readout phase is greater than a certain threshold and value and predicts spin-down otherwise.

We are currently optimizing Stage 1 of a two-stage RF amplifier circuit, shown in Figure 61, using a set of simulated spin-up and spin-down current traces with varying noise levels. The key circuit element is an ATF-34143 pseudomorphic High-Electricity Mobility Transistor (pHEMT). The circuit outputs filtered versions of traces in which both the signal and the noise have been amplified. While, in the process, additional noise is also introduced due to the components of the circuit board itself, the expectation is that the filtered current traces will have a higher calculated fidelity than the original, noisy traces.

To redesign the circuit board, we use reinforcement learning (RL) methods. In the RL paradigm, the algorithm (called an *agent*) is learning the properties of a

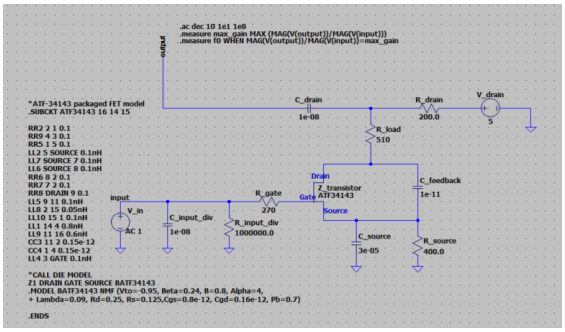

Figure 61. *Stage 1 of a two-stage RF amplifier circuit. Parameters are optimized using RL methods to maximize the fidelity of 1000 input current traces.*

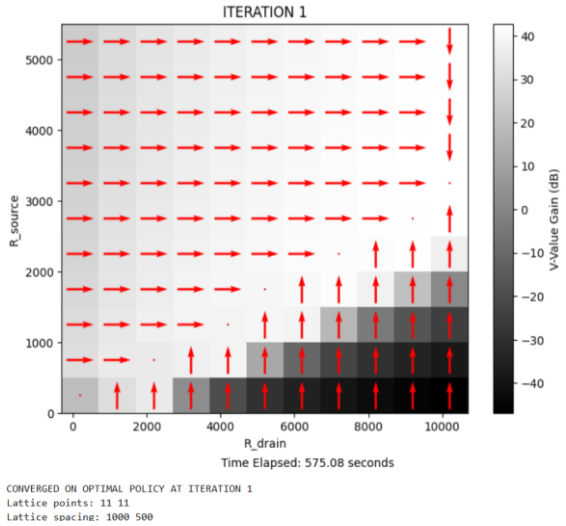

Figure 62. *2D heatmap and arrowmap depicting the RL results for how to maximize the gain by varying* $\boldsymbol{R_{source}}$ *and* $\boldsymbol{R_{drain}}$.

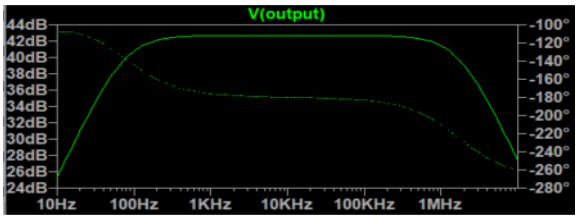

Figure 63. *Gain as a function of frequency for a particular circuit board arrangement. Note the gain is maximized at approximately 10 KHz at a value of approximately 43 dB. The bandwidth, defined as the range of frequencies in which the gain is within 3 dB of its maximum value, is approximately from 100 Hz to 2 MHz.*

dynamical system (called an *environment*) by interacting with it through a series of *actions* and *rewards* that depend on the *state* of the environment changed in response to a given action. The reward is some monotonic function of the fidelity, and the agent learns to maximize the fidelity. The system states are given by the values of the circuit components: V_{in} , $C_{\text{input\_div}}$, $R_{\text{input\_div}}$, R_{gate}, C_{source} , R_{source} , C_{feedback} , R_{load} , R_{drain} , V_{drain}, and C_{drain}. Our goal is to determine the optimal values of each of these components to maximize the overall fidelity. Up until this point, we have been focusing principally on R_{source} and R_{drain}, as it is known that the gain is highly sensitive to these two features. However, eventually, we seek to optimize all parameters.

To maximize the fidelity, there is a tradeoff between maximizing the gain and minimizing the bandwidth, defined as the range of frequencies in which the gain is within 3 dB of its maximum value. For each circuit state, the gain curve as a function of frequency is the key entity that determines how the current traces will be filtered. That is because each current trace can be regarded as a linear superposition over various Fourier frequencies, and it is these frequencies that get amplified by different amounts depending on the filter.

Up to this point, we have not yet concentrated on maximizing the fidelity but rather on the simpler problem of maximizing the *gain* using RL. In a 2D state space (R_{source} and R_{drain}), there are five possible actions: increasing or decreasing one of the two resistance parameters at the time and "no change"; see Figure 62. Actions that would take the agent out of the allowed range for either parameter are explicitly not allowed. We have found that in this configuration the gain appears to be maximized around the slope $R_{\text{source}} = 3/10\, R_{\text{drain}}$. Within the confines of our domain (in which R_{drain} cannot substantially exceed 10 000 Ω), the maximum gain is approximately 42 dB; see Figure 63. However, given that the gain increases as R_{source} and R_{drain} increase, there is good reason to suspect that the gain would increase further if the domain were enlarged.

In summary, our process is as follows: We have a particular circuit board arrangement that corresponds to a specific frequency gain function. The maximum gain, ideal frequency, and bandwidth together define a current trace filter. We simulate 1000 noisy current traces, corresponding to 1000 qubits, each either spin-up or spin-down. Our filter enhances these current signals, and the fidelity is calculated and recorded as a function of the particular circuit board arrangement. RL methods are then used to try to improve the circuit board arrangement, and the cycle begins again. Thus far, we have primarily used the policy iteration algorithm as the RL problem remains fairly simple with only two variables. However, as we consider an increasing number of variables and the problem becomes more complex, we will pivot to more sophisticated RL methods, likely deep Q-networks.

After building up an extensive memory of results and running through many iterations, we expect to identify the optimal circuit board arrangement.

[1] A.R. Mills, C.R. Guinn, M.M. Feldman, A.J. Sigillito, M.J. Gullans, M.T. Rakher, J. Kerckhoff, C.A.C. Jackson, and J. R. Petta. High-fidelity State Preparation, Quantum Control, and Readout of an Isotopically Enriched Silicon Spin Qubit. *Physical Review Applied* **18** (2022), 064028.

[2] J. P. Zwolak and J. M. Taylor. *Colloquium*: Advances in Automation of Quantum Dot Devices Control. *Reviews of Modern Physics* **95** (2023), 011006.

[3] J. M. Elzerman, R. Hanson, L. H. W. Van Beveren, B. Witkamp, L. M. K. Vandersypen, and L. P. Kouwenhoven. Single-shot Read-Out of an Individual Electron Spin in a Quantum Dot. *Nature* **430** (2004), 431.

Principled State Identification for Quantum Dot Data

Justyna P. Zwolak
Brian J. Weber (Intelligent Geometries, LLC)

Confining electrons in arrays of semiconductor nanostructures, called quantum dots (QDs), is a promising approach to quantum computing. Due to the ease of control of the relevant parameters, fast measurement of the spin and charge states, relatively long decoherence times, and their potential for scalability, QDs are gaining popularity as building blocks for solid-state quantum devices. However, the relevant parameter space scales exponentially with QD number (dimensionality), making heuristic control unfeasible. In semiconductor quantum computing, devices now have tens of individual electrostatic and dynamical gate voltages that must be carefully set to isolate the system to the single electron regime and to realize good qubit performance.

There has been recent work using machine learning (ML) techniques as part of the automating process [1]. However, training ML models require large amounts of labeled data indicating the true state of the device for a given voltage range. So far, ML efforts for QD rely on datasets that either come from simulations (and thus may lack some important features representing real-world noise and imperfections) or are labeled manually (and thus are subject to qualitative or erroneous classification). Automatic labeling will streamline creation of large, accurate datasets for purposes of ML training. Moreover, the ML approach currently lacks explainable and interpretable features for reliable diagnostics. It is thus desirable to have a simplified and theoretically motivated automated protocol for labelling experimental data.

The configuration space of a QD array supports irregular polytope tiling of the space, with each polytope indicating a distinct quantum state (e.g., a left or right single QD for a double QD device). The polytope shapes provide information about electron behavior within the discrete states they represent. Polytopes with similar characteristics will cluster together, allowing the subdivision of configuration space into distinct *domains* where the system exhibits a consistent behavior.

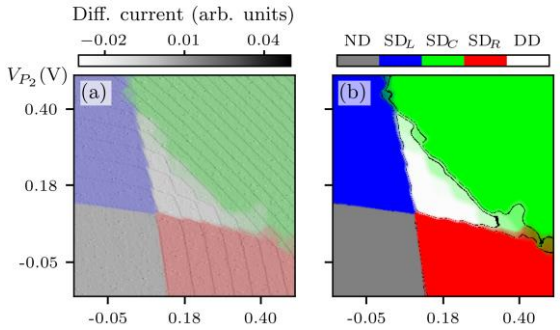

Figure 64. *(a) A probabilistic domain decomposition for a sample noisy simulated device overlaying the charge sensor data. (b) Regions with confidence in the dominant label of at least 70 %. Reproduced from [5].*

Our work is aimed at creating automatic procedures for identifying this domain decomposition and, if possible, automatic characterization of individual polytopes within each domain. The project currently focuses on the case of double QD devices, where the polygonal tessellation is readily understandable. In the past, we have successfully implemented the ray-based domain classification (RBC) schema, the theory behind which was developed in an earlier series of papers from our group [2, 3]. Building on this previous success, we are now developing an RBC-based domain decomposition methods for experimentally acquired large two-dimensional (2D) charge stability diagrams of double QD devices, see the left panel in Figure 64 for an example of such measurement. In this approach, we create a selection of *observation points* (OPs) using a simple centralization technique. From each OP we create a *fingerprint*, which is a list of distances along a set of evenly spaced rays from the OP to the nearest transition boundary along that ray. From each fingerprint we create a polygon model, an idealized representation of the charge region the OP lies within.

From theory, we know these polygons should cluster together by type into well-defined domains—hexagons, colored white in the left panel in Figure 64, should represent double-QD states. However, due to inherent noisiness in the measurements, many of these idealized models can be wrong. This means we cannot create a domain decomposition by individually classifying each polygon.

To overcome such limitations and facilitate the systematic processing of large volumes of experimentally acquired 2D charge stability diagrams, we have been developing tools for automated and unbiased analysis and labeling – *the QD auto-annotator* – that will streamline the creation of the QD data database for purposes of ML. The QD auto-annotator is a noise-robust automatic procedure for domain decomposition and characterization of individual polytopes within each domain. It leverages statistical methods for groupings of systematically similar polygons to create the desired domain divisions and

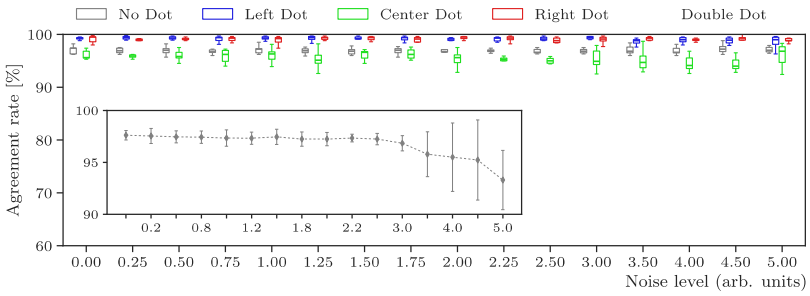

Figure 65. *The performance of the QD auto-annotator on a per-domain basis for different noise levels for the 7 simulated devices. The inset shows an overall performance across all domains and all devices for each noise level. Reproduced from [5].*

the principles of geometry to produce state labels for simulated and experimental double-QD charge stability diagrams. The exact locations where one domain transitions to another are also statistically determined. This is the reason for the "fuzziness" along domain boundaries in the right panel in Figure 64. Moreover, each point receives a probability of being in each of the five domains, which allows for definition of label confidence.

The fingerprinting method, developed in dimension two, is well suited to higher dimensional generalizations, where no serious theoretical barrier exists to using our methods of model-building followed by statistical grouping. Technical hurdles exist in the form of understanding details of high-dimensional geometry, such as ray placement and polytope recognition. A preliminary work on this in the form of creating ray-placement estimates and rough polytope classifications has been completed [2, 4].

An important aspect of developing automated data labeling software is determining the robustness of the method across various noise regimes. Using the ground truth labels assigned at a pixel level during simulations and the QD auto-annotator labels we can quantify both the overall per-device agreement between labels as well as the per-class performance [5]. We observe an overall state assignment agreement at around 97 % when averaged over all devices for noise levels up to 3.00, see the inset in Figure 65. Once the noise level surpasses 3.00, the agreement deteriorates slightly to 95.6(3.3) % at noise level 4.00 and 93.3(2.8) % at noise level 5.00. On a per-domain level the performance is defined as the proportion of correct pixel assignments to the total number of pixels in each of the five domain regions, as determined by the ground truth labels. Figure 64 shows the performance of the QD auto-annotator on a per-domain basis for each noise level for the simulated devices we considered. The ND, SD_L, and SD_R state identifications remain almost perfectly robust up to the highest considered noise level. The SD_L state shows a slight decay in performance at higher noise levels (at around noise level 3.00).

However, no substitute exists for real-world data. Although our methods work against the simulated datasets, relatively few experimental datasets are available. A major project goal is to collect datasets from many research teams around to world to establish a repository of datasets along with standardized labeling created using our methods hosted at data.nist.gov. Such a standardized repository of labelled data is consistent with the mission of NIST and would be of high value to the scientific community.

Another focus of future work is generalizing our methods to higher dimensions, with an aim of creating autotuning strategies for more than two QD at a time. Although theoretically straightforward, new challenges are expected related to high run-time expense and sparsity of available data. Theoretical understanding of higher-dimensional geometry will be a crucial component of this work.

[1] J. P. Zwolak and J. M. Taylor. *Colloquium*: Advances in Automation of Quantum Dot Devices Control. *Reviews of Modern Physics* **95** (2023), 011006.

[2] J. P. Zwolak, S. S. Kalantre, T. McJunkin, B. J. Weber, and J. M. Taylor. Ray-based Classification Framework for High-Dimensional Data. In *Third Workshop on Machine Learning and the Physical Sciences (ML4PS at NeurIPS 2020)*, Vancouver, Canada, December 11, 2020.

[3] J. P. Zwolak, T. McJunkin, S. S. Kalantre, S. F. Neyens, E. R. MacQuarrie, M. A. Eriksson, and J. M. Taylor. Ray-based Framework for State Identification in Quantum Dot Devices. *PRX Quantum* **2**:2 (2021), 020335.

[4] B. J. Weber, S. S. Kalantre, T. McJunkin, J. M. Taylor, and J. P. Zwolak. Theoretical Bounds on Data Requirements for the Ray-Based Classification. *SN Computer Science* **3**:1 (2022), 57.

[5] B. Weber and J. P. Zwolak. QDA^2: A Principled Approach to Automatically Annotating Charge Stability Diagrams. Preprint arXiv:2312.11206 (2023).

Data Generation for Machine-Learning Classification of Quantum Dot Devices

Donovan Buterakos (University of Maryland)
Justyna P. Zwolak
Jacob Taylor (NIST PML)

Quantum dot (QD) qubits are one of the most promising candidate platforms for realizing scalable quantum information technologies, due to their long coherence times, small physical size, and their integration with the current semiconductor industry. However, progress has been slow due, in part, to the difficulty and complexity of tuning QD devices. To date, tuning procedures have involved making many measurements, manually assessing the measured data, adjusting experimental device parameters in response, and repeating this process until the device is in its proper regime of operation. This process is time-consuming, exponentially more difficult with each additional QD added to the device. Thus, finding and automating a scalable tuning procedure is essential to creating industrial devices [1].

In 2020, we proposed using machine learning (ML) classification algorithms as a way to quickly analyze measured data and determine regimes of operation without the need for manual inspection [2]. More recently, by using a clever method of measuring data along so-called *rays* (a collection of evenly distributed one-dimensional (1D) sweeps) expanding outward from a central point, we have drastically reduced the number of measurements required to do so [3]. We have had success using these methods to classify data from experimental double-dot systems [4] and are currently expanding these techniques to larger devices.

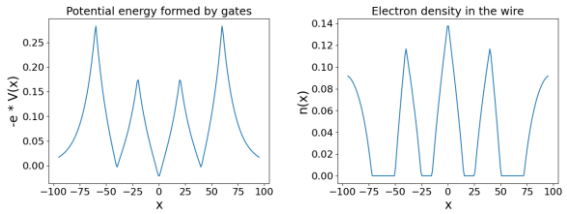

Figure 66. *(Left) The potential energy $\boldsymbol{V}(\boldsymbol{x})$ for a triple-QD device induced by electrostatic gates is input into the Thomas-Fermi calculation. (Right) The resulting electron density $\boldsymbol{n}(\boldsymbol{x})$ is found by solving Eqn. (1) and (2).*

Training ML models require large amounts of labeled data; however, experimental data is expensive and time-consuming to measure, and in addition, data labeling must be done manually. Thus, instead of using experimental data for training the model, we use a physical simulation of the device to create training data. This gives us two advantages. Firstly, data can be generated much more easily using a simulation than by using experimental devices. Secondly, having access to all the parameters of the simulation allows the data to be procedurally labeled, eliminating the need for manual data labeling. Using simulated data to train the ML model raises the concern that the simulation may not precisely reflect the reality of experimental devices. However, for DD devices, ML models trained on simulated data performed exceptionally well when benchmarked against experimental data [4].

Our simulation relies on a self-consistent Thomas-Fermi calculation [5] to solve the set of coupled integral equations for the electron density $n(x)$ of a (1D) nanowire:

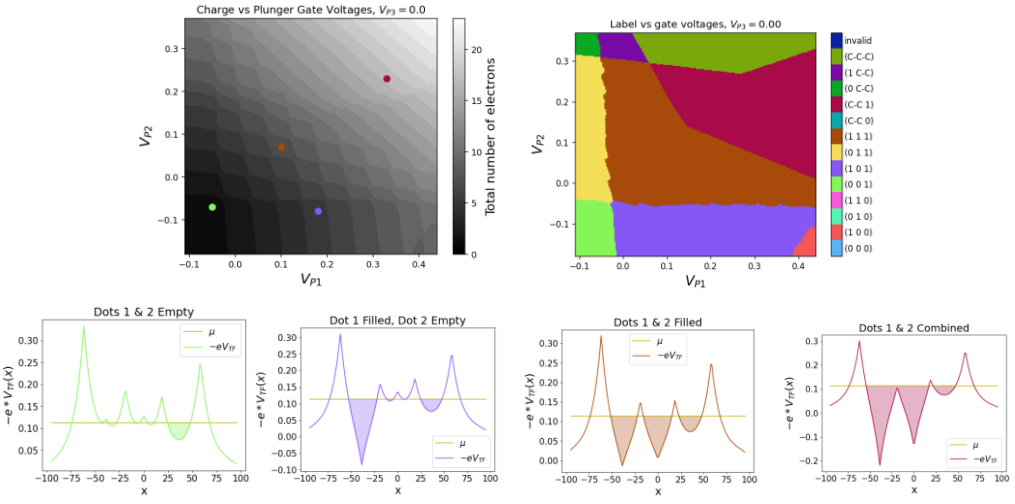

Figure 67. *(Top Left) Charge stability diagram plotting the total charge on the triple-QD device versus the plunger gate voltages on the first two QDs. The third plunger gate voltage is held constant, so this plot is a 2D slice of the full 3D space. (Top Right) State labels of the device for the same parameter space plotted on the left. There are 13 possible states, corresponding to whether each dot is empty (0), filled (1), or if multiple QDs are combined (C). (Bottom) Thomas Fermi potential $\boldsymbol{V_{TF}}(\boldsymbol{x})$ for four different points marked on the top-left plot. They depict how QDs 1 and 2 can be empty, filled, or combined, corresponding to the state labels above.*

$$n(x) = \int_{-eV_{TF}(x)}^{\infty} \frac{g_0}{1+e^{\beta(\epsilon - E_F)}} d\epsilon \quad (1)$$

$$V_{TF}(x) = V(x) - \int n(x')K(x-x')dx' \quad (2)$$

where $V(x)$ is the potential induced by the electrostatic gates, $K(\Delta x)$ is the Coulomb potential, and $V_{TF}(x)$ is the so-called Thomas-Fermi potential, which is the total potential after including a correction from the electron density itself. After the electron density $n(x)$ is calculated (see Figure 66), we can determine the preferred number of electrons that inhabit each QD, which is roughly proportional to the area under $n(x)$.

The voltages of the plunger gates on each of the QDs are varied and the Thomas-Fermi calculation is repeated for each new set of voltages. The total charge on the device is then calculated, and the points are classified into one of 13 classes based on whether each QD is empty, filled, or if two or more QDs have merged together, see Figure 67.

For training the ML model, points are uniformly selected from within the three-dimensional (3D) parameter space, and rays are extended outwards from each central point in multiple directions. For each point, the distance to the nearest transition line in each direction is recorded, along with the state of the central point. By averaging the inverse distance to the transition $\langle 1/distance \rangle$, we can quantify the defining features (so-called *fingerprints*) of each class. We plot the fingerprints of the 13 classes in Figure 68. Crucially, fingerprints have distinct enough features from each other that an ML model can learn to distinguish between them.

The rays we used are partitioned into 3 groups: (A) rays parallel to the +/- *x*, *y*, and *z* axes; (D) rays along the diagonals in each of the *xy*, *yz*, and *xz* planes; and (C) rays extending from the center to the corners of the unit cube. For each group or combination of groups, we train an ensemble of 20 deep neural network classifiers to map a fingerprint instance to one of the 13 charge-state classes. We find that the models can be trained to correctly classify over 94 % of the points with as few as 14 rays (see Figure 69). This accuracy can be improved to 96 % by increasing the number of rays to 30.

The ability to procedurally classify the current operating regime of experimental devices can potentially save large amounts of time and expense when tuning the devices. ML classification is a substantial step towards fully automating the tuning process, which is essential for building scalable devices going forward.

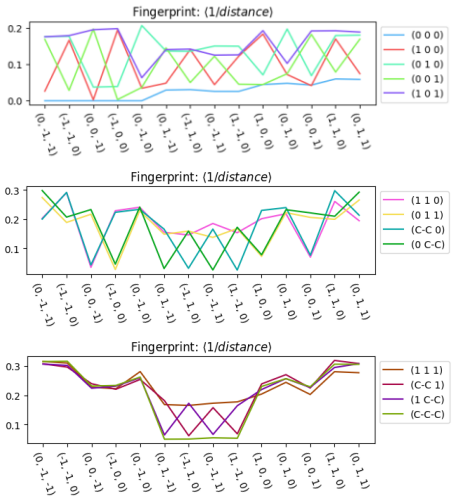

Figure 68. *Fingerprints of the 13 classes, created by averaging* $\langle \mathbf{1/distance} \rangle$ *over all points in a class.*

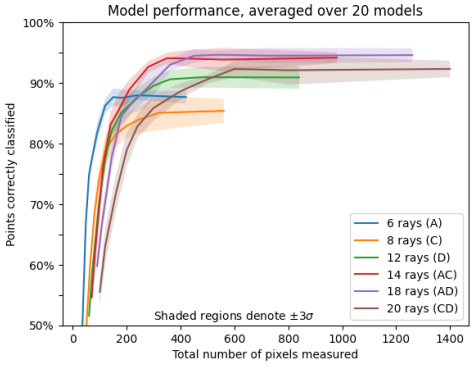

Figure 69. *Model performance as a function of the total number of measurements taken along all rays.*

[1] J. P. Zwolak, J. M. Taylor, et al. Data Needs and Challenges for Quantum Dot Devices Automation. *npj Quantum Information* **10** (2024), 105.

[2] J. P. Zwolak, T. McJunkin, et al. Autotuning of Double-Dot Devices in Situ with Ma-chine Learning. *Physical Review Applied* **13** (2020), 034075.

[3] J. P. Zwolak, T. McJunkin, S. S. Kalantre, S. F. Neyens, E. R. MacQuarrie, M. A. Eriksson, and J. M. Taylor. Ray-Based Framework for State Identification in Quantum Dot Devices. *PRX Quantum* **2** (2021), 020335.

[4] J. Ziegler, F. Luthi, M. Ramsey, F. Borjans, G. Zheng, and J. P. Zwolak. Tuning Arrays with Rays: Physics-informed Tuning of Quantum Dot Charge States. *Physical Review Applied* **20** (2023), 034067.

[5] J. P. Zwolak, S. S. Kalantre, X. Wu, S. Ragole, and J. M. Taylor. QFlow Lite Dataset: A Machine-learning Approach to the Charge States in Quantum Dot Experiments. *PLoS ONE* **13** (2018), e0205844.

Explainable Models for Quantum Dot Qubit Readout

Justyna P. Zwolak
Daniel Schug (University of Maryland)
Joshua Lou (University of Maryland)
Samuel Carter (Laboratory for Physical Sciences)
Adam Mills (Laboratory for Physical Sciences)

Semiconductor quantum dot (QD) devices are one of the promising platforms for realizing scalable quantum computing [1]. One of the big challenges when working with spin-based qubits in QD devices is the complexity of the high-dimensional control parameter space, which needs to be carefully adjusted to bring the device to an operating point. Tuning QD devices automatically requires robust, comprehensive, and precise routines and analysis [2].

There has been considerable interest in applying machine learning (ML) techniques to measurement characterization [2]. However, most of the ML used to date are black-box models that do not provide any insights into the inner workings of the algorithms. At the same time, in certain applications, it is desirable to have techniques that remain consistent with the underlying intuition behind these physical processes. Only recently have the first efforts at using explainable ML in QD autotuning subtasks been demonstrated [3].

The gates and gate combinations used to calibrate and control QD devices can be thoughts of as individual knobs. Any given configuration of knobs puts the system in a state which can be measured by determining how current flows when you vary one or more knobs while leaving the rest fixed. Experimentally, experimentalists heuristically study the effect of these knobs on a given device and learn the relationship between adjustments and the impact those adjustments have on the desired measurements. This poses a significant challenge as devices become more complex. As the number of adjustable knobs grows, the challenge of finding the precise optimal configuration becomes increasingly untenable for human practitioners, necessitating a shift towards automation.

We address this in a twofold fashion: through phenomenological modeling and explainable ML. To obtain meaningful representations of the measurement, we construct a function that 'mimics' the visual characteristics observed experimentally using simple basis functions. This yields a parametric representation of the data which can be immediately traced back to identifiable features of the measurement. The resulting parameters serve as meaningful ML features, ripe for exploration using explainable ML. Using explainable boosting machines (EBMs) [4], we train glass-box models targeted towards a variety of scientific processes, which in turn can be studied and scrutinized prior to deployment.

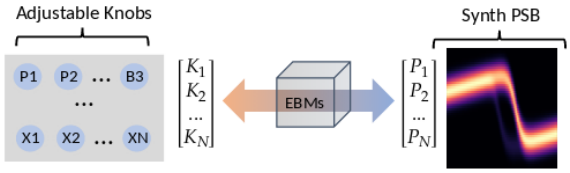

Figure 70. *Flow-chart diagram of process-flow for applying EBMs to map gate to phenomenological model relationships*

We are applying this approach to a tuning sub-problem where the objective is to optimize the result of a Pauli spin blockade (PSB) measurement, a critical prerequisite to qubit formation necessary to perform parity readout [5]. An example of this measurement can be seen in Figure 70. The objective is to determine whether this measurement shows a high-quality PSB measurement and, if not, which knobs need to be adjusted to improve the PSB quality. Our methodology allows us to train models that can actively infer the gate voltage adjustments needed to achieve desired outcomes using phenomenological models. This enables us to obtain parametric representations of the data which are ripe for interpretation using EBMs, giving us a means to ensure that the model holds up to expert scrutiny. Further, the model is constructed such that variations in its parameters directly reflect onto the experiment itself. This is critical, as it enables the model to learn the optimal adjustments directly.

The current phase of this project involves taking hundreds of measurements on a QD device and training models to encapsulate the relationship between adjusting the gate voltages and the desired measurement. The project also involves training models capable of distinguishing qualitative elements such as ideality or viability. The next steps include deploying this system in a live environment, giving the models access to the device in query mode, and allowing the model to learn and improve the measurement process until it reaches the specified optimal regime.

This work paves the way for techniques that will enable automated tuning of medium-scale QD devices, which will streamline the process of designing and testing candidate architectures.

[1] S. Resch and U. R. Karpuzcu. Quantum Computing: An Overview Across the System Stack. Preprint arXiv:1905.07240v3 (2019)

[2] J. P. Zwolak and J. M. Taylor. *Colloquium*: Advances in Automation of Quantum Dot Devices Control. *Reviews of Modern Physics* **95** (2023), 011006.

[3] D. Schug, T. J. Kovach, M. A. Wolfe, J. Benson, S. Park, J. P. Dodson, J. Corrigan, M. A. Eriksson, and J. P. Zwolak. Automation of Quantum Dot Measurement Analysis via Explainable Machine Learning, *Machine Learning: Science and Technology* **6** (2025), 015006.

[4] Y. Lou, R. Caruana, J. Gehrke, and G. Hooker, Accurate Intelligible Models with Pairwise Interactions, In *Proceedings of the 19th ACM SIGKDD International*

Conference on Knowledge Discovery and Data Mining, ACM, Chicago, IL, 2013, 623–631.

[5] A. M. Jones et al., Spin-Blockade Spectroscopy of Si/SiGe Quantum Dots. *Physical Review Applied* **12** (2019), 014026.

Quantum Information

An emerging discipline at the intersection of physics and computer science, quantum information science is likely to revolutionize 21st century science and technology in the same way that lasers, electronics, and computers did in the 20th century. By encoding information into quantum states of matter, one can, in theory, enable phenomenal increases in information storage and processing capability. At the same time, such computers would threaten the public-key infrastructure that secures all of electronic commerce. Although many of the necessary physical manipulations of quantum states have been demonstrated experimentally, scaling these up to enable fully capable quantum computers remains a grand challenge. We engage in (a) theoretical studies to understand the power of quantum computing, (b) collaborative efforts with the multi-laboratory experimental quantum science program at NIST to characterize and benchmark specific physical realizations of quantum information processing, and (c) demonstration and assessment of technologies for quantum communication.

Quantum Information Science

Shawn Geller
Scott Glancy
Emanuel Knill
Alex Kwiatkowski
Lynden K. Shalm (NIST PML)
Arik Agavayan (University of Colorado)
Mohammad Alhejji (University of New Mexico)
Stephen Becker (University of Colorado)
Akira Kyle (University of Colorado)
Karl Mayer (Quantinuum)
James R. van Meter (HRL Laboratories, Palo Alto)
Akshay Seshadri (University of Colorado)
Ariel Shlosberg (University of New Mexico)
Ezad Shojaee (IonQ)
Yanbao Zhang (Oak Ridge National Laboratory)

Quantum computing research has recently witnessed the first demonstrations of good fidelity 100 quantum bit (qubit) quantum computers with logical qubits closing in on having error lower than that of the physical qubits. These advances are rapidly progressing toward the realization of anticipated quantum advantages in computation, communication and measurement. Progress in quantum computing is perhaps the most visible result of research in the broad field of quantum information science.

ACMD has a long history of supporting quantum information science from foundations to implementation. Recent fundamental research performed by ACMD researchers in this field includes

- development of broad band pulsed (BBP) homodyne for measuring broad-spectrum light pulses,
- quantification of fidelity of homodyne measurements,
- efficient and robust statistical methods for certifying quantum device quality,
- boson sampling bunching and complexity, and
- improved security analysis of a quantum key distribution (QKD) protocol.

BBP Homodyne. Standard pulsed homodyne is a technique for measuring the complex amplitude or quadrature of a pulse of a signal light field. It involves combining the signal with a strong reference pulse (the local oscillator (LO)) and measuring the result with two photodetectors whose output is proportional to the number of photons in the pulse. Conventional photodetectors cannot efficiently measure octave-spanning pulses of light. Such pulses are increasingly common as witnessed by the many applications of femto-second pulsed lasers. Measurement of octave-spanning pulses is also needed to experimentally access fundamental features of relativistic fields.

ACMD researchers and their collaborators realized that broad-band efficiency is potentially achievable with calorimeters, but calorimeters measure energy, not number of photons. This motivated ACMD researchers' discovery that the homodyne measurement technique can be generalized to detectors such as calorimeters. The generalization requires a change of the LO pulse. They found that the well-known properties of homodyne still hold, including convergence of the moments of the measurement outcomes to those of the ideal quadrature measurement as the LO strength increases [1].

Quantification of Homodyne Fidelity. Optical quantum processing and computing based on continuous variable (CV) techniques heavily rely on homodyne quadrature measurements to control the state of light. The quantum state of the unmeasured light paths is determined by the quadrature measurement outcomes and actions depending on these outcomes. Homodyne measurements differ from exact quadrature measurements depending on the strength of the LO. Since CV techniques are designed with exact quadrature measurements in mind, it is necessary to quantify the error introduced by replacing these exact measurements with homodyne measurements. ACMD researchers and their collaborators developed a strategy for bounding the error in this replacement by readily determined properties of the signal state, the detectors and the strength of the LO [1].

Statistics for Certification. A perennial issue in applications of quantum devices is to verify that the devices or their output states perform according to specification. It is desirable for this verification to provide quantified statements of performance, where the statements are guaranteed to be correct with probability close to one. In many cases it is necessary for this probability to be extremely close to one. ACMD researchers and their collaborators have developed efficient strategies based on so-called estimation factors that accomplish this goal. A notable advance in the last year has been the development and analysis of a spot-checking strategy based on estimation factors. Spot-checking involves random, potentially destructive measurements of a small number of the states under test, leaving the remaining states for use in an application or protocol. ACMD researchers found that the new spot-checking method out-performs standard ones used in, for example, quantum protocols. Furthermore, their method works with states that are sequentially generated and need not be independent and identical. This weakens the assumptions required by other spot-checking methods.

Estimation-factor based verification provides good estimates, but the distance of the estimates from the truth is not guaranteed beforehand. In contrast, minimax methods provide such a guarantee at the cost of performing worse in some situations. ACMD researchers improved a minimax optimal method for estimating expectations and applied it to estimating expectations of observables for quantum states. They showed that the method's optimal performance is determined by a special norm and used this norm to show that their minimax method always performs better, sometimes even exponentially better, than a now standard minimax method called "classical shadow tomography".

Bosonic Sampling Bunching and Complexity. In quantum information experiments with bosonic atoms in optical lattices, the single-atom state space consists of visible and hidden degrees of freedom, where the hidden degree of freedom is often thermal. For applications such as boson sampling in quantum advantage demonstrations, the visible behavior of the atoms needs to be close to bosonic. However, as the temperature of the hidden degrees of freedom is increased, they behave less bosonically and more classically. In previous work [3], ACMD researchers and their collaborators established procedures to quantify the deviation from bosonic behavior. One such procedure measures the amount of visible bunching of the atoms. ACMD researchers are now investigating the dependence of this bunching on temperature. They are attempting to prove that bunching decreases monotonically as temperature is raised.

Boson sampling is a computational problem that is believed to be extremely difficult to accomplish on a classical computer but has a natural implementation on quantum devices. Any physical implementation is subject to noise, so it is important to determine whether

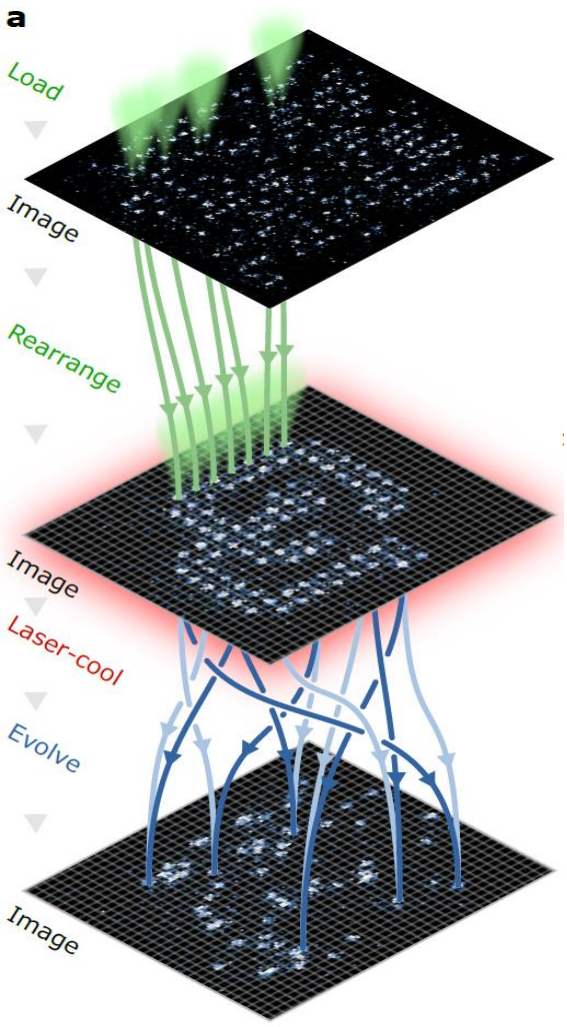

Figure 71. *Assembling strontium atoms in an optical lattice boson sampler. States containing up to 180 atoms are prepared and measured on-demand in an optical lattice (grey grid) via site- and atom-resolved imaging (pictured images are single-shot experimental data), parallelized rearrangement with optical tweezers (green cones and trajectories), and high-fidelity laser cooling. The evolution of these atoms in the lattice is described by factorially many (in particle number) different interfering multiparticle trajectories (light and dark blue lines show two possible interfering trajectories for a subset of atoms but are for illustration purposes only)*

noisy boson sampling is still classically difficult. In boson sampling with bosonic atoms in optical lattices, a primary source of noise arises from fluctuations of the optical lattice potential. This source of noise behaves differently from previously considered sources typically present in traditional boson sampling implementations with photons. The analysis of noise due to fluctuating potentials therefore requires different, specially tailored theoretical treatments. A particular type of potential fluctuations results in a simple noise model referred to as global dephasing noise. ACMD researchers have found that the sampling probabilities remain extremely hard to compute even with arbitrarily large global

dephasing noise. Further research is required to determine whether the hardness extends to sampling according to these probabilities.

QKD Analysis. Quantum key distribution is a protocol that establishes a shared secret key between two parties, where the secrecy of the key is based on the properties of quantum mechanics. Dispersive optics (DO-QKD) is one experimental technology that is considered promising by the community due to the potential for high key rates and the relative simplicity of the experimental setups that are required. However, the usual security analysis for this protocol assumes that the experiment is taking place in the high-dispersion limit. ACMD researchers and their collaborators discovered that the vast majority of current experiments are not in this limit, which invalidates the usual security analysis. In particular, in one experimental implementation the actual key rate is zero when finite dispersion is taken into account.

[1] E. Shojaee, J. R. van Meter, K. Mayer, S. Glancy, and E. Knill. Broadband Pulsed Quadrature Measurements with Calorimeters. In preparation.

[2] A. W. Young, S. Geller, W. J. Eckner, N. Schine, S. Glancy, E. Knill, and A. M. Kaufman. An Atomic Boson Sampler. *Nature* **629** (2024), 311. DOI: 10.1038/s41586-024-07304-4

[3] A. Shlosberg, A. Kwiatkowski, A. Kyle, and G. Smith. Security Assumptions in Dispersive-Optics QKD. Preprint arXiv:2403.08992 (2024). DOI: 10.48550/arXiv.2403.08992

Quantum Characterization Theory and Applications

Victor V. Albert
Thomas Gerrits
Shawn Geller
Scott Glancy
Emanuel Knill
Alex Kwiatkowski
Yi-Kai Liu
Adam D. Brandt (NIST PML)
Alejandra L. Collopy (NIST PML)
Michael J. Gullans (NIST PML)
Adam M. Kaufman (NIST PML)
Dietrich Leibfried (NIST PML)
Daniel Slichter (NIST PML)
Jacob M. Taylor (NIST PML)
Andrew Wilson (NIST PML)
Arik Avagyan (University of Colorado)
Christina M. Bowers (University of Colorado)
Riley Dawkins (Louisiana State University)
William J. Eckner (University of Colorado)
Stephen D. Erickson (University of Colorado)
Demitry Farfurnik (North Carolina State Universi-ty)
Srilekha Gandhari (University of Maryland)
Pan-Yu Hou (University of Colorado)
Kaixin Huang (University of Maryland)
Hannah Knaack (University of Colorado)
Marcel Mazur (University of Colorado)
Laurent J. Stephenson (University of Colorado)
Hilma Vasconcelos (Federal University of Ceará)
Jenny J. Wu (University of Colorado)
Aaron W. Young (University of Colorado)

Many emerging technologies already exploit or will exploit quantum mechanical effects to enhance metrology, computation, and communication. Developing these technologies requires improved methods to characterize the performance of quantum devices. This characterization requires solving statistical problems such as estimating an underlying quantum state, measurement, or process by using a collection of measurements made on the quantum system. Alternatively, one may also want to estimate figures-of-merit such as fidelity, error rates, entanglement measures, or success measures for particular tasks. Accurate quantum characterization allows experimentalists and engineers to answer questions like “What is happening in my quantum experiment?” or “How well will my system perform some quantum information protocol?” and to characterize uncertainty in that answer.

Randomized benchmarking is a very popular method to measure the error rates of quantum logic gates. Sequences of random logic gates are applied, and one observes how the probability of obtaining the correct output qubit state decreases with increasing sequence length. ACMD researchers have studied how to choose the sequence lengths so that one can obtain the most precise estimate of the individual gate error rate in a limited wall clock time. They have also studied how randomizing every sequence produces more accurate error rate estimates than repeating the same random sequence. ACMD researchers collaborated with the NIST Ion Storage Group to demonstrate the improvements to randomized benchmarking with a trapped-ion qubit [1].

To characterize nonlinear interactions between photons, such as those being developed for photon logic gates, ACMD researchers have developed a generalization of traditional homodyne detection. Traditional homodyne detection requires a strong reference beam and can only estimate the state in the mode matching the reference beam, but our generalization can use a weak reference beam (as required for some integrated circuit designs) and can learn about correlations between the signal mode and photons in nearby modes [2]. ACMD and PML researchers have performed an experiment to demonstrate this technique and are analyzing its results.

ACMD researchers have applied shadow tomography [3] to obtain new rigorous guarantees on well-established tomographic protocols for continuous-variable (CV) systems, such as optical fields or trapped ion

motion. Shadow tomography is a novel randomized tomographic framework that is based on approximating a quantum state by succinct "snapshots" or "shadows" that can be easily extracted and stored on a classical computer. The framework comes with rigorously proven guarantees on the minimum number of such shadows required to achieve high accuracy with high probability. While this framework was originally designed for intrinsically multi-qubit systems, we show that certain experimentally relevant CV protocols, such as homodyne and photon-number-resolving tomography, can also be viewed through the lens of this framework. This yields useful guarantees that dictate how many measurement rounds of a protocol are required to reach a desired accuracy of state estimation. The required number of rounds for a multi-mode CV system scales polynomially with both the number of CV modes and the maximum occupation (e.g., photon) number of each mode. ACMD researchers have benchmarked their bounds against numerical simulation and experimental data from a previous NIST optical homodyne experiment [4]. Details can be found in the manuscript [5].

A basic resource state for continuous-variable quantum information processing is a low-temperature squeezed state. Such states are often prepared in optical modes or in the motion of trapped ions. ACMD researchers have developed a method to estimate the amount of squeezing, temperature, and other parameters of a multi-mode squeezed state from measurements of the number of photons or phonons in the state [6, 7]. They have applied this method to ion motion and temperature in past experiments where the ions were previously assumed to have temperature 0 K. They are designing a new trapped-ion experiment to demonstrate this method.

Solid-state qubits often suffer from noise that contains non-Markovian effects, which can be characterized using noise spectroscopy. In systems with many qubits, such characterization procedures are time-consuming. To address this difficulty, ACMD researchers are developing random pulse sequences that can be used for compressed sensing of sparse noise spectra in quantum dots [8]. During the past year, progress has been made in two directions: first, generalizing this approach in order to reconstruct piece-wise linear noise spectra, and second, using simpler, uncorrelated pulse sequences that can be generated more easily by experimental apparatus.

A physical implementation of a qubit always involves choosing a preferred set of states out of a larger set of states that a system has. However, the presence of these other states can lead to deviations of the intended operations from the ideal operations on the qubit. For example, the logical information can leak out into the extra states, or corrupted in-formation that is contained in the extra states can seep back in. ACMD researchers have adapted standard randomized benchmarking techniques to characterize these effects. This research improves on the previous works in this area by using constraints implicit in the data to put stringent bounds on the relevant physical error rates. ACMD researchers are collaborating with PML researchers to implement their method on a superconducting quantum processor, where the logical qubit is a pair of states in two transmon qubits.

Some protocols for quantum information processing with trapped ions involve encoding and manipulating information using the ions' motion. Important goals are to transfer quanta from one oscillation mode to another and to show entanglement between oscillation modes. These capabilities were recently demonstrated at NIST with a three-ion, Beryllium-Magnesium-Beryllium crystal. ACMD researchers showed that the fidelity of the "beam splitter" operation that transfers quanta from one mode to another was at least 97.9 % with 84 % confidence [9]. Characterizing an ion's motion requires coupling the motion to the ion's spin and then measuring the spin. Obtaining full information about the motion requires many different couplings and measurements, which can take a long time. ACMD researchers are developing measurement schemes to reduce this time be robust against errors.

Researchers at JILA have an optical lattice atom trap, which consists of a lattice of cells, each of which may contain some number of Strontium atoms. See Figure 71. Single atoms can be loaded into any subset of the cells and allowed to hop from cell to cell as time evolves. If all atoms are indistinguishable, they behave as non-interacting bosons. Such "boson samplers" have computational powers beyond those of classical computers. ACMD researchers have characterized the performance of JILA's atomic boson sampler with up to 180 atoms distributed among ≈1000 cells. The atoms have in-distinguishability of 99.5 %, and their behavior shows critical features of boson samplers [10].

[1] A. Kwiatkowski, L. J. Stephenson, H. M. Knaack, A. L. Collopy, C. M. Bowers, D. Leibfried, D. H. Slichter, S. Glancy, and E. Knill. Optimized Experiment Design and Analysis for Fully Randomized Benchmarking. Preprint: arXiv:2312.15836 (2023).

[2] Avagyan, E. Knill, S. Glancy, and H. Vasconcelos. State Tomography with Photon Counting after a Beam Splitter. In preparation.

[3] H.-Y. Huang, R. Kueng, and J. Preskill. Predicting Many Properties of a Quantum System from Very Few Measurements. *Nature Physics* **16** (2020), 1050.

[4] T. Gerrits, S. Glancy, T. S. Clement, B. Calkins, A. E. Lita, A. J. Miller, A. L. Migdall, S. W. Nam, R. P. Mirin, and E. Knill. Generation of Optical Coherent-state Superpositions by Number-resolved Photon Subtraction from the Squeezed Vacuum. *Physical Review A* **82** (2010), 031802.

[5] S. Gandhari, V. V. Albert, T. Gerrits, J. M. Taylor, and M. J. Gullans. Precision Bounds on Continuous-Variable State Tomography using Classical Shadows. *PRX Quantum* **5** (2024), 010346.

[6] Bezerra, H. Vasconcelos, and S. Glancy. Quadrature Squeezing and Temperature Estimation from the Fock Distribution. *Quantum Information Processing* **21** (2022), 365.

[7] A. Avagyan, E. Knill, and S. Glancy. Multi-Mode Gaussian State Analysis with Photon Counting. *Journal of Physics B: Atomic, Molecular and Optical Physics* **56** (2023), 145501.

[8] K. Huang, A. Seif, D. Farfurnik, M. Hafezi, and Y.-K. Liu. Random Pulse Sequences for Qubit Noise Spectroscopy. Preprint: arXiv:2303.00909 (2023).

[9] P.-Y. Hou, J. J. Wu, S. D. Erickson, D. C. Cole, G. Zarantonello, A. D. Brandt, S. Geller, A. Kwiatkowski, S. Glancy, E. Knill, A. C. Wilson, D. H. Slichter, and D. Leibfried. Coherent Coupling and Non-Destructive Measurement of Trapped-Ion Mechanical Oscillators. *Nature Physics* **20** (2024), 1636.

[10] A. W. Young, S. Geller, W. J. Eckner, N. Schine, S. Glancy, E. Knill, and A. M. Kaufman. An Atomic Boson Sampler. *Nature* **629** (2024), 311.

Measurement-based and Autonomous Quantum Error Correction

Victor V. Albert
Alexey V. Gorshkov (NIST PML)
Shubham P. Jain (University of Maryland)
Simon Lieu (Amazon AWS)
Yu-Jie Liu (Technical University of Munich)
Oles Shtanko (IBM)

Error correction is necessary to develop useful quantum computers and to communicate quantum information in a robust fashion. In typical quantum computing systems, one or more rounds of "active" error detection and correction are done in a discrete or stroboscopic fashion. Many error-correcting codes are designed with such protocols, and our work highlights several codes that are capable of also performing large families of gates on the encoded information [1]. Such codes are based on a family of classical quadratic-residue codes and are, to our knowledge, the shortest codes to perform such gates for their distance.

An alternative approach to the "active" error correction is continuous or "passive" error correction [2], which allows such rounds to be applied in continuous and autonomous fashion. Autonomous error correction is possible by carefully engineering the environment underlying a target quantum system.

Despite being relevant to several experimental platforms, not much is known about the true power of the autonomous approach. For a large class of many-body quantum codes, we show [3] that, to achieve error suppression comparable to conventional error correction, autonomous decoders generally require correction rates that grow with code size. For codes with a threshold, we show that it is possible to achieve faster-than-polynomial decay of the logical error rate with code size by using super-logarithmic scaling of the correction rate.

[1] S. P. Jain and V. V. Albert. High-distance codes with transversal Clifford and T-gates. Preprint arXiv:2408.12752 (2024).

[2] C. Ahn, A. C. Doherty, and A. J. Landahl. Continuous Quantum Error Correction via Quantum Feedback Control. *Physical Review A* **65** (2002), 042301.

[3] O. Shtanko, Y.-J. Liu, S. Lieu, A. V. Gorshkov, and V. V. Albert. Bounds on Autonomous Quantum Error Correction. Preprint arXiv:2308.16233 (2023).

New Frontiers in Molecular Quantum Information Processing

Victor V. Albert
Wesley C. Campbell (UCLA)
Eric R. Hudson (UCLA)
Eric Kubischta (University of Maryland)
Mikhail Lemeshko (IST Austria)

The size of a quantum system's state space pro vides a fundamental upper bound to the system's memory and processing capacity. Many of today's state-of-the-art quantum devices are built out of single atoms, whose state space consists of electronic and nuclear-spin degrees of freedom. Molecular systems offer additional continuous degrees of freedom corresponding to molecular rotations and vibrations.

Molecular state space was assumed to be mostly uncontrollable because of the inability to isolate a single molecular species in aggregate experiments. However, working off past successes in trapping single atomic ions (in part, spearheaded by NIST), experimental attempts at isolating and trapping single molecules are well under way [1].

The theory of molecular state spaces, developed well before the end of the last century, has also been tailored mostly to aggregate molecular systems [2]. As experimental control of molecules improves and various quantum applications come to focus, it is important that the conventional theory be (1) re-tuned to model single trapped molecules and (2) re-examined considering several decades of development in quantum information science and technology.

We formulate a phase space for rotational and nuclear-spin states of arbitrary rigid closed-shell molecules. Taking in molecular geometry and nuclear-spin data, we reproduce a molecule's admissible angular momentum states known from spectroscopy, introduce its angular position states using quantization theory, and develop a generalized Fourier transform converting between the two. We classify molecules into three types,

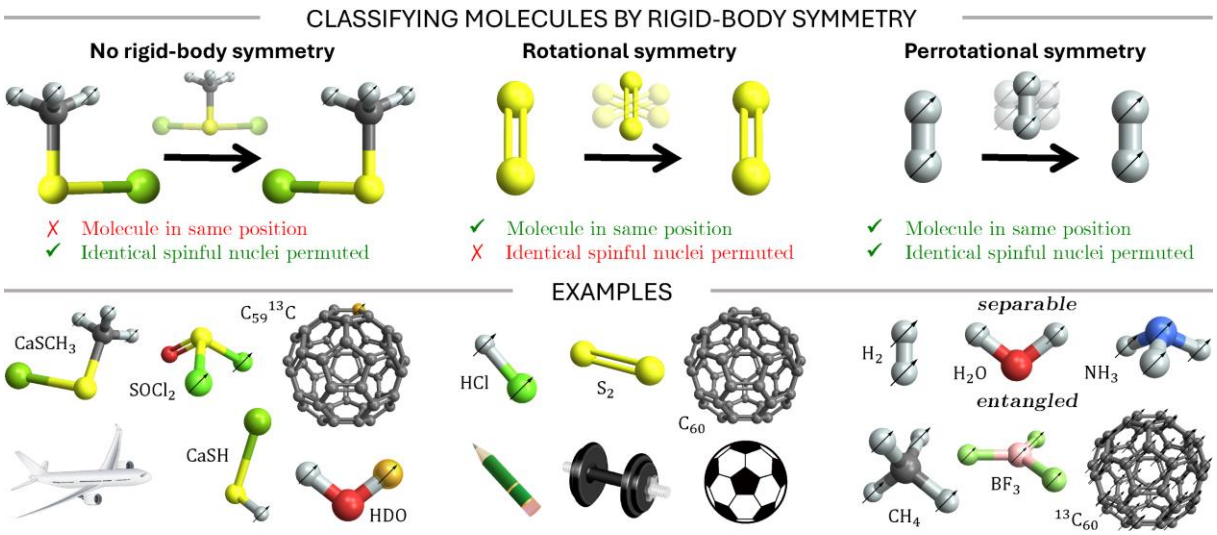

Figure 72. *Rigid bodies can be characterized by their behavior under orientation-preserving rotations. Orientations, or angular positions, of asymmetric molecules are the same as those of any rigid body (e.g., an airplane) whose center of mass is fixed. While every rotation moves an asymmetric molecule to a different position, rotationally symmetric molecules remain in the same position under some rotations. Such molecules can have nonzero nuclear spin (marked by "↗"), but any rotations that permute identical spinful nuclei must also rotate the rest of the molecule into a different position. Molecule-frame rotations that permute spinful nuclei and do leave the rest of the molecule invariant have to produce the molecule's nuclear-spin statistics. We call any molecule admitting such permutation-rotations a "perrotationally symmetric" molecule. The rotational state space of such molecules has no macroscopic analogue and exhibits several interesting and potential useful features. All molecules were drawn in Mathematica 13 [4]. The following public-domain photos from freesvg.org are pictured: dumbbell, round pencil, plane, and soccer ball.*

asymmetric, rotationally symmetric, and perrotationally symmetric, with the last type having no macroscopic analogue due to nuclear-spin statistics constraints.

We discuss two general features in perrotationally symmetric state spaces that are Hamiltonian-independent and induced solely by symmetry and spin statistics. First, we quantify when and how the state space of a molecular species is completely rotation-spin entangled, meaning that it does not admit any separable states. Second, we identify molecular species whose position states house an internal pseudo-spin or "fiber" degree of freedom, and the fiber's Berry phase or matrix after adiabatic changes in position yields naturally robust operations, akin to braiding anyonic quasiparticles or realizing fault-tolerant quantum gates. We outline how the fiber can be used as a quantum error-correcting code and discuss scenarios where these features can be experimentally probed.

In collaboration with an external team of experimentalists, we also develop more near-term practical error-correcting codes that require lower average energy, that can directly protect against photonic processes up to arbitrary order, and that are applicable to a broad set of atomic and molecular systems [3].

[1] B. L. Augenbraun, J. M. Doyle, T. Zelevinsky, and I. Kozyryev, Molecular Asymmetry and Optical Cycling: Laser Cooling Asymmetric Top Molecules. *Physical Review X* **10** (2020), 031022.

[2] P. R. Bunker and P. Jensen, *Molecular Symmetry and Spectroscopy*. 2nd ed. (2006).

[3] S. P. Jain, E. R. Hudson, W. C. Campbell, and V. V. Albert. Absorption-Emission Codes for Atomic and Molecular Quantum Information Platforms. *Physical Review Letters* **133** (2024), 26060.

[4] Wolfram Research Inc., *Mathematica*, Version 13.0 (2023), Champaign, IL.

Generalized Stabilizer Formalism for Phases of Quantum Matter

Victor V. Albert
David Aasen (Microsoft)
Jason Alicea (Caltech)
Christopher Fechisin (University of Maryland)
Wenjie Ji (UC Santa Barbara)
John Preskill (Caltech)
Nathanan Tantivasadakarn (Caltech)
Wenqing Xu (University of Maryland)

The Pauli stabilizer formalism [1] is the gold standard for defining and characterizing quantum error correcting codes, preparing entangled many-body states, understanding quantum circuits, and defining microscopic models that realize exotic and useful quantum phases of matter. While there has been progress in expanding the range of possible quantum phases realizable via this formalism, a broad swath of other phases remains unobtainable via a Pauli stabilizer description. As a result, such phases are very difficult to work with at the

level of lattice models and, consequently, also out of range of most of today's digital quantum devices. Realizing such phases would bring us closer to fully topological quantum computation, which, in contrast to the many other available blueprints for a quantum computer, holds the promise of computation in an inherently robust fashion.

We attempt to bring exotic non-Pauli-stabilizer phases closer to realization by generalizing the Pauli stabilizer formalism. Our generalization is applicable to systems comprised of qudits valued in finite groups G, which, most famously, realize non-abelian gauge theories as well as quantum-double topological order, the first known model capable of fault-tolerant topological quantum computation with anyons. We construct and analyze two models defined on such spaces which are computationally powerful and conceptually rich: gapped edges of the quantum double [2] and the generalized cluster state [3].

We derive a standalone Ising-like model for a general quantum double edge and show that this model is a generalized version of a previous studied model called the flux ladder [4]. Armed with this model, we map out a web of connections for quantum double models, generalizing the existing web for the Kitaev surface code, the current primary blueprint for a quantum computer. We develop Jordan-Wigner-like mode operators that are directly related to anyonic ribbon operators of the quantum double model. We obtain a continuum description of the general flux ladder and recast a particular case in terms of fermions with the help of non-Abelian bosonization. We make connections to established electronic systems, brightening the prospects of eventual realization of exotic quantum-double topological phases.

We also study the generalized cluster state on a group-valued Hilbert space [3], showing that it realizes symmetry-protected topological (SPT) order protected by a non-invertible symmetry (i.e., its symmetries no longer form a group). We identify several signatures of SPT order: gapped edge modes, algebraic structure under stacking, and topological response. We also discuss the implementation of measurement-based quantum computation (MBQC) using the generalized cluster state, generalizing the MBQC formalism to qudits valued in non-Abelian groups.

[1] D. Gottesman. Spin Chains, Stabilizer Codes and Quantum Error Correction. Preprint arXiv: quant-ph/9705052 (1997).

[2] V. V. Albert, D. Aasen, W. Xu, W. Ji, J. Alicea, and J. Preskill. Spin Chains, Defects, and Quantum Wires for the Quantum-Double Edge. Pre-print arXiv:2111.12096 (2021).

[3] C. Fechisin, N. Tantivasadakarn, and V. V. Albert. Non-invertible Symmetry-protected Topological Order in a Group-based Cluster State. *Physical Review X*. In press.

[4] M. I. K. Munk, A. Rasmussen, and M. Burrello. Dyonic Zero-energy Modes. *Physical Review B* **98** (2018), 245135.

New Frontiers in Continuous-variable Systems

Victor V. Albert
Michael J. Gullans (NIST PML)
Alexander Barg (University of Maryland)
Ansgar G. Burchards (Freie Universität Berlin)
Jonathan Conrad (Freie Universität Berlin)
Eric Culf (University of Ottawa)
Joseph T. Iosue (University of Maryland)
Shubham P. Jain (University of Maryland)
Kunal Sharma (IBM)
Thomas Vidick (Weizmann Institute of Science)
Christophe Vuillot (INRIA)
Yixu Wang (University of Maryland)
Yijia Xu (University of Maryland)

Utilization of quantum mechanical features promises to increase our understanding of chemical processes, communicate securely, and measure signals more accurately than with classical signals. However, most quantum protocols are focused on the abstract qubit (i.e., discrete-variable or DV) systems, and many of them cannot be readily available to bosonic or continuous-variable (CV) systems, e.g., optical fibers, free space, microwave and optical cavities, motional degrees of freedom of atoms and ions, and mechanical resonators, without substantial reformulation.

For example, quantum tomography is a field concerned with characterizing quantum systems, an important task whose completion is necessary for realizing most long-term goals in quantum information processing. However, tomography of quantum many-body systems is plagued with the "exponential wall" — the fact that complete characterization of a state or operation on a many-qubit quantum system requires either a computation time or a memory size that scales exponentially with the number of qubits. An active area of research is thus devoted to developing efficient protocols for such tasks. A recent breakthrough result called shadow tomography has substantially simplified the task of approximating quantum systems [1]. However, it is unclear how to develop similar important tools in CV systems because qubit shadows revolved around the notion of state designs, which have not, up to now, existed in the CV world.

For another example, fiber-based and free-space communication are described by CV systems, so development of secure CV protocols is critical to realizing quantum communication in the real world. However, there is a tradeoff between provable security and ease of

use, as some of the simplest CV protocols are not device independent, i.e., such protocols cannot be securely implemented without additional knowledge that the devices involved are also secure.

Last is quantum error correction for CV systems. While there has been substantial work on storing and processing quantum information in the amplitude of a single-frequency signal, or mode, there is a lack of understanding of the potential of multiple-frequency space. Members of Victor's group, along with collaborators at NIST and around the world, are spearheading a new research direction to extend state-of-the-art qubit-based tomographic, error-correction, and cryptographic quantum protocols to CV systems in the following ways.

Theory of Quantum Codes Defined on Quantum Systems Parameterized by Spheres and Tori. Such codes would encapsulate several physically relevant quantum coding schemes for CV, spin, and molecular systems. The framework of quantum spherical codes [2] provides a quantum analogue to the classical spherical codes, a subfield of coding theory that has been around since Shannon. Quantum spherical codes consist of a superposition of a handful of classical electro-magnetic signals. On the other hand, tiger code states [3] are superpositions of a continuous and compact set of signals. The tiger-code framework encompasses two-component cat, pair-cat, dual-rail, two-mode binomial, various bosonic repetition codes, and aspects of chi-squared encodings while also yielding codes from homological products, lattices, generalized coherent states, and algebraic varieties. We anticipate that both frameworks will pave the way for novel, well-protected, and experimentally feasible logical qubits.

Homological Error-Correcting Codes for Oscillators and Rotors. Conventional CV systems are characterized by linear position and momentum and are not thought to exhibit the unique topology of angular (a.k.a. rotor) quantum systems that are parameterized by periodic variables. Our work [4] shows that a mapping of an angular system into a CV system can be used to develop CV codes previously available only to rotor systems. We identify the (Clifford) group structure of rotor operations and show that analogous operations for conventional CV systems are available under the mapping.

CV state designs. Following up on our theory of appropriately defined CV state designs [5], we show that quantum lattice states (superpositions of electromagnetic signals whose amplitudes lie on a lattice) form CV two-designs [6]. This makes such states, colloquially known as GKP states, useful for CV shadow tomography, and we outline several tools for such use in the manuscript.

One-sided Device-independent Cryptographic Protocols. We utilize squeezed states whose proof of security is based on a CV extension of DV monogamy-of-entanglement games [7]. This work establishes this well-known protocol as the first one-sided device-independent CV protocol, to the authors' knowledge.

Review of Bosonic Coding [8] for computer scientists and others outside of physics.

[1] H.-Y. Huang, R. Kueng, and J. Preskill. Predicting Many Properties of a Quantum System from Very Few Measurements. *Nature Physics* **16** (2020), 1050.

[2] S. P. Jain, J. T. Iosue, A. Barg, and V. V. Albert. Quantum Spherical Codes. *Nature Physics* **20** (2024), 1300.

[3] Y. Xu, Y. Wang, C. Vuillot, and V. V. Albert. Letting the Tiger Out of Its Cage: Bosonic Coding Without Concatenation. Preprint arXiv:2411.09668 (2024).

[4] Y. Xu, Y. Wang, and V. V. Albert. Clifford Operations and Homological Codes for Rotors and Oscillators. *Physical Review A* **110** (2024), 022402.

[5] J. T. Iosue, K. Sharma, M. J. Gullans, and V. V. Albert. Continuous-variable Quantum State Designs: Theory and Applications. *Physical Review X* **14** (2023), 011013.

[6] J. Conrad, J. T. Iosue, A. G. Burchards, and V. V. Albert. Continuous-variable Designs and Design-Based Shadow Tomography from Random Lattices. Preprint arXiv:2412.17909 (2024).

[7] E. Culf, T. Vidick, and V. V. Albert. Group Coset Monogamy Games and an Application to Device-Independent Continuous-Variable QKD. Preprint arXiv:2212.03935 (2022).

[8] V. V. Albert. Bosonic Coding: Introduction and Use Cases. Preprint arXiv:2211.05714 (2022).

Navigating Noise in Quantum Metrology

Victor V. Albert
Anthony J. Brady
Jacob Bringewatt (Harvard, University of Maryland)
Alexey V. Gorshkov (NIST PML)
Cheng-Ju Lin (University of Maryland)
Zi-Wen Liu (Tsinghua University, Perimeter Institute)
Changhun Oh (Korea Advanced Inst. of Sci. and Tech.)
Alireza Seif (IBM Quantum)
Yu-Xin Wang (University of Maryland, QuICS)
Chao Yin (University of Colorado Boulder)
Sisi Zhou (Perimeter Institute, University of Waterloo)
Quntao Zhuang (University of Southern California)

Quantum metrology represents an exciting and rapidly advancing area within quantum information science. It focuses on estimating parameters (e.g., phase, magnetic field, strain caused by a gravitational wave) encoded in the quantum state of physical systems, such as spins, photonic modes, or mechanical oscillators. By leveraging quantum systems as sensors and designing specialized probe states, like highly entangled states of

spin systems and squeezed states of light, quantum metrology permits enhanced estimation precision that surpasses all known classical methods. Advancements in quantum metrology drive discoveries across a wide variety of realms, including searches for new physics, collective force and electric field sensing, and correlation spectroscopy in many-body quantum systems to name a few.

Noise, such as spin dephasing and random fluctuations of confined field modes, plays a dichotomous role in quantum metrology. On the one hand, noise limits measurement precision of parameters encoded into a quantum system through coherent (i.e., unitary) processes. Interestingly, quantum error correction, originally developed for realizing fault-tolerant quantum computation, offers promising strategies to mitigate such noise and maintain an entanglement advantage in coherent parameter estimation. On the other hand, estimating the noisy (incoherent) process itself often interests us — allowing us, for instance, to characterize properties of chaotic electromagnetic fields or noisy spin-spin correlations in many-body systems. ACMD researchers have contributed to both these key facets: coherent quantum metrology and quantum metrology of incoherent processes.

Coherent Quantum Metrology in Noisy Environments. In [1] we introduce a class of entangled quantum states that achieve optimal precision in coherent parameter estimation, even in noisy environments. To do so, we consider partitioning qubits into quasi-independent clusters, with strong intra-cluster entanglement and weak inter-cluster entanglement. This design balances the benefits of entanglement, which enhances estimation precision, while maintaining resilience against noise, which typically degrades precision. The quantum states can be prepared using local Hamiltonian evolution. Further, we propose efficient measurement protocols, including time-reversed dynamics (e.g., a many-body spin echo) with single-qubit measurements as well as quantum domino dynamics, which avoids the need for time reversal — thereby promoting the practical feasibility of our approach.

In [2] we introduce a framework for designing approximate quantum error-correcting codes (AQECCs) that afford a metrological entanglement advantage while simultaneously protecting against certain noise processes (e.g., heralded erasure errors). Leveraging symmetry considerations, we develop codes with transversal continuous gates, offering significant theoretical benefits. For example, we construct AQECCs using group-theoretic and algebraic methods that simplify the analyses and provide a systematic approach for generating codes. Numerical simulations confirm that the proposed metrological codewords within the AQECC retain their entanglement advantage under non-trivial noise for a particular coherent parameter estimation problem.

Quantum Metrology of (Correlated) Incoherent Processes. In [3] we introduce a novel method for estimating correlated dephasing in many-body spin systems. We theoretically demonstrate an exponential entanglement advantage in measurement sensitivity when estimating deviations from maximally correlated dephasing dynamics. This contrasts parameter estimation of uncorrelated noise, where it is known that entanglement offers zero advantage over "classical" (separable) approaches. Our approach showcases the potential of an entanglement advantage in characterizing decoherence in general and probing many-body correlated phases of spin systems in particular.

Lastly, in [4] we tackle the generic problem of estimating collective stochastic properties in many-body quantum systems, such as center-of-mass quadrature fluctuations in a system of bosonic modes or correlated dephasing in an ensemble of spins. We lay the theoretical groundwork to determine the ultimate precision limits for correlated noise estimation and identify conditions required to achieve an entanglement advantage for a broad class of problems. We elucidate optimal probe states and propose a sensing protocol (akin to a many-body echo sequence) which can, in principle, realize the advantage.

Our findings have broad implications for leveraging quantum sensor networks to accelerate searches for new physics, explore correlated noise processes in many-body quantum systems, and beyond. The inherent synergy between quantum computation, quantum error correction, and quantum metrology suggests untapped potential for breakthroughs in quantum sensor technology. Future efforts will aim to explore new possibilities across these domains.

[1] C. Yin, V. V. Albert, and S. Zhou. Small Correlation is Sufficient for Optimal Noisy Quantum Metrology. Preprint: arXiv:2408.00079 (2024).

[2] C. J. Lin, Z. W. Liu, V. V. Albert, and A. V. Gorshkov. Covariant Quantum Error-Correcting Codes with Metrological Entanglement Advantage. Preprint: arXiv:2409.20561 (2024).

[3] Y. X. Wang, J. Bringewatt, A. Seif, A. J. Brady, C. Oh, and A. V. Gorshkov. Exponential Entanglement Advantage in Sensing Correlated Noise. Preprint: arXiv:2410.05878 (2024).

[4] A. J. Brady, Y. X. Wang, V. V. Albert, A. V. Gorshkov, and Q. Zhuang. Correlated Noise Estimation with Quantum Sensor Networks. Preprint: arXiv:2412.17903 (2024).

Error Correction Zoo

Victor V. Albert
Philippe Faist (Freie Universität Berlin)

https://errorcorrectionzoo.org/

Classical and quantum error correction lies at the intersection of computer science, engineering, physics, and mathematics. Classical coding theory has been around for over 70 years, yielding an enormous literature collection. Quantum error correction is more recent but arguably wider, encompassing subfields from solid-state physics to complexity theory. Collecting and accurately synthesizing such a hyper-field is as formidable as it is useful.

We have created and actively maintain the Error Correction Zoo to categorize and organize known ways to encode classical and quantum information. The work involved is taxonomic, i.e., collecting and processing literature as well as developing a classification scheme for the thousands of available classical and quantum error-correcting codes.

This year, the EC Zoo's website enjoyed approximately 1100 unique visitors per day on average, peaking at 2300 around times when notable error-correction results were announced in the public sphere. There have been 128 external contributors so far.

Code entries form the primary content of the zoo. An entry can be a specific instance of a well-known code or a large family of codes, depending on community interest. There is a dedicated webpage for each family, collecting original work, related protocols, and real-world implementations.

Codes are organized into kingdoms by alphabet (or Hilbert space structure in the quantum case), with "parent" and "cousin" fields listing notable relations and connections. This year, a "primary" parent has been chosen for each code, and the corresponding primary taxonomy is listed in a graphical format on each code's page (see Figure 73). All data is automatically generated from the human- and machine-readable data files storing code information. At the time of writing, there are 910 codes, split roughly as 1/3 classical and 2/3 quantum.

During the summer of 2023, three undergraduate students contributed to the zoo through the REU-CAAR program at the University of Maryland College Park. Discussing the state of the art of the field led one of the students to publish a manuscript on an important class of codes called subsystem CSS codes [1].

[1] M. L. Liu, N. Tantivasadakarn, and V. V. Albert. Subsystem CSS Codes, a Tighter Stabilizer-to-CSS Mapping, and Goursat's Lemma. *Quantum* **8** (2024) 1403.

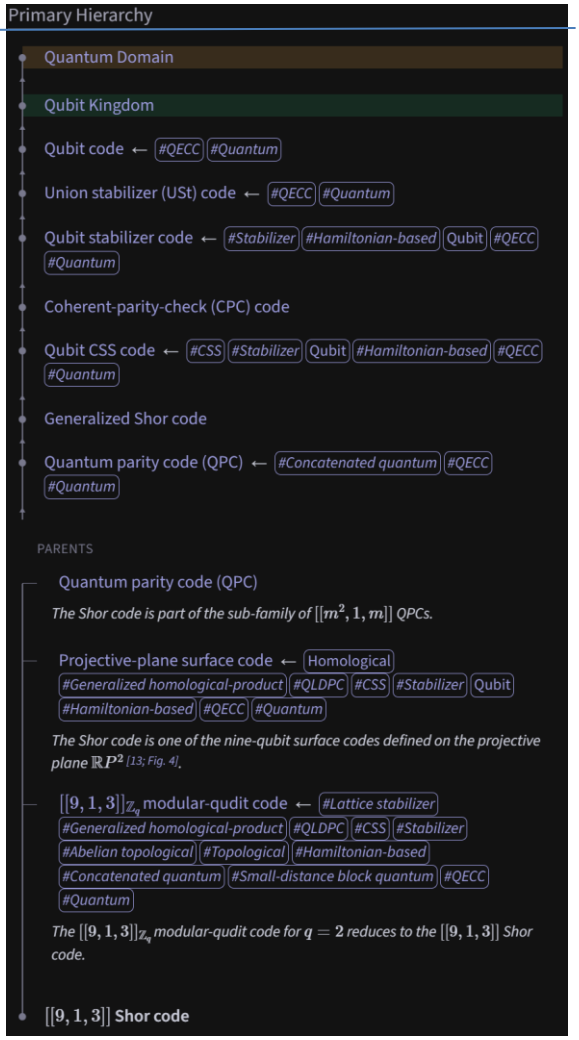

Figure 73. *Example primary parent hierarchy for the Shor nine-qubit quantum error-correcting code.*

Quantum Algorithms and Wavelet Transforms

Yi-Kai Liu
Marianna Podzorova (University of Maryland)

The quantum Fourier transform plays an important role in many quantum algorithms that achieve exponential speedups over classical algorithms. Could similar advantages be obtained by using quantum wavelet transforms? We are studying two areas where this question has practical significance: solving hard lattice problems, and simulating wave equations.

First, we are investigating the possibility (or impossibility) of fast quantum algorithms for solving shortest vector problems (SVP) and bounded distance decoding (BDD) in high-dimensional lattices. These problems are

believed to be computationally intractable, and their hardness is used to construct post-quantum cryptosystems, including several schemes recently standardized by NIST (see Post-Quantum Cryptography, page 104). Interestingly, the security proofs for some of these cryptosystems make use of a quantum reduction due to Regev [1], from SVP to an average-case problem called Learning with Errors (LWE), which uses a quantum Fourier transform. There have been unsuccessful attempts to strengthen this result to get a quantum algorithm for SVP, by using a quantum curvelet transform, a type of high-dimensional wavelet transform [2].

In recent work [3], we proved an uncertainty relation for the curvelet transform that suggests that the approach described in [2] is unlikely to succeed, for a natural class of curvelet transforms. In ongoing work, we are attempting to extend the above impossibility results, to larger classes of wavelet transforms. We are also attempting to prove some positive results, showing that the approach described in [2] can succeed in solving certain special cases of SVP.

Second, we are investigating how quantum wavelet transforms can be used to improve the performance of quantum algorithms for solving wave equations. As a first step, we are developing efficient quantum circuits for "wave atom" transforms [4], which are a family of hierarchical, tree-structured wavelet transforms. Our eventual goal is to make use of techniques from classical numerical algorithms, specifically, the use of "wave atoms" to construct sparse representations of the solutions of wave equations. This sparsity will help overcome some of the practical difficulties with preparing the initial states, and reading out the solutions, in quantum algorithms for solving wave equations.

[1] O. Regev. On Lattices, Learning with Errors, Random Linear Codes, and Cryptography. *Journal of the ACM* **56**:6 (2009), 1–40. DOI: 10.1145/1568318.1568324

[2] Y.-K. Liu. "Preparing Lattice Superpositions on a Quantum Computer." Workshop on Post-Quantum Information Security. Joint Quantum Institute, University of Maryland, College Park, MD. October 2010.

[3] Y.-K. Liu. An Uncertainty Principle for the Curvelet Transform, and the Infeasibility of Quantum Algorithms for Finding Short Lattice Vectors. Preprint arXiv: 2310.03735 (2023). URL: 10.48550/arXiv.2310.03735

[4] M. Podzorova and Y.-K. Liu. Quantum Wave Atom Transforms. In preparation.

Hamiltonians whose Low-Energy States Require Ω(n) T Gates

Matthew Coudron
Nolan J. Coble (University of Maryland)
Jon Nelson (University of Maryland)
Seyed Sajjad Nezhadi (University of Maryland)

After the publication of our result on Local Hamiltonians with No Low-Energy Stabilizer State [3], our research group made a technical breakthrough which allowed us to prove a significantly upgraded result using new and mathematically interesting techniques. Specifically, our new result constructs families of Local Hamiltonians whose low-energy states cannot be produced with fewer than $\Omega(n)$ T gates.

The minimum number of T gates required to produce a quantum state can be viewed as a measure of how far that state is from being a stabilizer state. Stabilizer states can be produced using only Clifford gates, and no T gates, and there are efficient classical algorithms for sampling from stabilizer states. In contrast, states that require a non-zero number of T gates to produce cannot always be efficiently classically sampled. There are known classical algorithms for sampling from any n-qubit quantum state that can be produced using at most k T-gates in time that scales better than $\mathrm{poly}(n)2^k$. Therefore, we can view the significance of our new result, constructing n-qubit local Hamiltonians whose low-energy states require $\Omega(n)$ T gates, as showing that we can construct simple Hamiltonians with the property that there is no "off the shelf" classical algorithm to sample from any of their low-energy states in less that exponential, $2^{\Omega(n)}$, time. This is interesting because it represents another resolved prerequisite, beyond our previous paper, to the No Low-energy Sampleable States (NLSS) conjecture of Gharibian and Le Gall [1]. Recall that the NLSS conjecture posits the existence of a family of local Hamiltonians where all quantum states of low-enough constant energy do not have succinct representations allowing perfect sampling access.

The recently-defined No Low-energy Sampleable States (NLSS) conjecture of Gharibian and Le Gall [1] posits the existence of a family of local Hamiltonians where all quantum states of low-enough constant energy do not have succinct representations allowing perfect sampling access. States that can be prepared using only Clifford gates (i.e. stabilizer states) are an example of sampleable states, so the NLSS conjecture implies the existence of local Hamiltonians whose low-energy space contains no stabilizer states. In our work, [3], we take a step towards the NLSS conjecture by constructing families of Hamiltonians that exhibit this requisite "no low-energy stabilizer states" property. Our construction works via a simple alteration to local Hamiltonians corresponding to CSS codes. Our method can also be

applied to the recent No Low-energy Trivial States (NLTS) Hamiltonians of Anshu, Breuckmann, and Nirkhe [2], resulting in a family of local Hamiltonians whose low-energy space contains neither stabilizer states nor trivial states. We hope that our techniques will eventually be helpful for constructing Hamiltonians which simultaneously satisfy NLSS and NLTS.

To understand the motivation behind our work it is important to take a step back and note that each of the conjectures in this particular branch of Hamiltonian complexity, including the NLTS conjecture, the NLSS conjecture, and many others, are all attempts to gain insight into a very widely known open problem in the field called the Quantum Probabilistically Checkable Proof (PCP) conjecture. Classical Probabilistically Checkable Proofs (PCPs) are considered to be one of the crowning achievements of modern theoretical computer science and have numerous emerging applications from cryptography (SNARKS) to hardness of approximation results. The Quantum PCP conjecture, if resolved, could have analogous applications to quantum computing, and would also have implications for the possibility of experimentally producing entangled quantum states that remain coherent at high temperatures, among other things.

The Quantum PCP conjecture itself is a complexity theoretic claim about a computational problem involved in simulating quantum mechanical systems which are governed by a Hamiltonian. Briefly put, the Quantum PCP conjecture postulates that it is QMA-hard (a computational hardness notion involving complexity classes) to approximate the ground state energy of a local Hamiltonian to within a constant. This simple statement, if proven, could have all the widespread implications discussed above, and the proof techniques would likely be valuable in and of themselves. However, a pre-requisite to proving that any problem is QMA-hard is to first prove that it cannot be solved in the smaller complexity class Non-Deterministic Polynomial Time (NP). This pre-requisite is the motivator for the NLTS conjecture, the NLSS conjecture, and for our own work. If the NLTS conjecture had been false, the ground state energy problem for local Hamiltonians would have been contained in NP. If the NLSS conjecture is false then the problem would be contained in a complexity class called MA, which is much smaller than QMA. Our result is a necessary pre-requisite of the NLSS conjectures, addressing the following important issue: The NLTS conjecture, while now proven, has only been proven with Hamiltonians whose ground state energy problem is clearly contained in MA because the ground states are stabilizer states and therefore efficiently sampleable (the exact reasoning behind all of these connections is non-trivial and is laid out in [1], where the NLSS conjecture was first stated).

At the level of techniques, we contribute a conceptually simple new procedure in which we begin with a regular local Hamiltonian and modify it by conjugating it (multiplying on either side) by low depth quantum circuit as shown in Figure 74. Part (a) of Figure 74 illustrates a generic low-depth quantum circuit C, comprised of a constant number of layers of quantum gates. Part (b) of Figure 74 illustrates what happens when a local Hamiltonian term H_i is conjugated by the low-depth quantum circuit C. A local Hamiltonian which is conjugated by a constant depth quantum circuit remains a local Hamiltonian since its Hamiltonian properties are preserved by the unitarity of the quantum circuit, and its locality is only increased by the spread of the "light cones" with in the circuit C which originate from one particular Hamiltonian term (these are the gates colored orange in part (b) of Figure 74). Since C is constant depth, the increase in the locality of the Hamiltonian is merely constant. In [3] we are able to show, through a series of combinatorial arguments that, if we take the local Hamiltonian from known constructions of quantum Low Density Parity Check (LDPC) error correcting codes, and conjugate those Hamiltonians by a $\frac{\pi}{8}$ rotation on every qubit (which is a low depth circuit), then no stabilizer state can have low energy relative to the resulting Hamiltonian. Since the resulting Hamiltonian must still be local, by the above argument and Figure 74, the desired result follows. We are hopeful that these techniques will prove useful in further extending known NLTS results to more general settings.

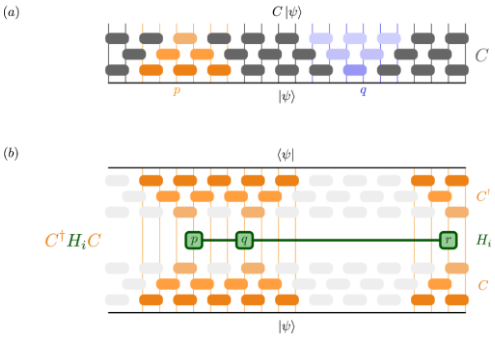

Figure 74. *Conjugation method for modifying local Hamiltonians.*

[1] S. Gharibian and F. Le Gall. Dequantizing the Quantum Singular Value Transformation: Hardness and Applications to Quantum Chemistry and the Quantum PCP Conjecture. In *Proceedings of the 54th Annual ACM SIGACT Symposium on Theory of Computing*, June 19-32, 2022. DOI: 10.1137/22M1513721

[2] A. Anshu, N. Breuckmann, and C. Nirkhe. NLTS Hamiltonians from Good Quantum Codes. Preprint arXiv:2206.13228 (2022). DOI: 10.1145/3564246.3585114

[3] N. J. Coble, M. Coudron, J. Nelson, and S. Sajjad Nezhadi. Local Hamiltonians with No Low-Energy Stabilizer States. In *18th Conference on the Theory of Quantum Computation, Communication and Cryptography* (TQC 2023). Leibniz International Proceedings in

Informatics (LIPIcs) **266** (2023), 14:1-14:21. DOI: 10.4230/LIPIcs.TQC.2023.14

[4] N. J. Coble, M. Coudron, J. Nelson, and S. Sajjad Nezhadi. Hamiltonians Whose Low-energy States Require Ω(n) T Gates. In *Proceedings of TQC 2024*. DOI: 10.48550/arXiv.2310.01347

Tests of Quantum Computational Advantage

Yi-Kai Liu
Alexey Gorshkov (NIST PML)
Andrew Childs (University of Maryland)
Dhruv Devulapalli (University of Maryland)
Alicia Kollar (University of Maryland)
Zhenning Liu (University of Maryland)
Joel Rajakumar (University of Maryland)
James Watson (University of Maryland)
Lucas T. Brady (NASA Ames Research Center)
Jacob Bringewatt (Harvard University)
Luis Pedro Garcia-Pintos (Los Alamos National Lab)
Dominik Hangleiter (University of California, Berkeley)

In recent years, there has been rapid progress in the development of experimental quantum information processors, leading to the first demonstrations of "quantum computational advantage," where a quantum device solves a computational problem that would be difficult or intractable on a classical computer. However, these experimental quantum devices have significant limitations: they suffer from noise and errors, and they do not have enough qubits to perform fault-tolerant quantum computation. Such devices are sometimes called noisy intermediate-scale quantum (NISQ) devices.

Quantum computational advantage using NISQ devices can be difficult to study, for two reasons. First, it is sometimes unclear how the presence of noise in a quantum computer affects the difficulty of simulating it using a classical computer. This has motivated the development of new classical algorithms for simulating NISQ devices. Second, it is sometimes unclear whether a NISQ device has actually solved a hard computational problem correctly, due to the effects of noise in the NISQ device, and the difficulty of reproducing the results using a classical computer. This has motivated the development of new methods for testing or verifying NISQ devices.

We have made progress on both of the above questions. First, we have developed a new classical algorithm for simulating noisy "IQP" quantum circuits with constant depth, using mathematical techniques from graph percolation theory [1]. IQP ("instantaneous quantum polynomial") circuits are a class of quantum circuits that have low depth and consist mostly of quantum gates that commute with each other. IQP circuits are relatively easy to implement on experimental quantum information processors yet are conjectured to be difficult to simulate on classical computers. Our results show that "noisy" IQP circuits can be simulated efficiently on a classical computer, when the noise strength is above some fixed threshold.

These results constrain the parameter regimes where quantum computational advantage can be achieved. They will likely be relevant to future experimental demonstrations, where fault-tolerant encodings will be able to correct many of the errors, but not all of them. These results are also more broadly applicable than previous results of this kind, because they do not require assumptions on the circuit's locality or anti-concentration properties, nor do they require the circuit depth to grow logarithmically with the number of qubits.

Second, we have developed a new method for verifying the performance of analog quantum simulators, when demonstrating quantum computational advantage, by preparing the Feynman-Kitaev history state [2]. Here, analog quantum simulators are NISQ devices that have large numbers of qubits, but have fewer degrees of control, compared to digital quantum computers. Analog quantum simulators are interesting for many reasons. They are easier to build than digital quantum computers, and they may be able to solve useful problems by performing adiabatic optimization, quantum annealing, and analog quantum simulation. But they cannot perform universal quantum computation or run quantum algorithms that are described by quantum circuits. They also cannot implement many of the methods that are used to verify the operation of digital quantum computers.

In this work [2], we consider a class of quantum computations that involve time evolution with a Hamiltonian consisting of Pauli ZZ + Z terms, and measurements in the Pauli X basis. This class of quantum computations serves as the basis for several proposed experiments (put forward by other authors) to demonstrate quantum computational supremacy on analog quantum simulators. We develop a novel technique for verifying these kinds of experiments, by using a globally accessible control qubit to prepare the Feynman-Kitaev history state for this time evolution operator. This allows efficient verification of the time-evolved state, and it produces a rigorous lower bound on the fidelity. This method has strengths and weaknesses: it only requires a constant number of samples, but it also requires trusted measurements.

Finally, we are developing a general framework for analyzing noisy implementations of quantum circuits, using perturbation theory [3]. One goal of this work is to examine the interactions between the dual goals of minimizing the running time and making the quantum computation robust to noise. For instance, when compiling a quantum algorithm into basic gates, one might hope that reducing the number of operations will decrease the chance of error. But this is not always the

case: minimizing the number of operations in a quantum algorithm can actually lead to increased noise sensitivity, and some compilations of an algorithm can be resilient against certain noise sources while being unstable against other noises.

[1] J. Rajakumar, J. D. Watson, and Y.-K. Liu. Polynomial-Time Classical Simulation of Noisy IQP Circuits with Constant Depth. In *Proceedings of the 2025 Annual ACM-SIAM Symposium on Discrete Algorithms (SODA)*, 1037-1056. DOI: 10.1137/1.9781611978322.30

[2] Z. Liu, D. Devulapalli, D. Hangleiter, Y.-K. Liu, A. Kollár, A. Gorshkov, and A. Childs. Efficiently Verifiable Quantum Advantage on Near-Term Analog Quantum Simulators. *Physical Review X Quantum*. In press.

[3] L. P. García-Pintos, T. O'Leary, T. Biswas, J. Bringewatt, L. Cincio, L. T. Brady, and Y.-K. Liu. Resilience-Runtime Tradeoff Relations for Quantum Algorithms. In review.

Welded Tree Path Finding: Implications for Classically Verifying Quantum Algorithms

Matthew Coudron
Chinmay Nirkhe (University of Washington)
Anand Natarjan (MIT)
Agi Villanyi (MIT)

Partially motivated by my work (with UMD collaborators) on Welded Tree Path Finding from last year, [1], this collaboration formed at the Berkeley Simons Institute workshop on Quantum Computing in Spring 2024 with the goal of investigating the implications that Welded Tree Path Finding impossibility results of [1] would have on our understanding of classical verification of quantum computation. The motivating idea, in short, is that, while we know that quantum computers can solve the welded tree problem efficiently and classical computers cannot [2], we believe that we can show that the only way a quantum computer could prove to a classical verifier that it has solved a particular Welded Tree type problem, of our own construction, is by exhibiting an Entrance-Exit path for that problem. This statement is non-trivial to prove and is the main goal of this project which is still underway. Once we prove this statement, we can combine it with the results of [1], which suggest that quantum computer cannot find Entrance-Exit paths, to establish that there are computational problems which quantum computers can solve exponentially faster than classical computers, and yet, counterintuitively, cannot produce an efficiently classically verifiable proof of their solution. In complexity theory terminology this result would constitute an oracle separation between the complexity class BQP (of computational problems solvable in quantum polynomial time) and IP_{BQP}, the class of problems for which a quantum computer can produce an efficiently classically verifiable proof of the answer. This would resolve an open problem in the field.

Many quantum computations rely on oracle constructions to yield an exponential advantage over their classical counterparts. What can we say about classically proving the correctness of such computations, assuming interaction between a classical verifier and a quantum prover (the quantum computer)? In [3], Mahadev pioneers the study of classical arguments for BQP by relying on interaction and the post-quantum assumption Learning-With-Errors (LWE) to obtain a verification protocol. We hope to better understand the types of quantum problems that can be classically verified by studying the relativizing properties of her protocol. Moreover, we aim to understand the structural difference between arguments and proofs in the quantum setting as highlighted in [1]. Specifically, it remains an open problem whether there exists a classical proof (an interactive protocol with completeness for provers in BQP and soundness against all-powerful provers) for all problems in BQP. It seems in part that the difficulty lies in finding a structural characterization of the underlying complexity classes related to quantum verification. A formal understanding of the structure that makes for successful interactive proofs between a BPP verifier and a BQP prover is lacking, and we hope to make progress by applying ideas from [1]. Formally, we study the relativized relationship between BQP and IP_{BQP}.

Our result uses an oracle which is a special modification of the welded tree oracle introduced in [2]. We construct an oracle consisting of two disjoint welded trees. Then, given access to the oracle, and the specific name of an Entrance vertex of one Welded Tree and an Exit vertex of one Welded tree, the quantum prover must determine when the two vertices belong to the same tree or different trees, and when they belong to the same tree, provide an efficiently verifiable classical proof of that. While the first determination task is known to be in BQP using a modified version of the result in [2], we can now prove that the second task, providing a proof of the positive case, is equivalent to being able to find Entrance-Exit paths in Welded Trees, which is suggested to be impossible by [1]. Thus, assuming the impossibility result in [1] we have established an oracle problem that can be solved in BQP but not in IP_{BQP}.

This outline is a substantial abbreviation/simplification of the full technical details required to establish mathematical proofs of these results. We are still writing out the proofs in their entirety and expect to submit the completed paper later this year.

[1] A. M. Childs, et al. Quantum Algorithms and the Power of Forgetting. In *14th Innovations in Theoretical Computer Science Conference* (ITCS 2023), Y. T. Kalai, ed.,

Leibniz International Proceedings in Informatics (LIPIcs) **251** (2023), 37:1-37:22. DOI: 10.4230/LIPIcs.ITCS.2023.37

[2] A. M. Childs, R. Cleve, E. Deotto, E. Farhi, S. Gutmann, and D. A. Spielman. Exponential Algorithmic Speedup by a Quantum Walk. In *Proceedings of the 35th Annual ACM Symposium on Theory of Computing*, San Diego, CA, June 9-11, 2003, 59–68. DOI: 10.1145/780542.780552

[3] U. Mahadev. Classical Homomorphic Encryption for Quantum Circuits. In *59th IEEE Annual Symposium on Foundations of Computer Science* (M. Thorup, ed.), Paris, France, October 7-9, 2018, 332–338.

Quantum Networking Testbeds at NIST and Beyond – A Multifaceted Collaboration Effort

Shawn Geller
Thomas Gerrits
Scott Glancy
Emanuel Knill
Paulina Kuo
Alexander Kwiatkowski
Lijun Ma
Oliver Slattery
Riley Dawkins
Jaden He
Daniel Jones
Nijil Lal
Anouar Rahmouni
Yicheng Shi
Pranish Shrestha
Jing Su
Xiao Tang
Ya-Shian Li-Baboud (NIST ITL)
Abdella Battou (NIST CTL)
Amar Abane (NIST CTL)
Abderrahim Amlou (NIST CTL)
Lydia Ait Oucheggou (NIST CTL)
Mheni Merzouki (NIST CTL)
Jabir Marakkarakath Vadakkepurayil (NIST CTL)
Joshua Bienfang (NIST PML)
Adriana Lita (NIST PML)
Alan Migdall (NIST PML)
Cory Nunn (NIST PML)
Sergey Polyakov (NIST PML)
Krister Shalm (NIST PML)
Daehyun Ahn (NIST PML)
Ivan Burenkov (NIST PML)
FNU Nur Fajar Rizqi Annafianto (NIST PML).
(The many non-NIST collaborators are not listed.)

The Quantum Networking (QN) research program at NIST is a multi-division, multi-lab and multi-agency collaboration to develop prototype QNs for cutting edge experiments and to enhance QNs though the development of QN components, metrology and testbeds, and through the implementation of QN experiments and applications. ACMD is actively involved in developing four distinct quantum networking testbeds. Three of the testbeds are being built within the NIST-Gaithersburg area, and while distinct from each other are fully interconnected. These testbeds are the NIST-Gaithersburg QN testbed (NG-QNet), the Washington Metropolitan QN Research Consortium (DC-QNet) and the DARPA

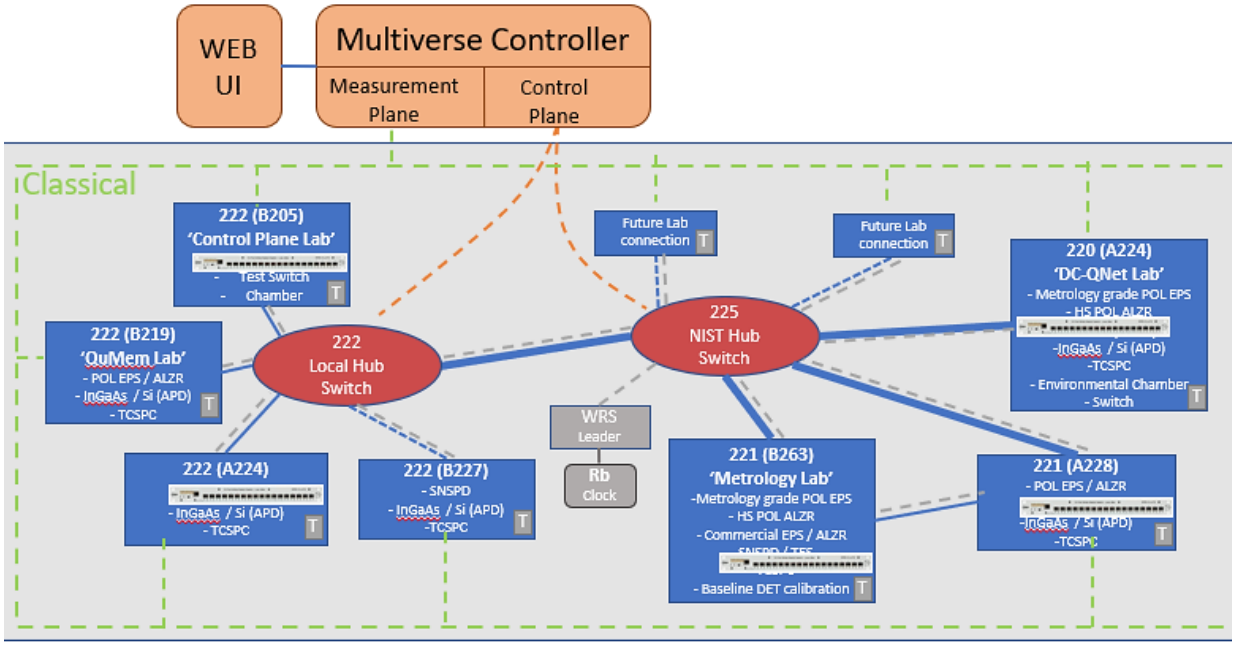

Figure 75. *Schematic of the NG-QNet.*

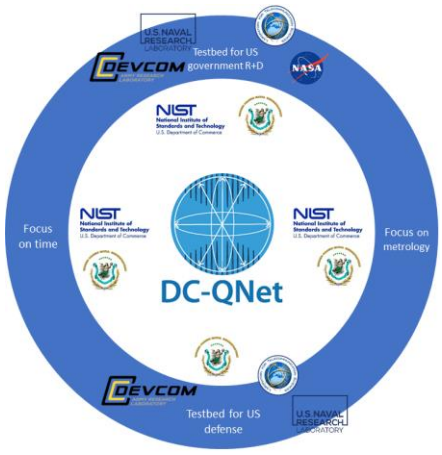

Figure 76. *Interagency Synergy of the DC-QNet.*

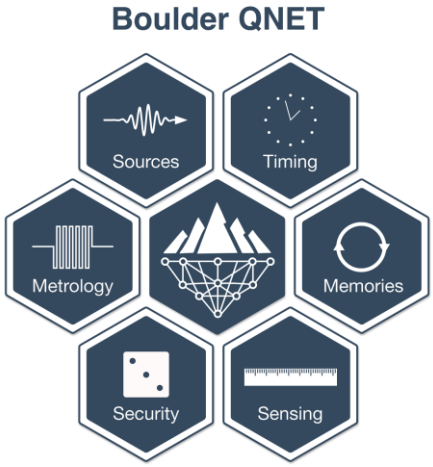

Figure 77. *Technologies and Application of the Boulder QNET.*

sponsored Quantum Augmented Network (QuANET). The NG-QNet includes the specialized management development network called the Platform for Quantum Network Innovation (PQNI) led by CTL in further collaboration with ITL and PML. The fourth testbed being built is the NIST-Boulder area QN testbed (Boulder-QNET).

The importance of QN testbeds was reiterated by the National Quantum Initiative Advisory Committee (NQIAC) in September 2024 when they concluded that "Quantum networking testbeds, if strategically chosen and properly timed, can play an important role in accelerating U.S. quantum information science leadership."

A central feature of the testbeds is the collaborative approach taken which ensures that unique skill sets (from a division, lab or agency) is coupled to unique mission and needs (e.g., metrology, security, defense) across NIST, the federal government, academia, and the emerging quantum industry. NIST personnel are leading in nationwide efforts to enhance cooperation and collaboration among US domestic QN entities. Several submitted and published papers [1-14] have resulted from this effort.

NG-QNet. The NIST Gaithersburg QN testbed (NG-QNet) is a research platform and testbed for NIST researchers to collaborate on experiments across quantum capable labs (Q-Labs) on the Gaithersburg campus in a real network environment. The NG-QNet has a dedicated facility (the DC-QNet Lab) that serves as the NIST 'node' connecting to the regional DC-QNet. It is a collaboration between ITL, CTL and PML.

DC-QNet. The DC-area area QN testbed (DC-QNet) is a six federal agency collaboration to enable strategic synergy and cooperation among agencies in QN experiments, research and development. It represents a non-proprietary environment for test and evaluation of QN concepts, components, protocols and architectures as well as a dedicated resource for the unique expertise and needs of the federal government. It is a collaboration between NIST, NASA, the Army Research Lab (ARL), the Naval Research Lab (NRL), the Laboratory for Telecommunication Sciences (LTS) and the US Naval Observatory (USNO). There are two non-regional associate collaborators, Air Force Research Lab (AFRL, Rome, NY) and Naval Information Warfare Center Pacific (NIWC, San Diego, CA).

QuANET. The Quantum Augmented Network (QuANET) is a DARPA sponsored program to implement a hybrid (quantum and classical) network enabling quantum enhancements to security on critical classical communications networks. The program is designed to address advanced persistent threat (APT) attacks on current classical networks that are defeating many state-of-the-art classical security schemes, increasing the cyber costs for US commercial and government entities. The goal is to develop an environmentally hardened quantum network interface card called a qNIC. The qNIC is intended to include the hardware, software and protocols to be fully compatible with the classical TCP/IP network stack. The DC-QNet will serve as the integration testbed for developed qNICs and quantum augmented security protocols. It is a collaboration between the federal government, industry and academia.

Boulder QNET. The NIST led Boulder quantum network testbed is focused on building scalable technologies for distributing entanglement between a number of dedicated network nodes in the Boulder area. The network aims to make NIST's world leading clock synchronization technologies compatible with quantum networks, allowing for next-generation quantum timing, sensing and secure communications applications. It is a collaboration between NIST (ITL, PML, and CTL) and the University of Colorado at Boulder (CU).

[1] W. McKenzie, A. M. Richards, S. Patel, T. Gerrits, T. G. Akin, S. Peil, A. T Black, D. Tulchinsky, A. Hastings, Y.-S. Li-Baboud, A. Rahmouni, I. A. Burenkov, A. Mink, M. Diaz, N. Lal, Y. Shi, P. Kuo, P. Shrestha, M. Merzouki, A. R. Perez, E. Onuma, D. E. Jones, A. A. Davis, T. A. Searles, J. D. Whalen, Q. S. Quraishi, K. S. Collins,

L. V. Cooper, H. Shaw, B. Crabill, O. Slattery, and A. Battou. Clock Synchronization Characterization of the Washington DC Metropolitan Quantum Network (DC-QNet). *Applied Physics Letters* **125**:16 (2024). DOI: 10.1063/5.0225082

[2] A. Rahmouni, P. Kuo, Y.-S. Li-Baboud, I. Burenkov, Y. Shi, M. V. Jabir, N. Lal, D. Reddy, M. Merzouki, L. Ma, A. Battou, S. Polyakov, O. Slattery, and T. Gerrits. 100-km Entanglement Distribution with Coexisting Quantum and Classical Signals in a Single Fiber. *Journal of Optical Communication Networks* **16** (2024), 781-787. DOI: 10.1364/JOCN.518226

[3] N. Lal, I. A. Burenkov, Y.-S. Li-Baboud, M. V. Jabir, P. Kuo, T. Gerrits, O. Slattery, and S. Polyakov. Synchronized Source of Indistinguishable Photons for Quantum Networks. *Optics Express* **32** (2024), 18257-18267. DOI: 10.1364/OE.521083

[4] M. V. Jabir, R. Dawkins, J. Sabines-Chesterking, D. V. Reddy, A. E. Lita, A. Battou, and T. Gerrits. Quantum Enhanced Precision Metrology for Quantum Networks. In *Quantum 2.0 Conference and Exhibition, Technical Digest Series (Optica Publishing Group, 2024).* Rotterdam, Netherlands, June 2024. DOI: 10.1364/QUANTUM.2024.QTh4C.5

[5] Y. Shi, T. Gerrits, and O. Slattery. Fiber Polarization Characterization and Stabilization in a Quantum Network. In *Proceedings Volume PC13025, Advanced Photon Counting Techniques XVIII; PC1302507.* National Harbour, MD, April 2024. DOI: 10.1117/12.3016179

[6] N. Lal, I. A. Burenkov, Y. Li-Baboud, M. V. Jabir, P. Kuo, T. Gerrits, O. Slattery, and S. V. Polyakov. Network-Ready Source of Indistinguishable Single Photons. In *CLEO 2024, Technical Digest Series (Optica Publishing Group, 2024).* Charlotte, May 2024. DOI: 10.1364/CLEO_FS.2024.FTh3R.8

[7] A. Rahmouni, P. S. Kuo, Y. Shi, M. V. Jabir, N. Lal, I. A. Burenkov, Y. S. Li-Baboud, M. Merzouki, A. Battou, S. V. Polyakov, O. Slattery, and T. Gerrits. Entanglement Distribution for Metropolitan-scale Quantum Networks with Classical Coexistence. In *CLEO 2024, Technical Digest Series (Optica Publishing Group, 2024).* Charlotte, NC, May 2024. DOI: 10.1364/CLEO_FS.2024.FTu3F.2

[8] N. Lal, I. A. Burenkov, Y.-S. Li-Baboud, M. V. Jabir, P. S. Kuo, T. Gerrits, O. Slattery and S. V. Polyakov. Synchronized Network Source of Indistinguishable Photons. In *Proceedings of SPIE Volume PC12911, Quantum Computing, Communication, and Simulation IV; PC129110T.* San Francisco, CA, February 2024. DOI: 10.1117/12.3002401

[9] A. Rahmouni, P. S. Kuo, Y. S. Li-Baboud, I. A. Burenkov, Y. Shi, M. V. Jabir, N. Lal, D. Reddy, M. Merzouki, L. Ma, A. Battou, S. V. Polyakov, O. Slattery, and T. Gerrits. 100-km Entanglement Distribution with Co-existing Quantum and Classical Signals in a Single Fiber. In *Quantum 2.0 Conference and Exhibition, Technical Digest Series (Optica Publishing Group, 2024).* Rotterdam The Netherlands, June 2024. DOI: 10.1364/QUANTUM.2024.QTh2B.4

[10] C. Nunn, N. L. C. Koyyottummal, I. Burenkov, Y.-S. Li-Baboud, P. Kuo, T. Gerrits, and S. Polyakov. Synchronized Pump Lasers for Network-Compatible Sources of Indistinguishable Photons. In review.

[11] F. Atzori, J. M. Vadakkepurayil, C. Nunn, N. L. C. Koyyottummal, I. Burenkov, and S. Polyakov. Characterization of Entanglement Distribution in a Quantum Network Using Quantum Resources Only. In review.

[12] J. M. Vadakkepurayil, D. Ahn, Ivan Burenkov, Abdella Battou, Sergey Polyakov, and N. Fajar R. Annafianto. Quantum Enhanced Phase Estimation and Locking of Metropolitan-Scale Fiber Link with Faint Light. In Review.

[13] J. M. Vadakkepurayil, D. Ahn, F. N. U. Nur Fajar Rizqi Annafianto, I. Burenkov, A. Battou, and S. Polyakov. Phase Stabilization of Metropolitan Quantum Networks Links with Single-Photon Detection. In review.

[14] A. Abane, M. Cubeddu, V. S. Mai, and A. Battou. Entanglement Routing in Quantum Networks: A Comprehensive Survey. In review.

Quantum Network and Component Metrology

Thomas Gerrits
Oliver Slattery
Anouar Rahmouni
Yicheng Shi
Jaden He
Pranish Shrestha
Jing Su
Scott Glancy
Manny Knill
Riley Dawkins
Paulina Kuo
Lijun Ma
Xiao Tang
Nijil Lal
Ya-Shian Li-Baboud (NIST ITL)
Abdella Battou (NIST CTL)
Amar Abane (NIST CTL)
Abderrahim Amlou (NIST CTL)
Lydia Ait Oucheggou (NIST CTL)
Mheni Merzouki (NIST CTL)
Jabir Marakkarakath Vadakkepurayil (NIST CTL)
Alan Migdall (NIST PML)
Sergey Polyakov (NIST PML)
Josh Bienfang (NIST PML)
Ivan Burenkov (NIST PML)

The Quantum Network and Component Metrology Project focusses on the characterization of quantum network links, components, and protocols. Measurement protocols and deployable tools are developed in our lab and used within our NIST Gaithersburg quantum network testbed (NG-QNet) and the regional quantum network called the DC-QNet. We collaborate with researchers across different NIST OUs (PML, ITL and CTL) as well as with researchers from other government agencies and industry. The project tackles measurement

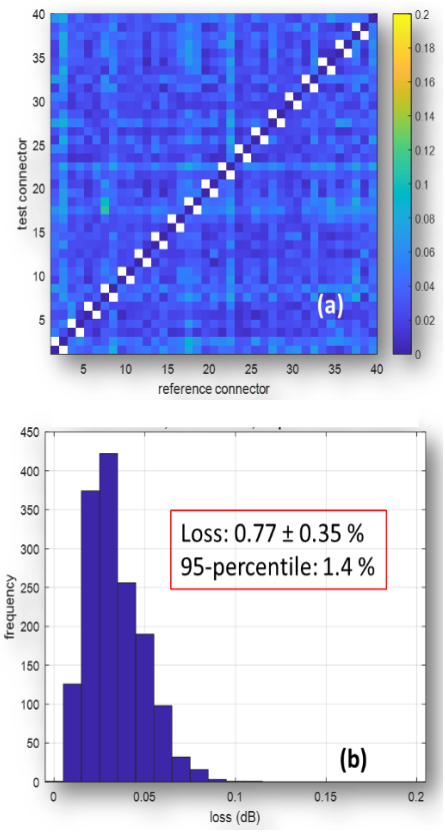

Figure 78. *Loss evaluation of 40x40 random fiber connector combinations. (a) fiber connector loss matrix. (b) histogram of fiber connector losses.*

challenges for single-photon devices and components and therefore works closely with companies within the Quantum Economic Development Consortium (QED-C) on component characterization and solving measurement challenges [1]. Highlights for the last year include:

- fiber polarization stabilization of our 60 km aerial fiber between NIST and our lab at the University of Maryland;
- collaboration with industry to develop and measure the loss and repeatability of ultra-low loss optical fiber connectors; measurement of optical fiber length to an accuracy of $1{:}10^{-9}$;
- quantum-assisted loss measurements based on a two-mode squeezed state, showing a 4 dB advantage over the best classical measurement;
- a nascent effort to develop remote single-photon detector calibration over the network; and
- continued built-up of infrastructure for continuous variable quantum states of light network metrology.

Some highlights are presented below in more detail.

Ultra-low loss fiber connectors. Quantum networks require low-loss components to preserve the quantum state they are carrying. Each component connected by optical fibers or fiber connected at fiber patch panels will contribute to the overall link loss, thus adding to the unavoidable optical fiber loss. While reducing optical loss is in fiber connections is the main goal of this project, the repeatability of fiber connections is also a challenge for the calibration of fiber-coupled single photon detectors. Currently, this repeatability poses the largest uncertainty component for the calibration of single-photon detectors [2]. We developed the measurement infrastructure and protocols to evaluate a fiber connector's loss and repeatability with measurement uncertainties of 0.01 %. Figure 78 shows an example of loss measurements for 40-by-40 fiber connectors, which were mated with random fiber connector unions. The probing wavelength was 1550 nm. Figure 78a shows an intensity plot of each individual connection. Light-blue streaks indicate a higher loss for a particular fiber connector. Figure 78b shows the histogram of all measurements presented in Figure 78a. The x-axis is shown in dB. The measured mean loss is 0.77 ± 0.35 % with a 95-percentile of 1.4 %. The evaluated uncertainty is already on the same order of uncertainty we can achieve with our single-photon detector calibration and when splicing the detector fibers [2] and is therefore an important milestone to achieving fiber-coupled single-photon detector calibrations with low uncertainties.

Accurate fiber length measurements. Synchronization of quantum nodes within a quantum network is paramount for the successful execution of quantum network protocols that rely on interference between individual photons originating from different nodes within the network. For example, when trying to perform entanglement swapping using single photons that are generated by spontaneous parametric downconversion, the photons need to arrive to within 10 ps of one another at the interference plane [3]. 10 ps corresponds to about 2 mm path difference in optical fibers. This level of synchronization in metropolitan (10's of kilometers) scale fiber, along with measurement and stabilization is about five orders of magnitude more stringent than for current classical networking. We therefore developed a method to measure fiber length with unprecedented precision. The method is based on measuring the time-of-flight of a single photon pulse through an optical fiber. Figure 79 shows the TDEV of our time-of-flight measurement for a 120 km roundtrip in an aerial fiber between NIST and the University of Maryland. The TDEV characterizes the average time offset between the injection of the single-photon pulse into the fiber and the arrival time of the single photon pulse at the single photon detector as a function of different averaging times. This can also be interpreted as the accuracy to which the fiber length can be estimated for different averaging times. We find a record 1.7 ps uncertainty in the determination of the 120 km round trip length. Note that TDEV increases for longer averaging

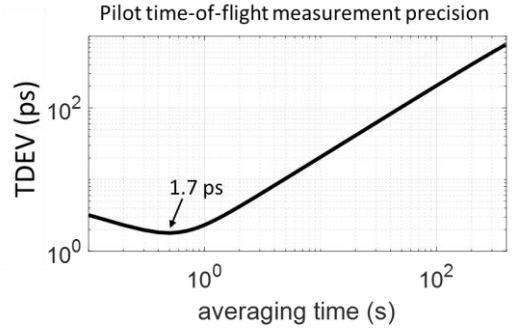

Figure 79. *TDEV of our time-of-flight measurement for a round-trip measurement of the aerial NIST-UMD fiber (≈120 km).*

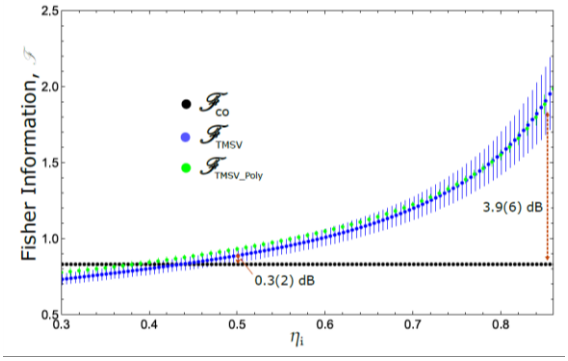

Figure 80. *Fisher Information of measuring transmissivity of an optical component using a two-mode squeezed state.*

times, which is due to the fact that the aerial fiber is changing in optical path length for such long integration times due to thermal effects related to the changing outside temperature.

Continuous Variable Quantum Network Metrology. Exotic quantum states of light exploiting the continuous variable (CV) nature of light are an important tool for optical quantum information processing and form the basis of a compelling platform for quantum computing, sensing and communication. They allow a greater range of states than are available with only discrete variable protocols. We are developing a measurement infrastructure for CV states of light at the telecom wavelengths around 1550 nm and have developed a source of two-mode squeezing at 1550 nm that we utilized to measure loss in optical components, e.g. an optical fiber. Using a two-mode squeezed state for loss estimation will give better uncertainties for each individual trial as compared to a classical coherent state [4]. Due to the fact that photon numbers are correlated in a two-mode squeezed vacuum state, the detection of a certain photon number in one mode signals the presence of the same photon number in the other (probing) mode, given there is no loss in both modes. This principle can be extremely sensitive to measurement of loss, as there is an expected photon number in the probing mode. Once loss is introduced, the expected mean photon number decreases and individual detection events become more randomized. However, this random character can still surpass the coherent state photon number randomness up to some total loss and noise in the system. Our two-mode squeezed photon source is a highly efficient source with a system efficiency of >80 %. Our protocol is based on photon-number resolved detection using transition edge sensors [5]. Figure 80 shows the Fisher information for the estimation of component transmissivity for our two-mode squeezed vacuum source and a weak coherent state. We see a clear advantage using a two-mode squeezed vacuum state over using a weak coherent state. This method can readily be implemented in quantum networks to measure in-situ component loss, where probing signals based on single photons are desired to minimize cross-talk between classical signals and the quantum signal due to, for example, Raman scattering.

[1] Single-Photon Measurement Infrastructure for Quantum Applications (SPMIQA): Needs and Priorities. Quantum Economic Development Consortium (QED-C), 2022. URL: https://quantumconsortium.org/single-photon-report

[2] T. Gerrits, et al. Calibration of Free-space and Fiber-coupled Single-photon Detectors. *Metrologia* **57** (2020), 015002.

[3] W. McKenzie, et al. Clock Synchronization Characterization of the Washington DC Metropolitan Quantum V. Network (DC-QNet). *Applied Physics Letters* **125**:16 (2024).

[4] V. Giovannetti, et al., Advances in Quantum Metrology. *Nature Photon*ics **5** (2011), 222–229.

[5] T. Gerrits, et al. Superconducting Transition Edge Sensors for Quantum Optics. In *Superconducting Devices in Quantum Optics*, Springer, Berlin, 2015.

Polarization Stabilization and Distributed Polarization Characterization Over Quantum Network Fibers

Yicheng Shi
Ben Werchowsky
Anouar Rahmouni
Pranish Shrestha
Thomas Gerrits
Oliver Slattery

In a fiber-based quantum network, transmitting polarization-encoded photons with good fidelity is a challenging task due to the presence of fiber birefringence, which induces a random rotational transformation to the polarization states of photons that changes over time. To enable quantum networking over the existing telecommunication fiber infrastructure, one needs to characterize the stability of the fibers in real

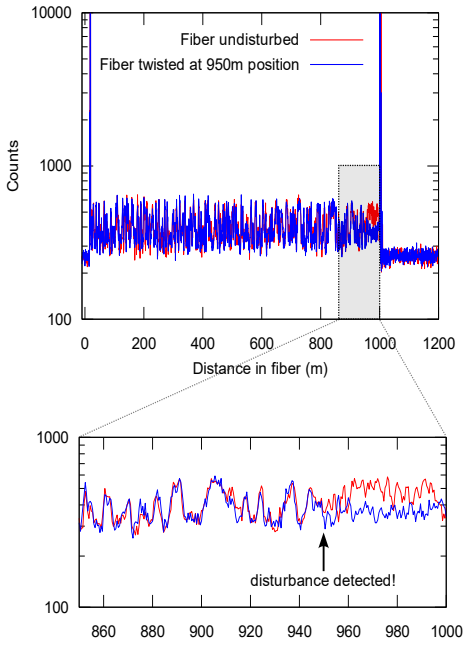

Figure 81. *Two sample P-OTDR traces of a 1-km fiber spool, measured at the H polarization basis. A small segment of the fiber was twisted about 50 meters from the tail, which is clearly indicated by the difference between the two traces.*

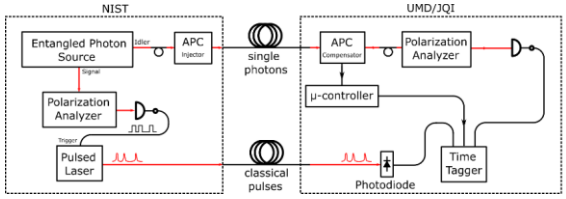

Figure 82. *Diagram of the entanglement distribution setup incorporated with the Qunnect APC modules.*

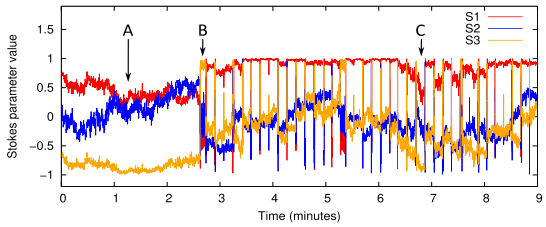

Figure 83. *Stokes parameters of probe light propagating across the 62km link between NIST and UMD, without (A) and with (B & C) polarization stabilization. The dips in the traces occurs once every 10 seconds and are due to the APC regularly checking up on the received polarization reference states.*

time and implement an active polarization stabilization scheme to compensate for the fiber-induced polarization transformation.

Distributed fiber polarization characterization with P-OTDR. In the fiber-optic communication industry, Optical Time-Domain Reflectometers (OTDRs) are commonly utilized by engineers to probe the loss profile of fiber links. An OTDR injects optical pulses into the fiber and monitors the amount of back-scattered light after each pulse, which provides a distributed measurement of the artifacts and optical losses at different points of the fiber. In an advance over conventional OTDR, we implemented a Polarization-sensitive Optical Time-Domain Reflectometer (P-OTDR) to perform distributed measurements of a fiber's polarization properties [1]. Unlike a conventional OTDR, the P-OTDR setup projects the back-scattered photons to different polarization measurement bases before detection, which allows us to observe the change of polarization states at different locations along the fiber. Such a technique can be used to characterize the birefringence properties of a long fiber in a distributed fashion or may be used to monitor the stability of different parts of a fiber link (see Figure 81).

Towards entanglement distribution over a 62 km polarization-stabilized fiber. Following the establishments of different quantum and classical network nodes in DC-QNet [2], we are moving towards an entanglement distribution demonstration between NIST and the University of Maryland, College Park campus (UMD). The two quantum nodes are connected by a 62 km fiber link with about 22 dB of optical loss. This fiber link is partially aerial-based and is stabilized with an active polarization compensator (APC), commercially developed by Qunnect Inc. As depicted in Figure 82, the APC injector module sends a set of polarization reference states across the link which are measured by a polarimeter inside the APC module. Based on the measurement results, the compensator adjusts an inline polarization controller to minimize the difference between the measured and the original reference states.

The performance of the APC is shown in Figure 83, which displays the stokes parameters of a probe light propagating across the 62 km fiber. In this nine-minute trace, the fiber was initially unattended (A) until the stabilization operation started at (B). The APC performs quick check on the received states once every 10 seconds and performs polarization compensation if they deviate too much from the reference states (C).

The APC polarization reference signal coexists with the entangled photons via time-division multiplexing, which means that entanglement distribution and polarization stabilization take place at different times. We incorporated the APC into an existing entanglement distribution setup (Figure 82), in which a microcontroller coordinates the order of the two operations. The setup has been tested in a lab environment and will be implemented over the 62 km deployed fiber between NIST and the University of Maryland in the coming months.

[1] Y. Shi et al. Fiber Polarization Characterization and Stabilization in a Quantum Network. In Proceedings Volume PC13025, *Advanced Photon Counting Techniques XVIII*, PC1302507. National Harbor, MD, April 2024.

[2] W. McKenzie et al. Clock Synchronization Characterization of the Washington DC Metropolitan Quantum Network (DC-QNet). *Applied Physics Letters* **125**:16 (2024).

Indistinguishability of Arbitrary Signal and Idler Photons

Nijil Lal
Paulina Kuo
Thomas Gerrits
Oliver Slattery
Ivan Burenkov (NIST PML)
Sergey Polyakov (NIST PML)

Indistinguishability of single photons is a requirement for scalable quantum networks to realize two photon interference-based network protocols such as entanglement swapping and quantum teleportation. While the indistinguishability, and resulting quantum interference, between signal and idler photons from a single parametric down-conversion (PDC) event has been well studied in the past, the indistinguishability of signal and idler photons that are not members of the same bi-photon pair enables the scalable and interchangeable use of any photon from any of the conjugated paths of down-conversion.

Following last year's work [1], we use the source of indistinguishable photons, designed and built at NIST, that satisfies the design constraints of a network compatible single photon source, i.e., picosecond-level jitter, single spatial and temporal-bandwidth mode, pulse duration of at least 10 ps, telecom C-band wavelength, as well as a high single-photon rate. In the ongoing work, we study the indistinguishability between signal and idler photons from independent down-conversion events. Our source uses a transform-limited pulsed pump laser (775 nm, 80 MHz, 10 ps Ti-Sapph) to generate telecom photons (1550 nm) so that the maximal fraction of energy in the crystal is utilized to generate indistinguishable biphotons. Due to the multimode nature of the PDC process, the generated photons are spectrally selected through additional narrow filtering using volume Bragg gratings. In our Type-II SPDC source, the generated photons are indistinguishable except in polarization (for their easy separation) which is later matched using polarization converters before their interference. Therefore, any two photons from any two signal/idler mode are expected to quantumly interfere.

The experimental schematic is given in Figure 84. A post processing algorithm looks for double-heralded coincidences between signal and idler photons originating from two independent PDC events (corresponding to different pump pulses separated in time). The delay line length is adjusted to match this separation between the

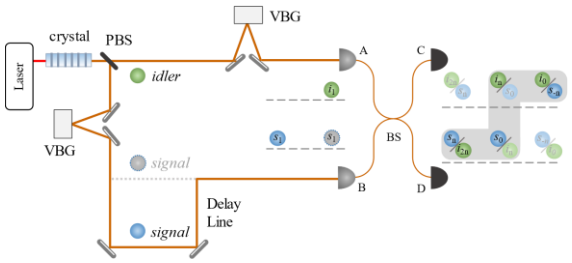

Figure 84. *Experimental schematic for studying indistinguishability between arbitrary signal and idler photons. The post-processing algorithm for the double-heralded coincidence detection is illustrated on the right.*

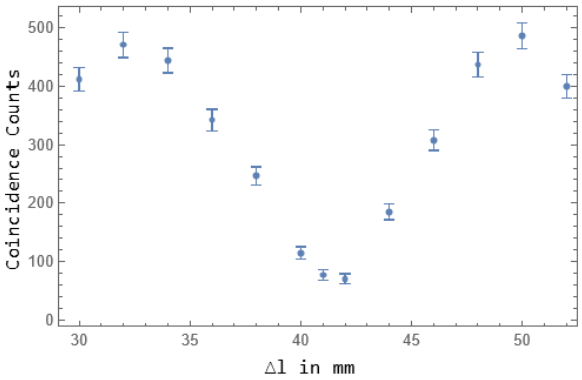

Figure 85. *HOM dip for the interference between correlated signal-idler pair from the same PDC event (without the delay line). By achieving right spectral and temporal overlap of the single photon wave functions, we expect to observe the indistinguishability for the case of arbitrary signal and idler photons as well.*

pump pulses under consideration. For the right delay matching, we observe double heralded coincidences. The post-processing of the detected time tags goes as follows: a detection in either of the detectors (resulting from idler *or* signal) marks the first herald; simultaneous clicks on both the detectors (due to an idler *and* delayed signal) in the central bin marks the coincidence event; and a final detection in either of the detectors (from idler *or* signal) marks the second herald. A successful combination of these marks a double heralded coincidence detection.

The Hong-Ou-Mandel dip for the case of correlated signal-idler pairs (originating from the same PDC event) is measured as a pre-requisite for the experiment (Figure 85) where the signal photon travels equal distance (gray dashed line in Figure 84) as the idler photon in the interferometer. An experiment is underway to verify the indistinguishability and observe the interference between the uncorrelated signal and idler photons originating from independent PDC events. We also plan to study the interference between multiple such FTL sources, synchronized over a network, which will further enable quantum network protocols between distant nodes.

[1] N. Lal, I. A. Burenkov, Y.-S. Li-Baboud, M. V. Jabir, P. Kuo, T. Gerrits, O. Slattery, and S. Polyakov. Synchronized Source of Indistinguishable Photons for Quantum Networks. *Optics Express* **32**:10 (2024), 18257-18267.

Photon-pair Sources for Quantum Networking

Paulina Kuo
Sesha Sai Pavan Kumar Challa

Entangled photon pairs are key resources for quantum networking and quantum information processing. Spontaneous parametric down-conversion (SPDC) in a second-order nonlinear crystal is often used to produce entangled-photons. SPDC is attractive because it is simple, requiring only a pump source and crystal. However, SPDC for photon-pair production has drawbacks, including probabilistic production of photons, and a need to trade-off pair-production rate with double down-conversion events that result in accidental-coincidence counts. Our research seeks to find ways to improve SPDC for entangled-photon pair generation and to explore the engineering of SPDC for improved properties.

Recently, we have investigated backward-wave SPDC for photon-pair production [1]. In collaboration with KTH Stockholm, we performed SPDC in a periodically poled KTiOPO4 (PPKTP) crystal with ultrashort poling period (500 nm). The ultrashort poling period allows counter-propagation of the longest-wavelength down-converted beam (that is, the longest-wavelength photons become backward-going compared to the other photons). This unique scenario results in new, potentially useful properties of the SPDC photons. Firstly, the backward-going photons have very narrow bandwidth, independent of the bandwidth of the pump photons. This could be useful for coupling to quantum nodes that have intrinsically narrow bandwidths, such as those based on atomic transitions. Secondly, we demonstrated that backward-wave SPDC can be used for frequency translation [1]. In this process, spectral properties of the pump can be transferred to the forward-going SPDC photons. Backward-wave SPDC that utilizing this property can be used as a source of spectrally shaped, heralded single-photons.

We are also investigating engineering of the periodic poling pattern of the crystal used in SPDC sources. Typically, SPDC crystals have uniform periodic poling patterns that allow phase matching of a desired set of wavelengths. Without periodic patterning, the indices of refraction of the crystal dictate the output wavelengths from the SPDC crystal. By using aperiodic poling patterns such as those utilizing the phase-modulation technique [2], not only can we choose the SPDC wavelengths, but we can also engineer the SPDC spectra. We are applying this technique to SPDC of 775 nm → 1530 nm (signal, s) + 1569 nm (idler, i) to generate the entangled photon-pair state $|\psi\rangle = (|H_s V_i\rangle + \exp(\mathrm{i}\varphi)|V_s H_i\rangle)/\sqrt{2}$. In the past year, we have worked with a company to produce custom poled PPKTP crystals. We are studying how the poling pattern affects the down-conversion spectra and how well we can produce the state $|\psi\rangle$.

[1] P. S. Kuo, D. V. Reddy, V. Verma, S. W. Nam, A. Zukauskas, and C. Canalias. Photon-pair Production and Frequency Translation Using Backward-Wave Spontaneous Parametric Downconversion. *Optica Quantum* **1**:2 (2023), 43.

[2] P. S. Kuo, V. B. Verma, and S. W. Nam. Demonstration of a Polarization-Entangled Photon-Pair Source Based on Phase-Modulated PPLN. *OSA Continuum* **3**:2 (2020), 295.

Thin-film Lithium Niobate Integrated Photonics for Quantum Information Processing

Sesha Sai Pavan Kumar Challa
Paulina Kuo

Performing quantum information processing using integrated optics is an attractive alternative to processing using free-space or bulk optics because integrated optics offers compact size and monolithic construction for high repeatability and phase stability. We have been exploring thin-film lithium niobate (TFLN) for integrated quantum photonics. TFLN offers multiple functionalities at the same time, including waveguiding, electro-optic modulation and optical frequency conversion (for quantum frequency conversion or entangled photon-pair generation) [1]. The initial step is to develop a process to fabricate low-loss waveguides in TFLN.

Using the NIST nanofabrication facility, we have performed a systematic study of argon-plasma dry etching of TFLN [2, 3]. We have identified masking materials (Figure 86a and b). We have also optimized parameters for dry etching to produce low-roughness waveguide sidewalls, which are needed to achieve low optical losses. Redeposited material forms during dry etching, so we have developed a wet-cleaning procedure to remove the redeposition. Scanning electronic microscope (SEM) images of the etching waveguides show highly promising results.

Using the established recipe, we modeled and fabricated self-focusing input/output grating couplers (Figure 86d and e) for telecom wavelengths with exhibited loss of 6 dB/coupler. Our initial micro-ring resonator (Figure 86f) devices exhibited a quality factor (Q) of ≈12000. We attribute this loss to the narrow waveguide widths which causes scattering of the optical

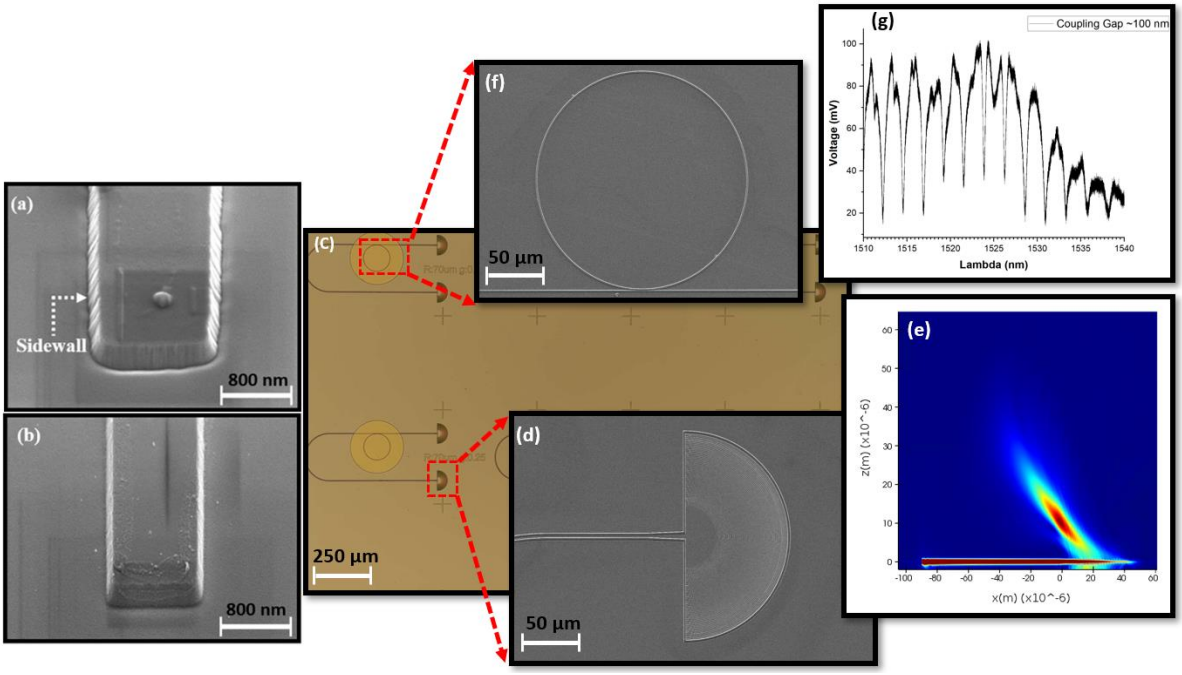

Figure 86. *SEM images of etched TFLN waveguides using (a) photoresist soft mask, (b) Cr hard mask. The Cr mask produces smoother sidewalls, (c) microscope image of focusing grating couplers (GCs) with micro-ring resonator, (d) SEM image of the GC, (e) numerical 3D-modeling of focusing GC showing that light travelling from the waveguide is focused at a height of ~10 µm above the GC, (f) SEM image of the micro-ring resonator, and (g) resonances at telecom wavelength for a micro-ring with coupling gap of 100 nm from the bus waveguide.*

fundamental mode along the bends of the waveguide. We are developing a process to further increase the quality factor of the resonator devices.

[1] D. Zhu, et al. Integrated Photonics on Thin-Film Lithium Niobate. *Advances in Optics and Photonics* **13** (2021), 242.

[2] S. Challa, N. Klimov, and P. Kuo. "Argon-Plasma Dry Etch of sub-Micron Feature-Size Waveguides in Thin-Film Lithium Niobate." AVS-69, American Vacuum Society, Portland, Oregon, November 5-10, 2023.

[3] Ch. S. S. P Kumar, N. Klimov, and P. Kuo. Optimization of Waveguide Fabrication Processes in Lithium-Niobate-On-Insulator Platform. *AIP Advances* **14** (2024), 065317.

Quantum Photonics Vocabulary Development

Paulina Kuo
Thomas Gerrits
Alan Migdall (PML)
Joshua Bienfang (PML)

Following the release of the NIST Single-Photon Sources and Detectors Dictionary in 2023 [1], we have worked with IEC/ISO (the International Electrotechnical Commission / International Organization for Standardization), on developing vocabularies and documentary standards for Quantum Technologies within the IEC/ISO, the Joint Technical Committee 3 (JTC 3) on quantum technologies which was established in 2024. We are participating in several JTC 3 discussion groups (so called "Ad Hoc groups (ahGs)") that are working to define the various technical areas in quantum technologies and identify areas that are ready for standards or other document development. The ahGs that we have worked on include: the Quantum Terminology and Metrics Ad Hoc Group (ahG2), the Quantum Random Number Generator (QRNG) Ad Hoc Group (ahG6) and the Quantum Enabling Technologies Ad Hoc Group (ahG7). We have also begun work to establish a project team (PT) to develop a Quantum Photonics Vocabulary, which is based on the dictionary [1].

[1] J. C. Bienfang, T. Gerrits, P. S. Kuo, A. Migdall, S. Polyakov, and O. Slattery. Single-Photon Sources and Detectors Dictionary. NIST IR 8486, National Institute of Standards and Technology, September 2023. DOI: 10.6028/NIST.IR.8486

Post-Quantum Cryptography

Yi-Kai Liu
Gorjan Alagic (NIST ITL)
Maxime Bros (NIST ITL)
Lily Chen (NIST ITL)
Pierre Ciadoux (NIST ITL)
David Cooper (NIST ITL)
Quynh Dang (NIST ITL)
Thinh Dang (NIST ITL)
John Kelsey (NIST ITL)
Jacob Lichtinger (NIST ITL)
Carl Miller (NIST ITL)
Dustin Moody (NIST ITL)
Rene Peralta (NIST ITL)
Ray Perlner (NIST ITL)
Angela Robinson (NIST ITL)
Hamilton Silberg (NIST ITL)
Daniel Smith-Tone (NIST ITL)
Noah Waller (NIST ITL)

Since 2016, the NIST Computer Security Division has been leading an open, competition-like process to develop standards for post-quantum cryptography (PQC). The goal is to standardize new schemes for public-key encryption, key establishment, and digital signatures in order to replace existing schemes, such as RSA, Diffie-Hellman, and elliptic curve cryptosystems, that would be vulnerable to cryptanalysis using quantum computers. These new post-quantum cryptosystems will be crucial for secure web browsing, digital certificates, secure software updates, and many other applications. While large quantum computers have not yet been built, NIST believes it is prudent to prepare for that possibility in order to provide long-term security for sensitive information that is transmitted over the Internet today and may remain sensitive for many years into the future.

In August 2024, NIST reached a milestone: the publication of the first three Federal Information Processing Standards (FIPS) for post-quantum cryptography:

- FIPS 203, Module-Lattice-Based Key-Encapsulation Mechanism (ML-KEM) Standard
- FIPS 204, Module-Lattice-Based Digital Signature (ML-DSA) Standard
- FIPS 205, Stateless Hash-Based Digital Signature (SLH-DSA) Standard.

These standards were derived from three post-quantum cryptosystems (CRYSTALS-Kyber, CRYSTALS-Dilithium and SPHINCS+) that were selected by NIST for standardization in 2022, following three rounds of intensive analysis and evaluation by NIST and the cryptographic community over several years. These standards consider the extensive feedback that NIST received on the initial public drafts in 2023.

In addition, NIST is soliciting public comments on an initial public draft of NIST SP 800-227, Recommendations for Key Encapsulation Mechanisms, which provides additional guidance on the usage of ML-KEM. NIST is also in the process of drafting FIPS 206, Fast-Fourier-Transform-Over-NTRU-Lattice-Based Digital Signature (FN-DSA) Standard, which is based on a fourth cryptosystem (Falcon) that was selected by NIST for standardization in 2022.

At the same time, NIST is continuing its evaluation process, and may select additional cryptosystems for standardization in the future, in order to mitigate the risk of unexpected advances in cryptanalysis, and to support use-cases that require cryptosystems with special properties. For this purpose, in 2022, NIST chose four key establishment algorithms (BIKE, Classic McEliece, HQC and SIKE) for a fourth round of evaluation, which is still ongoing. For similar reasons, in 2022, NIST also issued a new call for submissions of digital signature schemes. These submissions were due in June 2023 and are currently undergoing evaluation by NIST and the cryptography community. In October 2024, NIST selected a subset of these submissions to move on to a second round of evaluation [1].

To engage with the post-quantum cryptography community and other stakeholders, NIST has been organizing a series of virtual seminars on recent developments in PQC, and held its Fifth PQC Standardization Conference on April 10-12, 2024, in Rockville, MD (in-person). NIST is planning to hold a Sixth PQC Standardization Conference in September 2025.

Additional information on these activities is available on the NIST PQC web pages.[22] NIST is also working with industry on PQC migration issues, through the National Cybersecurity Center of Excellence (NCCoE).

To support these activities, NIST also carries out independent analysis and research on post-quantum cryptography and related topics. Recent work has focused on topics such as the implementation and testing of floating-point arithmetic operations in the signature scheme Falcon; the security of the signature schemes Dilithium and DME, and the key exchange protocol BIKE [2, 3, 4]; no-go theorems for certain approaches to solving lattice problems on a quantum computer [5]; and the potential applications of quantum technologies combined with post-quantum cryptography [6, 7, 8].

[1] G. Alagic, M. Bros, P. Ciadoux, D. Cooper, Q. Dang, T. Dang, J. M. Kelsey, J. Lichtinger, C. A. Miller, D. Moody, R. Peralta, R. Perlner, A. Robinson, H. Silberg, D. Smith-Tone, N. Waller, and Y.-K. Liu. Status Report on the First Round of the Additional Digital Signature Schemes for the NIST Post-Quantum Cryptography Standardization Process. NISTIR 8528 (2024). DOI: 10.6028/NIST.IR.8528

[22] https://csrc.nist.gov/Projects/post-quantum-cryptography

[2] K. A. Jackson, C. A. Miller, and D. Wang. Evaluating the Security of CRYSTALS-Dilithium in the Quantum Random Oracle Model. In *EUROCRYPT 2024 - Proceedings, Part VI*. Lecture Notes in Computer Science **14656** (2024), 418-446. DOI: 10.1007/978-3-031-58751-1_15

[3] P. Briaud, M. Bros, R. A. Perlner, and D. Smith-Tone. Practical Attack on All Parameters of the DME Signature Scheme. In *EUROCRYPT 2024 - Proceedings, Part VII*. Lecture Notes in Computer Science **14657** (2024), 3-29. DOI: 10.1007/978-3-031-58754-2_1

[4] S. Arpin, T. R. Billingsley, D. R. Hast, J. B. Lau, R. Perlner, and A. Robinson. A Graph-Theoretic Approach to Analyzing Decoding Failures of BIKE. Cryptology Preprint Archive 2024/1736. URL: https://eprint.iacr.org/2024/1736

[5] Y.-K. Liu. An Uncertainty Principle for the Curvelet Transform, and the Infeasibility of Quantum Algorithms for Finding Short Lattice Vectors. Preprint: arXiv:2310.03735. DOI: 10.48550/arXiv.2310.03735

[6] Y.-K. Liu and D. Moody. Post-Quantum Cryptography, and the Quantum Future of Cybersecurity. *Physical Review Applied* **21**:4 (2024), 040501. DOI: 10.1103/PhysRevApplied.21.040501

[7] Y. Alnawakhtha, A. Mantri, C. A. Miller, and D. Wang. Lattice-based Quantum Advantage from Rotated Measurements. *Quantum* **8** (2024), 1399. DOI: 10.22331/q-2024-07-04-1399

[8] C. A. Miller. Hidden-State Proofs of Quantumness. Preprint: arXiv:2410.06368. DOI: 10.48550/arXiv.2410.06368

Joint Center for Quantum Information and Computer Science

Victor Albert
Matthew Coudron
Yi-Kai Liu
Justyna Zwolak
Gorjan Alagic (NIST ITL)
Carl Miller (NIST ITL)
Alexey Gorshkov (NIST PML)
Michael Gullans (NIST PML)
Jacob Taylor (NIST PML)
Nicole Yunger Halpern (NIST PML)
Andrew Childs (University of Maryland)
Daniel Gottesman (University of Maryland)

http://quics.umd.edu/

Established in October 2014, the Joint Center for Quantum Information and Computer Science (QuICS) is a cooperative venture of NIST and the University of Maryland (UMD) to promote basic research in understanding how quantum systems can be effectively used to store, transport and process information. QuICS brings together researchers from the University of Maryland Institute for Advanced Computer Studies (UMIACS) and the UMD Department of Computer Science and Physics with NIST's Information Technology and Physical Measurement Laboratories, together with postdocs, students, and a host of visiting scientists.

QuICS has quickly established itself as a premier center for research in quantum information science. Fourteen Fellows, five Affiliate Fellows, one Adjunct Fellow, 19 postdocs, and 71 graduate students are currently associated with the center. QuICS also hosted 36 visiting scientists during CY 2024.

ACMD's Yi-Kai Liu's term as Co-Director of the Center will end in early 2025; Carl Miller of ITL's Computer Security Division will then take over as Co-Director. Andrew Childs' term as of the UMD Co-Director ended in July 2024; he is succeeded by Daniel Gottesman. Both are from the UMD Computer Science Department. QuICS welcomed a new Fellow, Runzhou Tao, who joined UMD as an assistant professor in the computer science department. Tao has experience in quantum programming languages, software engineering and theoretical computer science. His research interests center on building scalable and reliable software for quantum computing.

A QuICS-funded workshop "Advancing Quantum Computation Beyond Gate-Model" was held at UMD on October 7-9, 2024. It was organized by QuICS Fellow Xiaodi Wu, former QuICS Fellow Murphy Niu (now at UCSB), and Yuxiang Peng (Purdue). The workshop featured 24 speakers.[23]

The Center continues to be very productive. In CY 2024, 135 research papers were produced by those associated with the center. During CY 2024 two patents were granted based on work of the center and five new applications were filed.

Notably, five papers co-authored by QuICS members were accepted for presentation at the very high selective Quantum Information Processing (QIP) conference, which was held in Taipei in January 2024.

Among the recent technical accomplishments of QuICS researchers are the following:

- SimuQ, a programming language and compiler for analog quantum computers,
- a detailed analysis of quantum algorithms for simulating nuclear effective field theories,
- an experimental demonstration of a programmable quantum information processor with up to 48 logical qubits, implemented using up to 280 physical qubits based on neutral atoms, in a project led by Mikhail Lukin at Harvard University, with theoretical contributions from QuICS researchers,
- classical and quantum simulations of scattering dynamics of the Schwinger model,

[23] https://quics-beyond-2024.umiacs.io/

- generalizations of quantum state t-designs to continuous-variable systems,
- a new approach to constructing quantum error-correcting codes for continuous-variable systems, such as microwave and photonic oscillators,
- "Bell sampling," a technique for benchmarking the computational abilities of quantum computers, as well as diagnosing errors,
- a security proof for the signature scheme Dilithium (which is the basis for an upcoming NIST standard for post-quantum cryptography) in the quantum random oracle model,
- using cryptography to test quantum non-locality,
- progress towards analyzing the quantum security of the "sponge construction," which is well known for its use in the hash function SHA-3,
- using quantum analog machine-learning techniques to demonstrate improved quantum sensing to extract features of weak microwave signals,
- a proposed criterion to evaluate the quality of approximate quantum error-correcting codes which connects to the physics of high-energy and condensed-matter systems, and
- a demonstration of using partial knowledge of errors to improve the accuracy of optical lattice clocks.

Foundations of Measurement Science for Information Systems

ITL assumes primary responsibility within NIST for the development of measurement science infrastructure and related standards for IT and its applications. ACMD develops the mathematical foundations for such work. This can be very challenging. For example, many large-scale information-centric systems can be characterized as an interconnection of many independently operating components (e.g., software systems, communication networks, the power grid, transportation systems, financial systems). A looming example of importance to NIST is the Internet of Things. Exactly how the structure of such large-scale interconnected systems and the local dynamics of its components leads to system-level behavior is only weakly understood. This inability to predict the systemic risk inherent in system design leaves us open to unrealized potential to improve systems or to avoid potentially devastating failures. Characterizing complex systems and their security and reliability properties remains a challenging measurement science problem.

Uncertainty Quantification of Classification and Machine Learning

Paul Patrone
Anthony Kearsley
Amudhan Krishnaswamy-Usha
Stephen Tennyson
Andrew Henrichsen

Uncertainty quantification (UQ) for machine learning remains a largely open problem. While the community has a strong understanding of classification algorithms such as *k*-nearest neighbors, little of the underlying mathematical machinery carries over to more exotic machine-learning (ML) models such as neural networks. Given the increasing rate at which ML and artificial intelligence (AI) are being adopted in both research and real-world applications, it stands to reason that the community would benefit from an understanding of how such tools encode uncertainty.

To address this problem, we have been conducting a multi-year research program on the probabilistic underpinnings of classification theory. See, for example, [1, 2]. The key idea behind our analysis is to recognize that the concept of prevalence, i.e. fraction of elements in a class, is fundamental to UQ for ML in a surprising, albeit indirect, way. A binary classification setting illustrates the point most simply [3, 4].

If we let $C \in \{0,1\}$ denote the class of a sample and r denote an input to the classifier, one way to incorporate UQ into classification is to estimate the probability $\Pr[C|r]$. By the definition of conditional probability, we find that

$$\Pr[C|r] = \frac{\Pr[r|C]\Pr[C]}{\Pr[r]}$$

In general, $\Pr[C]$ can be interpreted as the prevalence, and $\Pr[r|C]$ is the probability of a measurement outcome conditioned on the class. Given these, $\Pr[r]$ can always be constructed after the fact. Several recent works have demonstrated that $\Pr[C]$ can always be estimated in an unbiased and converging manner given sufficient training data for each class. Thus, the challenge of estimating uncertainties in class assignments can essentially be reduced to determining $\Pr[r|C]$.

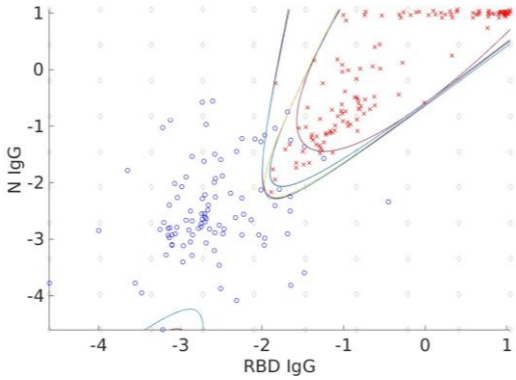

Figure 87. *Example of relative probability level sets numerically extracted from training data associated with SARS-CoV-2 serology measurements. The horizontal and vertical axes correspond to different antibody levels, whereas red and blue points are positive and negative training data. The dim black diamonds are a numerical tool used to ensure that the level sets do not cross.*

In a general ML model, we do not have direct access to $\Pr[r|C]$, nor is it even obvious that the underlying conditional distributions exist in a meaningful sense. However, we recently showed that under reasonable conditions, the ratio $\frac{\Pr[r|0]}{\Pr[r|1]}$ can always be extracted by training a family $\{\hat{C}(q,r)\}$ of classifiers $\hat{C}(q,r)$ that minimize the objective function

$$\mathcal{E}\left(\hat{C}(r)\right) = q\Pr\left[\hat{C}(r)|C=1\right] + (1-q)\Pr\left[\hat{C}(r)|C=0\right]$$

where $q \in [0,1]$ is a parameter indexing a classifier within the family. In particular, one can show that $\hat{C}(q,r)$ is a monotone function of q for fixed r, and the value of q at which $C(q,r)$ changes class corresponds to the situation

$$\Pr[r|0]/\Pr[r|1] \;=\; q/(1-q).$$

See Figure 87. Thus, one can extract the relative probability of a point belonging to a given class, which is sufficient for downstream UQ analyses.

We have also proved several related results about inequality structures associated with classifiers [5]. Current work is finishing extensions of these methods to multiclass settings and situations in which training data is corrupted by data from the wrong class.

[1] P. Bedekar, A. J. Kearsley, and P. N. Patrone. Prevalence Estimation and Optimal Classification Methods to Account for Time Dependence in Antibody Levels. *Journal of Theoretical Biology* **559** (2023), 111375.

[2] P. N. Patrone and A. J. Kearsley. Minimixing Uncertainty in Prevalence Estimates. *Statistics and Probability Letters* **205** (2024), 109946.

[3] P. N. Patrone, R. A. Binder, C. S. Forconi, A. M. Moorman, and A. J. Kearsley. Analysis of Diagnostics (Part I): Prevalence, Uncertainty Quantification, and Machine Learning. In review.

[4] P. N. Patrone, R. A. Binder, C. S. Forconi, A. M. Moorman, and A. J. Kearsley. Analysis of Diagnostics (Part II): Prevalence, Linear Independence, and Unsupervised Learning. In review.

[5] P. N. Patrone and A. J. Kearsley. Inequalities for Optimization of Diagnostic Assays. In preparation.

Measurements of Service Interference Between Network Slices in 5G/6G Networks

Richard J. La
Van Sy Mai (NIST CTL)
Tao Zhang (NIST CTL)

Many network applications and services demand widely varying quality-of-service (QoS) requirements. Network slicing has been proposed as a possible solution to provide an efficient and flexible network architecture capable of offering differentiated service in 5G/6G systems. It supports a set of end-to-end (E2E) logical networks, called network slices (NSs), on the same physical network, which can be dynamically set up and torn down to meet time-varying requirements. The overall network slicing framework is shown in Figure 88. Each NS is tailored to support a specific set of QoS services and, in principle, is isolated from other NSs to prevent performance degradation when sharing (virtual) resources with other NSs, such as communication links, and virtual machines on which virtual network functions are run.

However, recent studies [1-3] demonstrated that NSs can experience service interference when they share physical or virtual resources. Thus, from the perspective of providing E2E service quality assurance in 5G/6G systems, it is crucial to discover possible service interference among the existing NSs in a timely manner and isolate potential issues before it can cause violations of service level requirement (SLRs).

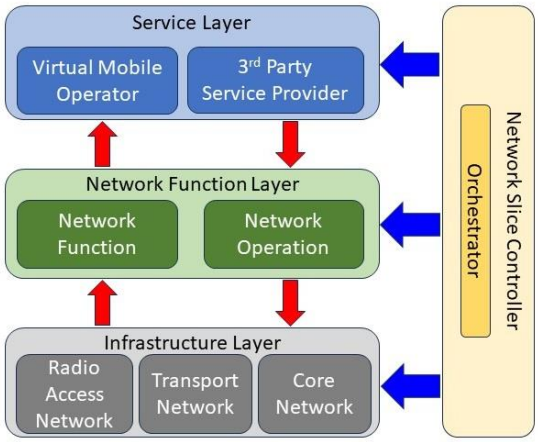

Figure 88. *5G network slicing function.*

A key challenge arises from the fact that the internal operations of each autonomous system (AS), such as an access network, are unlikely to be known to or controllable by other ASs (e.g., core networks). Such internal AS operations include how physical and virtual resources—such as VFNs, computing capacities, network routes, and communication bandwidth—are assigned at any given time, often dynamically, at different protocol layers to each NS across an AS. As a result, no single entity in the network may possess complete knowledge of how (physical or virtual) resources are shared among NSs at any time end to end across multiple ASs.

This naturally leads to the following important question: *Is it possible to detect or even predict potential service interference among NSs, using only E2E key performance indicator (KPI) measurements, such as E2E delay and packet drops?*

The overarching goal of this project is to design a suite of algorithms for (a) identifying groups of interfering NSs and (b) finding appropriate remedial actions to avoid violation of SLRs, which can lead to unacceptable performance. Our efforts so far focused on finding suitable metrics for measuring interference among NSs and based on the metrics, identifying the interference patterns among NSs based on E2E network measurements, such as E2E packet delays and packet loss rates.

Our proposed algorithm [4] consists of three phases: it first discovers pairwise interference among NSs, which is measured using the Spearman's rank correlation coefficient. The pairwise interference is represented as an interference graph. In the second phase, we identify all maximal cliques in the interference graph. Then, for each maximal clique in the interference graph, we search for a set of cliques in the maximal clique, where each clique represents a group of NSs that share a resource and can cause service interference via the shared resource. Our algorithm employs *factor analysis*, which is a dimensionality reduction

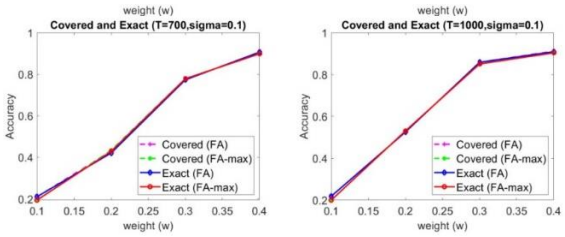

Figure 89. *Plot of the fraction of shared resources correctly identified with sharing NSs, sigma=0.1, T=number of measurements.*

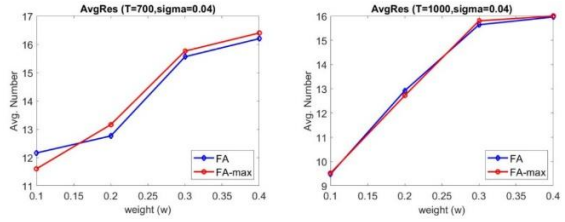

Figure 90. *Plot of the fraction of shared resources correctly identified with sharing NSs, sigma=0.04, T=number of measurements.*

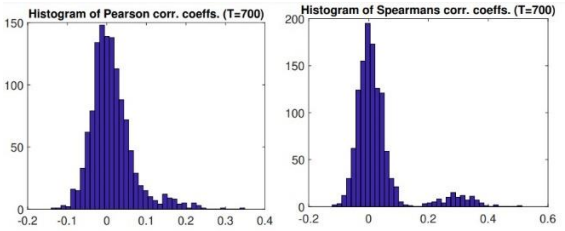

Figure 91. *Histograms of pairwise correlation coefficients for weight 0.3 and T=700.*

technique, for identifying a set of shared resources from the maximal cliques [5].

To evaluate the performance of the proposed algorithm, we carried out extensive numerical studies with varying network sizes and E2E delays as the KPI measurements. Figure 89 shows the fraction of correctly identified shared resources in a network with 15 resources shared by 50 NSs using 700 (T = 700) or 1,000 (T = 1000) E2E delay measurements; a shared resource is correctly discovered if all the NSs that share the resource are correctly identified. The weight along the x-axis is used to change the strength of service interference among the NSs; as the weight increases, so does the service interference at shared resources. As the plots indicate, when enough measurements are available and service interference is non-negligible, the proposed algorithm can correctly identify over 80 percent of shared resources (when the weight is at least 0.3).

In addition, Figure 90 shows the estimated number of shared resources by our proposed algorithm. When the weight is at least 0.3, the estimates are only slightly larger than the correct number of 15, suggesting that the proposed algorithm does not produce many false positives, while correctly detecting most of the shared resources in the network.

Figure 91 plots the histogram of the pairwise correlation measured by Pearson correlation coefficient and Spearman's rank correlation coefficient for T = 700. The plots indicate that when the weight is set to 0.3, the pairwise correlations are weak to moderate between interfering NSs, with most of the Pearson correlation coefficients lying below 0.25. Together with the plots in Figure 89 and Figure 90, they demonstrate that the proposed algorithm can correctly discover most NSs that can potentially interfere with each other only using E2E measurements.

[1] S. Amri, H. Hamdi, and Z. Brahmi. Inter-VM Interference in Cloud Environments: A Survey. In *14th IEEE/ACS International Conference on Computer Systems and Applications*, October 2017.

[2] W. Lin, C. Xiong, W. Wu, F. Shi, K. Li, and M. Xu. Performance Interference of Virtual Machines: A Survey. *ACM Computing Surveys* **55**:254 (2023), 1–37.

[3] Q. Zhang, F. Liu, and C. Zeng. Adaptive Interference-Aware VNF Placement for Service-Customized 5G Network Slices. In *IEEE Conference on Computer Communications*, May 2019

[4] V.-S. Mai, R.J. La and T. Zhang. Detection of Performance Interference Among Network Slices in 5G/6G Systems. In review.

[5] D.J. Bartholomew and M. Knott. *Latent Variable Models and Factor Analysis: Kendall's Library of Statistics 7*. Wiley, 2nd edition, 1999.

Methods for Improving Robustness of Federated Learning Against Byzantine Attacks

Richard J. La
Van Sy Mai (NIST CTL)
Tao Zhang (NIST CTL)

With rapid advances in sensing technologies, in many applications, e.g., the Internet of Things (IoTs), a large amount of data is generated at many spatially distributed devices. Given the expected volume of data, it is often impractical to transfer all data to a server where centralized learning can be performed. Federated Learning (FL) is a distributed learning paradigm proposed to address this challenge and has garnered much interest from the research community in recent years [1].

In FL, a coordinating server (CS) maintains a global machine learning (ML) model that is communicated to (a subset of) clients at each round, which perform learning using their own local datasets. Once they finish updating their local ML models, the updated models are forwarded to the CS, which then aggregates the forwarded models to update the global ML model. Since

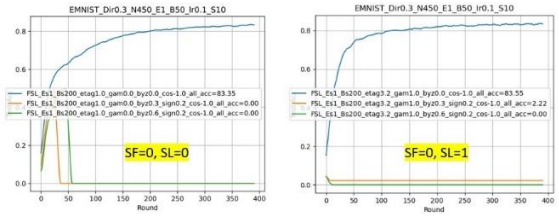

Figure 92. *Plot of test accuracy under sign-flipping attacks as a function of epoch for EMNIST dataset without server learning (SL=0) and with server learning (SL=1). Blue = no malicious clients, red = 30% malicious clients, green = 60% malicious clients.*

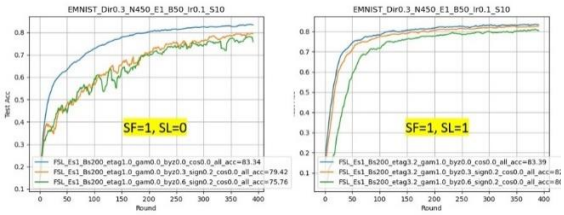

Figure 93. *Plot of test accuracy under sign-flipping attacks with server filter as a function of epoch for EMNIST dataset without server learning (SL=0) and with server learning (SL=1). Blue = no malicious clients, red = 30% malicious clients, green = 60% malicious clients.*

local datasets are only used to update the local ML models at the clients, no data is shared among the clients or with the CS.

Unfortunately, the performance of FL can degrade significantly when some clients are malicious and employ different types of attacks, such as data poisoning or model poisoning [2, 3]. Figure 92 shows the test accuracy of FL on EMNIST dataset under sign-flipping attacks by malicious clients with and without server learning. The plots show that when more than 30 percent of clients are malicious, FL cannot achieve stable learning in either case. Various methods have been proposed to mitigate the effects of malicious clients whose goal is to prevent the CS from learning a good model.

In some applications, it may be possible to collect a small dataset at the CS, e.g., training an ML model for object recognition by autonomous vehicles. Earlier we investigated how the CS can make use of its local dataset to improve the learning process in FL. Our studies [4, 5] demonstrated that incremental learning by the CS, even on a small dataset, can improve the learning process significantly at the beginning. However, they also showed that care must be taken when integrating server learning with existing FL techniques by carefully considering how the server learning interacts with the aggregation of clients' updates.

Recently, we explored how the CS dataset can be used to mitigate the adverse effects of malicious clients. In particular, we examined how two different types of filters that can be employed by the CS based on its local dataset to remove some of the updates reported by suspected malicious clients. Our preliminary experimental results show that the proposed filters can help stabilize the learning process even in extreme cases where a majority of the clients are malicious.

The key idea behind these filters is to evaluate the quality of the updates reported by the clients using the local dataset available at the CS and aggregate only the updates that are deemed acceptable. Figure 93 shows the test accuracy of the same setup with one of the two filters in place, which is based on the gradient of the server's loss function. It is evident from the plots that when the filter is place, FL is able to perform stable distributed learning. Slower learning rates with malicious clients are due to the fact that not all reported updates from the polled clients are aggregated for updating the global model at the CS, thereby reducing the effective number of polled clients.

Comparing the left plots of Figure 92 and Figure 93 shows that the filter alone is able to cope with the adverse effects of sign flipping attacks by malicious clients. The right plot of Figure 93 demonstrates that local server learning speeds up the learning process significantly, even when 60 percent of clients are malicious and report misleading updates, suggesting that the combination of server filter and learning can deliver considerable performance improvement for FL in the presence of malicious clients.

We are currently investigating the effectiveness of the proposed filters against other types of attacks. In addition, we are working towards providing performance guarantees as a function of the fraction of malicious clients.

[1] B. McMahan, E. Moore, D. Ramage, S. Hampson, and B.A. y Arcas. Communication-efficient Learning of Deep Networks from Decentralized Data. In *20th International Conference on Artificial Intelligence and Statistics*, April 2017.

[2] P. Sun, X. Liu, Z. Wang, and B. Liu. Byzantine-robust Decentralized Federated Learning via Dual-domain Clustering and Trust Bootstrapping. In *IEEE/CVF Conference on Computer Vision and Pattern Recognition* (CVPR), June 2024.

[3] J. Shi, W. Wan, S. Hu, J. Lu, and L.Y. Zhang. Challenges and Approaches for Mitigating Byzantine Attacks in Federated Learning. In *IEEE International Conference on Trust, Security and Privacy in Computing and Communications* (TrustCom), December 2022.

[4] V. S. Mai, R. J. La, and T. Zhang, A Study of Enhancing Federated Learning on Non-IID Data with Server Learning. *IEEE Transactions on Artificial Intelligence* **5**:11 (2024), 5589-5604.

[5] V. S. Mai, R. J. La, T. Zhang, Y. Huang, and A. Battou. Federated Learning with Server Learning for Non-IID Data. In *57th Annual Conference on Information Sciences and Systems*, March 2023.

On Risk Evaluation & Mitigation

Vladimir Marbukh

Systemic events in large-scale networked systems typically occur through contagion at well-defined values of exogenous parameters. In cases of undesirable systemic events, e.g., cascading failures, propagation of computer or human viruses, etc., the corresponding systemic risk is often measured by the distance to the point of the undesirable transition in the space of exogenous parameters. However, this measure does not account for potential losses if such a transition occurs due to unavoidable uncertainties in the exogenous parameters. It is known that even in a case of gradual/continuous transition, a higher safety margin with respect to contagion threshold may be associated with higher losses if this threshold is breached.

Attempts to overcome this problem with Viral Conductance (VR) risk metrics suffer from unrealistic assumptions about the uncertainties and disregard for the risk tolerance of the decision maker. This motivates us to propose and demonstrate the advantages of the Entropic Value at Systemic Risk (EVaSR) metric, which overcomes these limitations of VR [1, 2]. The EVaSR metric treats systemic events as phase transitions under Landau approximation. Figure 94 shows the corresponding effective Landau potential for continuous systemic events represented by phase transitions of the first kind [1]. EVaSR for discontinuous systemic events, represented by phase transitions of the second kind, is discussed in [2].

Conventional game-theoretic models of systemic risk evaluation and mitigation in networks with selfish components are based on classical economics which assumes risk neutral/averse decision makers. While the corresponding game-theoretic models have unique Nash equilibria, our analysis [3] of the Susceptible-Infected-Susceptible (SIS) contagion under a behavioral economic model for selfish components, indicates the possibility of multiple Nash equilibria. This possibility has important practical implications, e.g., an "unacceptably" high Price of Anarchy (PoA) associated with "non-efficient" Nash equilibria may warrant additional mechanisms for the purpose of avoiding the inefficient Nash equilibria. The infeasibility of centralized control of dynamic processes in large-scale networks necessitates some level of decentralization. On an example of SIS contagion, [3] discusses the feasibility of decentralized mitigation of systemic risk, which is inherently a collective phenomenon. Also, [3] reports our initial results on microeconomic modeling of cyber security investments.

System-specific cyber security risk depends on the likelihoods of potential multi-step attacks that combine multiple vulnerabilities and the corresponding losses.

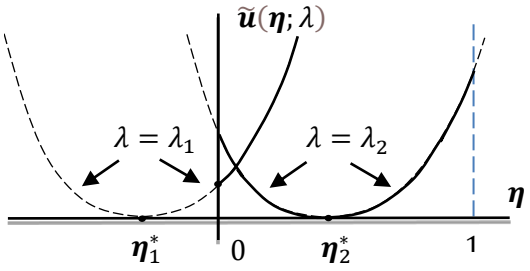

Figure 94. *Effective Landau potential:* $\boldsymbol{\rho_1 < \gamma^{-1} < \rho_2}$

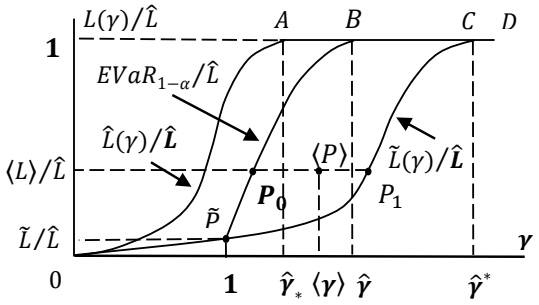

Figure 95. *System-specific cybersecurity risk envelope.*

These likelihoods are typically obtained under assumptions that exploitations of individual vulnerabilities are statistically independent and probabilities of these events can be estimated from the data on vulnerability exploits in the wild. However, these assumptions, which do not account for the inherently adversarial nature of the attacker-defender interactions, may lead to significant inaccuracies in cyber risk estimation and thus result in highly inefficient risk mitigation decisions. In [4] we propose a framework for system-specific cyber security risk evaluation, which addresses some of these shortcomings. Figure 95 shows the corresponding cybersecurity risk envelope 0ABC0, which represents the feasible region for relative system losses resulting from a cyber-attack of "relative force" γ [4].

In [5] we suggest that contact tracing abilities to alleviate the impact of and even disrupt a pandemic can be significantly improved with the support of a specialized Recommender System (RS). Based on the combination of up-to-date contact tracing and medical data, such a RS can identify and test through an Exposure Notification System (ENS) not only high-risk individuals but also potential superspreaders to suppress infection propagation. Due to incomplete information, the dynamic nature of the problem, and a large state and action spaces, the RS should be supported by Deep Reinforcement Learning (DRL) for solving the corresponding Partially Observable Markov Decision Process (POMDP).

[1] V. Marbukh. "Towards Evaluation & Mitigation of the Entropic Value at Systemic Risk in Networked Systems."

12th International Conference on Complex Networks and their Applications, Menton, France, November 28-30, 2023.

[2] V. Marbukh. "Systemic Risk of Discontinuous Failures in Large-Scale Networks within Time Horizon: Work in Progress." 12th International Conference on Complex Networks and their Applications, Menton, France, November 28-30, 2023.

[3] V. Marbukh and M. Marbukh. "Towards Systemic Risk Evaluation, Attribution, and Mitigation in Networked Systems: Work in Progress." First International Workshop on Safeguarding Social Networks: Privacy, Security, Trust, and Truth in the Age of Misinformation (SAFE-SN 2024), ASONAM 2024, Rende, Italy, September 2-5, 2024.

[4] V. Marbukh. From Exploit Prediction in the Wild to System-Specific Cyber Security Risk Metrics: Work in Progress. In *Proceedings of the 21st ACM International Conference on Computing Frontiers* (ACM CF' 24), Ischia, Italy, May 7-9, 2024

[5] V. Marbukh. "Position Paper: Towards Recommender System Supported Contact Tracing for Cost-Efficient and Risk Aware Infection Suppression." Workshop on Health Recommender Systems, 18th ACM Conference on Recommender Systems (RecSyS'24), Bari, Italy, October 18, 2024.

Towards Mitigating Green Energy Intermittency in Distributed Systems

Vladimir Marbukh
Brian Cloteaux

Our contemporary society relies heavily on communication and computing, both of which consume a significant share of generated energy. The production and usage of energy have become deeply intertwined with our daily lives. Unfortunately, the negative ecological impact of carbon-based energy sources has escalated in recent years. Mitigating this impact through the broader adoption of green energy, while still fostering technological advancements, is becoming one of the foremost challenges of our time.

A major obstacle to the broad acceptance of renewable energy for computing and communication, which has strict latency requirements, is the intermittency of green energy sources [1]. This obstacle can be overcome by a combination of the following three strategies: (a) using batteries allowing for smoothing the energy supply by absorbing unpredictable fluctuations in renewable energy availability, (b) shaping demand to fit green energy supply, and (c) dynamic allocation of computationally extensive jobs based on the green energy availability in geographically distributed systems.

It is likely that the successful path to green energy acceptance will include some combination of all strategies (a), (b), and (c). This path will require balancing various tradeoffs between cost, performance, and reliability. Additional complexity is due to the necessity of decentralized management of large-scale interconnected networked systems which are geographically distributed. From our earlier research, we developed a simulation framework which allowed us to perform initial investigation of tradeoffs involved in of the potential mitigation of intermittency of green energy sources via various job replication strategies [2, 3].

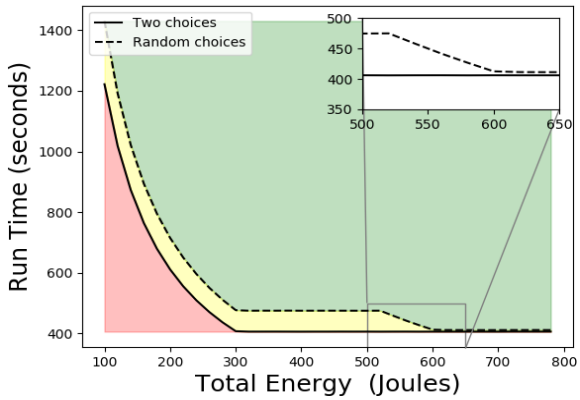

Figure 96. *Simulation results from [4] showing the differing feasible regions for run time versus energy usage.*

Last year, we extended this simulation framework by combining redundancy and power-of-two choices in random load balancing when an incoming job randomly selects two queues and joins the shortest one [4] to mitigate the negative effect of intermittency on a longer time scale than the acceptable latency. Such a "long time scale" intermittency may significantly diminish the power of two choices since the chosen shortest queue may become a subject to a "long" slowdown due to intermittency which started after the job joined the queue. On the other hand, pure redundancy may not be effective since job replica(s) which join an "already slow" queue due to intermittency, waste communication and computing resources. Our simulation results [4] suggested benefits of combining redundancy and power-of-d choices load balancing for $d > 2$.

In a continuation of this research, we proposed [5] a distributed Green Network Optimization (GNO) with Multi-Agent Reinforcement Learning (MARL). GNO-MARL combines: (a) Network Utility Maximization (NUM) based network management, given the capacity constraints, on a "fast" time scale, and (b) network dimensioning which balances the maximal network utility with the "carbon cost" of the transmissions on "slower" time scales. Inherent non-convexity of the GNO due to dominance of the idle power in network devices, including routers, makes exact solutions of the GNO even by centralized algorithms for realistic size networks intractable. We also conjectured in [5] that GNO-MARL may lead to a practically acceptable sub-optimal solution.

[1] G. Gowrisankaran, et al. Intermittency and the Value of Renewable Energy. National Bureau of Economic Research Working Paper No. 17086, May 2011, Revised December 2011.

[2] V. Marbukh and B. Cloteaux. "Towards Mitigating Intermittency of Renewable Energy Supply in Large-Scale Computing Infrastructure with Job Replication." Carbon Aware Networks Workshop, University of Oxford, September 29-20, 2023.

[3] B. Cloteaux and V. Marbukh. "Simulating Computing Redundancy vs. its Energy Usage." Winter Simulation Conference, San Antonio, TX, December 10-13, 2023.

[4] B. Cloteaux and V. Marbukh. Towards Mitigating Effects of Intermittency on a Green Computing/Communication Infrastructure. In review.

Combinatorial Testing for Software Based Systems

Raghu N. Kacker
James F. Lawrence
D. Richard Kuhn (NIST ITL)
M. S. Raunak (NIST ITL)
Yu Lei (University of Texas at Arlington)
Dimitris E. Simos (SBA-Research, Austria)
Eric Wong (University of Texas at Dallas)
Itzel Dominguez-Mendoza (CENAM, Mexico)

https://csrc.nist.gov/projects/automated-combinatorial-testing-for-software

In 1997, the Mars Pathfinder began experiencing system resets at seemingly unpredictable times soon after it landed and began collecting data. Fortunately, engineers were able to deduce and correct the problem, which occurred only when (1) a particular type of data was being collected, and (2) intermediate priority tasks exceeded a certain load, resulting in a blocking condition that eventually triggered a reset. Situations of this type are known as interaction faults. Many real-time failures of software-based systems have been traced to such faults. These are often insidious in that they may remain hidden until the unfortunate combination is encountered during system operation.

Combinatorial testing (CT) is a versatile methodology for detecting interaction faults. CT began as pairwise (2-way) testing in which all pairs of the test values for all pairs of test factors are checked. Thus, pairwise testing can detect faults involving single factors or interactions between two factors. CT is based on an empirical observation, referred to as the interaction rule, that while the behavior of a software system may be affected by many factors, only a few are involved in any given failure. NIST investigations of failures in actual systems have shown that while most faults involved a single factor or interaction between two factors, some faults involved three or more factors [1]. (A fault involving more than six factors has not yet been reported.) Thus, pairwise testing is useful, but it may not be adequate for detecting interaction faults involving more than two test factors.

Table 2. *A covering array of 13 rows includes all eight triplets (000, 001, 010, 011, 100, 101, 110, and 111) of the possible values (0 and 1) for every one of the 120 possible sets of 3 out of 10 test factors represented by the columns (for example, see colored entries)*

	Columns									
Rows	**1**	**2**	**3**	**4**	**5**	**6**	**7**	**8**	**9**	**10**
1	0	0	0	0	0	0	0	0	0	0
2	1	1	1	1	1	1	1	1	1	1
3	1	1	1	0	1	0	0	0	0	1
4	1	0	1	1	0	1	0	1	0	0
5	1	0	0	0	1	1	1	0	0	0
6	0	1	1	0	0	1	0	0	1	0
7	0	0	1	0	1	0	1	1	1	0
8	1	1	0	1	0	0	1	0	1	0
9	0	0	0	1	1	1	0	0	1	1
10	0	0	1	1	0	0	1	0	0	1
11	0	1	0	1	1	0	0	1	0	0
12	1	0	0	0	0	0	0	1	1	1
13	0	1	0	0	0	1	1	1	0	1

More than fifteen years ago, NIST took the initiative to extend pairwise (2-way) CT to higher strength *t*-way CT for $t > 2$. NIST has helped make CT practical by developing research tools and techniques for generating combinatorial test suites. CT has now gained significant interest from the international software testing community. Many successful results from the use of CT in aerospace, automotive, and financial service industries, as well as defense, security, and electronic medical systems have since been reported.

A suite of test cases for combinatorial *t*-way testing includes (covers) at least once all possible *t*-tuples of the test values for every set (combination) of t factors out of the complete set of all *k* factors that are tested ($k > t$). Use of mathematical objects called covering arrays makes it possible to check all *t*-tuples of the test values with a small number of test cases. Table 2 shows a covering array of 13 rows and 10 columns each having two possible value 0 and 1. Columns correspond to the factors and the rows correspond to the test cases. The number of possible sets (combinations) of 3 out of 10 test factors is $\binom{10}{3} = \frac{10!}{(10-3)!\,3!} = 120$. When each factor has two possible values, each set of 3 factors can have $2^3 = 8$ possible triples of test values ((0, 0, 0), (0, 0, 1), (0, 1, 0), (0, 1, 1), (1, 0, 0), (1, 0, 1), (1, 1, 0), (1, 1, 1)). So, the total number of possible triples of values for all 10 factors is $120 \times 8 = 960$. A test suite based on Table 2 includes (covers) at least once all 960 distinct triples of the test values of ten factors using just 13 tests.

In practice, one wants a minimal covering array, that is an array which covers all possible *t*-tuples of the test values for every set of *t* out of all *k* factors with the least number of rows (test cases). In practice, many factors have dependencies and constraints, and hence not all combinations of the test values may be logically or physically valid. A combinatorial test suite must avoid such forbidden combinations. Generating minimal covering arrays that avoid forbidden combinations is a difficult computational problem [2]. A great deal of research has been done to develop mathematical and computational methods to generate minimal covering arrays of this type. NIST and its collaborators have developed several such algorithms.

NIST-Developed Tools. NIST has developed several research tools to make CT practical. ACTS (for Automated Combinatorial Testing for Software), which was developed in cooperation with the University of Texas at Arlington, includes several algorithms to generate high strength test suites for CT [3]. The ACTS algorithms are optimized to efficiently avoid forbidden combinations of test settings. More than 4925 users have downloaded executable versions of the ACTS algorithms from the NIST webpage for CT. (It is difficult to ascertain the number of users because some users have redistributed to others, and some are students who may have used it only once for a single project.).

A second research tool, CCM (for Combinatorial Coverage Measurement), developed jointly by NIST and a guest researcher from CENAM, the national metrology institute of Mexico, describes the incompleteness of a test suite that may not have been developed from a CT viewpoint. Basic combinatorial coverage measurements describe the incompleteness of a test suite relative to a test suite based on a covering array that includes all possible *t*-tuples of values for every *t*-factor combination for various values of *t*. The combinatorial deficiency of a test suite can be remedied by additional tests. Thus, CCM can help guide the expansion of a test suite to satisfy stated combinatorial requirements [4]. The latest version of CCM supports constraints which exclude forbidden combinations of values. A parallel processing version is also available.

Impact of NIST Research. NIST efforts have sparked a surge of research and application of combinatorial testing technology. A 2010 NIST Special Publication on CT was downloaded more than 30 000 times by the end of 2014 [5]. In 2013, we published a book with Chapman and Hall/CRC Press on this topic [6].

One of the first large-scale users that we worked with is a group at the U.S. Air Force Base in Eglin, Florida. The behavior of one of their systems depended on the sequential order of certain events. This led to the problem of testing sequences of events, which required development of new mathematical objects called *sequence covering arrays* [7, 8, 9]. Lockheed Martin, a large U.S. defense contractor, reported (based on eight projects) that use of CT reduced cost of testing by about 20 % with 20 % to 50 % improvement in test coverage [10]. CT methods are now being used in many areas such as financial services, automotive, automation, avionics, video coding standards, and for security testing. The NIST webpage for CT cites more than forty application papers.

For testing a software-based system, no single approach is enough. Multiple approaches are generally needed at various stages of software development and installation. CT complements other approaches for testing, verification, and validation of software-based systems. CT is now included in software engineering courses taught in many universities. NIST efforts on technology transfer of CT tools and techniques received the 2009 Excellence in Technology Transfer Award from the Federal Laboratory Consortium-Mid Atlantic Region. A 2013 paper describing the ACTS research tool [3] received the Most Influential Paper of the Decade Award by the 2023 IEEE International Conference on Software, Testing, Verification and Validation (ICST) held in Dublin, Ireland, April 16-22, 2023.

CT has also gained significant interest from the research community. In 2012, NIST took lead in organizing a workshop on CT[24] in conjunction with the 2012 IEEE International Conference on Software Testing, Verification, and Validation (ICST), a premier conference in this field. Since then, an International Workshop on Combinatorial Testing (IWCT) has become an annual event for sharing advancements in CT tools and techniques, as well as results from practical industrial use of CT. The thirteenth such IWCT[25] was held in Toronto, Canada on May 27, 2024, in conjunction with the ICST 2024[26]. Four of us (Kacker, Kuhn, Lei, and Simos) were among the co-organizers. The IWCT 2024 received nine submissions. The Program Committee accepted seven papers.

Recent accomplishments. The following accomplishments occurred during this reporting period.

SmartExecutor: coverage-driven symbolic execution guided by a function dependency graph [11]: Symbolic execution of smart contracts suffers from sequence explosion. Some existing tools limit the sequence length, thus being unable to adequately evaluate some functions. In this paper, we propose a symbolic execution approach without limiting the sequence length. In our approach, the symbolic execution process is guided by a function dependency graph aiming to maximize code coverage while reducing the number of sequences to be

[24] https://doi.org/10.1109/ICST19380.2012

[25] https://conf.researchr.org/home/icst-2024/iwct-2024

[26] https://conf.researchr.org/home/icst-2024

executed. Our approach consists of two major phases. The first phase executes all sequences up to a length limit while the second attempts to cover the not-fully covered functions. We have developed a tool called SmartExecutor and conducted an experimental evaluation on the SGUARD dataset. The experimental results indicate that, compared with a state-of-the-art symbolic execution tool Mythril, SmartExecutor achieves higher code coverage and detects more vulnerabilities with less time.

A combinatorial approach to hyperparameter optimization [12]: In machine learning, hyperparameter optimization (HPO) is essential for effective model training and significantly impacts model performance. Hyperparameters are predefined model settings which fine-tune the model's behavior and are critical to modeling complex data patterns. Traditional HPO approaches such as Grid Search, Random Search, and Bayesian Optimization have been widely used in this field. However, as datasets grow and models increase in complexity, these approaches often require a significant amount of time and resources for HPO. This research introduces a novel approach using *t*-way testing — a combinatorial approach to software testing used for identifying faults with a test set that covers all *t*-way interactions — for HPO. *T*-way testing substantially narrows the search space and effectively covers parameter interactions. Our experimental results show that our approach reduces the number of necessary model evaluations and significantly cuts computational expenses while still outperforming traditional HPO approaches for the models studied in our experiments.

A proxy model-based approach to influence analysis [13]: Machine learning (ML)-based artificial intelligence (AI) systems rely on training data to function, but the internal workings of how ML models learn from this data are often inscrutable. Influence analysis provides valuable insights into the model's behavior by evaluating the effect of individual training instances on the model's predictions. However, calculating the influence of each training data can be computationally expensive. In this paper, we propose a proxy model-based approach to influence analysis called Proxima. The main idea of our approach is to use a subset of training instances to create a proxy model that is simpler than the original model, and then use the proxy model and the subset of training instances to perform influence analysis. We evaluate Proxima on ML models trained using seven real-world datasets. We compare Proxima to two state-of-the-art influence analysis tools, FastIF and Scaling-Up. Our experimental results suggest that the proposed approach can successfully perform and speed up the influence analysis process, and, in most cases, perform better than FastIF and Scaling-Up.

Assessing the degree of feature interactions that determine a model prediction [14]: ML models rely on capturing important feature interactions to generate predictions. This study is focused on validating the hypothesis that model predictions often depend on interactions involving only a few features. This hypothesis is inspired by *t*-way combinatorial testing for software systems. In our study, we utilize the notion of Shapley Additive Explanations (SHAP) values to quantify each feature's contribution to model prediction. We then use a greedy approach to identify a minimal subset of features (*t*) required to determine a model prediction. Our empirical evaluation is performed on three datasets: Adult Income, Mushroom, and Breast Cancer, and three classification models: Logistic Regression, XGBoost, and SVM. Through our experiments, we find that the majority of predictions are determined by interactions involving only a subset of features.

Constructing surrogate models in machine learning using combinatorial testing and active learning [15]: ML-based models are often black box, making it challenging to understand and interpret their decision-making processes. Surrogate models are constructed to approximate the behavior of a target model and are an essential tool for analyzing black-box models. The construction of a surrogate model typically includes querying the target model with carefully selected data points and using the responses from the target model to infer information about its structure and parameters. In this paper, we propose an approach to surrogate model construction using combinatorial testing and active learning, aiming to efficiently capture the essential interactions between features that drive the target model's predictions. Our approach first leverages *t*-way testing to generate data points that capture all the *t*-way feature interactions. We then use an iterative process to isolate the essential feature interactions, i.e., those that can determine a model prediction. In the iterative process, we remove nonessential feature interactions, generate additional data points to contain the remaining interactions, and employ active learning techniques to select a subset of the data points to update the surrogate model. This process is continued until we construct a surrogate model that closely mirrors the target model's behavior. We evaluate our approach on 4 public datasets and 12 ML models and compare the results with the state-of-the-art (SOTA) approaches. Our experimental results show that our approach can perform in most cases better than the SOTA approaches in terms of accuracy and efficiency.

Combinatorial security testing for the Tor anonymity network client [16]: In this paper, we present an application of combinatorial security testing to the well-known anonymity network Tor. Rigorous testing of the Tor network is important to evaluate not only its functionality, but also the security it provides to its users. However, such testing efforts are facing challenges including accurate modeling as well as creation of automated and

security focused test oracles. We argue that combinatorial test sets fulfilling coverage criteria can be used to enhance and augment currently employed testing approaches of Tor in practice. Results from a case study demonstrate that combinatorial methods are a promising avenue for security testing of the Tor anonymity network client.

Leveraging combinatorial coverage in machine learning product lifecycle [17]: The data-intensive nature of ML-enabled systems introduces unique challenges in test and evaluation. We present an overview of combinatorial coverage, exploring its applications across the ML-enabled system lifecycle and its potential to address key limitations in performing test and evaluation for ML-enabled systems.

Combinatorial testing for building reliable systems [18]: Stakeholders of technology-oriented systems expect some level of reliability from them. IEEE defines reliability as "the ability of a system or component to perform its required functions under stated conditions for specified period of time". One of the crucial factors in determining a system's quality is based on how reliable it is. However, ensuring reliability is hard, especially for systems that are large and complex in nature. In this article, we introduce combinatorial testing and its use in developing highly reliable systems.

Ensuring reliability through combinatorial coverage measures [19]: Verification of complex software systems is an important, yet challenging task. Testing is the most common method for assuring that software meets its specifications and is defect-free. To claim that software is defect-free and thus reliable, one has to show that it produces the "correct" output or "behaves" according to specification without failing under all possible parameter values and configurations. In the software verification world, this is known as exhaustive testing. For any software of reasonable size and complexity, exhaustive testing is completely infeasible. Thus, during the testing process, a small subset of parameter values and configurations is selected to ensure that the software is producing its output or maintaining its behavior as "expected." The selected parameter value for one test execution is called a Test Case, and the set of test cases selected for testing a system is called a Test Suite. The essence of software testing, therefore, lies in effective ways of identifying the test cases and building the test suite. Two overarching questions related to this process include: 1) how to select the test cases and 2) how to decide when enough test cases have been selected. Over the years, researchers have proposed different Test Adequacy criteria for answering these two questions.

We are continuing research involving use of combinatorial methods for trust and assurance of machine learning models, autonomous systems, for model debugging, for security of smart contracts, cybersecurity, and risk factors identification. The research includes the development of supporting tools.

[1] D. R. Kuhn, D. R. Wallace, and A. M. Gallo, Jr. Software Fault Interactions, and Implications for Software Testing. *IEEE Transactions on Software Engineering* **30** (2004), 418-421. DOI: 10.1109/TSE.2004.24

[2] L. Kampel and D. E. Simos. A Survey on the State of the Art of Complexity Problems for Covering Arrays. *Theoretical Computer Science* **800** (2019), 107-124. DOI: 10.1016/j.tcs.2019.10.019

[3] L. Yu, Y. Lei, R. N. Kacker, and D. R. Kuhn. ACTS: A Combinatorial Test Generation Tool. In *Proceedings of the 2013 IEEE Sixth International Conference on Software Testing, Verification and Validation* (ICST), Luxembourg, Luxembourg, March 18-22, 2013, 370-375. DOI: 10.1109/ICST.2013.52

[4] D. R. Kuhn, R. N. Kacker, and Y. Lei. Combinatorial Coverage as an Aspect of Test Quality. *CrossTalk: The Journal of Defense Software Engineering* (March/April 2015), 19-23.

[5] D. R. Kuhn, R. N. Kacker, and Y. Lei. Practical Combinatorial Testing, NIST Special Publication 800-142, October 2010, NIST. URL: http://nvlpubs.nist.gov/nistpubs/Legacy/SP/nistspecialpublication800-142.pdf

[6] D. R. Kuhn, R. N. Kacker, and Y. Lei. *Introduction to Combinatorial Testing.* CRC Press, 2013.

[7] D. R. Kuhn, J. M. Higdon, J. F. Lawrence, R. N. Kacker, and Y. Lei. Combinatorial Methods for Event Sequence Testing. In *Proceedings of the 5-th IEEE International Conference on Software Testing, Verification and Validation Workshops* (ICSTW), Montreal, Quebec, Canada, April 17-21, 2012, 601-609. DOI: 10.1109/ICST.2012.147

[8] D. R. Kuhn, J. M. Higdon, J. F. Lawrence, R. N. Kacker, and Y. Lei. Efficient Methods for Interoperability Testing using Event Sequences. *CrossTalk: The Journal of Defense Software Engineering*, (July/August 2012), 15-18. URL: https://apps.dtic.mil/docs/citations/ADA566540

[9] Y. M. Chee, C. J. Colbourn, D. Horsley, and J. Zhou. Sequence Covering Arrays. *SIAM Journal of Discrete Mathematics* **27** (2013), 1844-1861. DOI: 10.1137/120894099

[10] J. Hagar, D. R. Kuhn, R. N. Kacker, and T. Wissink. Introducing Combinatorial Testing in a Large Organization. *IEEE Computer* **48** (2015), 64-72. DOI: 10.1109/MC.2015.114

[11] Q. Wei, F. Sikder, H. Feng, Y. Lei, R. N. Kacker, and D. R. Kuhn. SmartExecutor: Coverage-Driven Symbolic Execution Guided by a Function Dependency Graph. In *Proceedings of the 5th Conference on Blockchain Research & Applications for Innovative Networks and Services* (BRAINS), Paris, France, October 11-13, 2023. DOI: 10.1109/BRAINS59668.2023.10316942

[12] K. Khadka, J. Chandrasekaran, Y. Lei, R. N. Kacker, and D. R. Kuhn. A Combinatorial Approach to Hyperparameter Optimization. In *Proceedings of the 2024 IEEE/ACM International Conference on AI Engineering - Software*

Engineering for AI (*CAIN 2024*), Lisbon, Portugal, April 14-15, 2024. DOI: 10.1145/3644815.3644941

[13] S. Shree, Y. Lei, R. N. Kacker, and D. R. Kuhn. A Proxy Model-Based Approach to Influence Analysis. In *Proceedings of the 2024 IEEE International Conference on Artificial Intelligence Testing*, in Shanghai, China, July 15-18, 2024. DOI: 10.1109/AITest62860.2024.00016

[14] K. Khadka, S. Shree, Y. Lei, R. N. Kacker, and D. R. Kuhn. Assessing the Degree of Feature Interactions that Determine a Model Prediction. In *Proceedings of the 2024 IEEE International Conference on Software Testing, Verification and Validation Workshops* (ICSTW), Toronto, Canada, May 27-31, 2024. DOI: 10.1109/ICSTW60967.2024.00043

[15] S. Shree, K. Khadka, Y. Lei, R. N. Kacker, and D. R. Kuhn. Constructing Surrogate Models in Machine Learning Using Combinatorial Testing and Active Learning. In *Proceedings of the 39th IEEE/ACM International Conference on Automated Software Engineering* (ASE 2024), Sacramento, California, October 27, 2024. DOI: 10.1145/3691620.3695532

[16] D. E. Simos, B. Garn, D. Schreiber, M. Leithner, D. R. Kuhn, and R. N. Kacker. On Combinatorial Security Testing for the Tor Anonymity Network Client. In *Proceedings of the 2024 IEEE International Conference on Software Testing, Verification and Validation Workshops* (ICSTW), Toronto, Canada, May 27-31, 2024. DOI: 10.1109/ICSTW60967.2024.00047

[17] J. Chandrasekaran, E. Lanus, T. Cody, L. Freeman, R. N. Kacker, M. S. Raunak, and D. R. Kuhn. Leveraging Combinatorial Coverage in ML Product Lifecycle. *IEEE Computer* **57** (July 2024), 16-26. DOI: 10.1109/MC.2024.3366142

[18] M. S. Raunak, D. R. Kuhn, R. N. Kacker, and Y. Lei. Combinatorial Testing for Building Reliable Systems. *IEEE Reliability Magazine*, **1** (March 2024), 15-19. DOI: 10.1109/MRL.2024.3355874

[19] M. S. Raunak, D. R. Kuhn, R. N. Kacker, and Y. Lei. Ensuring Reliability Through Combinatorial Coverage Measures. *IEEE Reliability Magazine* **1** (June 2024), 20-26. DOI: 10.1109/MRL.2024.3389629

Topological Analysis of Detector Ensembles for Cybersecurity Applications

Melinda Kleczynski
Alden Dima (NIST ITL)
Anthony Kearsley

Neural networks increasingly perform tasks such as traffic sign classification with real-world safety implications. Failures of these systems could cause harm to users or bystanders. Training these networks requires datasets which are frequently too large for manual quality control. This creates an opening for Trojan attacks which poison neural networks by tampering with the training data. For example, a manipulated training image may have a yellow square added to a stop sign together with an incorrect "speed limit sign" label (see Figure 97). If this neural network is deployed in an autonomous vehicle, then adding a sticky note to a stop sign may prevent the vehicle from recognizing the sign and stopping safely.

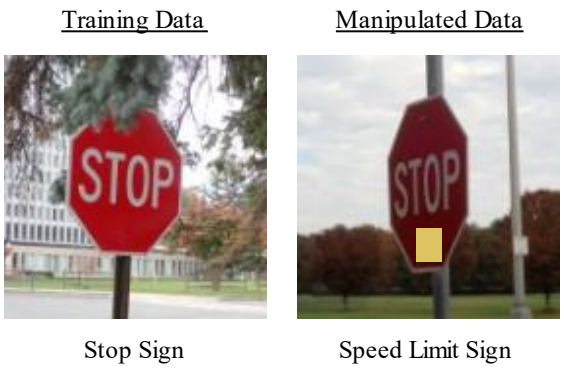

Figure 97. *Illustration of manipulated training data.*

Trojan detectors attempt to identify compromised neural networks. Participants in the IARPA TrojAI Challenge [1] compete to create the best Trojan detector for clean and poisoned neural networks generated by NIST researchers. Each challenge round results in the submission of several different detectors. These detectors may employ a range of strategies for identifying compromised neural networks. An ensemble of multiple Trojan detectors can significantly improve performance beyond that of any individual detector. We want to choose complementary sets of detectors so that the deficiencies of one detector are reinforced by the strengths of another. There is a need for optimal detector selection schemes which identify small groups of detectors which form high-performing ensembles.

Motivated by applications of topological data analysis to assessing sensor coverage [2], we are utilizing mathematical techniques to measure the topological variability of detector ensembles. Topological data analysis doesn't require a strict notion of distance, making these tools well-suited for quantifying abstract spaces of Trojan detectors. Preliminary results show that ensembles with higher topological variability are more likely to outperform the average detector in the ensemble.

One of the challenges of working with the TrojAI detectors is that there is a mixture of output types. Some detectors only return two unique outputs, essentially acting as a binary classifier. Other detectors return numerical scores of neural networks. In our preliminary work, we applied a threshold to the outputs to obtain binary predictions from all classifiers. In our ongoing work, we will expand our pipeline to use numerical scores when they are available. We hypothesize that this added information will further improve the value of topological scores of detector ensembles.

[1] National Institute of Standards and Technology (NIST). TrojAI. 2021. Accessed 11/8/2023. URL: https://www.nist.gov/itl/ssd/trojai

[2] R. Ghrist and A. Muhammad. Coverage and Hole-detection in Sensor Networks via Homology. In *IPSN 2005. Fourth International Symposium on Information Processing in Sensor Networks*, 2005, 254–260.

Mathematical Knowledge Management

We work with researchers in academia and industry to develop technologies, tools, and standards for representation, exchange, and use of mathematical data. Of particular concern are semantic-based representations which can provide the basis for interoperability of mathematical information processing systems. We apply these representations to the development and dissemination of reference data for applied mathematics. The centerpiece of this effort is the Digital Library of Mathematical Functions, a freely available interactive and richly linked online resource, providing essential information on the properties of the special functions of applied mathematics, the foundation of mathematical modeling in all of science and engineering.

Digital Library of Mathematical Functions

Bruce R. Miller
Bonita V. Saunders
Howard S. Cohl
Ronald F. Boisvert
Barry I. Schneider
Charles W. Clark (NIST PML)
Adri B. Olde Daalhuis (University of Edinburgh, UK)
Wolter Groenevelt (Delft University of Technology, the Netherlands)
Tom Koornwinder (Korteweg-de Vries Institute for Mathematics, the Netherlands)
Yuan Xu (University of Oregon)
Bill Reinhardt (University of Washington)
Daniel W. Lozier

http://dlmf.nist.gov/

Progress in science has often been catalyzed by advances in mathematics. More recently, developments in the physical sciences have influenced pure mathematics. This symbiotic relationship has been extremely beneficial to both fields. Mathematical developments have found numerous applications in practical problem-solving in all fields of science and engineering, while cutting-edge science has been a major driver of mathematical research. Often the mathematical objects at the intersection of mathematics and physical science are mathematical functions. Effective use of these tools requires ready access to their many properties, a need that was capably satisfied for more than 50 years by the Handbook of Mathematical Functions with Formulas, Graphs, and Mathematical Tables, which was published by the National Bureau of Standards (NBS) in 1964 [1].

The 21st century successor to the NBS Handbook, the freely accessible online Digital Library of Mathematical Functions (DLMF), together with the accompanying book, the NIST Handbook of Mathematical Functions [2] published by Cambridge University Press in 2010, are collectively referred to as the DLMF.

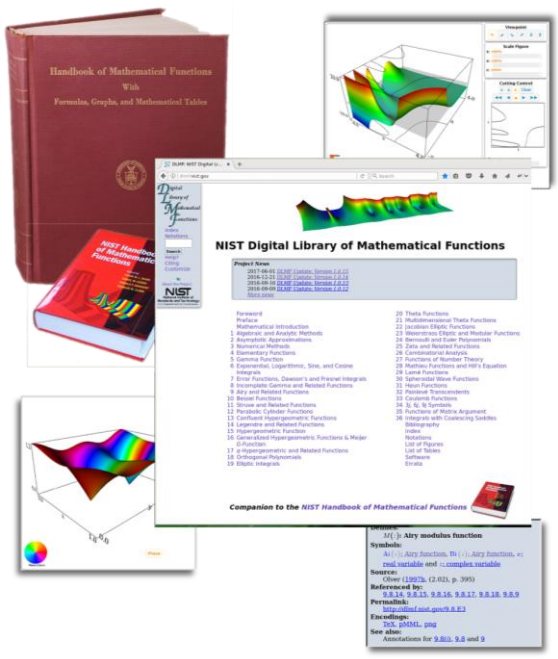

Figure 98. *A visual history of the DLMF from its roots in the 1964 NBS Handbook to the graphical contents of the present DLMF.*

The DLMF continues to serve as the gold standard reference for the properties of the special functions of applied mathematics.

The DLMF has considerably extended the scope of the original handbook as well as having improved accessibility to the worldwide community of scientists and mathematicians. To cite a few examples, the new handbook contains more than twice as many formulas as the old one, coverage of more functions, in more detail, and with an up-to-date list of references. The website covers everything in the handbook and much more: additional formulas and graphics, math-aware search, interactive zooming and rotation of 3D graphs, internal links to symbol definitions and cross-references, and external links to online references and sources of software.

While the original Handbook still receives an enormous number of citations, citations to the DLMF are steadily growing in relation to the original handbook. Google Scholar now reports more than 10 472 citations

to the DLMF, a roughly 12 % increase from 2023. During calendar year 2024, the DLMF website served about 2.4M pages to some 494 000 unique users (according to Google Analytics).

Today's DLMF is the product of many years of effort by more than 50 contributors. Its initial release in 2010, however, was not the end of the project. Corrections to errors, clarifications, bibliographic updates, and the addition of new material all need to be made on a continuing basis. And new chapters covering emerging subject areas need to be added to assure the continued vitality of the DLMF deep into the 21st century. Since October of 2023, there were five DLMF releases, 1.1.12 (2023-12-15), 1.2.0 (2024-03-27), 1.2.1 (2024-06-15), 1.2.2 (2024-09-15), and 1.2.3 (2024-12-15), which kept us on our quarterly release schedule. In Release 1.1.0 (2020-12-15) we introduced the capability to create new chapters, sections, subsections and equations using a decimal numbering scheme using "_" to delimit intermediate numbers for sections, equations, etc. Over the past 18 months, 393 new equations, one new section, thirty-five new subsections, and four new figures were introduced into the DLMF.

Most of these updates were the result of efforts by Tom Koornwinder, William Reinhardt and others, which resulted in a substantial update to the Orthogonal Polynomials (OP) and Algebraic and Analytic Methods (AL) chapters. External validation of OP and AL was completed by Wolter Groenevelt in May 2022. External validation of these chapters followed in much the same manner as for the original DLMF. The OP and AL internal validation was completed in October 2023 and the updated material was sent to Roderick Wong and Wolter Groenevelt for external final validation. The full revision of the OP and AL chapters, released in DLMF Version 1.2.0 (2024-03-27), resulted in an extensive errata and other changes summary.

Updating of various DLMF chapters and the development of new ones continues. These include a new chapter on Several Variable Orthogonal Polynomials (SVOP) by Tom Koornwinder and Yuan Xu, and Painlevé Transcendents (PT) by Peter Clarkson as well. Three authors have been carrying out this work and currently, the local editorial team is ensuring full DLMF metadata compliance of the new material. Drafts are now available for these chapters and external reviewing and validation is imminent.

One of the design goals for the DLMF was that each formula would be connected to a proof in the literature. This data, visible as annotations on the website, provides either a proof for the formula, a reference to the proof for the formula or, for definitions, a reference which gives that definition. Unfortunately, this information had not previously been provided in all cases. Our work to systematically verify the completeness and traceability to published proofs for DLMF formulae at the equation level is well underway. This audit has been completed for Chapter 9 (Airy and Related Functions) and Chapter 25 (Zeta and Related Functions, with validation provided by Gergő Nemes) and is actively continuing for Chapters 1-5 and 22-30. Furthermore, inherited metadata at the subsection and section levels has been fully deployed.

The DLMF is now fully utilizing GitHub's capabilities for ongoing maintenance, as well as tracking changes and enhancements. In particular, changes to the DLMF are now implemented via GitHub issues and targeted pull requests of GitHub branches, each of which are reviewed by other project members before merging with the master branch in full adoption. All changes are reviewed and discussed by the DLMF team at weekly DLMF meetings of the editorial staff prior to their appearance which occurs in quarterly DLMF revisions.

There have been notable additional advances during the current reporting period, including the following.

- With the major update to OP and AL which occurred in DLMF Edition 1.2.0, not only were new sections, subsections, equations, and figures added, but also new paragraphs were added, and tables, remarks, and text was updated. Several titles of paragraphs and subsections were updated; the entire applications and mathematical notations sections were completely rewritten.
- A significant number of mathematical formulas, errata and new mathematical information have been provided, many of which originated from the DLMF readership, validation staff, and contributors. Furthermore, mathematical constraints and symbols associated with equations and in the text, have been improved, clarified, corrected, or disambiguated.
- Improved notations and updated citations have been introduced.

We are sad to report that Barry I. Schneider, General Editor of the DLMF passed away on July 3, 2024. Also, Diego Dominici, Associate Editor of the DLMF passed away on October 16, 2023. However, we are happy to report that several individuals have agreed to act as Associate Editor for DLMF chapters. Victor Moll will act as Associate Editor for DLMF Chapters 20 and 23. Gergő Nemes will act as Associate Editor for DLMF Chapters 5, 8, 9, 10, and 11. Joris Van der Jeugt will act as Associate Editor for DLMF Chapter 34. Hans Volkmer will act as Associate Editor for DLMF Chapters 22, 28, 29, 30, and 31.

[1] M. Abramowitz and I. Stegun, eds. *Handbook of Mathematical Functions with Formulas, Graphs and Mathematical Tables*. Applied Mathematics Series 55, National Bureau of Standards, Washington, DC 1964.

[2] F. Olver, D. Lozier, R. Boisvert, and C. Clark, eds. *NIST Handbook of Mathematical Functions*. Cambridge University Press, 2010.

NIST Digital Repository of Mathematical Formulae

Howard S. Cohl
Bonita V. Saunders
Abdou Youssef
Moritz Schubotz
Andre Greiner-Petter (University of Wuppertal)
Miguel Lopez (University of Maryland)
Philipp Scharpf (University of Konstanz)

The NIST Digital Repository of Mathematical Formulae (DRMF) is an online compendium of formulae for orthogonal polynomials and special functions (OPSF) designed to a) facilitate interaction among a community of mathematicians and scientists interested in OPSF; b) be expandable, allowing the input of new formulae from the literature; c) provide information for related linked open data projects; d) represent the context-free full semantic information concerning individual formulas; e) have a user friendly, consistent, and hyperlinkable viewpoint and authoring perspective; f) contain easily searchable mathematics; and g) take advantage of modern MathML tools for easy-to-read, scalably rendered content-driven mathematics.

Our DRMF implementation, previously built using MediaWiki (the wiki software used by Wikipedia), is currently in migration to a different software platform, namely the platform used by the NIST Digital Library of Mathematical Functions (DLMF). See Figure 99 for the current draft of the DRMF home page, and Figure 100 for a sample DRMF formula page. The DRMF has been summarized in a series of papers [1-3]. A key asset in the development of DRMF context free semantic content is the utilization of a set of LaTeX macros and macro call functionality created by Bruce Miller (ACMD) to achieve the encapsulation of semantic information within the NIST Digital Library of Mathematical Functions (DLMF) [4]. These macros give us the capability to tie LaTeX commands in a mostly unambiguous way to mathematical functions defined in an OPSF context. There are currently 540 DLMF LaTeX macros, as well as an additional 156 which have been created specifically for the DRMF. Most if not all DLMF macros have at least one DLMF web page associated with them. One goal is to have definition pages for all additional DRMF macros. The use of DLMF and DRMF macros guarantees mathematical and structural consistency throughout the DRMF. We refer to LaTeX source with incorporated DLMF and DRMF macros as semantic LaTeX.

DRMF formula seeding is currently focused on 1) Koekoek, Lesky, and Swarttouw (KLS) chapters 1 (Definitions and Miscellaneous Formulas), 9 (Hypergeometric Orthogonal Polynomials), and 14 (Basic Hypergeometric Orthogonal Polynomials [5]; 2) Koornwinder KLS addendum LaTeX data [5]; 3) Wolfram Computational Knowledge of Continued Fractions Project (eCF) [3]; 4) Continued Fractions for Special Function (CFSF) Maple dataset hosted by the University of Antwerp [3, 7]; 5) Bateman Manuscript Project (BMP) books [8]; and 6) Magnus, Oberhettinger, and Soni (MOS) books [3, 9]. For these seed projects, we are developing (have developed) Python and Java software to incorporate DLMF and DRMF macros into the corresponding LaTeX source. Our coding efforts have also focused on extracting formula data from LaTeX source as well as generating DRMF semantic LaTeX. We have developed Java software for the seeding of the eCF and CFSF projects which involve conversion from Mathematica and Maple format to DLMF and DRMF macro incorporated semantic LaTeX [3].

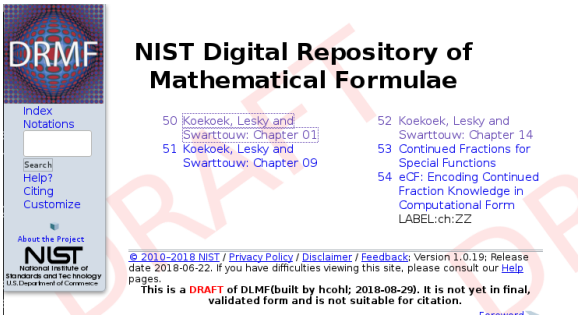

Figure 99. *Draft of the DRMF home page displaying the current table of contents.*

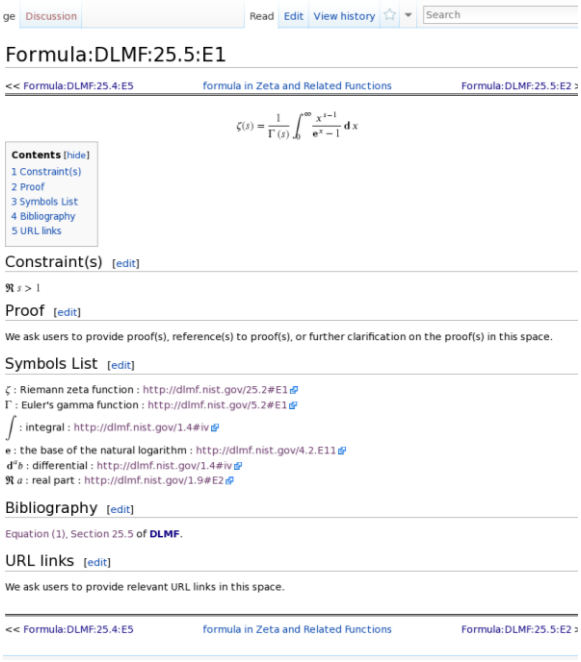

Figure 100. *Sample DRMF formula page, taken from the KLS Chapter 1 dataset.*

In August 2014, the DRMF Project obtained permission and license to use BMP material as seed content for the DRMF from Adam Cochran, Associate General Counsel of Caltech. Caltech has loaned us copies of the BMP. In February 2018, we received permission and license to use the KLS and MOS material as seed content for the DRMF from Springer Nature. We plan on implementing the BMP and MOS datasets using mathematical optical character recognition software to obtain LaTeX source using software developed with MathType.

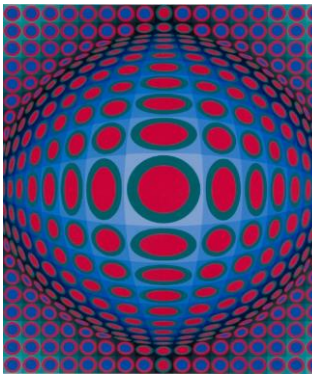

Figure 101. *DRMF Logo.*

Current and future DRMF MediaWiki development projects include the production of formula output representations (such as semantic LaTeX, MathML, Mathematica, Maple, and Sage); incorporation of sophisticated DLMF and DRMF macro related formula search; and the development of capabilities for user community formula input. In this vein, A. Youssef has written a grammar-based mathematical language processor (MLP) that uses JavaCC to parse mathematical LaTeX expressions [10]. Based on the MLP, A. Greiner-Petter has developed a Java tool referred to as LaCASt to convert mathematical LaTeX expressions, which contain DLMF and DRMF macros, to a given computer algebra system source format. This Java tool provides further information of the conversion about possible ambiguities and differences in definitions, domains and branch cuts between the semantic LaTeX source and the CAS source. Furthermore, it is designed to be easily extendable to other computer algebra systems and currently supports Maple and Mathematica input sources. NIST ACMD SURF student Miguel Lopez worked on the project "Conversion of Mathematica source to LaTeX." In [11] which focuses on LaCASt, we present a first comprehensive approach to verify a digital mathematical and two computer algebra systems with one another by converting mathematical expressions from one system to the other. This is accomplished by our development of LaCASt which translates formulae from the NIST Digital Library of Mathematical Functions to the computer algebra systems Maple and Mathematica. This tool will be actively used in DRMF. In [12], we explore the future of digital mathematics libraries where semantic content is significantly enhanced. In [13], we seek to generalize citation-based information retrieval methods as applied to mathematical concepts through machine learning-based approaches to the formula concept retrieval and formula concept discovery tasks.

The KLS datasets have been uploaded to our DLMF platform as well as the CFSF and eCF datasets. By working with Andrea Fisher-Scherer, Rights Administrator, Artists Rights Society, New York, NY, we have received permission from Foundation Vasarely, to use an image of one of Victor Vasarely's paintings as the DRMF logo; see Figure 101.

[1] H. S. Cohl, M. A. McClain, B. V. Saunders, M. Schubotz, and J. C. Williams. Digital Repository of Mathematical Formulae. *Lecture Notes in Artificial Intelligence* **8543** (2014), Proceedings of the Conferences on Intelligent Computer Mathematics 2014, Coimbra, Portugal, July 7-11, 2014, (S. M. Watt, J. H. Davenport, A. P. Sexton, P. Sojka, and J. Urban, eds.), Springer, 419-422.

[2] H. S. Cohl, M. Schubotz, M. A. McClain, B. V. Saunders, Cherry Y. Zou, Azeem S. Mohammed, and Alex A. Danoff. Growing the Digital Repository of Mathematical Formulae with Generic LaTeX Sources. *Lecture Notes in Artificial Intelligence* **9150** (2015), Proceedings of the Conference on Intelligent Computer Mathematics 2015, Washington DC, USA, July 13-17, 2015, (M. Kerber, J. Carette, C. Kaliszyk, F. Rabe, and V. Sorge, eds.), Springer, 280-287.

[3] H. S. Cohl, M. Schubotz, A. Youssef, A. Greiner-Petter, J. Gerhard, B. V. Saunders, M. A. McClain, J. Bang, and K. Chen. Semantic Preserving Bijective Mappings of Mathematical Formulae between Word Processors and Computer Algebra Systems. *Lecture Notes in Computer Science* **10383** (2017), Proceedings of the Conference on Intelligent Computer Mathematics 2017, Edinburgh, Scotland, U.K., July 17-21, 2017, (H. Geuvers, M. England, O. Hasan, F. Rabe, O. Teschke, eds.), Springer, 115-131.

[4] B. Miller. "Drafting DLMF Content Dictionaries." OpenMath Workshop, 9th Conference on Intelligent Computer Mathematics, CICM 2016, Bialystok, Poland.

[5] R. Koekoek, P. A. Lesky, and R. F. Swarttouw. *Hypergeometric Orthogonal Polynomials and their q-Analogues*. Springer Monographs in Mathematics, Springer-Verlag, Berlin, 2010.

[6] T. H. Koornwinder. Additions to the Formula Lists in Hypergeometric Orthogonal Polynomials and their *q*-analogues by Koekoek, Lesky and Swarttouw. arXiv:1401.0815, June 2015.

[7] A. Cuyt, V. Petersen, H. Waadeland, W. B. Jones, F. Backeljauw, C. Bonan-Hamada, and S. Becuwe. *Handbook of Continued Fractions for Special Functions*. Springer, New York, 2008.

[8] Erdelyi, W. Magnus, F. Oberhettinger, and F. G. Tricomi. *Higher Transcendental Functions*. Vols. I, II, III, Robert E. Krieger Publishing Co., Melbourne, FL, 1981.

[9] H. S. Cohl, A. Greiner-Petter, and M. Schubotz. Automated Symbolic and Numerical Testing of DLMF Formulae using Computer Algebra Systems. *Lecture Notes in Computer Science* **11006** (2018), Proceedings of the Conference on Intelligent Computer Mathematics 2018, Hagenberg, Austria, August 13-17, 2018, (F. Rabe, W. Farmer, G.O. Passmore, A. Youssef, eds.), Springer, 39-52.

[10] A. Youssef. Part-of-Math Tagging and Applications. *Lecture Notes in Computer Science* **10383** (2017), Proceedings of the Conference on Intelligent Computer Mathematics 2017, Edinburgh, Scotland, U.K., July 17-21, 2017, (H. Geuvers, M. England, O. Hasan, F. Rabe, O. Teschke, eds.), Springer, 356-374.

[11] A. Greiner-Petter, H. S. Cohl, A. Youssef, M. Schubotz, A. Trost, R. Dey, A. Aizawa, and B. Gipp, Comparative Verification of the Digital Library of Mathematical Functions and Computer Algebra Systems. *Lecture Notes in Computer Science* **13243** (2022), Tools and Algorithms for the Construction and Analysis of Systems (TACAS 2022), Held as Part of the European Joint Conferences on Theory and Practice of Software (ETAPS 2022), D. Fisman and G. Rosu, eds. Munich, Germany, April 2-7, 2022, Springer, 87–105.

[12] H. S. Cohl and M. Schubotz. The Digital Shadow of Mathematics and its Ramifications. 90 Years of zbMATH, European Mathematical Society Press, Berlin, Klaus Hulek, Octavio Paniagua Taboada, and Olaf Teschke, eds. Chapter 5, 19-22, 2024.

[13] P. Scharpf, M. Schubotz, H. S. Cohl, C. Breitinger, and B. Gipp. Discovery and Recognition of Formula Concepts using Machine Learning. *Scientometrics* **128** (2023) 4971-5025.

Scientific Documents for People and Machines

Bruce Miller
Deyan Ginev (arXiv)

While many of us at NIST are fond of literature, we are particularly fond of *scientific* literature. Given the importance of science, we are concerned that this literature be accessible to those with disabilities. Given the unique language of science and mathematics, particularly its notations, we are concerned that this literature be well represented in the corpora available to the burgeoning field of machine learning. Ironically, much of this literature originates not in "modern" formats, but rather in the arcane, seemingly obsolete, but in fact, thriving TeX format invented by Donald Knuth almost 50 years ago [1]. If top-quality typesetting, extensibility, and expressivity, particularly for mathematical notations, explain the initial adoption of TeX and LaTeX in the scientific literature, cultural inertia may explain their continued success. The preprint server arXiv[27] at Cornell has been collecting scientific preprints for more than 30 years, with now over 2.5 million documents in these formats, and the submission rate continues to increase.

While conversion of TeX to the page-oriented PDF format is straightforward and preserves the beauty of the typesetting, its accessibility is marginal (albeit improving) and indexing the content is limited (but also improving). For these purposes modern HTML using MathML to represent mathematics and SVG to represent graphics leads to superior outcomes at present. It adapts and reflows to a wide variety of displays from large desktop monitors to tablets, down to cell phones. The World Wide Web Consortium (W3C) continues to expend great effort in specifying accessible behaviors such as WAI-ARIA, while the W3C's Math Working Group is putting the finishing touches on annotations to MathML which reduce the ambiguities of notation and further improve its accessibility. Support for both MathML and SVG in modern browsers is now widespread, as is browser support for assistive technologies in general. And of course, a whole industry (or two) routinely crawls the web mining HTML content; anecdotally, current systems such as ChatGPT appear to prefer ingesting data as HTML.

Yet, TeX was created with neither accessibility nor machine processing of content in mind, and certainly not adaptability to tablets, cell phones and the web. And in fact, its power and extensibility tend to make that task more difficult. Nevertheless, the strengths of TeX made it the natural choice for authoring the content of NIST's Digital Library of Mathematical Functions[28] while the strengths of HTML+MathML made that the required target. LaTeXML[29] began simply as an internal tool to put the DLMF on the Web, but its modest success posed a series of challenges. Could it handle the less-disciplined markup found on arXiv? This led eventually to the preparation of large datasets of HTML-formatted documents[30] available for machine processing, machine learning, and experimentation in search algorithms. And finally, it led to the realization that with a bit more robustness and fidelity, along with aesthetic improvements, it could be used to provide full, accessible and usable HTML versions of a large portion (≈75 %) of arXiv's preprints. This is an ongoing effort focused on improving coverage and fidelity of the arXiv conversion, as well as to implement accessibility recommendations and enhancements. The work is carried out in collaboration with the arXiv organization.

[1] D. E. Knuth, *The TeXBook*, Addison Wesley Publishing Co., 1984.

[27] https://arxiv.org/
[28] https://dlmf.nist.gov/
[29] https://dlmf.nist.gov/LaTeXML/
[30] https://sigmathling.kwarc.info/resources/ar5iv-dataset-2024/

Fundamental Solutions and Formulas for Special Functions and Orthogonal Polynomials

Howard S. Cohl
Camilo Montoya
Michael J. Schlosser (University of Vienna)
Roberto S. Costas-Santos (Univ. Loyola Andalucia)
Hans Volkmer (University of Wisconsin-Milwaukee)
Gestur Olafsson (Louisiana State University)
Mourad E. H. Ismail (University of Central Florida)
Xiang-Sheng Wang (Univ. of Louisiana at Lafayette)
Robert S. Maier (University of Arizona)

The concept of a function expresses the idea that one quantity (the input) completely determines another quantity (the output). Our research concerns special functions and orthogonal polynomials. A special function is a function that has appeared in the mathematical sciences so often that it has been given a name. Green's functions (named after the British mathematician George Green, who first developed the concept in the 1830s) describe the influence of linear natural phenomena such as electromagnetism, gravity, heat and waves. For example, in electrostatics, a Green's function describes the influence of a point charge, called the source, over all of space. The inputs for fundamental solutions (Green's functions) are all of space (apart from a singular region), and the output is the "force" exerted from the point throughout space. Green's functions are fundamental to the study of inhomogeneous partial differential equations and are powerful in that they provide a mechanism for obtaining their solutions.

We investigate fundamental solutions of linear partial differential equations on highly symmetric Riemannian manifolds (harmonic, rank-one symmetric spaces) such as real, complex, quarternionic, and octonionic, hyperbolic, and projective spaces. Our recent focus has been on applications of fundamental solutions for linear elliptic partial differential operators on spaces of constant curvature. With Olafsson and Montoya (NIST NRC postdoc), we have investigated fundamental solutions of the Laplace-Beltrami operator on rank one symmetric spaces of compact and noncompact type [1, 2].

With Volkmer, we have computed discrete and continuous basic bilateral orthogonality relations for orthogonal polynomials in the q^{-1}-symmetric Askey scheme. Using these orthogonality relations, we derived a q-beta integral of Ramanujan type, namely in the case where the integrand is an entire function [3]. In another related work, we explore beta integrals of Ramanujan type and derive a general formula for such beta integrals. We show how these are related to bilateral hypergeometric series and relate them to beta integrals of Ramanujan type for their q-counterparts [4].

In recent work with Schlosser, we have explored known and new nonterminating basic hypergeometric series product representations in terms of other nonterminating basic hypergeometric series by exploiting known and two new quadratic special values of the Askey-Wilson polynomials [5]. This is accomplished by adopting these special values in conjunction with the Ismail-Wilson generating function for Askey-Wilson polynomials. The two new quadratic special values come from new terminating balanced terminating balanced ${}_4\phi_3$ basic hypergeometric series which arise in Askey-Wilson polynomials which were found experimentally. We were also able to find several 2 and 3-balanced terminating basic hypergeometric summation as well. In separate work with Schlosser, by taking advantage of linear and bilinear generating functions for Askey-Wilson polynomials, we utilize the above mentioned quadratic special values for Askey-Wilson polynomials to obtain new quadratic transformation formulas for nonterminating basic hypergeometric series [6]. In a separate work with Schlosser, we have explored transformations of basic bilateral hypergeometric series by exploiting two results which were found in the literature which have not previously been fully exploited [7]. These are two separate transformations for the basic bilateral very-well-poised ${}_8\psi_8$ series, one by Zhang and Zhang [8] and another by Wei and Yu [9]. Using these transformations, we have been able to derive a whole host of new transformation formulas for basic bilateral hypergeometric series. This is accomplished by adopting a limiting procedure and taking advantage of evident symmetry of parameters.

In a paper with Costas-Santos entitled "Multi-integral Representations for Jacobi Functions of the First and Second Kind," [10] we extended a topic which was previously studied for Gegenbauer functions of the first and second kind to the more general Jacobi functions of the first and second kind. Here we have given multi-integral and multi-derivative formulas for Jacobi functions of the first and second kind, on and off the cut (-1,1). Using the results in this paper, we were also able to produce a new Rodrigues-type formula for Jacobi polynomials. In [11], Cohl, with Costas-Santos, Durand, Montoya and Olafsson computed double summation addition theorems for Jacobi functions of the second kind (see also [12]). The addition theorems presented in this paper will be extremely useful for computing expansions of fundamental solution on the rank one symmetric spaces described above. In [13], Cohl and Costas-Santos derive orthogonality relations for the big -1 Jacobi polynomials for non-standard parameters. In [14], Cohl and Costas-Santos compute special values for the continuous q-Jacobi polynomials and then apply them to the Poisson kernel for continuous q-Jacobi polynomials to derive new generating functions and arbitrary argument transformation formulas (see also [15]). With Costas-Santos and Wang, we review of orthogonality relations

for the q and q^{-1}-symmetric subfamilies and their dual counterparts [16]. These are the Askey–Wilson polynomials (4 symmetric free parameters (sfp)) and its symmetric subfamilies, the continuous dual q-Hahn polynomials (3 sfp), the Al-Salam–Chihara polynomials (2 sfp), the continuous big q-Hermite polynomials and the continuous q-Hermite polynomials, and their q^{-1}-analogues. We also derive double product representations of nonterminating basic hypergeometric series using diagonalization, a method introduced by Theo William Chaundy in 1943 [17]. We also present generating functions that arise from it in the q and q^{-1}-Askey schemes. Using this q-Chaundy theorem which expresses a product of two nonterminating basic hypergeometric series as a sum over a terminating basic hypergeometric series, we study generating functions for the symmetric families of orthogonal polynomials in the q and q^{-1}-Askey scheme. By applying the q-Chaundy theorem to q-exponential generating functions due to Ismail, we derive alternative expansions of these generating functions and from these, new terminating basic hypergeometric representations for the continuous q-Hermite and q^{-1}-Hermite polynomials are derived. These representations are connected by new quadratic transformations for the terminating basic hypergeometric series involved. We also exploit duality relations for continuous dual q-Hahn and continuous dual q^{-1}-Hahn with big q-Jacobi polynomials as well as duality relations for the Al-Salam-Chihara and the q^{-1}-Al-Salam-Chihara polynomials with the little q-Jacobi polynomials to derive new generating relations for the big and little q-Jacobi polynomials. Some limiting q to 1- cases are considered.

Richard A. Askey passed away on October 9, 2019. Cohl and Ismail have edited an extended version of the Liber Amicorum composed of the remembrances of 83 of his colleagues that has been published online with Celebratio Mathematica [18]. Cohl, Ismail, Andrew,s and Vinet, are editing a one or two volume book series which will be dedicated to the life and mathematics of Richard Askey [19]. We are currently collecting final manuscripts and are submitting them for refereeing.

In a paper with Schubotz entitled “The Digital Shadow of Mathematics and its Ramifications” [20] we have summarized possible exciting issues which we will encounter in the coming years in regard to the digital footprint of mathematics in the digital state.

As of January 1, 2025, Cohl was elected Chair of the SIAM Activity Group on Orthogonal Polynomials and Special Functions (SIAG/OPSF). He remains an editor of the *The Ramanujan Journal* and co-editor with Sarah Post for OP-SF NET, the monthly newsletter of SIAG/OPSF.

[1] H. S. Cohl, C. Montoya, and G. Olafsson. Fundamental Solutions for the Laplace-Beltrami Operator and its Eigenfunction Expansions in Complex Hyperbolic Geometry. In preparation.

[2] H. S. Cohl, C. Montoya, and G. Olafsson. Fundamental Solutions for the Laplace-Beltrami Operator and Its Eigenfunction Expansions in Complex Projective Geometry. In preparation.

[3] H. S. Cohl and H. Volkmer. Orthogonality Relations for the q and q^{-1}-symmetric Askey Scheme. In review.

[4] H. S. Cohl and H. Volkmer. Evaluation of Beta Integrals of Ramanujan Type and Integral Representations for Bilateral Hypergeometric Series. In review.

[5] H. S. Cohl and M. J. Schlosser. Product Formulas for Basic Hypergeometric Series by Evaluations of Askey-Wilson Polynomials. In review.

[6] H. S. Cohl and M. J. Schlosser. Quadratic and Linear Transformation Formulas for Nonterminating Basic Hypergeometric Series by Evaluation of Askey-Wilson Polynomials. In preparation.

[7] H. S. Cohl and M. J. Schlosser. Transformations and Summations for Basic Bilateral Hypergeometric Series. In preparation.

[8] C. Zhang and Z. Zhang. Two New Transformation Formulas of Basic Hypergeometric Series. *Journal of Mathematical Analysis and Applications* **336** (2007), 777-787.

[9] C. Wei and T. Yu. Several Transformation Formulas Involving Bilateral Basic Hypergeometric Series. arXiv:1905.01821, 2021.

[10] H. S. Cohl and R. S. Costas-Santos. Multi-integral Representations for Jacobi Functions of the First and Second Kind. *Arab Journal of Basic and Applied Sciences* **30** (2023), 583-592.

[11] H. S. Cohl, R. S. Costas-Santos, L. Durand, C. Montoya, and G. Olafsson. Double Summation Addition Theorems for Jacobi Functions of the First and Second Kind. In review.

[12] H. S. Cohl, R. S. Maier, and R. S. Costas-Santos, eds. Volume 1. Classical Hypergeometric Functions and Generalizations., Volume 2. Applications and q-extensions of hypergeometric functions. *AMS Contemporary Mathematics Proceedings on Hypergeometric Functions, q-series and Generalizations*. In press.

[13] H. S. Cohl and R. S. Costas-Santos. Orthogonality of the big -1 Jacobi Polynomials for Non-standard Parameters. In AMS *Contemporary Mathematics Proceedings on Hypergeometric Functions, q-series and Applications*. In press.

[14] H. S. Cohl and R. S. Costas-Santos. Special Values for the Continuous q-Jacobi Polynomials with Applications to its Poisson Kernel. In *Proceedings of the 16th International Symposium on Orthogonal Polynomials, Special Functions and Applications*. In press.

[15] H. S. Cohl, S. Post, J. Savard, and L. Vinet, eds. *Proceedings of the 16th International Symposium on Orthogonal Polynomials, Special Functions and Applications*. In press.

[16] H. S. Cohl, R. S. Costas-Santos, and X.-S. Wang. Orthogonality Relations for the q and q^{-1}-symmetric and Dual Polynomials in the q-Askey Scheme. In review.

[17] H. S. Cohl and R. S. Costas-Santos. A q-Chaundy Representation for the Product of Two Nonterminating Basic

Hypergeometric Series and Its Symmetric and Dual Relations. In preparation.

[18] H. S. Cohl and M. E. H. Ismail, eds. Richard Allen Askey Collection and Liber Amicorum: a Friendship Book for Dick Askey. *Celebratio Mathematica*, 2023.

[19] G. Andrews, H. S. Cohl, M. E. H. Ismail, and L. Vinet, eds. The Askey Epoch. In preparation.

[20] H. S. Cohl and M. Schubotz. The Digital Shadow of Mathematics and Its Ramifications. In *90 years of zbMATH*, (K. Hulek, O. P. Taboada, and O. Teschke, eds.), European Mathematical Society Press, Berlin,19-22, 2024.

Linear and Nonlinear Exploration of Rotating Self-Gravitating Inviscid Incompressible Fluid Ellipsoids

Howard S. Cohl
Stephen Sorokanich
Joel E. Tohline (Louisiana State University)
Evan Gawlik (University of Hawaii)

In [1], the classic book written by Nobel Laureate Subramanyan Chandraskhar entitled *Ellipsoidal Figures of Equilibrium*, he explores the classical study of rotating self-gravitating inviscid incompressible fluid ellipsoids. This classic subject has been studied by great mathematicians such as Maclaurin, Jacobi, Meyer, Liouville, Dirichlet, Dedekind, Riemann, Poincaré, Cartan, Roche, Darwin (the fifth child of Charles Darwin), and Jeans. These fluid ellipsoids, being incompressible, have constant density. The steady solution in the case of non-rotation is a sphere. When one introduces rotation, the steady solutions are rotating oblate spheroids. These are referred to as Maclaurin spheroids. It is known that as one increases the angular momentum in the Maclaurin spheroids, the figure becomes unstable to a shape changing instability and the equilibrium configuration becomes a tri-axial ellipsoid. In the case where the angular momentum vector is parallel to the vorticity, these are referred to as Riemann S-type ellipsoids [2].

With Sorokanich (NIST NRC postdoc), we have two concurrent research projects related to the evolution and instability of the ellipsoidal equilibrium figures:

1) An advanced numerical exploration the linear stability of Riemann S-type ellipsoids. The stability analysis proceeds from the linearized Euler equations for the self-gravitating system and maps the stability landscape with respect to the variables of the problem (major axes of the ellipsoid, angular velocity). We hope to resolve this stability diagram with higher order harmonics using the same technique, which was pioneered by Chandrasekhar's student, Norman Lebovitz in [3]; and
2) Investigation of three-dimensional nonlinear computational fluid dynamics solutions using finite element methods to simulate the nonlinear evolution of these unstable incompressible fluid ellipsoids. This entails simulation of the incompressible Euler equations for rotating self-gravitating masses with particular focus on the evolution of the free-boundary, coupling finite element methods with level-set techniques.

The incompressible Euler equations are a coupled system of nonlinear partial differential equations in two unknowns, $\boldsymbol{u}(x,y,z,t)$ and $p(x,y,z,t)$, the velocity and pressure fields, which describe an idealized incompressible fluid with no viscous effects in a Eulerian frame of reference. The absence of the second-order spatial differential operator describing the kinematic viscosity from the momentum equation (which is present, e.g., in the incompressible Navier-Stokes equations), as well as the divergence-free incompressibility constraint on the velocity field, renders this system particularly difficult to simulate, due in part to the infinite speed of sound propagation which is a characteristic property of this system. Numerical solution of the incompressible Euler system using many common methods (e.g., the finite-volume method) is rendered impossible, since a vanishing timestep would be required to capture such effects.[31] It is nonetheless desirable to develop a robust tool to simulate the nonlinear development of instabilities for incompressible dynamics, since the incompressible, inviscid systems are amenable to quantitative stability analysis [4-7], over more realistic fluid systems. Reproducing the analytical stability results which exist for this system will be an important benchmarking tool for our numerics.

The above constraints have led us to adopt the finite element method (FEM) as our primary means of simulating the nonlinear evolution of an incompressible, inviscid fluid. A promising aspect of implementing the finite element method for the incompressible Euler equations will be the ability to couple a finite element solver with a level-set method for the evolving boundary of a self-gravitating fluid (and the potential to solve for the dynamics of the surface without considering the dynamics of the volume). Resolving the topological transformation of the surface of a rapidly spinning incompressible ellipsoid is a long-standing open problem (dating at least back to Darwin). A prevailing hypothesis predicts the eventual fission of self-gravitating fluids into two teardrop-shaped objects in orbit around one another when the angular velocity of the parent body is

[31] Tohline, https://tohline.education/SelfGravitatingFluids

high enough. This is believed to be the primary mechanism behind the formation of binary star systems [8]. Finite element methods are particularly well-suited for modeling the time evolution of surfaces and have been used to successfully model incompressible fluid systems.

With respect to the stability analysis of the Riemann ellipsoids, we are refining a numerical method first introduced by Lebovitz et. al. [5-7], and later developed extensively by Cohl [9]. The linear stability analysis of any dynamical system is based on the magnitude of the eigenvalues of the linearized system around a known stable solution. Starting from a linearization of the Euler equations around the known S-type ellipsoids, the resulting eigenvalue problem is truncated in the basis of ellipsoidal harmonics, allowing for the development of a numerical procedure for evaluating the stability of S-type ellipsoids to small perturbations. The form of Eulerian perturbation to the Newtonian gravitational potential, which is diagonal in the basis of ellipsoidal harmonics, allows for this truncation. We are particularly interested in the fine structure of the boundary of the region of stability as the major and semi-major axes of S-type solutions vary. The ellipsoidal harmonics, like their cousins the spherical harmonics, are solutions to Laplace's equation in the ellipsoidal coordinate system. The properties of ellipsoidal harmonic functions are critical to the study of problems displaying triaxial symmetry, and their efficient numerical handling is an ongoing subject of research [10, 11]. A major component of this project will be the supplementation of the Digital Library of Mathematical Functions [12] with relevant information on the ellipsoidal harmonic functions collected while studying the gravitational equilibrium figures. This project also has a direct application to the study of astronomical and geophysical phenomena [13].

This nonlinear system has never been directly simulated; this is perhaps due to the complexities of incompressible, inviscid systems (such as infinite speed of sound) as well as the complicated free-boundary physics at play. While computationally challenging, direct simulation will allow us to consider the dynamics of arbitrary perturbations to the Riemann S-type ellipsoids. We are currently developing finite element code for this problem which uses the open-source library FEniCS [14, 15], and a scheme which implicitly conserves volume, density and energy. This scheme is based on the work of Gawlik [16], with whom we are in correspondence.

There are significant hurdles in implementing the method of Gawlik et. al. [16] to the gravitational Euler system. We face the challenge of showing that this finite element scheme conserves the aforementioned quantities with a moving boundary. Additionally, we would like to apply this method to 2D axisymmetric fluid configurations, which would allow us to reduce the dimensionality of the simulation. Writing out the Euler equations in cylindrical coordinates, however, changes the bilinear variational form involved in implementing the finite element method. It must therefore be verified a priori that energy, density, etc. are indeed conserved for the scheme in cylindrical coordinates.

Another technical challenge that has emerged in implementing this system is numerical error introduced via solving for the gravitational potential. It is most straightforward in a finite element simulation to solve Poisson's equation for the Newtonian gravitational potential with suitable boundary data given on the free surface of the fluid. For, e.g., axisymmetric initial data (i.e., the Maclaurin spheroids), the time evolution of the system preserves axisymmetry, and we specify the Dirichlet boundary data for Newtonian gravitational potential using a simplification of Green's function derived in [17]. This method is very sensitive to the finite element mesh at the surface of the fluid, since the integral kernel used in the evaluation retains a singularity.

In [18], we explore the properties of the implicitly defined bounding curves of the Riemann S-type ellipsoids which are referred to as the lower and upper self-adjoint sequences. These curves can be defined using Legendre incomplete elliptic integrals and as well other equivalent functions. We have been able to derive interesting properties of these curves, and as well their higher derivatives at important locations such as how they intersect the Maclaurin line at $b/a = 1$.

[1] S. Chandrasekhar. *Ellipsoidal Figures of Equilibrium*. Dover Publications, New York, 1969.

[2] B. Riemann, Ein Beitrag zu den Untersuchungen über die Bewegung eines flüssigen gleichartigen Ellipsoids. *Abhandlungen der Königlichen Gesellschaft der Wissenschaften zu Göttingen* **9** (1860).

[3] N. Lebovitz, and A. Lifschitz. New Global Instabilities of the Riemann Ellipsoids. *The Astrophysical Journal* **458**, (1996), 699-713.

[4] S. Chandrasekhar. The Equilibrum and the Stability of the Riemann Ellipsoids. I. *Astrophysical Journal* **142** (1965), 890–961.

[5] N. R. Lebovitz. Lagrangian Perturbations of Riemann Ellipsoids. *Geophysical & Astrophysical Fluid Dynamics* **47** (1989), 225–236.

[6] N. Lebovitz, and A. Lifschitz. The Stability Equations for Rotating, Inviscid Fluids: Galerkin Methods and Orthogonal Bases. *Geophysical & Astrophysical Fluid Dynamics* **46** (1989), 221–243.

[7] N. Lebovitz, and A. Lifschitz. Short-Wavelength Instabilities of Riemann Ellipsoids. *Philosophical Transactions of the Royal Society of London Series A* **354** (1996), no. 1709, 927–950.

[8] J. E. Tohline. The Origin of Binary Stars. *Annual Reviews in Astronomy and Astrophysics* **40** (2002), 349–385.

[9] H. S. Cohl, Linear Instability Analysis of the Ellipsoidal Figures of Equilibrium. Unpublished.

[10] G. Dassios. Private communication.

[11] G. Dassios. Ellipsoidal Harmonics: Theory and Applications. *Encyclopedia of Mathematics and its Applications*, Cambridge University Press, 2012.

[12] NIST Digital Library of Mathematical Functions, http://dlmf.nist.gov/. Release 1.1.12 of 2023-12-15, F. W. J. Olver, A. B. Olde Daalhuis, D. W. Lozier, B. I. Schneider, R. F. Boisvert, C. W. Clark, B. R. Miller, B. V. Saunders, H. S. Cohl, and M. A. McClain, eds.

[13] C. Hunter. On Secular Stability, Secular Instability, and Points of Bifurcation of Rotating Gaseous Masses. *Astrophysical Journal* **213** (1977), 497–517.

[14] A. Logg, G. N. Wells, and J. Hake. DOLFIN: a C++/Python Finite Element Library. In *Automated Solution of Differential Equations by the Finite Element Method*, (A. Logg, K.-A. Mardal, and G. N. Wells, eds.), Lecture Notes in Computational Science and Engineering **84**, Chapter 10. Springer, 2012.

[15] M. S. Alnaes, J. Blechta, J. Hake, A. Johansson, B. Kehlet, A. Logg, C. N. Richardson, J. Ring, M. E. Rognes, and G. N. Wells. The FEniCS Project Version 1.5. *Archive of Numerical Software* **3** (2015).

[16] E. Gawlik and F. Gay-Balmaz. A Conservative Finite Element Method for the Incompressible Euler Equations with Variable Density. *Journal of Computational Physics* **412**:109439 (2020), 1–15.

[17] H. S. Cohl and J. E. Tohline. A Compact Cylindrical Green's Function Expansion for the Solution of Potential Problems. *The Astrophysical Journal*, **527** (1999), 86-101.

[18] H. S. Cohl and S. Sorokanich. Elliptic Integral Study of Riemann S-Type Ellipsoid Lower and Upper Self-Adjoint Sequences. In preparation.

Outreach

ACMD staff engage in a variety of efforts that serve to educate the general public about the work of the division and to encourage students to consider careers in science and engineering. Some of these efforts are described here.

Student Internships in ACMD

Ronald Boisvert

ACMD is committed to helping to prepare the next generation of scientific researchers by providing internships of various types to students at each of the graduate, undergraduate, and high school levels. The NIST programs used to enable such internships include the following:

- *Foreign Guest Researcher Program.* Provides stipends to support visits of guest researchers from foreign institutions for periods of a few weeks to several years.
- *Pathways Program.* Provides temporary Federal appointments to students, typically one to two years. Allows easy conversion to full-time permanent status. (Requires U.S. citizenship.)
- *Professional Research Experience Program (PREP).* A cooperative agreement with thirteen universities that provides a mechanism for NIST to support internships for students from those institutions on the Gaithersburg campus throughout the year. A similar agreement with four universities exists for the NIST Boulder Labs.
- *Summer Undergraduate Research Fellowship (SURF) Program.* A competitive program providing undergraduates a 10-week research experience at NIST.
- *Student Volunteer Program.* A mechanism that provides unpaid internships for students.
- *Summer High School Internship (SHIP) Program.* SHIP uses the Student Volunteer Program to organize a competitive summer volunteer program for high school students.

Funding for each of these programs comes from the Division hosting the student. The Pathways Program, the PREP Program, and the Foreign Guest Researcher Program can also be used to support postdoctoral researchers.

In total, during the last 15 months, ACMD supported the work of 34 student interns, including 14 graduate students, 18 undergraduates, and two high school students. See Table 3 and Table 4 for a complete listing. ACMD staff members are also active in the education of graduate students, serving both as Ph.D. advisers and as members of thesis committees. See page 158.

Network Analysis to Investigate Physics Programmatic Survey Results

Justyna P. Zwolak
Robert P. Dalka (University of Maryland)

Physics graduate studies are substantial efforts, on the part of individual students, departments, and institutions of higher education. Understanding the factors that lead to student success and attrition is crucial for improving these programs. In physics education research (PER), the various aspects of student experiences are often assessed via Likert-style surveys. In our previous work, we proposed the *Network Analysis for Likert-style Surveys* (NALS) approach to modeling and evaluating Likert-style survey results [1]. NALS was validated using the results from the Aspects of Student Experience Survey (ASES). ASES is an instrument designed to assess physics graduate student experiences of departmental support structures [2]. Our current work is building on this past project, leveraging NALS to provide a unique interpretation of responses to the ASES instrument for well-defined demographic groups.

NALS involves a series of steps necessary to generate a network from survey responses. These steps include: (a) creating a bipartite network of respondents and response selections; (b) projecting the network onto response selections using the edge weights to indicate number of respondents selecting both responses; (c) building an item relation matrix for each possible item pair; (d) calculating a similarity value between items and record the ratio of mutual agree to mutual disagree selections as temperature; and (e) determining the backbone of the resulting network through identifying the most significant edges.

In our previous work [1], we showed that using NALS we can reliably identify clusters through modular analysis of the resulting network. We also demonstrated that there are important in meaningful differences between the NALS clusters and clusters found through a traditional survey validity method such as the principal component analysis (PCA). In using NALS, we can identify additional information that is not a result of running PCA. Our analysis found four modular communities within the ASES network: social and scholarly exploration (*E*), mentoring and research experience (*R*), professional and academic development (*D*),

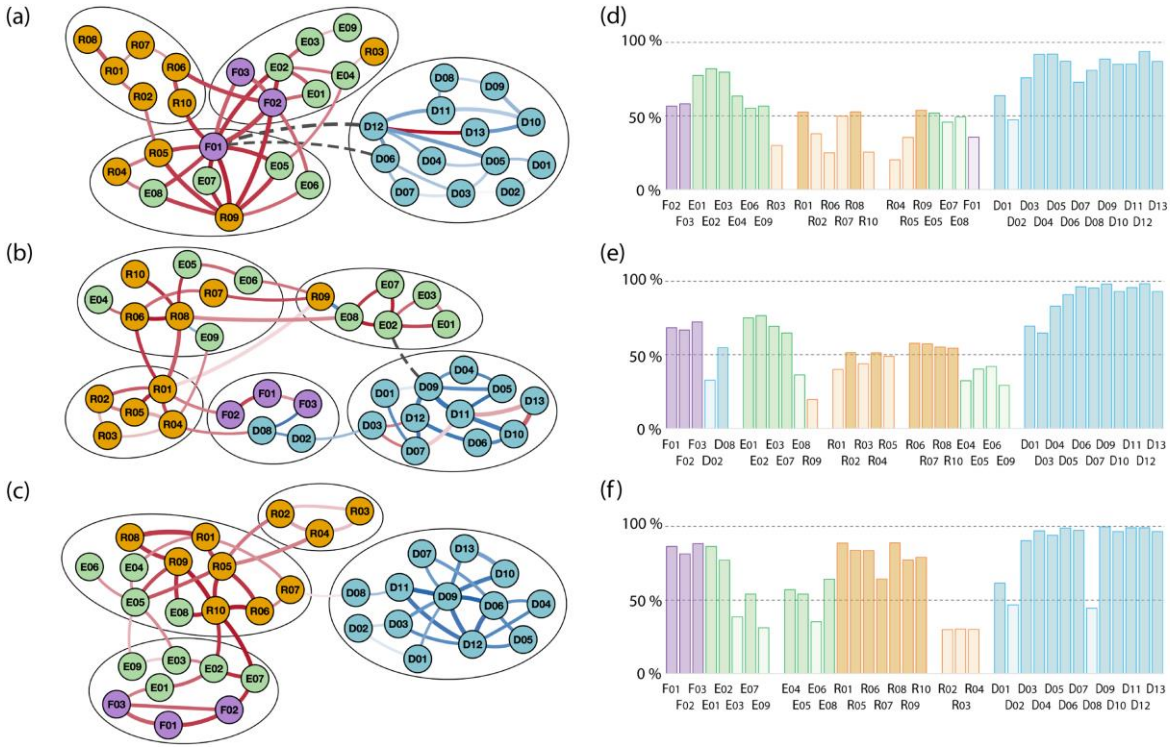

Figure 102. *Plots and histograms for networks based on respondent's indicated funding source: (a) research, (b) non-research, and (c) mixed funding. Plots (d) – (f) show the corresponding bootstrapped frequency. In the network plots, the four original themes are highlighted with different colors. Positive temperature edges are indicated in red and negative temperature edges are indicated in blue. New clusters are indicated by the circled regions. Each histogram is grouped by the clusters in the respective network, with nodes not reaching 50 % stability made transparent.*

and financial support (*F*). While Mentoring and Research Experience and Financial Support had been previously identified through PCA, Social and Scholarly Exploration and Professional and Academic Development were unique to the NALS approach.

In our current work, we leverage NALS to provide a unique interpretation of responses to the ASES instrument for well-defined demographic groups. Each demographic split results in distinct set of networks built only from the relevant responses. In additional to NALS, we also perform a stability analysis of the NA clusters to further confirm the validity of the observed themes. We chose to focus on four demographics for which the subgroups were well-defined and sufficiently large to apply the NALS methodology: type of program students are enrolled in (bridge and non-bridge), gender (women and men), the number of semesters since enrollment (less than five semesters and five or more semesters), and type of support available since enrollment (research, non-research, and mixed).

Our analysis reveals that for some demographic groups, NALS produces several new clusters that typically include nodes from multiple original clusters. However, some of the new clusters, especially the smaller ones, turn out to be unstable and tend to revert to the original *R*, *E*, *D*, and *F* clusters during bootstrapping tests. Overall, we find that a certain level of divergence from the full network persists in the demographic-based networks, indicating that there are aspects of experiences that are unique to specific demographic groups.

Figure 102 shows a comparison of the three networks generated based on financial support data. Out of the four original thematic clusters, the professional and academic development theme (cluster *D*) is most often recovered in the demographic-based networks. However, while in the network based on full ASES dataset the *D* nodes form a separate component connected exclusively through negative temperature similarity, in both research [Figure 102(b)] and non-research [Figure 102(b)] funding-based networks some *D* nodes are connected via positive temperature similarity. This indicates that students with exclusively research or non-research support experience some of the aspects of professional and academic development identified above. However, the significant prevalence of negative temperature edges for this theme suggests that the majority of students, regardless of their demographics, are not experiencing these supports within their department.

Looking at the types of connections that the *D* nodes have extending outside of that thematic cluster allows for additional interpretation. For example, in the research network, there are the two edges of dissimilarity

connecting tuition (F_{01}) to both time management training and PI training (D_{06} and D_{12}, respectively). This means that while graduate students supported solely through research assistantships have their tuition fully supported (all other edges connecting this node within the network have a positive temperature) and may not worry about their financial stability in graduate school, they are not supported in advancing certain skills important for their academic careers.

The second theme persistent in all but one considered network is financial support (cluster *F*). The three *F* nodes are almost always clustered together within the demographic-based networks, however, they often tend to get grouped into larger clusters with additional nodes from other themes, Figure 102(b, c). The only network in which the *F* nodes are separated is the research network, shown in Figure 102(a), where the central position played by the tuition item (F_{01}) helps to mix around the clustering in the sampled networks. In fact, it is the only one in which an *F* node is most central in terms of both the local and global connectivity, as quantified by the closeness and betweenness centrality measures, with $\mathcal{C}_{\mathcal{D}}(F_{01}) = 11$ and $\mathcal{C}_{\mathcal{B}}(F_{01}) = 348$, respectively. [3] presents a detailed analysis of all 10 demographic-based networks.

Using the full ASES dataset, we have confirmed that the thematic clusters found through NALS are stable against small data perturbation which indicates that the themes are well suited to capture patterns in graduate students' experiences. Additionally, we have shown that for demographic-based networks, NALS can reveal certain unique features that shed light on the needs of particular demographic groups. More details about this work can be found in our report recently published in *Physical Review Physics Education Research* [3].

[1] R. P. Dalka, D. Sachmpazidi, C. Henderson, and J.P. Zwolak. Network Analysis Approach to Likert-Style Surveys. *Physical Review Physics Education Research* **18** (2022), 020113.

[2] D. Sachmpazidi and C. Henderson. Departmental Support Structures for Physics Graduate Students: Development and Psychometric Evaluation of a Self-Report Instrument. *Physical Review Physics Education Research* **17** (2021), 01012

[3] R. P. Dalka and J. P. Zwolak. Network Analysis of Graduate Program Support Structures Through Experiences of Various Demographic Groups. *Physical Review Physics Education Research* **20** (2024), 020106.

Aspects of Postdoctoral Researcher Experience Scale Survey

Justyna P. Zwolak
Robert P. Dalka (University of Maryland)

High attrition rates in science, technology, engineering, and mathematics disciplines are an ongoing problem. Most studies to date have focused on undergraduate and graduate student attrition, with a particular emphasis on students' attributes, undergraduate preparation, and mentoring relationships. Systematic studies looking into the experiences of postdoctoral researchers are few and far between. One example is a recent post-COVID survey organized by *Nature* [1]. The responses to Nature's survey uncovered a list of issues that postdoctoral researchers face: "high pressure, long hours, relatively low wages compared with those for analogous research positions outside academia, and pervasive job insecurity" [2]. Another example is a study that investigates challenges that female postdocs face in academia [3]. The study revealed that a sense of belonging, and the overall work environment are critical for female postdocs to overcome the decision to leave academia.

The goal of the Aspects of Postdoctoral Researcher Experience Scale Survey (APRES) study is to assess the experiences of postdoctoral researchers at NIST. This study will be used to inform what changes might be necessary to ensure that the time postdoctoral researchers spend at NIST prepares them well for the next steps on their career path.

The "Aspects of Student Experience Scale" (ASES) survey was developed by researchers at Western Michigan University to study what factors foster a supportive environment for graduate students [4]. The questions included in ASES were developed based on prior literature and the American Physical Society Bridge Program (APSBP) recommendations, revised based on APSBP feedback, and subjected to psychometric evaluation. It has been demonstrated that ASES meets the standard criteria for divergent validity, discriminant validity, and internal consistency. Our APRES is a revised version of the ASES survey, modified to be relevant to postdoctoral researchers. The revisions include replacing references to the "department" with "OU" or "division", as appropriate, replacing "graduate student" with "postdoctoral researcher", "courses" with "professional development," etc. The resulting APRES was discussed with researchers having prior experience working with ASES. We have made every attempt to ensure the resulting APRES survey is as anonymous as possible while ensuring we are able to capture data that will enable us to tease out where we may have concerns about the postdoctoral researchers' experiences at NIST.

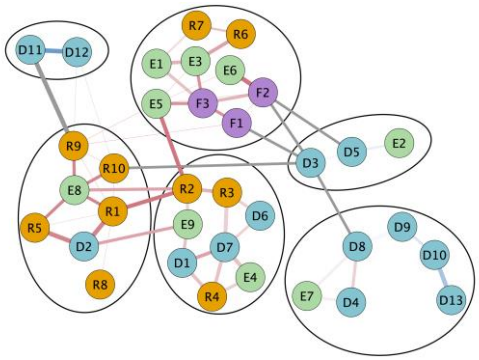

Figure 103. *The full network created based on the APRES dataset. Mutual agree responses are indicated in red while mutual disagree responses are indicated in blue. Questions to which the respondents disagree are shown in gray. The colors indicate the original ASES survey themes. The ovals highlight the new emerging clustering.*

The APRES survey was administered in FY 24 and in FY 25 to all postdoctoral and early career researchers, including Federal and non-Federal employees, in the NIST Information Technology Laboratory (ITL). Non-Federal employees may include guest researchers, contractors, and other early-career researchers working at or for NIST. For the purpose of this work, early-career researchers are defined as researchers no more than seven years from receiving their Ph.D. This includes NRC postdocs, federal term employees, and guest researchers (US citizens and foreign nationals) supported via the NIST PREP program or other agreements with external institutions.

The survey responses are currently being analyzed to identify common themes in responses; see Figure 103. These themes may include postdoctoral researchers' social and scholarly exploration support, mentoring and research experience, professional and academic development, and financial stability. The proposed analysis plan includes a quantitative summary for each question, with count per response for multiple-choice questions and mean response for scaled questions. Secondary analysis will include using the Network Analysis Approach to Likert-style Surveys (NALS) of the full response data [5]. We will be looking for areas where we need to improve postdoctoral researchers' experiences at NIST. Finally, the results will be shared in an annual report. (in preparation) to NIST leadership, staff, and the public. The results will be posted to NIST internal and external websites.

[1] C. Woolston. Pandemic Darkens Postdocs' Work and Career Hopes. *Nature* **585** (2020), 309-31.

[2] C. Woolston. Postdocs Under Pressure: 'Can I Even Do This Any More?' *Nature* **587** (2020), 689-692.

[3] R. Ysseldyk, K. H. Greenaway, E. Hassinger, S. Zutrauen, J. Lintz, and M. P. Bhatia. A Leak in the Academic Pipeline: Identity and Health Among Postdoctoral Women. *Frontiers in Psychology* **10** (2019), 1297.

[4] D. Sachmpazidi and C. Henderson. Departmental Support Structures for Physics Graduate Students: Development and Psychometric Evaluation of a Self-Report Instrument. *Physical Review Physics Education Research* **17** (2021), 010123.

[5] R.P. Dalka, D. Sachmpazidi, C. Henderson, and J.P. Zwolak. Network Analysis Approach to Likert-style Surveys. *Physical Review Physics Education Research* **18** (2022), 020113.

An Evaluation of the NIST Scientific Integrity Program

Justyna P. Zwolak
Anne Andrews (LP)

The NIST Scientific Integrity Program was formally established in policy in 2011. It is NIST's policy to promote scientific integrity by creating a culture of personal and organizational responsibility where the practice and management of scientific research and its products are free from undue influences that are not essential to the practice of science, such as personal or social allegiances, beliefs, or interests. NIST's dedication to scientific integrity is highlighted with this assertion on the internal website: *NIST is an organization with strong values, reflected both in our history and our current work*. NIST leadership and staff will uphold these values to ensure a high-performing environment that is safe and respectful of all. The annual evaluation of the NIST Scientific Integrity Program provides a summary of activities and updates about the program status for the period between 1 June 2022 and 30 September 2023.

A baseline evaluation of the program was conducted in May 2023 and included a survey of NIST staff. The purpose of the baseline evaluation was to get a sense of the current staff's awareness before implementing planned updates. In addition, it served to identify areas where the program needs to focus or improve.

The survey, sent by email with an invitation from the Associate Director for Laboratory Programs, was open to all staff. The survey remained open for three weeks, with a reminder sent one week before the closing date. Of 3416 Federal employees and 4646 Associates included in the NIST Federal Workforce database, 373 Federal and 33 non-Federal respondents completed the survey, resulting in 10.9 % and 0.7 % response rates, respectively. Since the participants were not required to answer any of the questions, a survey was considered completed whenever the participant selected the *Submit*

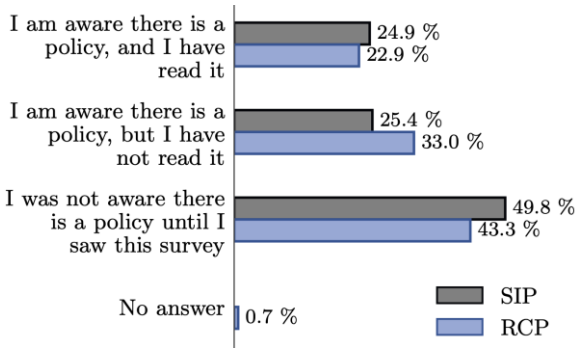

Figure 104. *A comparison of responses to questions about the respondents' familiarity with the Scientific Integrity Policy (SIP) and the Research Conduct Policy (RCP).*

button, regardless of how many questions were answered. All survey questions were answered by at least 97.5 % of respondents, while the demographic questions included at the end of the survey were responded to by at least 94.8 %.

The first two sets of survey questions pertained to the respondents' knowledge of the Scientific Integrity Policy (SIP) and the Research Conduct Policy (RCP) as well as their attitudes toward handling allegations related to scientific integrity and research misconduct. Figure 104, showing a comparison of responses to questions about the respondents' familiarity with SIP and RCP, indicates slightly more responses were aware of the RCP than of the SIP, at about 56 % vs. 50 %, respectively. A detailed analysis of all survey questions is presented in a NIST Special Publication [1].

In addition to answering survey questions, the respondents were given an opportunity to provide general comments and feedback about NIST's SIP and RCP. The most common theme in the open-ended questions was a request for more training about both policies. Respondents also asked for resources that would present these policies in a more accessible format, such as a course on the Commerce Learning Center or via NIST internal web pages and should be included as part of the annual training requirements. A number of respondents expressed disappointment with how the NIST Editorial Review Board process is being handled, requesting authorship guidelines that would explain who should be included in publications.

The program evaluation highlighted several areas where the program could be improved, and more guidance would be helpful. The baseline assessment validated our assumption that while staff believe scientific integrity is important at NIST, they are not familiar with our established program. Earlier in FY 24, the SIO finalized and deployed the awareness training program. In addition, the SIO and SIP team continue to work with the SOSI to develop an implementation and evaluation. The full report has been published in FY 24 [1] and updated in FY 25 [2].

[1] A. Andrews and J. P. Zwolak. NIST Scientific Integrity Program. Annual Report. NIST Special Report 1313, March 2024. DOI: 10.6028/NIST.SP.1313

[2] A. Andrews and J. P. Zwolak. NIST Scientific Integrity Program. Annual Report. NIST Special Report 1313, December 2024. DOI: 10.6028/NIST.SP.1313e2024

Table 3. *Student interns in ACMD –High School and Undergraduate*

Name	From	Program		Mentor	Topic
Choi, Daniel	US Marine Corps	U	SURF	L. Ma	Characterization of SiC-based Quantum Devices
Cooksey, Isaac	U. of Maryland	U	DGR	A. Kearsley	Mathematical Optimization
Deye, William	UCLA	U	SURF	R. Evans	Simulation and Analysis of a Model for BioFET Experiments
Egleston, Brady	U. of Maryland	U	DGR	J. Zwolak	Machine Learning Methods for Control of Laser Cooled Atoms
Ford, Davis	Florida State U.	U	SURF	M. Mascagni	Developing Artifacts for Testing of Publication of New Mathematical Software
Hakala, Sonja	U. Maryland	U	PREP	T. Gerrits	Quantum Network Node Metrology
Harvey, Katherine	Hillsdale College	U	SURF	R. Evans	Approximate Solutions to a Nonlinear Model for BioFET Experiments
He, Dongxing	U. Maryland	U	PREP	T. Gerrits	Quantum Network Component Metrology
Ko, Morgan	U. Maryland	U	PREP	J. Terrill	Parallel Programming HydratiCA, a Parallel Stochastic Reaction-diffusion Model of Cement Hydration
Krepets, Mikhail	U. Maryland	U	SURF	M. Mascagni	Parallelizing Monte Carlo Codes using C++Threads
Lee, Sydney	Texas A & M U.	U	SURF	L. Jia	Interdisciplinary Analysis of Deformable Cells
Leonard, Navek	Montgomery Blair H. S.	H	VOL	A. Kearsley	Calculations Associated with Physical Experiments including Simulating Parabolic Trajectories
Liu, Alexander	Georgia Tech	U	SURF	S. Su	Digital Twin 3D Immersive Visualization and Computational Algorithm Data Analysis for Metrology
Pourifarsi, Shawn	U. Maryland	U	SURF	S. Su	Graphics Shaders
Shaikh, Faadil Abdullah	U. Maryland	U	SURF	M. Mascagni	Using Stochastic Point Estimates to Create a Reliable Field Estimate
Shi, Irving	U. Maryland	U	SURF	B. Cloteaux	Optimizing Energy Use in Job Replication
Werchowsky, Benjamin	U. Virginia	U	DGR	T. Gerrits	Quantum Network Component Metrology
Wolcott, Thomas	U. Maryland	U	SURF	B. Schneider	The Atomic, Molecular and Optical Sciences Gateway
Wu, Ryan	Mississippi School of Math and Science	H	VOL	S. Su	Digital Twin 3D Immersive Visualization and Computational Algorithm Data Analysis for Metrology
Xiao, Lilian	U. of Pennsylvania	U	SURF	J. Terrill	Lighting in 3D Visualization

Legend

G Graduate Student
U Undergraduate
H High School

PREP Professional Research Experience Program
FGR Foreign Guest Researcher
DGR Domestic Guest Researcher
SHIP Summer High School Internship Program
SURF Summer Undergraduate Research Fellowship
PATH Pathways Program

Table 4. *Student interns in ACMD – Graduate Students.*

Name	From	Program		Mentor	Topic
Chalfin, Harry	U. of Maryland	G	DGR	J. Zwolak	Tuning High-Fidelity Operation of Spin Qubits
Fox, Matthew	U. Colorado Boulder	G	DGR	S. Glancy	Topics in Theoretical Quantum Information Science
Hall, Carole	Stony Brook U.	G	DGR	G. Dogan	Measure of Shape Similarity and Complexity
Henrichsen, Andrew	Johns Hopkins U.	G	PREP	P. Patrone	Uncertainty Quantification for Artificial Intelligence
Kyle, Akira	U. Colorado Boulder	G	DGR	S. Glancy	Topics In Theoretical Quantum Information Science
Ladic, Katjana	U. Zagreb, Croatia	G	FGR	K. Sayrafian	Analysis and Modeling of Wireless Channels for Wearables and Implants
Liu, Xinyi	Northwestern U.	G	FGR	L. Jia	Mathematical Modeling of Membranes
Mazur, Marcel	U. Colorado Boulder	G	DGR	S. Glancy	Topics in theoretical quantum information science
Patra, Soumyadip	U. of New Orleans	G	FGR	S. Glancy	Analysis of Quantum Optical Measurements
Schneider, Ryan	U. C. San Diego	G	DGR	B. Schneider	Collocation Methods to Solve the Electronic Schrödinger Equation
Seshadri, Akshay	U. Colorado Boulder	G	PREP	E. Knill	Quantum Measurement Statistics
Shrestha, Pranish	Morgan State University	G	PREP	T. Gerrits	Optical fiber-link noise characterization
Tennyson, Stephen	U. Maryland	G	PREP	P. Patrone	Applied Diagnostics
van de Poll, May An	U. Colorado Boulder	G	PREP	E. Knill	Analysis of quantum optical measurements

Legend

G Graduate Student
U Undergraduate
H High School

PREP Professional Research Experience Program
FGR Foreign Guest Researcher
DGR Domestic Guest Researcher
NSF NSF Mathematical Sciences Graduate Internship Program

Part IV

Activity Data

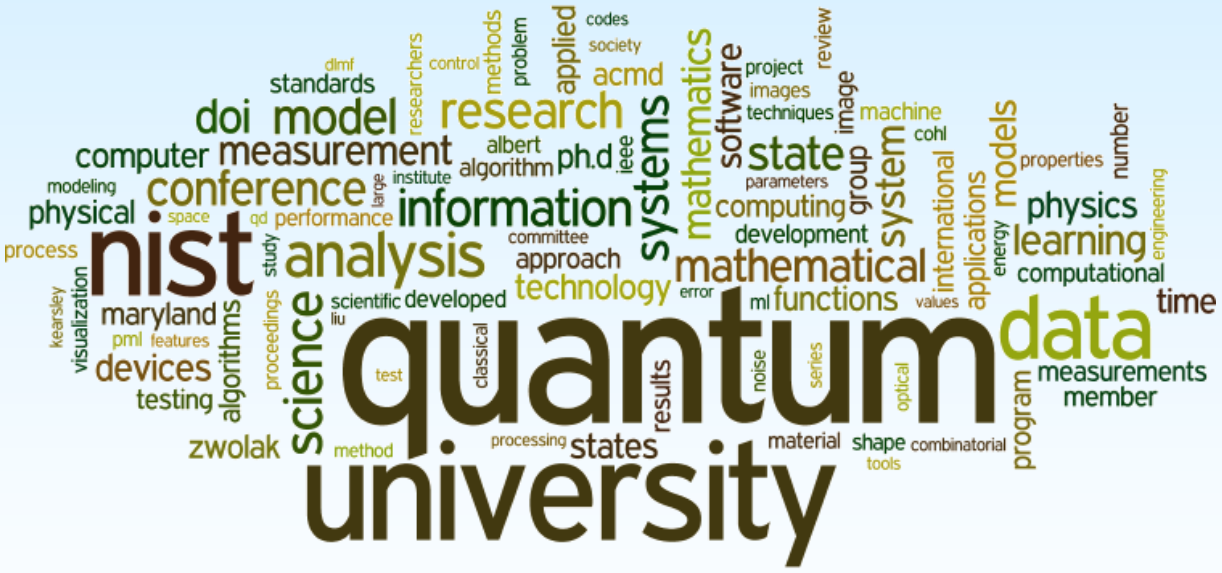

Publications

Note: Names of (co-)authors with an ACMD affiliation during this reporting period are underlined.

Appeared

Refereed Journals

1. F. Abel, E. Correa, T. Bui, A. Biacchi, M. Donahue, M. Merritt, J. Seppala, S. Woods, A. Hight Walker, and C. Dennis. Strongly Interacting Nanoferrites for Magnetic Particle Imaging and Spatially Resolved Thermometry. *ACS Applied Materials & Interfaces* **16**:40 (2024), 54328. DOI: 10.1021/acsami.4c03076

2. M. A. Alhejji and E. Knill. Towards a Resolution of the Spin Alignment Problem. *Communications in Mathematical Physics* **405** (2024), 119. DOI: 10.1007/s00220-024-04980-1

3. D. M. Anderson, D. C. Brager, and A. J. Kearsley. Spatially-dependent Model for Rods and Cones in the Retina. *Journal of Theoretical Biology* **579** (2024), 111687. DOI: 10.1016/j.jtbi.2023.111687

4. P. Bedekar, A. J. Kearsley, and P. N. Patrone. Prevalence Estimation and Optimal Classification Methods to Account for Time Dependence in Antibody Levels. *Journal of Theoretical Biology* **559** (2023), 111375**.** DOI: 10.1016/j.jtbi.2022.111375

5. P. P. Bedekar, R. A. Luke, and A. J. Kearsley. Prevalence Estimation Methods for Time-Dependent Antibody Kinetics of Infected and Vaccinated Individuals: a Markov Chain Approach. *Bulletin of Mathematical Biology* **87**:26 (2025). DOI: 10.1007/s11538-024-01402-0

6. J. Borchers, K. Krycka, B. Bosch-Santos, E. de Lima Correa, A. Sharma, H. Carlton, Y. Dang, M. Donahue, C. Grüttner, R. Ivkov and C. Dennis. Magnetic Anisotropy Dominates Over Physical and Magnetic Structure in Performance of Magnetic Nanoflowers. *Small Structures* (2024), 2400410**.** DOI: 10.1002/sstr.202400410

7. J. Chandrasekaran, E. Lanus, T. Cody, L. Freeman, R. N. Kacker, M. S. Raunak, and D. R. Kuhn. Leveraging Combinatorial Coverage in ML Product Lifecycle. *IEEE Computer* **57** (July 2024), 16-26. DOI: 10.1109/MC.2024.3366142

8. G. A. Cooksey, S. Iavarone-Garza, N. Drachman, and P. N. Patrone. Accuracy and Dynamics of Flow Measurements to 1 NL/min Using an Optofluidic Flow Meter. *Measurement: Sensors* (2024) 101548. DOI: 10.1016/j.measen.2024.101548

9. R. P. Dalka and J. P. Zwolak. Network Analysis of Graduate Program Support Structures Through Experiences of Various Demographic Groups. *Physical Review Physics Education Research* **20**:2 (2024), 020106. DOI: 10.1103/PhysRevPhysEducRes.20.020106

10. R. DeCrescent, Z. Wang, J. Bush, P. Imany, A. Kwiatkowski, D. Reddy, S. Nam, R. Mirin, and K. Silverman. Coherent Dynamics in an Optical Quantum Dot with Phonons and Photons. *Optica* **11** (2024), 1526-1532. DOI: 10.1364/OPTICA.537726

11. L. Devroye and J. P. Nolan. Random Variate Generation for the First Hit of a Ball for the Symmetric Stable Process in R^d. *Journal of Statistical Theory and Practice* **18**:11 (2024), DOI: 10.1007/s42519-023-00364-1

12. N. Drachman, P. N. Patrone, and G. A. Cooksey. Relaxation Times and Dynamic Behavior of an Optofluidic Flow Meter in the Nanoliter Per Minute Regime. *Physics of Fluids* **36** (2024) 022029. DOI: 10.1063/5.0193599

13. J. T. Fong, S. Freiman, and N. Heckert. An Error-Analysis-based Multi-Scale Reliability Model for Predicting the Minimum Time-to-Failure of Brittle Components with Environment-Assisted Crack Growth. *Journal of Strength, Fracture, and Complexity*. **17** 2024. DOI: 10.3233/SFC-230020

14. S. Gandhari, V. V. Albert, T. Gerrits, J. M. Taylor, and M. J. Gullans. Precision Bounds on Continuous-Variable State Tomography Using Classical Shadows. *PRX Quantum* **5**, 010346 (2024). DOI: 10.1103/PRXQuantum.5.010346

15. P.-Y. Hou, J. J. Wu, S. D. Erickson, D. C. Cole, G. Zarantonello, A. D. Brandt, S. Geller, A. Kwiatkowski, S. Glancy, E. Knill, A. C. Wilson, D. H. Slichter, and D. Leibfried. Coherent Coupling and Non-Destructive Measurement of Trapped-Ion Mechanical Oscillators. *Nature Physics* **20** (2024), 1636. DOI: 10.1038/s41567-024-02585-y

16. J. T. Iosue, K. Sharma, M. J. Gullans, and V. V. Albert. Continuous-variable Quantum State Designs: Theory and Applications. *Physical Review X* **14** (2023), 011013. DOI: 10.1103/PhysRevX.14.011013

17. S. P. Jain, J. T. Iosue, A. Barg, and V. V. Albert. Quantum Spherical Codes. *Nature Physics* **20** (2024), 1300. DOI: 10.1038/s41567-024-02496-y

18. S. P. Jain, E. R. Hudson, W. C. Campbell, and V. V. Albert. Absorption-Emission Codes for Atomic and Molecular Quantum Information Platforms. *Physical Review Letters* **133**, 260601 (2024). DOI: 10.1103/PhysRevLett.133.260601

19. R. N. Kacker and K. K. Irikura. The SI Unit Mole and Avogadro Constant. *Measurement Sensors* (29 January 2025), 101767. DOI: 10.1016/j.measen.2024.101767

20. CH. S. S. Pavan Kumar, N. N. Klimov, and P. S. Kuo, Optimization of Waveguide Fabrication Processes in Lithium-Niobate-On-Insulator Platform. *AIP Advances* **14** (2024), 065317. DOI: 10.1063/6.0003522

21. P. S. Kuo, D. V. Reddy, V. Verma, S. W. Nam, A. Zukauskas, and C. Canalias. Photon-pair Production and Frequency Translation Using Backward-Wave Spontaneous Parametric Downconversion. *Optica Quantum* **1**:2 (2023), 43. DOI: 10.1364/OPTICAQ.500021

22. N. Lal, I. A Burenkov, Y.-S. Li-Baboud, M. V. Jabir, P. S. Kuo, T. Gerrits, O. Slattery, and S.V. Polyakov, Synchronized Source of Indistinguishable Photons for Quantum Networks, *Optics Express* **32** (2024), 18257-18267. DOI: 10.1364/OE.521083

23. M. L. Liu, N. Tantivasadakarn, and V. V. Albert. Subsystem CSS codes, a Tighter Stabilizer-to-CSS Mapping, and Goursat's Lemma. *Quantum* **8**, 1403 (2024). DOI: 10.22331/q-2024-07-10-1403

24. Y. K. Liu and D. Moody. Post-Quantum Cryptography and the Quantum Future of Cybersecurity. *Physical Review Applied* **21** (2024), 040501. DOI: 10.1103/PhysRevApplied.21.040501

25. V.-S. Mai, R. J. La and T. Zhang. Distributed Optimization with Global Constraints Using Noisy Measurements, *IEEE Transactions on Automatic Control* **69**:3 (2024), 1089-1096. DOI: 10.1109/TAC.2023.3277312

26. V.-S. Mai, R. J. La and T. Zhang. A Study of Enhancing Federated Learning on Non-IID Data with Server Learning, *IEEE Transactions on Artificial Intelligence* **5**:11 (2024), 5589-5604. DOI: 10.1109/TAI.2024.3430250

27. W. McKenzie, A. M. Richards, S. Patel, T. Gerrits, T. G. Akin, S. Peil, A. T. Black, D. Tulchinsky, A. Hastings, Y.-S. Li-Baboud, A. Rahmouni, I. A. Burenkov, A. Mink, M. Diaz, N. Lal, Y. Shi, P. Kuo, P. Shrestha, M. Merzouki, A. R. Perez, E. Onuma, D. E. Jones, A. A. Davis, T. A. Searles, J. D. Whalen, Q. S. Quraishi, K. S. Collins, L. V. Cooper, H. Shaw, B. Crabill, O. Slattery, and A. Battou, Clock Synchronization Characterization of the Washington DC Metropolitan Quantum Network (DC-QNet), *Applied Physics Letters* **125**:16 (2024), DOI: 10.1063/5.0225082

28. N. Nakamura, P. Szypryt, A. Dagel, B. Alpert, D. Bennett, W. Bertrand Doriese, M. Durkin, J. Fowler, D. Fox, J. Gard, R. Goodner, J. Zachariah Harris, G. Hilton, E. Jimenez, B. Kernen, K. Larson, Z. Levine, D. McArthur, K. Morgan, G. O'Neil, C. Pappas, C. Reintsema, D. Schmidt, P. Schulz, K. Thompson, J. Ullom, L. Vale, C. Vaughan, C. Walker, J. Weber, J. Wheeler, and D. Swetz. Nanoscale Three-Dimensional Imaging of Integrated Circuits Using a Scanning Electron Microscope and Transition-Edge Sensor Spectrometer. *Sensors* **24**:9 2890, 2024. DOI: 10.3390/s24092890

29. J. P. Nolan, D. H. Audus, and J. F. Douglas. Computation of Riesz α-Capacity C_α of General Sets in R^d Using Stable Random Walks. *SIAM Journal on Applied Mathematics*, **84**:2, 317-337 (2024) DOI: 10.1137/23M1568077

30. K. Quelhas, M. Henn, R. Farias, W. Tew, S. Woods. GPU-Accelerated Parallel Image Reconstruction Strategies for Magnetic Particle Imaging. *Physics in Medicine and Biology* **69** 2024, 13500. DOI: 10.1088/1361-6560/ad5510

31. P. N. Patrone and A. J. Kearsley. Minimixing Uncertainty in Prevalence Estimates. *Statistics and Probability Letters* **205** (2024) 109946. DOI: 10.1016/j.spl.2023.109946

32. P. N. Patrone, M. DiSalvo, A. J. Kearsley, G. B. McFadden, G. A. Cooksey. Reproducibility in Cytometry: Signals Analysis and its Connection to Uncertainty Quantification. *PLoS One* **18** (2023) e0295502. DOI: 10.1371/journal.pone.0295502

33. A. Rahmouni, P. S. Kuo, Y.-S. Li-Baboud, I. A. Burenkov, Y. Shi, M. V. Jabir, N. Lal, D. Reddy, M. Merzouki, L. Ma, A. Battou, S. V. Polyakov, O. Slattery, and T. Gerrits. 100-km Entanglement Distribution with Coexisting Quantum and Classical Signals in a Single Fiber. *Journal of Optical Communication Networks* **16** (2024), 781-787. DOI: 10.1364/JOCN.518226

34. M. S. Raunak, D. R. Kuhn, R. N. Kacker, and Y. Lei. Combinatorial Testing for Building Reliable Systems. *IEEE Reliability Magazine* **1** (March 2024), 15-19. DOI: 10.1109/MRL.2024.3355874

35. M. S. Raunak, D. R. Kuhn, R. N. Kacker, and Y. Lei. Ensuring Reliability Through Combinatorial Coverage Measures. *IEEE Reliability Magazine* **1** (June 2024), 20-26. DOI: 10.1109/MRL.2024.3389629

36. W. Sherman and S. Su. Introduction to the Presence Special Edition on Immersive Visualization Laboratories. *PRESENCE: Virtual and Augmented Reality* **33**:1 (2024). URL: https://direct.mit.edu/pvar/issue/volume/33

37. L. Wang, P. N. Patrone, A. J. Kearsley, J. R. Izac, A. K. Gaigalas, J. C. Prostko, H. J. Kwon, W. Tang, M. Kosikova, H. Xie, L. Tian, E. B. Elsheikh, E. Kwee, T. Kemp, S. Jochum, N. Thornburg, L. C.

McDonald, A. Gundlapalli, and S. Lin-Gibson. Monoclonal Antibodies as SARS-CoV-2 Serology Standards: Experimental Validation and Broader Implications for Correlates of Protection. *International Journal of Molecular Sciences* **24**:21 (2023), 15705. DOI: 10.3390/ijms242115705

38. J. C. Wu and R. N. Kacker. Statistical Analysis for Speaker Recognition Evaluation with Data Dependence and Three Score Distributions. *IEEE/ACM Transactions on Audio, Speech, and Language Processing* **32** (2024), 1-14. DOI: TASLP.2023.3313447

39. Y. Xu, Y. Wang, and V. V. Albert. Clifford Operations and Homological Codes for Rotors and Oscillators. *Physical Review A* **110** (2024), 022402. DOI: 10.1103/PhysRevA.110.022402

40. A. W. Young, S. Geller, W. J. Eckner, N. Schine, S. Glancy, E. Knill, and A. M. Kaufman. An Atomic Boson Sampler. *Nature* **629** (2024), 311. DOI: 10.1038/s41586-024-07304-4

41. J. P. Zwolak, J. Taylor, R. Andrews, J. Benson, G. Bryant, D. Buterakos, A. Chatterjee, S. Das Sarma, M. Eriksson, E. Greplova, M. Gullans, F. Hader, T. Kovach, P. Mundada, M. Ramsey, T. Rasmussen, B. Severin, A. Sigillito, B. Undseth, and B. Weber. Data Needs and Challenges of Quantum Dot Devices Automation. *npj Quantum Information* **10**:1 (2024), 105. DOI: 10.1038/s41534-024-00878-x

Books

1. H. S. Cohl and M. E. H. Ismail, eds. *Richard Allen Askey*. Celebratio Mathematica, 2024. URL: https://celebratio.org/Askey_RA/cover/888/

Book Chapters

1. H. S. Cohl and M. Schubotz. The Digital Shadow of Mathematics and its Ramifications. In *90 Years of zbMATH* (K. Hulek, O. P. Taboada, and O. Teschke, eds.), European Mathematical Society Press, Berlin, Chapter 5, 19-22, 2024. DOI: 10.4171/ZBL90/11

In Conference Proceedings

1. U. Bengi, K. Krhac, K. Sayrafian, and S. Dumanli. A Wearable Flexible Loop Antenna for In-Body Beamforming. In *IEEE International Symposium on Antennas and Propagation* (IEEE AP-S 2024), Florence, Italy, July. 14-19, 2024. DOI: 10.1109/AP-S/INC-USNC-URSI52054.2024.10686699

2. J. C. Bienfang, P. Kuo, T. Gerrits, A. L Migdall, S. Polyakov, and O. Slattery, A Dictionary for Single Photonics. In *Proceedings Volume PC13025, Advanced Photon Counting Techniques XVIII*, PC1302508, 2024. DOI: 10.1117/12.3016082

3. J. Fong, S. Freiman, M. Cohn, and N. Heckert. A Multi-Scale Minimum Time-To-Failure Reliability Model for Creep, Creep Crack Initiation, and Creep Crack Growth of a 2-1/4-CR-1-MO Steel at 565 OC and a BK-7 Glass at 20 OC. In *Proceedings of the 2024 ASME Pressure Vessels & Piping Division Conference*, July 28-Aug. 01, 2024, Bellevue, WA, PVP2024-123443. DOI: 10.1115/PVP2024-123443

4. J. Fong. A Multi-Scale Minimum Time-to-Failure Reliability Model for Estimating Reliability Lower Bound of a Structural Health Monitored Cracked 316L(N) Stainless Steel Component in Creep at Elevated Temperatures. In *Proceedings of ASME 2024: 51st Annual Review of Progress in Quantitative Nondestructive Evaluation Conference*, July 21-24, 2024, Denver, CO, QNDE2024-135261. DOI: 10.1115/QNDE2024-135261

5. G. A. Kavuri, J. Palfree, D. V. Reddy, Y. Zhang, M. D. Mazurek, M. J. Stevens, J. C. Bienfang, C. Abellán, M. W. Mitchell, R. P. Mirin, S. W. Nam, E. Knill, and L. K. Shalm. Traceable Device-Independent Randomness as a Service. In *Proceedings Quantum 2.0 Conference and Exhibition*, Rotterdam, Netherlands, June 23–27, 2024. DOI: 10.1364/QUANTUM.2024.QM5A.3

6. K. Khadka, J. Chandrasekaran, Y. Lei, R. N. Kacker, and D. R. Kuhn. A Combinatorial Approach to Hyperparameter Optimization. In *Proceedings of the 2024 IEEE/ACM International Conference on AI Engineering - Software Engineering for AI* (CAIN 2024), Lisbon, Portugal, April 14-15, 2024. DOI: 10.1145/3644815.3644941

7. K. Khadka, S. Shree, Y. Lei, R. N. Kacker, and D. R. Kuhn. Assessing the Degree of Feature Interactions that Determine a Model Prediction. In *Proceedings of the 2024 IEEE International Conference on Software Testing, Verification and Validation Workshops* (ICSTW), Toronto, Canada, May 27-31, 2024. DOI: 10.1109/ICSTW60967.2024.00043

8. R. J. La. Effects of Homophily in Epidemic Processes. In *Proceedings of the 12th International Conference on Complex Networks and Their Applications* (Complex Networks 2023), Menton, France, November 28-30, 2023, DOI: 10.1007/978-3-031-53499-7_24

9. N. Lal, I. A. Burenkov, Y.-S. Li-Baboud, M. V. Jabir, P. S. Kuo, T. Gerrits, O. Slattery, and S. V. Polyakov, Synchronized Network Source of Indistinguishable Photons. In *Proceedings Volume PC12911, Quantum Computing, Communication,*

and Simulation IV, SPIE Quantum West, PC129110T, 2024. DOI: 10.1117/12.3002401

10. N. Lal, I. A. Burenkov, Y. Li-Baboud, M. V. Jabir, P. Kuo, T. Gerrits, O. Slattery, and S. V. Polyakov. Network-ready Source of Indistinguishable Single Photons. In *CLEO 2024, Technical Digest Series* (Optica Publishing Group, 2024), FTh3R.8. DOI: 10.1364/CLEO_FS.2024.FTh3R.8

11. V. Marbukh. Towards Recommender System Supported Contact Tracing for Cost-Efficient and Risk Aware Infection Suppression. In *Health Recommender Systems 2024*, Proceedings of the 6th International Workshop on Health Recommender Systems (HealthRecSys 2024), 63-66. URL: https://ceur-ws.org/Vol-3823/7_Marbukh_position_8.pdf

12. R. Pozo. Approximate Algorithms for k-Median Problems on Complex Networks: Theory and Practice. In *Complex Networks and Their Applications XII*, Proceedings of The Twelfth International Conference on Complex Networks and their Applications: COMPLEX NETWORKS 2023, Volume 3, Studies in Computational Intelligence **1143,** 89-101. Springer. DOI: 10.1007/978-3-031-53472-0_8 89-101

13. K. Quelhas, M. Henn, R. Farias, W. Tew, S. Woods. Parallel 3D Temperature Image Reconstruction Using Multi-Color Magnetic Particle Imaging (MPI). In *AIP Conference Proceedings* **3230**. DOI: 10.1063/5.0234268

14. D. Schug, T. J. Kovach, M. A. Wolfe, J. Benson, S. Park, J. P. Dodson, J. Corrigan, M. A. Eriksson, and J. P. Zwolak. Explainable Classification Techniques for Quantum Dot Device Measurements. In *Proceedings of the XAI4Sci: Explainable Machine Learning for Sciences Workshop* (AAAI 2024), Vancouver, Canada, February 26, 2024. URL: https://xai4sci.github.io/papers/2024/12_explainable_classification_techniques_for_quantum_dot_device_measurements.pdf

15. D. Schug, S. Yerramreddy, R. Caruana, C. Greenberg, and J. P. Zwolak. Extending Explainable Boosting Machines to Scientific Image Data. In *Proceedings of the Machine Learning and the Physical Sciences Workshop* (NeurIPS 2023), New Orleans, LA, December 15, 2023. URL: https://ml4physicalsciences.github.io/2023/files/NeurIPS_ML4PS_2023_35.pdf

16. S. Shree, K. Khadka, Y. Lei, R. N. Kacker, and D. R. Kuhn Constructing Surrogate Models in Machine Learning Using Combinatorial Testing and Active Learning. In *Proceedings of the 39th IEEE/ACM International Conference on Automated Software Engineering* (ASE 2024), October 27, 2024. DOI: 10.1145/3691620.3695532

17. A. Rahmouni, P. S. Kuo, Y. Shi, M. V. Jabir, N. Lal, I. A. Burenkov, Y. S. Li-Baboud, M. Merzouki, A. Battou, S. V. Polyakov, O. Slattery, and T. Gerrits, Entanglement Distribution for Metropolitan-scale Quantum Networks with Classical Coexistence. In *CLEO 2024, Technical Digest Series* (Optica Publishing Group, 2024), FTu3F.2. DOI: 10.1364/CLEO_FS.2024.FTu3F.2

18. S. Shree, Y. Lei, R. N. Kacker, and D. R. Kuhn. A Proxy Model-Based Approach to Influence Analysis. In *Proceedings of the 2024 IEEE International Conference on Artificial Intelligence Testing*, Shanghai, China, July 15-18, 2024. DOI: 10.1109/AITest62860.2024.00016

19. D. E. Simos, B. Garn, D. Schreiber, M. Leithner, D. R. Kuhn, and R. N. Kacker. On Combinatorial Security Testing for the Tor Anonymity Network Client. In *Proceedings of the 2024 IEEE International Conference on Software Testing, Verification and Validation Workshops* (ICSTW), Toronto, Canada, May 27-31, 2024. DOI: 10.1109/ICSTW60967.2024.00047

20. Q. Wei, F. Sikder, H. Feng, Y. Lei, R. N. Kacker, and D. R. Kuhn. SmartExecutor: Coverage-Driven Symbolic Execution Guided by a Function Dependency. In *Proceedings of the 2023 Conference on Blockchain Research & Applications for Innovative Networks and Services* (BRAINS), Paris, France, October 11-13, 2023. DOI: 10.1109/BRAINS59668.2023.10316942

Technical Reports

1. A. M. Andrews and J. P. Zwolak. NIST Scientific Integrity Program. Annual Report. NIST Special Report 1313, March 2024. DOI: 10.6028/NIST.SP.1313

2. J. Bernal and J. Lawrence. Partial Elastic Shape Registration of 3D Surfaces Using Dynamic Programming. NIST Technical Note 2274, November 2023. DOI: 10.6028/NIST.TN.2274

3. J. Bernal and J. Lawrence. Elastic Shape Registration of Surfaces in 3D Space with Gradient Descent and Dynamic Programming. NIST Technical Note 2310, October 2024. DOI: 10.6028/NIST.TN.2310

4. R. Boisvert (ed.). Applied and Computational Mathematics Division, Summary of Activities for Fiscal Year 2023. NISTIR 8518, April 2023, 225 pages. DOI: 10.6028/NIST.IR.8518

5. A. Brady, Y. Wang, V. Albert, A. Gorshkov, and Q. Zhuang. Correlated Noise Estimation with Quantum Sensor Networks. Preprint arXiv:2412.17903. DOI: 10.48550/arXiv.2412.17903

6. A. S. Carasso and A. Vladar. Linnik Point Spread Functions, Time Reversed Logarithmic Diffusion

Equations, and Blind Deconvolution of Electron Microscope Imagery. NIST TN 2324. DOI: 10.628/NIST.TN.2324

7. A. S. Carasso. Data Assimilation in 2D Incompressible Navier-Stokes Equations using a Stabilized Explicit O(Δt) 2 Leapfrog Finite Difference Scheme Run Backward in Time. NIST TN 2299. DOI: 10.628/NIST.TN.2299
8. A. S. Carasso. Data Assimilation in 2D Nonlinear Coupled Sound and Heat Flow using a Stabilized Explicit Finite Difference Scheme Run Backward in Time. NIST TN 2322. DOI: 10.628/NIST.TN.2322
9. D. F. Flater, R. N. Kacker, and D. Foxvog. A Unified Model of Core Metrological Concepts. NISTIR: 8530, July 2024. DOI: 10.6028/NIST.IR.8530
10. Z. Grey, N. Fisher, G. Dogan, and A. Glaws. Explainable Binary Classification of Separable Shape Ensembles. Preprint arXiv:2410.12994. DOI: 10.48550/arXiv.2410.12994

Other Publications

1. S. Geller. Characterization of Noninteracting Bosons, with Applications. Dissertation, University of Colorado at Boulder, 2024. DOI: 10.48550/arXiv.2410.10593
2. A. Kwiatkowski. Optimized Experiment Design and Analysis for Fully Randomized Benchmarking. Dissertation, University of Colorado at Boulder, 2024. URL: https://scholar.colorado.edu/concern/graduate_thesis_or_dissertations/79407z849

Blog Posts

1. Z. Grey. Riding the Wind: How Applied Geometry and Artificial Intelligence Can Help Us Win the Renewable Energy Race. Taking Measure Blog, NIST Public Affairs Office, January 10, 2024. URL: https://www.nist.gov/blogs/taking-measure/riding-wind-how-applied-geometry-and-artificial-intelligence-can-help-us-win
2. S. Ressler. What's in a Name: The Magnetic Weber. Taking Measure Blog, NIST Public Affairs Office, October 23, 2024. URL: https://www.nist.gov/blogs/taking-measure/whats-name-magnetic-weber
3. M. Kleczynski. Math Will Help Us Make Better Medications. In *From Diamonds in Your Computer to Safer Medications, NIST Researchers Look at What's Next for 2024 and Beyond*. Taking Measure Blog, NIST Public Affairs Office, January 3, 2024. URL: https://www.nist.gov/blogs/taking-measure/diamonds-your-computer-safer-medications-nist-researchers-look-whats-next-2024

Accepted

1. V. V. Albert. Bosonic Coding: Introduction and Use Cases. *Proceedings of the International School of Physics "Enrico Fermi."*
2. P. Bedekar, R. Luke, and A. J. Kearsley. Prevalence Estimation Methods for Time- dependent Antibody Kinetics of Infected and Vaccinated Individuals: a Markov Chain Approach. *Bulletin of Mathematical Biology*.
3. N. Coble, M. Coudron, J. Nelson, and S. Sajjad Nezhadi. Hamiltonians Whose Low-Energy States Require Ω(n) T Gates. *19th Conference on the Theory of Quantum Computation, Communication and Cryptography* (TQC 2024).
4. H. S. Cohl and R. S. Costas-Santos. Special Values of the Continuous *q*-Jacobi Polynomials. In: *Proceedings of 16th International Symposium on Orthogonal Polynomials, Special Functions and Applications*.
5. H. S. Cohl and R. S. Costas-Santos. Orthogonality of the Big -1 Jacobi Polynomials for Non-standard Parameters. *AMS Contemporary Mathematics Volume on Hypergeometric Functions, q-series and Generalizations*.
6. H. S. Cohl, R. S. Costas-Santos, L. Durand, C. Montoya and G. Olafsson. Double Summation Addition Theorems for Jacobi Functions of the First and Second Kind. *AMS Contemporary Mathematics Volume on Hypergeometric Functions, q-series and Generalizations*.
7. O. Doronina, B. Lee, Z. Grey and, A. Glaws. Aerodynamic Sensitivities Over Separable Shape Tensor. *AIAA Journal.*
8. C. Fechisin, N. Tantivasadakarn, and V. V. Albert. Non-invertible Symmetry-Protected Topological Order in a Group-Based Cluster State. *Physical Review X*.
9. K. Katzis, N. Evetovic, B. Cloteaux, K. Sayrafian, and D. Bajić. Evaluation of LoRaWAN for Remote Health Monitoring: A Preliminary Study. *IEEE Conference on Standards for Communications and Networking* (IEEE CSCN 2024), Belgrade, Serbia, November 25-27, 2024.
10. K. Ladic, K. Sayrafian, and K. Yekeh Yazdandoost. An Immersive Visualization System to Study UWB Propagation Channel in Smart Pills Applications. *IEEE Conference on Standards for Communications and Networking* (IEEE CSCN 2024), Belgrade, Serbia, November 25-27, 2024.

11. Z. Liu, D. Devulapalli, D. Hangleiter, Y. K. Liu, A. J. Kollar, A. V. Gorshkov, and A. M. Childs. Efficiently Verifiable Quantum Advantage on Near-Term Analog Quantum Simulators. *Physical Review X Quantum*.
12. L. Melara, R. Evans, S. Cho, A. Balijepalli, A. Kearsley. Optimal Bandwidth Selection in Stochastic Regression of Bio-FET Measurements. *Journal of Mathematical Biology*.
13. J. Rajakumar, J. D. Watson, and Y. K. Liu. Polynomial-Time Classical Simulation of Noisy IQP Circuits with Constant Depth. *ACM-SIAM Symposium on Discrete Algorithms* (SODA25).
14. D. Schug, T. J. Kovach, M. A. Wolfe, J. Benson, S. Park, J. P. Dodson, J. Corrigan, M. A. Eriksson, and J. P. Zwolak. Automation of Quantum Dot Measurement Analysis via Explainable Machine Learning. *Machine Learning: Science and Technology*.
15. A. Zubchenko, D. Middlebrooks, T. Rasmussen, L. Lausen, F. Kuemmeth, A. Chatterjee, and J. P. Zwolak. Autonomous Bootstrapping of Quantum Dot Devices. *Physical Review Applied*.

In Review

1. R. Adkins, J. Robaszewski, S. Shin, F. Brauns, L. L. Jia, A. Khanra, P. Sharma, R. Pelcovits, T. R. Powers, Z. Dogic. Topology and Kinetic Pathways of Colloidosome Assembly and Disassembly.
2. V. V. Albert, E. Kubischta, M. Lemeshko, and L. R. Liu. Quantum theory of Molecular Orientations: Topological Classification, Complete Entanglement, and Fault-Tolerant Encodings.
3. V. V. Albert, D. Aasen, W. Xu, W. Ji, J. Alicea, and J. Preskill. Spin Chains, Defects, and Quantum Wires for the Quantum-Double Edge.
4. E. Atindama, C. Miller-Lynch, C. Mattice, G. Doğan, and P. Athavale. Hybrid Algorithm for Filling in Missing Data in Electron Backscatter Diffraction Maps.
5. A. Avagyan, E. Knill, and S. Glancy. Multi-mode Gaussian State Analysis with One Bounded Photon Counter.
6. P. Bedekar, M. A. Catterton, M. DiSalvo, G. A. Cooksey, A. J. Kearsley, and P. N. Patrone. Per-event Uncertainty Quantification for Flow Cytometery using Calibration Beads.
7. I. Bell and B. Alpert. Exceptionally Reliable Density Solving Algorithms for Multiparameter Mixture Models from Chebyshev Expansion Root-finding.
8. A. J. Brady, Y.-X. Wang, V. V. Albert, A. V. Gorshkov, and Q. Zhuang. Correlated Noise Estimation with Quantum Sensor Networks.
9. T. Q. Bui, S. D. Oberdick, F. M. Abel, M. J. Donahue, K. N. Quelhas, C. L. Dennis, T. Cleveland, Y. Liu, and S. I. Woods. Magnetodynamics of Few-nanoparticle Chains.
10. M. A. Catterton, M. DiSalvo, P. N. Patrone, and G. A. Cooksey. Uncertainty Quantification for Cytometry Part II: Comparison of Serial and Traditional Cytometers.
11. N. J. Coble, M. Coudron, J. Nelson, and S. Sajjad Nezhadi. Hamiltonians whose Low-Energy States Require $\Omega(n)$ T Gates.
12. H. S. Cohl, R. S. Costas-Santos, and X.-S. Wang. Asymptotics, Orthogonality Relations and Duality for the q and q^{-1}-symmetric Polynomials in the q-Askey Scheme.
13. H. S. Cohl and H. Volkmer. Bilateral Discrete and Continuous Orthogonality Relations in the q^{-1}-symmetric Askey Scheme.
14. H. S. Cohl and R. S. Costas-Santos. A q-Chaundy Representation for the Product of Two Nonterminating Basic Hypergeometric Series and Its Symmetric Generating Functions.
15. H. S. Cohl and H. Volkmer. Evaluation of Beta Integrals of Ramanujan Type and Integral Representations for Bilateral Hypergeometric Series.
16. J. Conrad, J. T. Iosue, A. G. Burchards, and V. V. Albert. Continuous-variable Designs and Design-Based Shadow Tomography from Random Lattices.
17. E. Culf, T. Vidick, V. V. Albert. Group Coset Monogamy Games and an Application to Device-Independent Continuous-variable QKD.
18. R. P. Dalka and J. P. Zwolak. Restoring the Structure: A Modular Analysis of Ego-driven Organizational Networks.
19. R. P. Fitzgerald, B. K. Alpert, D. E. Bergeron, M. B. Carlson, R. M. Essex, K. M. Morgan, S. Muramoto, S. Nour, G. C. O'Neil, D. R. Schmidt, G. A. Shaw, D. S. Swetz, and R. M. Verkouteren. Absolute Spectroscopic Activity Assay of Microliter Aliquots of Radioactive Solution Without Tracers or Calibrants.
20. L. P. García-Pintos, T. O'Leary, T. Biswas, J. Bringewatt, L. Cincio, L. T. Brady, and Y. K. Liu. Resilience-Runtime Tradeoff Relations for Quantum Algorithms.

21. K. Huang, D. Farfurnik, A. Seif, M. Hafezi, and Y. K. Liu. Random Pulse Sequences for Qubit Noise Spectroscopy.
22. J. T. Fong. A Comparative Study of Three Approaches to Fatigue-Life Prediction and Design for Uncracked and Cracked Components: Deterministic, Probabilistic, and Reliability Target.
23. Z. Grey, A. Glaws, N. Fisher, and G. Doğan. Explainable Binary Classification of Separable Shape Ensembles.
24. S. P. Jain and V. V. Albert. High-distance Codes with Transversal Clifford and T-gates.
25. R. N. Kacker and K. K. Irikura. The Avogadro Constant is not the Defining Constant of the Mole.
26. R. N. Kacker and K. K. Irikura. The SI Approach to Redefine Units does not Apply to the Mole
27. K. Khadka, J. Chandrasekaran, Y. Lei, R. N. Kacker, and D. R. Kuhn. A Combinatorial Approach to Synthetic Data Generation.
28. K. Krhac, K. Sayrafian, U. Bengi, and S. Dumanli. Monitoring Excess Fluid in the Lungs Using a Wearable Wireless System.
29. A. Krishnaswamy-Usha, G. Cooksey, and P. Patrone. Uncertainty Quantification in Flow Cytometry using a Cell Sorter.
30. A. Krishnaswamy-Usha, B. Capistran, and A. Kearsley. Novel Probabilistic Similarity Scores for Sets of Replicate Mass Spectra.
31. A. Kwiatkowski, L. J. Stephenson, H. M. Knaack, A. L. Collopy, C. M. Bowers, D. Leibfried, D. H. Slichter, S. Glancy, and E. Knill. Optimized Experiment Design and Analysis for Fully Randomized Benchmarking.
32. A. Lavasani, M. J. Gullans, V. V. Albert, and M. Barkeshli. On Stability of k-local Quantum Phases of Matter.
33. C.-J. Lin, Z.-W. Liu, V. V. Albert, and A. V. Gorshkov. Covariant Quantum Error-Correcting Codes with Metrological Entanglement Advantage.
34. V.-S. Mai, R. J. La, and T. Zhang. Detection of Performance Interference Among Network Slices in 5G/6G Systems.
35. P. N. Patrone, L. Wang, S. Lin-Gibson, and A. J. Kearsley. Uncertainty Quantification of Antibody Measurements: Physical Principles and Implications for Standardization.
36. P. N. Patrone, A. J. Kearsley, M. A. Catterton, and G. A. Cooksey. Uncertainty Quantification in Cytometry Part I: An Analytical Perspective Beyond Q and B.
37. P. N. Patrone and A. J. Kearsley. Inequalities for Optimization of Diagnostic Assays.
38. P. N. Patrone, R. A. Binder, C. S. Forconi, A. M. Moorman, and A. J. Kearsley. Analysis of Diagnostics (Part I): Prevalence, Uncertainty Quantification, and Machine Learning.
39. P. N. Patrone, R. A. Binder, C. S. Forconi, A. M. Moorman, and A. J. Kearsley. Analysis of Diagnostics (Part II): Prevalence, Linear Independence, and Unsupervised Learning.
40. J. Schreiber, Z. Grey, G. Dogan, and A. Crueziger. Topology of Shape and Data Analysis.
41. A. Shlosberg, A. Kwiatkowski, A. Kyle, and G. Smith. Security Assumptions in Dispersive-Optics QKD.
42. O. Shtanko, Y.-J. Liu, S. Lieu, A. V. Gorshkov, and V. V. Albert. Bounds on Autonomous Quantum Error Correction.
43. Y. X. Wang, J. Bringewatt, A. Seif, A. J. Brady, C. Oh, and A. V. Gorshkov. Exponential Entanglement Advantage in Sensing Correlated Noise.
44. B. Weber and J. P. Zwolak. QDA^2: A Principled Approach to Automatically Annotating Charge Stability Diagrams.
45. Y. Xu, Y. Wang, C. Vuillot, and V. V. Albert. Letting the Tiger Out of Its Cage: Bosonic Coding Without Concatenation.
46. C. Yin, V. V. Albert, and S. Zhou. Small Correlation is Sufficient for Optimal Noisy Quantum Metrology.

Patents

1. S. Buckley, A. McCaughan, A. Dienstfrey, S. W. Nam. System and Method for Parameter Multiplexed Gradient Descent. Provisional Patent Application, US20240028879A1, January 25,2024.
2. G. Cooksey, A. Kearsley, and P. Patrone. Multiplexed Amplitude Modulation Photometer and Performing Multiplexed Amplitude Modulation Photometry. US Patent 12,072,277, August 27, 2024.
3. K. Sayrafian. Lung Fluid Monitor and Monitoring Fluid Level in a Lung. Patent Application Serial Number PCT/US2022/048217, January 23, 2024.

4. A. Seif, M. Hafezi and Y. K. Liu. Systems and Methods for Compressed Sensing Measurement of Long-Range Correlated Noise. Patent US 12,014,247 B2, June 18, 2024.
5. J. P. Zwolak and B. Weber. QD Auto-annotator: Principled Approach to Automatically Annotating Experimental Data. U.S. Provisional Patent Application serial number 63/673,882, July 22, 2024.

ACMD in the News

1. A Framework to Construct Quantum Spherical Codes. Phys.org, June 3, 2024.
2. The Interference of Many Atoms, and a New Approach to Boson Sampling. JILA News, May 7, 2024.
3. Carving Up Infinite Quantum Spaces into Simpler Surrogates. Joint Center for Quantum Information and Computer Science, March 4, 2024.
4. NIST Tool Will Make Math-Heavy Research Papers Easier to View Online. NIST News, January 3, 2024.

Presentations

Note: When multiple presenters are listed, names of co-presenters with an ACMD affiliation during this reporting period are underlined.

Invited Talks

1. V. V. Albert. "Letting the Tiger Out of Its Cage: Homological Bosonic Coding Without Concatenation." Quantum Information Dynamics and Non-Equilibrium Quantum Matter." Simons Center for Geometry and Physics, Stony Brook, NY, December 3, 2024.
2. V. V. Albert. "Fourier in the Quantum Realm." Fall Fourier Talks, University of Maryland College Park, College Park, MD, October 25, 2024.
3. V. V. Albert. "Entanglement and Topology of Molecular Phase Space." PChem Seminar, University of Maryland College Park, College Park, MD, October 2, 2024.
4. V. V. Albert. "Entanglement and Topology of Molecular Phase Space." Condensed Matter-AMO-QIS Seminar, Purdue University, Lafayette, IN, May 31, 2024.
5. V. V. Albert. "Entanglement and Topology of Molecular Phase Space." Workshop on Fundamental Limitations to Quantum Computation, Banff, Canada, March 7, 2024.
6. V. V. Albert. "Frontiers of Bosonic Error Correction." Quantum Information and Foundations Group (QUINFOG) Seminar, Spanish National Research Council (CSIC), Online, February 27, 2024.
7. V. V. Albert. "Tutorial on Bosonic Codes." Advances in Quantum Coding Theory." Simons Institute for the Theory of Computing, Berkeley, CA, February 16, 2024.
8. V. V. Albert. "Entanglement, Geometry, and Topology of Molecular Position States." Molecular Quantum Science and Technology Conference (MQST2024), Vienna, Austria, January 31, 2024.
9. V. V. Albert. "Introduction to Quantum Error Correction." SPIE Photonics West, San Francisco, CA, January 29, 2024.
10. V. V. Albert. "Quantum Spherical Codes." MQC Frontiers in Quantum Information and Technology Seminar, Online, University of Michigan, Ann Arbor, MI, November 16, 2023.
11. P. Bedekar. "Time-Dependent Antibody Kinetics for Previously Infected and Vaccinated Individuals via Graph-Theoretic Modeling." Society for Industrial and Applied Mathematics (SIAM) Annual Meeting, Spokane, WA, July 8, 2024.
12. P. Bedekar. "Time-Dependent Antibody Kinetics for Previously Infected and Vaccinated Individuals via Graph-Theoretic Modeling." American Mathematical Society (AMS) Spring Eastern Sectional Meeting, Howard University, Washington, DC, April 6, 2024.
13. P. Bedekar. "Prevalence Estimation to Account for Time-Dependent Antibody Kinetics for Previously Infected and Vaccinated Individuals." Department of Bioengineering, Indian Institute of Science, Bengaluru, India, February 21, 2024.
14. P. Bedekar. "Prevalence Estimation to Account for Time-Dependent Antibody Kinetics for Previously Infected and Vaccinated Individuals." Biology Seminar, Computational Biology Group, The Institute of Mathematical Sciences, Chennai, India, February 14, 2024.
15. P. Bedekar. "Prevalence Estimation to Account for Time-Dependent Antibody Kinetics for Previously Infected and Vaccinated Individuals." Postdoctoral Seminar, Johns Hopkins University, Baltimore, Maryland, November 2023.
16. A. J. Brady. "Quantum Sensing, with Applications to Fundamental Physics." Friday Quantum Seminar, University of Maryland, Joint Center for Quantum Information and Computer Science (QuICS), College Park, MD, October 11, 2024.

17. H. S. Cohl. "A q-Chaundy Representation for the Product of Two Nonterminating Basic Hypergeometric Series and Its Symmetric and Dual Relations." Department of Mathematics, University of Central Florida, Orlando, FL, January 26, 2024.
18. H. S. Cohl. "Bilateral Discrete and Continuous Orthogonality Relations in the q^{-1}-symmetric Askey scheme." International Conference on Analysis and Applications, Hong Kong, China, June 3-6, 2024.
19. H. S. Cohl. "Dick Askey (1933-2019) and What I've Learned About Him and His Life." The Legacy of Ramanujan Conference, State College, PA, June 8, 2024.
20. H. S. Cohl. "Bilateral Discrete and Continuous Orthogonality Relations in the q^{-1}-symmetric Askey Scheme." Seminar in Partition Theory, q-Series and Related Topics, Department of Mathematical Sciences, Michigan Technological University, Houghton, MI, September 5, 2024.
21. H. S. Cohl. "Dick Askey (1933-2019) and What I've Learned About Him and His Life." Department of Mathematics, University of Central Florida, Orlando, FL, September 6, 2024.
22. H. S. Cohl. "Dick Askey (1933-2019) and What I've Learned About Him and His Life." Rutgers Experimental Mathematics Seminar, Department of Mathematics, Rutgers University, New Brunswick, NJ, September 12, 2024.
23. H. S. Cohl. "Transformations and Summations for Basic Bilateral Hypergeometric Series. Joint Meeting of the New Zealand Mathematical Society, Australian Mathematical Society, and the American Mathematical Society, December 13, 2024.
24. H. S. Cohl. "Bilateral and Quadratic Transformations for Basic Hypergeometric Functions." Department of Mathematics and Statistics, University of Otago, Dunedin, New Zealand, December 16, 2024.
25. G. Doğan. "Variational Models and Algorithms for Image Segmentation." Joint Mathematics Meetings, San Francisco, CA, January 3-6, 2024.
26. G. Doğan. "Optimal Algorithms for Large-scale Elastic Shape Analysis." Society for Industrial and Applied Mathematics (SIAM) Annual Meeting, Spokane, WA, July 8-12, 2024.
27. R. M. Evans. "Applied Mathematics and Biological Field Effect Transistors." Mathematics Colloquium, Hillsdale College, Hillsdale, MI, February 22, 2024.
28. R. M. Evans and A. J. Kearsley. "Spectral and Fictitious Domain Methods for Efficient Simulation of DNA Origami." Society for Industrial and Applied Mathematics (SIAM) Annual Meeting, Spokane, WA, July 9, 2024.
29. S. Geller. "The Weak Generalized Bunching Conjecture," Special Seminar, University of Maryland, Joint Center for Quantum Information and Computer Science (QuICS), College Park, MD, Wed, November 13, 2024
30. Z. Grey. "Pareto Tracing Ridge Profiles for Wind Turbine Design." Society for Industrial and Applied Mathematics (SIAM) Conference on Uncertainty Quantification, Trieste, Italy, March 2024
31. Z. Grey. "Topological Shape and Data Analysis." Society for Industrial and Applied Mathematics (SIAM) Conference on Imaging Science. Atlanta, GA, May 2024
32. Z. Grey. "Towards Trustworthiness through the Lens of Geometric Interpretation." 16th World Congress on Computational Mechanics and 4th Pan American Congress on Computational Mechanics, Vancouver, BC, July 2024
33. Z. Grey. "Explainable Binary Classification of Separable Shape Ensembles." Colorado School of Mines, Golden, CO, November 22, 2024.
34. K. Huang and Y. K. Liu. "Random Pulse Sequences for Qubit Noise Spectroscopy." Institute for Robust Quantum Simulation (RQS) Workshop, Princeton University, Princeton, NJ, June 24, 2024.
35. M. Kleczynski and C. Giusti. "Topological Data Analysis of Long-Term Plant-Pollinator Data." Special Session on Discrete, Algebraic, and Topological Methods in Mathematical Biology, American Mathematical Society Fall Central Sectional Meeting, Creighton University, Omaha, NE, October 7, 2023.
36. M. Kleczynski. "Topological Data Analysis of Coordinate-Based and Interaction-Based Datasets." Mathematics and Statistics Colloquium, American University, Washington, DC, October 31, 2023.
37. M. Kleczynski, C. Bergonzo, and A. J. Kearsley. "Topological Data Analysis of the NIST Monoclonal Antibody: Cycle Representatives and Protein Structure." Special Session on Applied Topology Beyond Persistence Diagrams, Joint Mathematics Meetings, San Francisco, CA, January 6, 2024.
38. M. Kleczynski, C. Bergonzo, and A. J. Kearsley. "Topological Data Analysis of Artificial Antibodies." Special Session on Mathematical Modeling, Computation, and Data Analysis in Biological and Biomedical Applications, American Mathematical Society Sectional Meeting, Washington, DC, April 6, 2024.

39. M. Kleczynski, C. Bergonzo, and A. J. Kearsley. "Topological Data Analysis of Molecular Dynamics Simulations of Monoclonal Antibodies." Mathematical Modeling and Dynamics of Biological Systems Minisymposium, Society for Industrial and Applied Mathematics Annual Meeting, Spokane, WA, July 10, 2024.
40. M. Kleczynski, C. Bergonzo, and A. J. Kearsley. "Topological Data Analysis of Molecular Dynamics Simulations of Monoclonal Antibodies." Applied Mathematics and Statistics Postdoc Seminar, Johns Hopkins University, Baltimore, MD, March 8, 2024.
41. M. Kleczynski, C. Bergonzo, and A. J. Kearsley. "Topological Data Analysis of Molecular Dynamics Simulations of Monoclonal Antibodies." Theoretical Biology and Biophysics Seminar, Online, Los Alamos National Laboratory, May 8, 2024.
42. M. Kleczynski, C. Giusti, and A. J. Kearsley. "Persistent Homology of Plant-Pollinator Interactions: The Importance of Flowering Plant Surveys." Applied Topology Seminar, Applied Algebraic Topology Research Network (AATRN), Online, August 21, 2024.
43. M. Kleczynski, C. Bergonzo, and A. J. Kearsley. "Topological Data Analysis of Molecular Dynamics Simulations of Monoclonal Antibodies." Applied and Computational Math Seminar, George Mason University, Fairfax, VA, November 15, 2024.
44. A. Krishnaswamy-Usha, G. Cooksey, and P. Patrone. "Uncertainty Quantification in Flow Cytometry Using a Cell Sorter." Applied and Computational Mathematics Seminar, George Mason University, Fairfax, Virginia, September 27, 2024.
45. A. Krishnaswamy-Usha, "Spectral Operators in Finite von Neumann algebras", Mathematics Colloquium, Institute of Mathematical Sciences, Chennai, India, February 8, 2024.
46. A. Kwiatkowski "Optimized Experiment Design and Analysis for Fully Randomized Benchmarking." Center for Robust Quantum Simulation and Center for Quantum Information and Computer Science Joint Seminar, University of Maryland, November 2023.
47. A. Kwiatkowski. "Optimized Experiment Design and Analysis for Fully Randomized Benchmarking." Quantum Systems Accelerator (QSA) Trapped Ion Topical Group Seminar, Boulder, CO, October 2023.
48. A. Kwiatkowski. "Optimized Experiment Design and Analysis for Fully Randomized Benchmarking." Ph.D. Thesis Defense, University of Colorado, Boulder, CO, April 2024.
49. Y. K. Liu. "Quantum Curvelet Transforms, and the Infeasibility of Quantum Algorithms for Finding Short Lattice Vectors." Workshop on Distributed Quantum Computing and Cryptography, Virginia Tech, Arlington, VA, June 12, 2024.
50. R. A. Luke. "A Mathematical Understanding of Antibody Tests: Testing Accuracy, Prevalence Estimation, and Time-Dependence." Society for Industrial and Applied Mathematics Faculty Symposium, George Mason University, Fairfax, VA, February 23, 2024.
51. R. A. Luke. "A Mathematical Understanding of Antibody Tests: Testing Accuracy, Prevalence Estimation, and Time-Dependence." Institute for Biohealth Innovation "Lunch and Learn" Seminar Series, George Mason University, Manassas, VA, March 20, 2024.
52. R. A. Luke. "A Mathematical Understanding of Antibody Tests: Testing Accuracy, Prevalence Estimation, and Time-Dependence." Keynote Address, Villanova University Student Research Symposium. Villanova, PA. December 9, 2024.
53. P. N. Patrone and A. J. Kearsley. "From Data to Diagnostics: Advancements in Prevalence Estimating and Testing." Society for Industrial and Applied Mathematics (SIAM) Conference on Life Sciences, Portland, OR, June 13, 2024.
54. P. N. Patrone. "Career Panel: Shedding Light on Opportunities for Applied Mathematicians in Industry and Government." Society for Industrial and Applied Mathematics (SIAM) Conference on Life Sciences, Portland, OR, June 11, 2024.
55. P. N. Patrone, G. A. Cooksey, and A. J. Kearsley. "Uncertainty Quantification and Metrology in Cytometry." SelectBio Conference on Innovations in Flow Cytometry and Extracellular Vesicles, Laguna Hills, CA, November 20, 2024.
56. K. Sayrafian. "Wireless Wearable, Implantable and Ingestible Technology in Healthcare: A Perspective on Opportunities and Challenges." IEEE Baltimore Technical Colloquium, Baltimore, MD, November 2, 2024.
57. K. Sayrafian. "Standardization Landscape for 6G *in vivo* milli/micro/nano-Robotic Services." IEEE Conference on Standards for Communications and Networking, Munich, Germany, 6–8 Nov. 8, 2023.

58. J. P. Zwolak. "Machine Learning and Dynamical Systems in Quantum Computing: Intelligent Tuning of Quantum Dot Devices." Machine Learning and Dynamical Systems Seminar, Alan Turing Institute, Virtual, October 2024.
59. J. P. Zwolak. "Tuning Quantum Dot Arrays with Rays." Global Conference on Materials in an Explosively Growing Informatics World, Montecatini Terme, Italy, June 2024.
60. J. P. Zwolak. "International Practices of Reproducibility and Scientific Integrity." Panelist, International Conference on Reproducibility in Condensed Matter Physics, University of Pittsburgh, Pittsburgh, PA, May 2024.
61. J. P. Zwolak. "Enabling AI Adoption in Research." Roundtable, AI Meets Science Conference, New York University, New York, NY, April 2024.
62. J. P. Zwolak. "AI-induced Trends in Science." Keynote, AI Meets Science Conference, New York University, New York, NY, April 2024.
63. J. P. Zwolak. "Autonomous Control of Experiments: Quantum Dots and Beyond." WECode Conference, Harvard University, Boston, MA, February 2024.
64. J. P. Zwolak. "Tuning Quantum Dot Arrays with Rays." Center for Emergent Matter Science, RIKEN, Tokyo, Japan, November 2023.

Conference Presentations

1. V. V. Albert. "Quantum Spherical Codes." 6th International Conference on Quantum Error Correction (QEC2023), Sydney, Australia, November 2, 2023.
2. J. C. Bienfang, P. Kuo, T. Gerrits, A. L. Migdall, S. Polyakov, and O. Slattery. "A Dictionary for Single Photonics." Advanced Photon Counting Techniques XVIII, SPIE Defense + Commercial Sensing Conference, National Harbor, MD, April 24, 2024.
3. D. Buterakos, J. M. Taylor, and J. P Zwolak. "Data Generation for Triple-Quantum-Dot Machine-Learning Autotuning." American Physical Society March Meeting, Minneapolis, MN, March 4-8, 2024.
4. H. S Chalfin, T. O Boykin II, M. D Stewart, M. J. Gullans, and J. P. Zwolak. "Optimizing High-Fidelity Readout Circuit Using Reinforcement Learning Methods." American Physical Society March Meeting, Minneapolis, MN, March 4-8, 2024.
5. G. Doğan. "Efficient Algorithms to Compute Elastic Shape Distances for Closed Curves." Society for Industrial and Applied Mathematics (SIAM) Conference on Imaging Science, Atlanta, GA, May 28-31, 2024.
6. J. T. Fong, "A Multi-Scale Minimum Time-To-Failure Reliability Model for Estimating Reliability Lower Bound of a Structural Health Monitored Cracked 316l(N) Stainless Steel Component in Creep At Elevated Temperatures." Quantitative NDE Conference, Denver, CO, July 23, 2024.
7. J. T. Fong, "A Multi-Scale Minimum Time-To-Failure Reliability Model For Creep, Creep Crack Initiation, And Creep Crack Growth of a 2-1/4-Cr-1-Mo Steel at 565 Oc and a Bk-7 Glass at 20 Oc." ASME Pressure Vessel and Piping PVP Conference, Bellevue, WA, July 31, 2024.
8. T. Gerrits, A. Abane, A. Amlou, L. Ait Oucheggou, Y.-S. Li-Baboud, A. Battou, J. Bienfang, I. A. Burenkov, R. Dawkins, D. He, P. Kuo, L. Ma, M. Merzouki, A. Migdall, Jabir MV, S. Polyakov, A. Rahmouni, Y. Shi, P. Shrestha, O. Slattery, J. Su, H. Georgieva, H. Hofer, M. López, S. Kück, B. Korzh, and M. Shaw. "Enabling Quantum Networks through Metrology." Single Photon Workshop, Edinburgh, UK, November 2024.
9. Z. Gimbutas, M. Rachh, and J. Hoskins, "Self-interaction Quadratures for Weakly Singular and log(r) Singularities." Computational Tools for PDEs with Complicated Geometries and Interfaces, Flatiron Institute, New York, NY, June 12, 2024.
10. S. P. Jain, J. T. Iosue, A. Barg, and V. V. Albert. "Quantum Spherical Codes." 19th Theory of Quantum Computation, Communication and Cryptography Conference (TQC2024), Okinawa, Japan, September 9-13, 2024.
11. L. L. Jia and X. Liu. "A Plateau Problem for Membranes." 77th Annual Meeting of the American Physical Society Division of Fluid Dynamics, Salt Lake City, UT, November 24-26, 2024.
12. K. Keenan, A. Peskin, A. Dienstfrey, Z. Gimbutas, K. Jordanova, S. Ogier, J. Chalfoun, and S. Lund, "Using SI Traceable Training Data to Improve Network Performance." Conference on Precision Electromagnetic Measurements, Denver, CO, July 8-12, 2024.
13. M. Kleczynski, C. Bergonzo, and A. J. Kearsley. "Topological Data Analysis of Molecular Dynamics Simulations of Monoclonal Antibodies." Biology and Medicine Through Mathematics Conference, Virginia Commonwealth University, Richmond, VA, May 15, 2024.
14. T. J. Kovach, D. Schug, M. A. Wolfe, P. Walsh, J. Benson, E. R. MacQuarrie, D. Middlebrooks, M. A.

Erikkson, and J. P. Zwolak. "Autotuning Quantum Dot Qubits with FrEQuENTS." 36th International Conference on the Physics of Semiconductors, Ottawa, Canada, July 28-Aug 2, 2024.

15. A. Krishnaswamy-Usha and K. Dykema, "Spectral Operators in Finite von Neumann Algebras." Joint Mathematics Meetings, San Francisco, CA, January 5, 2024
16. D. R. Kuhn, R. N. Kacker, M. S. Raunak, and S. Rekhi. "Combinatorial Methods for Functional Verification and Hardware Vulnerability Detection." Symposium and Bootcamp on the Science of Security (HoTSoS). Online, April 2-4, 2024.
17. A. Kwiatkowski "Optimized Experiment Design and Analysis for Fully Randomized Benchmarking." Southwestern Quantum Information and Technology Conference, Albuquerque, NM, October 2023.
18. A. Kwiatkowski "Optimized Experiment Design and Analysis for Fully Randomized Benchmarking." Assessing the Performance of Quantum Computers, Estes Park, CO, October 2023.
19. A. Kwiatkowski "Optimized Experiment Design and Analysis for Fully Randomized Benchmarking." Meeting of the American Physical Society (APS) Division of Atomic and Molecular Physics, Fort Worth, TX, June 2024.
20. R. J. La. "Effects of Homophily in Epidemic Processes." 12th International Conference on Complex Networks and Their Applications (Complex Networks 2023), Menton, France, November 28-30, 2023.
21. N. Lal, I. A. Burenkov, Y. Li-Baboud, M. V. Jabir, P. Kuo, T. Gerrits, O. Slattery, and S. V. Polyakov, "Network-ready Source of Indistinguishable Single Photons." CLEO Fundamental Science, Charlotte, NC, May 5-10, 2024.
22. N. Lal, I. A Burenkov, Y.-S. Li-Baboud, M. V. Jabir, P. S Kuo, T. Gerrits, O. Slattery, and S. V. Polyakov. "Synchronized Network Source of Indistinguishable Photons." SPIE Quantum West, San Francisco, CA, March 13, 2024.
23. X. Liu, L. L. Jia, S. Halder, P. Kahrilas, J. Pandolfino, N. Patankar. "Mechano-pathogenesis of Esophageal Hypertophy and Remodeling." 77th Annual Meeting of the American Physical Society (APS) Division of Fluid Dynamics, Salt Lake City, UT, November 24-26, 2024.
24. R. A. Luke. "Time-Dependent Antibody Kinetics for Infected and Vaccinated Individuals via Graph-Theoretic Modeling." Biology and Medicine Through Mathematics Conference, Virginia Commonwealth University, Richmond, VA, May 15-17, 2024.
25. R. A. Luke. "Time-Dependent Antibody Kinetics for Infected and Vaccinated Individuals via Graph-Theoretic Modeling." Society for Industrial and Applied Mathematics (SIAM)Conference on the Life Sciences, Portland, OR, June 10-13, 2024.
26. V. Marbukh. "Towards Recommender System Supported Contact Tracing for Cost-Efficient and Risk Aware Infection Suppression." Workshop on Health Recommender Systems (HealthRecSys'24) 18th ACM Conference on Recommender Systems (RecSys'24), Bari, Italy, October 18, 2024.
27. V. Marbukh. "Towards Evaluation & Mitigation of the Entropic Value at Systemic Risk in Networked Systems." 12th International Conference on Complex Networks and their Applications, Menton, France, November 28-30, 2023.
28. V. Marbukh. "Systemic Risk of Discontinuous Failures in Large-Scale Networks within Time Horizon: Work in Progress." 12th International Conference on Complex Networks and their Applications, Menton, France, November 28-30, 2023.
29. V. Marbukh and M. Marbukh. "Towards Systemic Risk Evaluation, Attribution, and Mitigation in Networked Systems: Work in Progress." First International Workshop on Safeguarding Social Networks: Privacy, Security, Trust, and Truth in the Age of Misinformation (SAFE-SN 2024, 16th International Conference on Advances in Social Networks Analysis and Mining (ASONAM 2024), University of Calabria, Rende, Italy, September 2-5, 2024.
30. A. Rahmouni, P. S. Kuo, Y. Shi, M. V. Jabir, N. Lal, I. A. Burenkov, Y. S. Li-Baboud, M. Merzouki, A. Battou, S. V. Polyakov, O. Slattery, and T. Gerrits, "Entanglement Distribution for Metropolitan-scale Quantum Networks with Classical Coexistence." CLEO Fundamental Science, Charlotte, NC, May 5-10, 2024.
31. T. Rasmussen, A. Zubchenko, D. Middlebrooks, L. Lausen, F. Kuemmeth, J. P. Zwolak, and A. Chatterjee. "Fully Automated Coldstart Protocol for Semiconductor Quantum Dot Tune-up." American Physical Society (APS) March Meeting, Minneapolis, MN, March 4-8, 2024
32. A. Rao, D. Buterakos, V. John, C. Yu, S. Oosterhout, L. Stehouwer, G. Scappucci, M. Veldhorst, F. Borsoi, and J. P. Zwolak. "Automated Real-Time Gate Virtualization of a 10 Quantum Dot Germanium 2D Array." Silicon Quantum Electronics

Workshop, Davos, Switzerland, September 4-6, 2024.

33. K. Sayrafian. "An Immersive Visualization System to Study UWB Propagation Channel in Smart Pills Applications." IEEE Conference on Standards for Communications and Networking, Belgrade, Serbia, November 25-27, 2024.
34. K. Sayrafian. "Evaluation of LoRaWAN for Remote Health Monitoring: A Preliminary Study." IEEE Conference on Standards for Communications and Networking (IEEE CSCN 2024), Belgrade, Serbia, November 25-27, 2024.
35. D. Schug, T. J. Kovach, M. A. Wolfe, J. Benson, S. Park, J. P. Dodson, J. Corrigan, M. A. Eriksson, and J. P. Zwolak. "Explainable Classification Techniques for Quantum Dot Device Measurements." XAI4Sci: Explainable Machine Learning for Sciences Workshop (AAAI 2024), Vancouver, Canada, February 22-25, 2024.
36. W. Sherman and S. Su. Advances to the ParaView Immersive Interface. 2nd Workshop on Immersive Visualization Laboratories: Past, Present and Future, IEEE VR, Orlando FL, March 17, 2024.
37. W. Sherman. Considerations on Preserving VR Experiences (ideas collected over 30 years). Archiving VR Workshop, IEEE VR, Orlando FL, March 17, 2024.
38. W. Sherman. Immersive Visualization with ParaView for HMDs & CAVE VR Systems. Sandia Annual XR Conference, Online, July 24, 2024.
39. W. Sherman and S. Su. ParaView's Immersive Interface for CAVE and HMD, CAAV Conference, Madison WI, November 14, 2024.
40. W. Sherman. Integrating ANARI into Virtual Reality. Birds-of-a-Feather Session on ANARI, The International Conference for High Performance Computing, Networking, Storage, and Analysis (SC24), Atlanta GA, November 19, 2024.
41. D. E. Simos, B. Garn, D. Schreiber, M. Leithner, D. R. Kuhn, and R. N. Kacker. "A Combinatorial Perspective Towards Security Testing of Anonymity Networks." Symposium and Bootcamp on the Science of Security (HoTSoS). Online, April 2-4, 2024.
42. P. J. Walsh, T. J. Kovach, M. A. Wolfe, P. Marciniec, E.S. Joseph, Brighton X. Coe, J. A. Reily, A. Rogers, J. Benson, D. Middlebrooks, D. Schug, G. J. Bernhardt, and J. P. Zwolak, and M. A. Eriksson. "Methods of Automated Gate-Voltage Selection for Quantum Dot Device Initialization." University of Wisconsin Undergrad Symposium, Madison, WI, April 25, 2024.
43. Y. Xu, Y. Wang, and V. V. Albert. "Clifford Operations and Homological Codes for Rotors and Oscillators." 19th Theory of Quantum Computation, Communication and Cryptography Conference (TQC2024), Okinawa, Japan, September 9-13, 2024.
44. J. P. Zwolak, B. Weber, F. Luthi, and F. Borjans. "Principled Approach to Automatically Annotating Charge Stability Diagrams." American Physical Society (APS) March Meeting, Minneapolis, MN, March 4-8, 2024.

Poster Presentations

1. P. Bedekar. "Sperm-egg Interaction for Fertilization Success." Biology and Medicine Through Mathematics Conference, 2024, Virginia Commonwealth University, Richmond, VA, May 15, 2024.
2. D. Buterakos, J. M. Taylor, and J. P. Zwolak. "Data Generation for Triple-Dot Machine-Learning Autotuning." QuICS Stakeholder Day, College Park, MD, April 17, 2024.
3. S. Challa, N. Klimov, and P. Kuo, "Argon-Plasma Dry Etch of sub-Micron Feature-Size Waveguides in Thin-Film Lithium Niobate," American Vacuum Society Conference, Portland, OR, November 5-10, 2023.
4. B. Cloteaux and V. Marbukh. "Simulating Computing Redundancy vs. its Energy Usage." Winter Simulation Conference, San Antonio, TX, December 10-13, 2023.
5. N. J. Coble, M. Coudron, J. Nelson, and S. Sajjad Nezhadi. Hamiltonians whose Low-Energy States Require $\Omega(n)$ T Gates. 27th Conference on Quantum Information Processing (QIP), Taipei, Taiwan, January 13-19, 2024.
6. H. Cui, Z. Shamsi, X. Ma, G. Cheon, S. Li, M. Tikhanovskaya, N. Mudur, M. B. Plomecka, P. C. Norgaard, P. Raccuglia, V. V. Albert, Y. Bahri, P. Srinivasan, H. Pan, P. Faist, B. A. Rohr, M. J. Statt, D. Morris, D. Purves, E. Kleeman, R. Alcantara, M. Abraham, M. Mohammad, E. P. VanLee, C. Jiang, E. Dorfman, E.-A. Kim, M. Brenner, S. S. Ponda, and S. Venugopalan. "CURIE: Evaluating LLMs on Multitask Scientific Long-Context Understanding and Reasoning." Machine Learning and the Physical Sciences Workshop, The Thirty-Eighth Annual Conference on Neural Information Processing Systems (Neurips 2024), Vancouver, Canada, December 15, 2024.

7. G. Doğan. “Scikit-Shape: Python Toolbox for Shape and Image Analysis.” Society for Industrial and Applied Mathematics (SIAM) Conference on Imaging Science, Atlanta, GA, May 28-31, 2024.
8. G. Doğan. “VEMOS: A GUI for Evaluation of Similarity Metrics on Complex Data Sets.” Society for Industrial and Applied Mathematics (SIAM) Conference on Imaging Science, Atlanta, GA, May 28-31, 2024.
9. S. Geller. “The Weak Generalized Bunching Conjecture,” Southwestern Quantum Information and Technology Conference, Broomfield, CO, October 30, 2024.
10. S. Glancy. “Open Quantum Challenge.” Assessing Performance of Quantum Computers, Estes Park, CO, October 7, 2024.
11. L. L. Jia. “Serial Flow Cytometry as a Method to Measure Membrane Elasticity.” International Soft Matter Conference, Raleigh, NC, July 29-August 2, 2024.
12. E. Knill. “Pulsed, Multi-octave Bandwidth Quadrature Measurements with Calorimeters,” Southwestern Quantum Information and Technology Conference, Broomfield, CO, October 30, 2024.
13. T. Kovach, M. Wolfe, P. Marciniec, P. Walsh, E. Joseph, B. Coe, J. Reily, A. Rogers, J. Benson, D. Middlebrooks, D. Schug, G. Bernhardt, J. P. Zwolak, and M. Eriksson. “Quantum Dot Device Screening at 1.2K.” Silicon Quantum Electronics Workshop 2023, Kyoto, Japan, October 31 - November 2, 2023.
14. A. Krishnaswamy-Usha, G. Cooksey, and P. Patrone. “Distinguishing Population and Instrument Induced Uncertainties using a Cell Sorter.” 37th Annual Congress of the International Society for the Advancement of Cytometry (CYTO 2024), May 7, 2024
15. A. Krishnaswamy-Usha, B. Capistran, and A. Kearsley. “A Novel Statistical Similarity Score Using Replicate Electron-Ionization Mass Spectra.” American Society for Mass Spectrometry Conference on Mass Spectrometry and Allied Topics, Anaheim, CA, June 5, 2024.
16. A. Kwiatkowski. “High-fidelity Fully Randomized Benchmarking and Testing for Time-dependent Errors.” Assessing the Performance of Quantum Computers, Estes Park, CO, October 2024.
17. A. Kwiatkowski. “High-fidelity Fully Randomized Benchmarking and Testing for Time-dependent Errors.” Southwestern Quantum Information and Technology Conference, Broomfield, CO, October 2024.
18. V. Marbukh. “Green Network Optimization with Multi-Agent Reinforcement Learning: Work in Progress.” 2024 IEEE International Conference on Cyber, Physical and Social Computing (CPSCom 2024), Copenhagen, Denmark, August 19-22, 2024.
19. A. S. Rao, D. Buterakos, V. John, C. Yu, S. Oosterhout, L. Stehouwer, G. Scappucci, M. Veldhorst, F. Borsoi, and J. P. Zwolak. “Automated Barrier Gate Virtualization of a 10-Quantum-Dot Array.” Quantum Computing Program Review, Strata Center, MIT, Boston, MA, July 22-26, 2024.
20. T. Rasmussen, J. Benestad, A. Zubchenko, D. Middlebrooks, B. Brovang, E. van Nieuwenburg, O. Krause, J. P. Zwolak, J. Danon, F. Kuemmeth, and A. Chatterjee. “Optimizing Gate Control in Quantum Point Contacts and Quantum Dot Devices.” Spin Qubit 6, Sydney, Australia, November 4-8, 2024.
21. D. Schug, T. J. Kovach, M. A. Wolfe, J. Benson, S. Park, J. P. Dodson, J. Corrigan, M. A. Eriksson, and J. P. Zwolak. “Explainable Classification Techniques for Quantum Dot Device Measurements.” QuICS Stakeholder Day, College Park, MD, April 17, 2024.
22. D. Schug, T. J. Kovach, M. A. Wolfe, J. Benson, S. Park, J. P. Dodson, J. Corrigan, M. A. Eriksson, and J. P. Zwolak. “Explainable Classification Techniques for Quantum Dot Device Measurements.” Workshop on XAI4Sci: Explainable Machine Learning for Sciences, Vancouver, Canada, February 22-25, 2024.
23. D. Schug, S. Yerramreddy, R. Caruana, C. Greenberg, and J. P. Zwolak. “Extending Explainable Boosting Machines to Scientific Image Data.” Workshop on Machine Learning and the Physical Sciences, NeurIPS 2023, New Orleans, LA, December 11-15, 2023.
24. W. Zhong, A. Krishnaswamy-Usha, B. Capistran, A. Kearsley, “A Robustness Analysis of High Dimensional Consensus (HDC) Mass Spectra in Forensic Drug Identification.” American Society for Mass Spectrometry Conference on Mass Spectrometry and Allied Topics, Anaheim, CA, June 6, 2024.
25. J. P. Zwolak, B. Weber, F. Luthi, and F. Borjans. “Principled Approach to Automatically Annotating Experimental Data.” Silicon Quantum

Electronics Workshop 2023, Tokyo, Japan, October 31 - November 2, 2023.

Multimedia

1. S. Ressler. DLMF in VR. Interactive WebVR application. URL: https://math.nist.gov/~SRessler/dlmfvr.html

Web Services

Note: ACMD provides a variety of information and services on its website. Below is a list of major services provided that are currently under active maintenance. If there are a group of authors, ACMD staff names are underlined.

1. *Atomic, Molecular and Optical Sciences Gateway*: a portal for research and education in atomic, molecular and optical science.
2. *Digital Library of Mathematical Functions:* a repository of information on the special functions of applied mathematics.
3. *Digital Repository of Mathematical Formulae*: a repository of information on special function and orthogonal polynomial formulae.
4. *DLMF Standard Reference Tables on Demand*: an online software testing service providing tables of values for special functions, with guaranteed accuracy to high precision.
5. *Error-correction Zoo*: a repository of information about classical and quantum error-correcting codes.
6. *muMAG*: a collection of micromagnetic reference problems and submitted solutions.
7. *thermalmagic.pythonanywhere.com*: a web based magnetic particle imaging (MPI) simulation tool.

Software Released

Note: ACMD distributes many software packages that have been developed in the course of its work. Listed below are packages which have seen new releases during the reporting period.

1. Scikit-shape: Python Package for Shape and Image Analysis. Version 0.4.1 (5/26/23). G. Doğan.
2. CAVE Interaction Plugin and XR Interface. ParaView Version 5.13.0. W. Sherman, S. Su, S. Wittenburg, S. Satterfield, T. Griffin, and J. E. Terrill.
3. OOMMF: Object Oriented MicroMagnetic Framework. Version 2.1a1 (9/27/24). M. J. Donahue and D. G. Porter.
4. OOF2: Image Based Analysis of Materials with Complex Microstructures. Versions 2.3.2 (10/4/23) and 2.3.3 (4/10/24). S. A. Langer, A. C. E. Reid, G. Doğan.
5. Thread: Thread management commands for Tcl. Version 2.8.1 (8/9/2017). D. G. Porter.
6. FMM3D: A set of libraries to compute N-body interactions governed by the Laplace and Helmholtz equations, to a specified precision in three dimensions on a multi-core shared-memory machine. Version 1.0.4, February 27, 2024. T. Askham, Z. Gimbutas, L. Greengard, L. Lu, J. Magland, D. Malhotra, M. O'Neill, M. Rachh, V. Rokhlin. F. Vico.
7. ParaView: Post-processing Visualization Engine. Version 5.13.0. W. Sherman, S. Su, J. E. Terrill.
8. Tcl/Tk: Extensible scripting language and GUI toolkit. Versions 8.6.14 (2/28/2024), 8.6.15 (9/16/2024), 8.6.16 (12/11/2024), 9.0b1 (1/5/2024), 9.0b2 (5/20/2024), 9.0b3 (7/31/2024), 9.0.0 (9/26/2024), 9.0.1 (12/21/2024). D. G. Porter.
9. Itcl: C++ inspired Object Oriented commands for Tcl. Versions 4.2.4 (1/5/2024), 4.2.5 (5/20/2024), 4.3.0 (9/16/2024), 4.3.1 (9/26/2024), 4.3.2 (12/11/2024). D. G. Porter.
10. Thread: Thread management commands for Tcl. Versions 2.8.8 (11/22/2022), 2.8.9 (2/28/2024), 2.8.10 (9/16/2024), 2.8.11 (12/11/2024), 3.0b1 (1/5/2024), 3.0b2 (5/20/2024), 3.0b4 (7/31/2024), 3.0.0 (9/26/2024), 3.0.1 (12/21/2024). D. G. Porter.
11. TDBC: Database connection commands for Tcl. Versions 1.1.6 (1/5/2024), 1.1.7 (2/28/2024), 1.1.8 (5/20/2024), 1.1.9 (9/16/2024), 1.1.10 (12/11/2024). D. G. Porter.

Data Released

1. J. Bernal. Computing a Partial Elastic Shape Registration of 3D Surfaces Using Dynamic Programming. DOI: 10.18434/mds2-3056
2. J. Bernal. Computing the Elastic Shape Registration of Two Surfaces in 3D Space with Gradient Descent and Dynamic Programming. DOI: 10.18434/mds2-3519
3. R. DeJaco. Software and data associated with "DeJaco, R. F.; Kearsley, A. J. Understanding Fast Adsorption in Breakthrough-curve Measurements." DOI: 10.18434/mds2-3103

4. G. Dogan. Training and Validation Datasets for Neural Network to Fill in Missing Data in EBSD Maps. DOI: 10.18434/mds2-3694
5. S. Geller. Code for "An Atomic Boson Sampler." DOI: 10.18434/mds2-3140
6. O. Doronina, A. Glaws, Z. Grey, B. Lee. G2Aero Database of Airfoils – Curated Airfoils. URL: https://www.osti.gov/biblio/2448331
7. M.-A. Henn. A Library to Enable the Modeling of Optical Imaging of Finite Multi-Line Arrays. DOI: 10.18434/T42C7D

Conferences, Minisymposia, Lecture Series, Courses

ACMD Seminar Series

There were 18 talks in our division seminar series presented during this period; talks are listed chronologically.

1. Andrew Rukhin (NIST Statistical Engineering Division). Parity Based Statistics, Extreme Value Theory and the Bible of Mathematics. October 17, 2023.
2. Wonjun Lee (University of Minnesota). Monotone Generative Modeling via a Gromov-Monge Embedding. October 31, 2023.
3. William Sherman (NIST ACMD). Immersive ParaView. November 13, 2023.
4. Brennan Sprinkle (Colorado School of Mines). The Countoscope: Measuring Self and Collective Diffusion with Fancy Counting. November 28, 2023.
5. Jennifer Wei (OpenFold). Applications in Machine Learning for Structure Elucidation. December 12, 2023.
6. Christine Parrish (Compact Membrane Systems), Computational Models as Integral Product Development Tools. January 11, 2024.
7. Jeanie Schreiber (George Mason University). Topological Shape and Data Analysis. January 23. 2024.
8. Drew Henrichsen (Johns Hopkins University). Rendezvous Search on a Sphere: The Astronaut Problem. February 6, 2024.
9. Gustavo Rohde (University of Virginia). Representing and Classifying Data with Optimal Transport. February 20, 2024.
10. Prashant Athavale (Clarkson University). Toward Parameter-free Restoration of Noisy Orientation Maps. March 19, 2024.
11. John Cobb (University of Wisconsin-Madison). Missing Data and Likelihood Geometry. March 26, 2024.
12. Kirk Cameron (Virginia Tech). The Impact and Influence of Power Measurement on GreenHPC. July 23, 2024.
13. Xinyi Liu (Northwestern University). Mechanopathogenesis of Esophageal Hypertrophy and Atrophy. August 6, 2024.
14. Pranava Jayanti (University of Southern California). Mass Transfer, Energy Dissipation, and Global Solutions in a Micro-scale Model of Superfluidity. August 20, 2024.
15. Stephen Sorokanich (ACMD). Many-body Physics in Superconducting Devices. September 17, 2024.
16. Lindsey Brown (Princeton University). Neural Circuit Models for Evidence Accumulation and Graded Information Transfer in Decision Making. October 15, 2024.
17. Edinah Gnang (Johns Hopkins University). From Graph Decomposition to Matrix Apportionment and Back. October 24, 2024.
18. Brian McKenzie (Carnegie Mellon University). Interfacial Flows Driven by Solute Concentration Gradients in Complex Fluids. November 14, 2024.

Shortcourses

1. V. V. Albert. "Boot Camp: Modern Quantum Coding Theory with Four Qubits." Quantum World Congress, Tysons Corner, VA, September 9, 2024.
2. S. Geller. "A Differential Geometry Approach to the Fisher Information." Center for Theory of Quantum Matter University of Colorado, Boulder, CO, August 5, 2024.
3. D. R. Kuhn, R. N. Kacker, M. S. Raunak, E. Lanus, J. Chandrasekaran, and B. Lee. "Workshop on Testing Strategies for Artificial Intelligence-enabled Systems using Combinatorial Testing." Virginia Tech Research Center, Arlington, Virginia, September 04, 2024.
4. W. Sherman. The Ins and Outs of Fixed-Screen Immersive Displays (aka CAVE-style VR). IEEE VR, Orlando FL, March 17, 2024.

Conference Organization

Leadership

1. P. S. Kuo. Program Chair. Conference on Lasers and Electro-optics (CLEO), Charlotte, NC, May 5-10, 2024.
2. P. S. Kuo. Co-Organizer, Symposium: Celebrating the International Year of Quantum, 2025 Conference on Lasers and Electro-optics (CLEO), Long Beach, CA, May 4-9, 2025.
3. K. Sayrafian. Co-Chair. Industry Panel, IEEE Global Communications Conference, Kuala Lumpur, Malaysia, December 4-8, 2023.
4. O. Slattery. Chair, Steering Committee. Workshop for Quantum Repeaters and Networks (WQRN) Series.
5. J. P. Zwolak. Co-organizer. XAI4Sci: Explainable Machine Learning for Sciences, Vancouver, Canada, February 26, 2024.

Committee Membership

1. V. V. Albert. Member, Program Committee. International Conference on Quantum Information Processing (QIP), Taipei, Taiwan, January 13-19, 2024.
2. V. V. Albert. Member, Program Committee. International Conference on Quantum Communication, Measurement and Computing (QCMC2024), Chennai, India, August 26-30, 2024.
3. V. V. Albert. Member, Scientific Committee. Quantum Technology International Conference (QTech 2024), Berlin, Germany, September 10-12, 2024.
4. H. Cohl. Member, Steering Committee. Orthogonal Polynomials and Special Functions Conference Series.
5. T. Gerrits. Member, Scientific Committee. Single Photon Workshop (SPW) Series.
6. T. Gerrits. Member, Program Committee. SPIE Quantum Technologies, Strasbourg, France. April 8-10, 2024.
7. Z. Gimbutas. Member, External Organizing Committee. Frontiers in Applied and Computational Mathematics (FACM 17). New Jersey Institute of Technology, Newark, NJ, June 24–25, 2017.
8. S. Glancy. Member, Program Committee. Southwest Quantum Information Technology Workshop (SQuInT 2024), Broomfield, CO, October 30 – November 1, 2024.
9. S. Glancy. Member, Program Committee. Assessing Performance of Quantum Computers (APQC 2024), Estes Park, CO, October 7 – 10, 2024.
10. S. Glancy. Member, Program Committee. Quantum Information and Probability: from Foundations to Engineering (QIP24), Växjö, Sweden, June 11 – 14, 2024.
11. R. N. Kacker. Member, Program Committee. International Workshop on Combinatorial Testing, (IWCT 2024), Toronto, Canada, May 27, 2024
12. P. S. Kuo. Member, Steering Committee. Conference on Lasers and Electro-optics (CLEO), Long Beach, CA, May 4-9, 2025.
13. P. S. Kuo. Member, Program Committee. SPIE Quantum West: Quantum Computing, Communication, and Simulation IV, San Francisco, CA, January 27 – February 1, 2024.
14. R. La. Member, Technical Program Committee. International Conference on Complex Networks and Their Applications (Complex Networks 23), Menton, France, November 28-30, 2023.
15. R. J. La. Member, Technical Program Committee. IEEE International Conference on Computer Communications (INFOCOM 25). London, United Kingdom, May 19-22, 2025.
16. R. J. La. Member, Technical Program Committee. IEEE International Conference on Computer Communications (INFOCOM 24). Vancouver, Canada, May 20-23, 2024.
17. R. J. La. Member, Technical Program Committee. International Conference on Complex Networks and Their Applications (Complex Networks 24). Istanbul, Turkey, December 10-12, 2024.
18. W. Sherman. Member, Executive Board. Community Alliance for Advanced Visualization (CAAV) Series.
19. O. Slattery. Member, Program Committee. Workshop for Quantum Repeaters and Networks (WQRN), Montreaux, Switzerland, September 11-13, 2024.
20. S. Su. Member, Program Committee. IEEE Virtual Reality (VR) 2024.
21. Simon Su, Member, Board Member, 2024, 15th International Conference on Virtual, Augmented and Mixed Reality, HCI International 2024.
22. S. Su, Member, Program Board. 16th International Conference on Virtual, Augmented and Mixed Reality, HCI International, 2024.

Session Organization

1. P. Bedekar. Co-Organizer, Special Session: Early Career Researchers in Mathematical Biology and Differential Equations. Association for Women in Mathematics (AWM) Research Symposium, Atlanta, Georgia, October 1-2, 2023.
2. G. Doğan. Co-Organizer, Minisymposia 40, 48, 56: Shapes, Manifolds and Geometry in Imaging. SIAM Conference on Imaging Science, Atlanta, GA, May 28-31, 2024.
3. G. Doğan and Z. Grey. Co-Organizers, Minitutorial 19: Computing Distances, Similarity Metrics to Enable Analysis of Complex Multimodal Data. SIAM Mathematics of Data Science, Atlanta, GA, October 20-25, 2024.
4. R. M. Evans. Organizer, Minisymposium 5: Contemporary Models in Mathematical Biology Part I of II. SIAM Annual Meeting, Spokane, WA, July 8, 2024.
5. R. M. Evans. Organizer, Minisymposium 22: Contemporary Models in Mathematical Biology Part II of II. SIAM Annual Meeting, Spokane, WA, July 9, 2024.
6. S. Glancy. Organizer, Special Session: Quantum Intersubjective Agreement. Quantum Information and Probability: from Foundations to Engineering (QIP24), Växjö, Sweden, June 11 – 14, 2024.
7. K. Sayrafian. Co-Organizer and Co-Chair: Measurement & Modelling of Radio Waves Propagation for Indoor Communication. 4th URSI Atlantic Radio Science Meeting, Gran Canaria, Spain, May 19-24, 2024.
8. W. Sherman and T. Bednarz. Organizers: Birds of a Feather: Immersive Visualization, SIGGRAPH Conference, Denver CO, August 1, 2024.
9. J. Stone, K. Griffin, W. Sherman, and V. Mateevitsi. Organizers: Birds of a Feather: ANARI Open Rendering Standard, The International Conference for High Performance Computing, Networking, Storage, and Analysis (SC24), Atlanta GA, November 19, 2024.
10. S. Su and W. Sherman. Co-Organizers. Workshop on Immersive Visualization Laboratory – Past, Present and Future, IEEE VR, 2024.

Other Professional Activities

Internal

1. R. Boisvert. Coordinator. ITL Quantum Information Program.
2. R. Boisvert. Member. NIST Research Computing Advisory Committee.
3. R. Boisvert. Member. NIST Open Access to Research (OAR) Committee.
4. B. Cloteaux. Member. Editorial Review Board.
5. W. George, Member, NIST High Performance Computing Resource Allocation Committee.
6. T. Gerrits. Organizer. Quantum Optics Seminar Series.
7. Z. Gimbutas. Member. ITL Awards Committee.
8. Z. Grey. Co-Chair. ACMD Seminar Series.
9. Z. Grey. Coordinator and Facilitator. Applied Geometry Reading Group (AGRG).
10. L. L. Jia. Member, Association of NIST Asian-Pacific Americans (ANAPA) Events Committee.
11. L. L. Jia, Member, NIST SBIR Proposals Review Panel.
12. L. L. Jia. Secretary, Association of NIST Asian-Pacific Americans (ANAPA).
13. L. L. Jia. Co-Chair. ACMD Seminar Series.
14. D. Porter. Member. ITL Awards Committee
15. B. Schneider. Chair. High Performance Computing Working Group, NIST Research Computing Advisory Committee.
16. J. P. Zwolak. Committee Chair. NIST Chapter of Sigma Xi Early Career Poster Presentation Competition.

External

Editorial

1. R. Boisvert. Associate Editor. *ACM Transactions on Mathematical Software*.
2. H. Cohl. Co-Editor. *OP-SF NET*, SIAM Activity Group on Orthogonal Polynomials and Special Functions.
3. H. Cohl. Editor. *The Ramanujan Journal.*
4. T. Gerrits. Associate Editor. *Optics Express*.
5. Z. Gimbutas. Member, Editorial Board. *Advances in Computational Mathematics.*
6. S. Glancy. Associate Editor. *Quantum Information Processing*.
7. R. La. Associate Editor. *IEEE/ACM Transactions on Networking*.

8. Bonita Saunders. Associate Editor, MAA *Mathematics Magazine*.
9. B. Saunders. Webmaster/SIAM Engage Moderator, SIAM Activity Group on Orthogonal Polynomials and Special Functions (SIAG/OPSF).
10. K. Sayrafian. Associate Editor. *International Journal of Wireless Information Networks*.
11. B. Schneider. Associate Editor in Chief. *IEEE Computing in Science and Engineering*.
12. B. Schneider. Specialist Editor. *Computational Physics Communications.*
13. S. Su. Associate Editor. *PRESENCE: Virtual and Augmented Reality*.
14. J. P. Zwolak. Guest Editor. Focus on Explainable Machine Learning in Sciences. *Machine Learning: Science and Technology*.
15. J. P. Zwolak. Member, Advisory Board. *Newton*.

Boards and Committees

1. R. Boisvert. Member. International Federation of Information Processing Working Group 2.5 (Numerical Software).
2. R. Boisvert. Member. Reproducibility Badging and Definitions Working Group, National Information Standards Organization (NISO).
3. R. Boisvert. NIST Representative. National Science and Technology Council (NSTC) Subcommittee on Future Advanced Computing Ecosystem (FACE).
4. B. Cloteaux. Member, Advisory Board. Department of Computer Science, New Mexico State University.
5. A. Dienstfrey. Chair. International Federation of Information Processing Working Group 2.5 (Numerical Software).
6. J. T. Fong. Member. American Society of Mechanical Engineers (ASME) Boiler and Pressure Vessel Code Committee.
7. T. Gerrits. NIST Representative. DC-QNet Science and Technology Advisory Committee.
8. P. Kuo. Member. ISO/IEC JTC-3 Quantum Technologies.
9. P. Kuo. Member. ISO/IEC JTC 3/ahG 6 Quantum Random Number Generator (QRNG) Ad Hoc Group.
10. P. Kuo. Member. ISO/IEC JTC 3/ahG 7 Quantum Enabling Technologies Ad Hoc Group.
11. P. Kuo. Member. Selection Committee, Max Born Award, Optica.
12. L. Ma. Co-principal Investigator. Center for Quantum Error Correction, Joint Korea-US Quantum Research Center.
13. L. Ma. Member. ISO/TC229 (Nanotechnology Standards Development), WG2 on the Standard ISO/TS 80004-12 (Nanotechnologies Vocabulary Part 12: Quantum Phenomena in Nanotechnology).
14. D. Porter. Member Tcl Core Team.
15. S. Ressler. Member. Immersive Web Working Group, World Wide Web Consortium (W3C).
16. S. Ressler. NIST Representative. W3C Advisory Committee.
17. S. Ressler. NIST Representative. Khronos Group.
18. S. Ressler. Member. 3D Formats Working Group, Khronos Group.
19. S. Ressler. Member. Working Groups, Metaverse Standards Forum.
20. S. Ressler. Member, Steering Committee. IEEE Metaverse Initiative.
21. B. Saunders. Member, Board of Trustees. Society for Industrial and Applied Mathematics (SIAM).
22. B. Saunders. Member, SIAM Systems Oversight Committee.
23. B. Saunders. Member, SIAM Human Resources Committee.
24. B. Saunders. Chair, AWM-MAA Falconer Lecture Nominating Committee.
25. B. Saunders. Member, Awards Review Panel, Washington Academy of Sciences.
26. B. Saunders. Secretary, SIAM Activity Group on Geometric Design.
27. K. Sayrafian. Voting Member. IEEE802.15 Task Group 6ma (Body Area Networks).
28. K. Sayrafian. Member. IEEE P2731 Standard Working Group (Unified Terminology for Brain-Computer Interfaces).
29. K. Sayrafian. Core Member. COST CA20120: Intelligence-Enabling Radio Communications for Seamless Interactions.
30. K. Sayrafian. Co-Chair, Vertical Track 1: Health and Well-Being. COST CA20120: Intelligence-Enabling Radio Communications for Seamless Interactions.
31. K. Sayrafian. Member. Digital Health Research and Development Interagency Working Group, Networking and Information Technology Research and Development (NITRD) Program.

32. K. Sayrafian. Co-Chair, Semi-smart Med-Tech Initiative Working Group on Standards and Modeling.
33. B. Schneider. NIST Representative. High End Computing (HEC) Interagency Working Group, Networking and Information Technology Research and Development (NITRD) Program.
34. W. Sherman. Member. OpenXR Working Group, Khronos Group.
35. W. Sherman. Member. ANARI Working Group, Khronos Group.
36. O. Slattery. Co-Chair. Interagency Working Group on Quantum Networks (QN-IWG), Office of Science and Technology Policy (OSTP).
37. O. Slattery. Co-Chair. DC-QNet Experiments Working Group.
38. S. Su. Member. 3D Formats Working Group, Khronos Group.
39. S. Su. Member. OpenXR Working Group, Khronos Group.
40. S. Su. Member. ANARI Working Group, Khronos Group.

Adjunct Academic Appointments

1. V. Albert. Adjunct Assistant Professor. Department of Physics, University of Maryland, College Park, MD.
2. V. V. Albert. Adjunct Assistant Professor. Department of Computer Science, University of Maryland, College Park, MD.
3. V. Albert. Affiliated Faculty Member. Applied Mathematics & Statistics, and Scientific Computation (AMSC) Program, University of Maryland, College Park, MD.
4. M. Coudron. Adjunct Assistant Professor. Department of Computer Science, University of Maryland, College Park, MD.
5. S. Glancy. Lecturer. Department of Physics, University of Colorado, Boulder, CO.
6. E. Knill. Lecturer. Department of Physics, University of Colorado, Boulder, CO.
7. E. Knill. Fellow. Center for Theory of Quantum Matter, Department of Physics, Colorado University, Boulder, CO.
8. P. Kuo. Adjunct Associate Professor. Department of Physics, University of Maryland, College Park, MD.
9. Y. Liu. Co-Director. Joint Center for Quantum Information and Computer Science (QuICS), University of Maryland, College Park, MD.
10. Y. Liu. Adjunct Associate Professor. Department of Computer Science, University of Maryland, College Park, MD.
11. K. Sayrafian. Affiliate Associate Professor. Electrical & Computer Engineering Department, Concordia University, Montreal Canada.
12. W. Sherman. Adjunct Faculty. Luddy School of Informatics, Computing, and Engineering, Indiana University, Bloomington, IN.
13. S. Su. Adjunct 1. Media Arts and Technologies, Department, Montgomery College, Rockville, MD.
14. J. Zwolak. Adjunct Assistant Professor, Department of Physics, University of Maryland, College Park, MD.

Thesis Direction

1. V. V. Albert. Member, Ph.D. Thesis Committee, University of Maryland, College Park: A. Rad.
2. V. V. Albert. Advisor, University of Maryland: S. Jain.
3. V. V. Albert. Advisor, University of Maryland: E. Kubischta.
4. V. V. Albert. Advisor, University of Maryland: Y. Xu.
5. V. V. Albert. Co-Advisor, University of Maryland: J. Iosue.
6. M. Coudron, Member, Master's Thesis Committee, University of Maryland: A. Gilani.
7. M. Donahue. Member, Ph.D. Thesis Committee, University of Southampton: M. Lang.
8. S. Glancy. Member, Ph.D. Thesis Committee, University of Colorado: H. Knaack.
9. S. Glancy. Member, Ph.D. Thesis Committee, University of Colorado: J. Wu.
10. S. Glancy. Co-Advisor, University of Colorado: S. Geller.
11. S. Glancy. Co-Advisor, University of Colorado: A. Kwiatkowski.
12. Z. Grey. Member, Ph.D. Thesis Committee, George Mason University: J. Schreiber
13. L. L. Jia. Co-advisor, Northwestern University: X. Liu.

14. A. Kearsley. Member, Ph.D. Thesis Committee, Drexel University: A. Chen.
15. E. Knill. Advisor, University of Colorado: S. Geller.
16. E. Knill. Advisor, University of Colorado: A. Kwiatkowski.
17. Y. K. Liu. Member, Ph.D. Thesis Committee, University of Maryland: J. Bringewatt.
18. Y. K. Liu. Member, Ph.D. Thesis Committee, University of Maryland: J. Leng.
19. K. Sayrafian. Co-Advisor, University of Zagreb, Zagreb, Croatia: K. Krhac.
20. J. P. Zwolak. Member, Ph.D. Thesis Committee, University of Maryland: R. P. Dalka,
21. J. P. Zwolak. Ph.D. Advisor, University of Maryland: H. S. Chalfin.
22. J. P. Zwolak. Ph.D. Advisor, University of Maryland: A. Rao.
23. J. P. Zwolak. M.S. Advisor, University of Maryland: D. Schug.

Community Outreach

1. V. Albert. Undergraduate Advisor, University of Maryland.
2. B. Alpert. Member, Computer Science Advisory Committee, Fairview High School, Boulder, CO.
3. G. Dogan. Organizer, Coding Club, Cabin John Middle School, Potomac, MD.
4. L. L. Jia. Mentor, Georgia Tech Alumni Association.
5. Simon Su. "Immersive ParaView for Scientific Visualization." Poolesville High School, October 2, 2024.
6. J. P. Zwolak. "Careers in Industry and Government." Panelist at the Spectra Panel, Online, September 2024.
7. J. P. Zwolak. Science Education Volunteer, Mary of Nazareth Elementary School.

Awards and Recognition

External

1. S. Challa. American Vacuum Society Nanoscale Science and Technology Division Early Career Award. November 2023.
2. J. P. Zwolak. Fellow, Washington Academy of Sciences. May 2024.
3. J. P. Zwolak. Excellence in Research Award in Applied Mathematics, Washington Academy of Sciences. May 2024.

Internal

1. P. Bedekar. Associate of the Year, NIST Information Technology Laboratory. July 2024.
2. M. Coudron. Outstanding Conference Paper: "Quantum Algorithms and the Power of Forgetting," NIST Information Technology Laboratory, July 2024.
3. M. Donahue. 2024 DOC Bronze Medal. (Joint with PML and MML.)
4. T. Gerrits. 2024 DOC Gold Medal. (Joint with PML)
5. T. Gerrits, P. Kuo, and O. Slattery. 2024 DOC Bronze Medal. (Joint with PML)
6. A. Kearsley. Outstanding Mentorship. NIST Information Technology Laboratory, July 2024.
7. M. Kleczynski. Most Outstanding Poster, Civil/Mechanical Engineering & Manufacturing, Cybersecurity & Wireless Communication Technologies, Computer Sciences, and Mathematical Sciences Category, NIST Chapter of Sigma Xi, May 2024.
8. T. Gerrits, P. Kuo, and O. Slattery. Outstanding Standards Document. NIST Information Technology Laboratory, July 2024.
9. B. Miller. 2024 DOC Bronze Medal.
10. B. Miller. Outstanding Technology Transfer. NIST Information Technology Laboratory, July 2024.
11. J. P. Zwolak. 2024 DOC Bronze Medal. (Joint with PML)
12. J. P. Zwolak. Outstanding Journal Paper: "Colloquium: Advances in Automation of Quantum Dot Devices Control." NIST Information Technology Laboratory, July 2024.

Funding Received

During FY 2024 ACMD's yearly allocation of base funding from the NIST Information Technology Laboratory was supplemented with funding from a variety of internal and external competitions. Below we list the major sources of such funding.

Note: For joint projects, names of ACMD participants are underlined.

External

1. T. Gerrits, L. Ma, O. Slattery, Z. Levine. Free-Space Memory-Based High-Rate Single Photon Source. Air Force Research Laboratory.
2. O. Slattery. Quantum Augmented Networking (QuANET). DARPA.

Internal

1. V. Albert. Entanglement, Geometry, and the Topology of Molecular State Space. ITL Building the Future Program.
2. B. Alpert, et al. Ture Becquerel: A New Paradigm for 21st Century Radioactivity Measurements. NIST Innovations in Measurement Science.
3. J. Bienfang, A. Migdall, S. Polyakov; PML/686: S. Buckley, J. Lehman, T. Gerrits, P. Kuo, and O. Slattery. Quantum Photonics Standards Development. NIST Emerging Technologies Standards Engagement (NETSE).
4. B. Cloteaux and V. Marbukh. Towards Developing Carbon Aware Algorithms. ITL Building the Future Program.
5. G. Cooksey, S. Sakar, and P. Patrone. A Framework and Platform for Uncertainty Quantification of Absolute Particle Count. NIST Emerging Technologies Standards Engagement (NETSE).
6. G. Doğan and S. Lund. Image Alignment Tool to Enable Fast and Objective Analysis of Footwear Evidence. NIST Accelerating Forensics Innovation for Impact Program.
7. M. Donahue. Metrology for Integration of New Magnetic Materials. CHIPS Metrology Program.
8. S. Geller, E. Knill, and S. Glancy. Computational Power of Atomic Boson Samplers. ITL Building the Future Program.
9. T. Gerrits, S. Glancy, E. Knill, and M. A. Van de Poll. Metrology for Continuous Variable Quantum Computing and Networking. ITL Building the Future Program.
10. Z. Grey and G. Doğan. Topological Shape and Data Analysis for Material Microstructures. ITL Building the Future Program.
11. A. Kearsley, D. McGlynn, and S. Stein. Novel Algorithms for Identification of Forest Fire Analytes. ITL Building the Future Program.
12. P. Kuo, S. Challa, and S. Klimov. Thin-film Lithium Niobate for Quantum Information Processing. ITL Building the Future Program.
13. K. Sayrafian, S. Su, and K. Ladic. A Virtual 3D Platform to Study Wireless Propagation in Brain-Computer Interfaces. ITL Building the Future Program.
14. L. Ma, O. Slattery, T. Gerrits, X. Tang, and A. Rahmouni. Integrated Entangled Photon Source Based on Silicon Carbide Devices. ITL Building the Future Program.
15. M. Mascagni, W. Keyrouz, and D. Juba. A Stochastic Library for Solving Partial Differential Equations. ITL Building the Future Program.
16. K. Ramu, M. Daniels, W. Borders, J. McClelland, S. Buckley, A. McCaughan, and A. Dienstfrey. Standardizing New Materials, Processes, and Equipment for Microelectronics. CHIPS Metrology Program.
17. S. Su, W. Sherman, and K. Sayrafian. Development of Visualization Infrastructure to Support Future Collaborations in a Hybrid Data Analysis Environment. ITL Building the Future Program.
18. S. Su and W. Sherman. Advancing Forensic Science in an Immersive Digital Twin to Enable Virtual Measurement through 3D Immersive Visualization and Computational Algorithm Analysis. NIST Accelerating Forensics Innovation for Impact Program.
19. J. P. Zwolak and C. S. Greenberg. Explainable Boosting Machines for Scientific and Medical Image Data. ITL Building the Future Program.

Grants Funded

ACMD awards a small amount of funding through the NIST Grants Program for projects that make direct contributions to its research programs. During FY 2024 the following cooperative agreements were active.

1. Carnegie Mellon University: *Entangled Photon Pair Source in an Integrated Silicon Carbide Platform*. PI: Qing Li.
2. Louisiana State University: *Metrology for Continuous Variable Quantum Computing and Networking*. PI: Omar S. Magana-Loaiza.

3. Theiss Research: *Exploiting Alternate Computing Technologies*. PI: Alan Mink.
4. University of Edinburgh: *Applicable Resurgence and Uniform Asymptotics*. PI: Adri Olde-Daalhuis.
5. University of Maryland: *Joint Center for Quantum Information and Computer Science (QuICS)*. PI: Andrew Childs.
6. University of Texas at Arlington: *Explaining and Debugging Machine Learning Models by Neighborhood Exploration*. PI: Yu Lei.

External Contacts

ACMD staff members interact with a wide variety of organizations in the course of their work. Examples of these follow.

Industrial Labs

Amazon
Boeing Company
Computational Physics, Inc.
Extreme Event Risk
Fraunhoffer IGD (Germany)
GE Global Research Center
HRL Laboratories
IBM
Intel Corporation
Intelligent Geometries, LLC
IonQ
KDDI Research Inc. (Japan)
Kitware
Lumos NanoLabs
Microsoft Research
NTT Corporation (Japan)
Photon Spot Inc.
Prorenata Labs
Quantinuum
Qunnect
Raicol Crystals (Israel)
Regeneron
Roche
Rolls-Royce Corp.
SINTEF (Norway)

Government/Non-profit Organizations

American Society of Mechanical Engineers
Argonne National Laboratory
Army Research Laboratory
Center for Disease Control
Centro Nacional de Metrologia (Mexico)
Constellation Research Center
Defense Advanced Research Projects Agency
El Centro Nacional de Metrología – CENAM (Mexico)
European University Cyprus (Cyprus)
Federal Communications Commission
Fermi National Lab
Food and Drug Administration
IEEE
IEEE Computer Society
INRIA (France)
Institute of Science and Technology Austria
Intelligence Advanced Research Projects Agency
Johns Hopkins University Applied Physics Laboratory
Khronos Group
Korteweg-de Vries Inst. for Mathematics (Netherlands)
Korean Institute of Science and Technology (S. Korea)
Los Alamos National Laboratory
Massachusetts Institute of Technology
Max Planck Institute for Quantum Optics (Germany)
Metaverse Standards Forum
Mid-Atlantic Crossroads (MAX)
NASA Goddard Space Flight Center
National Cancer Institute
National Institute of Biomedical Imaging and Bioengineering
National Institutes of Health
National Physical Laboratory (UK)
National Science Foundation
National Renewable Energy Laboratory (NREL)
Naval Research Laboratory
Oak Ridge National Laboratory
Pacific Northwest National Laboratory
Perimeter Institute (Canada)
Physikalisch-Technische Bundesanstalt (Germany)
Poolesville High School
Quantum Economic Development Consortium
Sandia National Laboratories
US Holocaust Memorial Museum
US Naval Observatory
Washington Metro Quantum Network Research Consortium
World Wide Web Consortium

Universities

American University
Beihang University (China)
Beijing Institute of Technology (China)
Bogazici University (Turkey)
Brown University
CalTech
Carnegie Mellon University
China University of Petroleum (China)
Clarkson University
Clemson University
Colorado School of Mines
Columbia University
Concordia University (Canada)
Courant Institute of Mathematical Sciences
Dalian University of Science and Tech (China)

Delft University of Technology (Netherlands)
Drake University
Drexel University
East China U. of Science and Tech (China)
ETH Zurich (Switzerland)
European University Cyprus (Cyprus)
Federal University of Ceará (Brazil)
Florida State University
Freie Universität Berlin (Germany)
Friedrich-Alexander-University (Germany)
Gdansk University of Technology (Poland)
George Mason University
Harvard University
Hillsdale College
Imperial College London (UK)
Indian Institute of Science, Bangalore (India)
Indian Institute of Technology (India)
IST Austria
Johns Hopkins University
Khallikote College (India)
Koç University (Turkey)
KTH Stockholm (Sweden)
Louisiana State University
Lund University (Sweden)
Massachusetts Institute of Technology (MIT)
Morgan State University
National University of Singapore (Singapore)
Northwestern University
Oregon State University
Polytechnic University of Valencia (Spain)
Portland State University
Rhode Island School of Design
Shandong University (China)
Stanford University
Stony Brook University
Swiss Federal Technology Institute of Lausanne (EPFL)
Technische Universitat München
Texas A&M University
Tokyo University of Science (Japan)
Toronto University (Canada)
Tsinghua University (China)
Tufts University
University of Akron
University of Antwerp (Belgium)
University of Arizona
Universidad Loyola Andalucia (Spain)
University of Bologna, Bologna, Italy
University of British Colombia (Canada)
University of California, Berkeley
University of California, Davis
University of California, Los Angeles
University of California, Santa Barbara
University of Central Florida
University of Chicago
University of Colorado, Boulder
University of Colorado, Denver
University of Copenhagen (Denmark)
University of Edinburgh (UK)
University of Erlangen (Germany)
University of Hawaii
University of Houston
University of Illinois, Urbana-Champaign
University of Konstanz (Germany)
University of Lisbon (Portugal)
University of Louisiana, Lafayette
University of Manchester (UK)
University of Maryland, Baltimore County
University of Maryland, College Park
University of Massachusetts
University of New Mexico
University of Munich (Germany)
University of North Carolina
University of Novi Sad (Serbia)
University of Oregon
University of Oulu (Finland)
University of Ottawa (Canada)
University of Pennsylvania
University of Scranton
University of Sheffield (UK)
University of Southampton (UK)
University of Southern California
University of South Carolina
University of Strathclyde (UK)
University of Texas at Arlington
University of Texas at Dallas
University of Vienna (Austria)
University of Virginia
University of Washington
University of Waterloo (Canada)
University of Wisconsin, Madison
University of Wisconsin, Milwaukee
University of Wuppertal (Germany)
University of Zagreb (Croatia)
Virginia Polytechnic Institute
Weizmann Institute of Science (Israel)
Worcester Polytechnic University
Yale University

Part V

Appendix

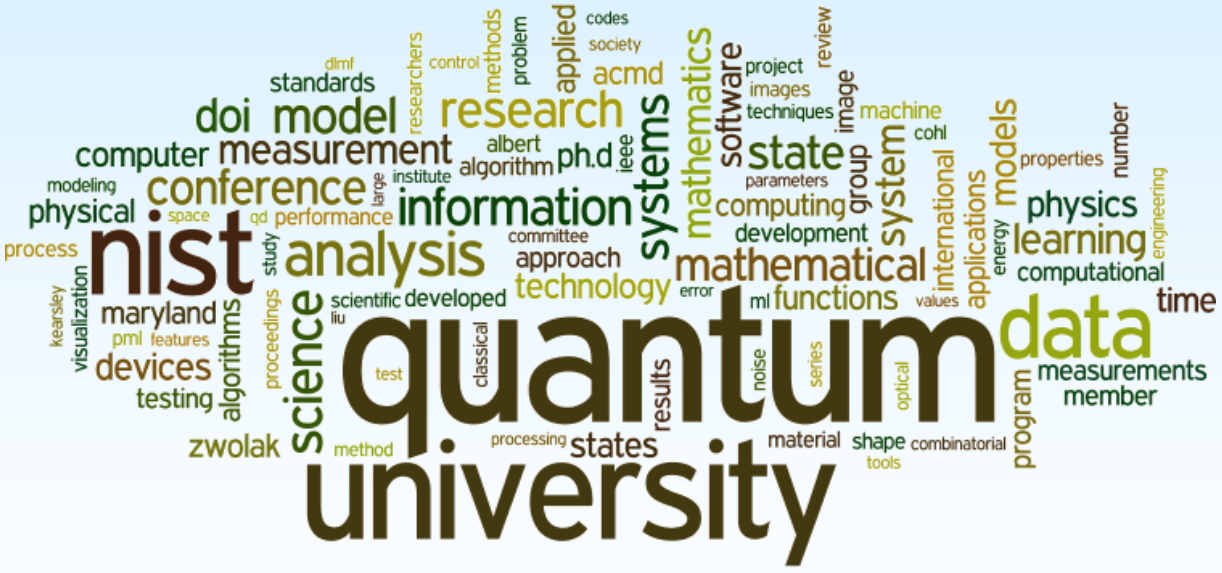

Staff

ACMD consists of full-time permanent Federal staff located at NIST laboratories in Gaithersburg, MD and Boulder, CO. This full-time staff is supplemented with a variety of special appointments. The following list reflects all non-student appointments held during any portion of the reporting period (October 2023 – December 2024). Students and interns are listed on page 134 and page 135.

* Denotes staff at NIST Boulder.
† Denotes part-time Federal staff.

Division Staff

Ronald Boisvert, *Chief*, Ph.D. (Computer Science), Purdue University, 1979
*Andrew Dienstfrey, *Deputy Chief*, Ph.D. (Mathematics), New York University, 1998
*Elsie (Meliza) Lane, *Administrative Assistant*
Lochi Orr, *Administrative Assistant*, A.A. (Criminal Justice), Grantham University, 2009
Lakshmi Venkataramanan, *Administrative Assistant*, M.S. (Cybersecurity), University of MD, 2021
†Alfred Carasso, Ph.D. (Mathematics), University of Wisconsin, 1968
†Roldan Pozo, Ph.D. (Computer Science), University of Colorado at Boulder, 1991
Kamran Sayrafian, Ph.D. (Electrical and Computer Engineering), University of Maryland, 1999
Christopher Schanzle, B.S. (Computer Science), University of Maryland Baltimore County, 1989

Mathematical Analysis and Modeling Group

*Bradley Alpert, *Leader*, Ph.D. (Computer Science), Yale University, 1990
Ryan Evans, Ph.D. (Applied Mathematics), University of Delaware, 2016
†Jeffrey Fong, Ph. D. (Applied Mechanics and Mathematics), Stanford University, 1966
*Zydrunas Gimbutas, Ph.D. (Applied Mathematics), Yale University, 1999
*Zachary Grey, Ph.D. (Computational and Applied Mathematics), Colorado School of Mines, 2019
Leroy Jia, Ph.D. (Applied Mathematics), Brown University, 2018
Raghu Kacker, Ph.D. (Statistics), Iowa State University, 1979
Anthony Kearsley, Ph.D. (Computational and Applied Mathematics), Rice University, 1996
Vladimir Marbukh, Ph.D. (Mathematics) Leningrad Polytechnic University, 1986
Paul Patrone, Ph.D. (Physics), University of Maryland, 2013

NRC Postdoctoral Associates
Melinda Kleczynski, Ph.D. (Applied Mathematics), University of Delaware, 2023
Deborah McGlynn, Ph.D. (Civil and Environmental Engineering), Virginia Tech, 2022
Anne Talkington, Ph.D. (Computational Biology), University of North Carolina, 2021

Faculty Appointee (Name, Degree / Home Institution)
Daniel Anderson, Ph.D. / George Mason University
James Lawrence, Ph.D. / George Mason University
Richard La, Ph.D. / University of Maryland
Michael Mascagni, Ph.D. / Florida State University
John Nolan, Ph.D. / American University

Guest Researchers (Name, Degree / Home Institution)
Prajakta Bedekar, Ph.D. / Johns Hopkins University
Robert DeJaco, Ph.D. / Compact Membrane Systems
Kaitlyn Hood, Ph.D. / Purdue University
Fern Hunt, Ph.D. / *NIST Scientist Emeritus*
Rayanne Luke, Ph.D. / George Mason University
Amudhan Krishmaswamy Usha, Ph.D. / Chakra Consulting Inc.

Yu (Jeff) Lei, Ph.D. / University of Texas at Arlington
Geoffrey McFadden, Ph.D. / *NIST Scientist Emeritus*
Dimitrios Simos, Ph.D. / SBA Research, Austria
Stephen Tennyson, B.S. / University of Maryland

Mathematical Software Group

Bonita Saunders, *Leader,* Ph.D. (Mathematics), Old Dominion University, 1985
Javier Bernal, Ph.D. (Mathematics), Catholic University, 1980
Brian Cloteaux, Ph.D. (Computer Science), New Mexico State University, 2007
Howard Cohl, Ph.D. (Mathematics), University of Auckland, 2010
Günay Doğan, Ph.D. (Applied Mathematics and Scientific Computing), University of Maryland, 2006
Michael Donahue, Ph.D. (Mathematics), Ohio State University, 1991
Stephen Langer, Ph.D. (Physics), Cornell University, 1989
Bruce Miller, Ph.D. (Physics), University of Texas at Austin, 1983
Donald Porter, D.Sc. (Electrical Engineering), Washington University, 1996
Barry Schneider, Ph.D. (Physics), University of Chicago, 1969

NRC Postdoctoral Associates
William Earwood, Ph.D. (Chemistry), University of Mississippi, 2022
Camilo Montoya, Ph.D. (Mathematics), Florida International University, 2022
Stephen Sorokanich, Ph.D. (Mathematics), University of Maryland, College Park, 2022

Faculty Appointees (Name, Degree / Home Institution)
Abdou Youssef, Ph.D. / George Washington University

Guest Researchers (Name, Degree / Home Institution)
Luca Argenti, Ph.D. / University of Central Florida
Joel Bowman, Ph.D. / Emory University
Nicolas Douguet, Ph.D. / Kennesaw State University
Heman Gharibnejad, Ph.D. / Computational Physics Inc.
Mark Alexander Henn, Ph.D. / University of Maryland
Daniel Lozier, Ph.D. / NIST, Retired
Carlos Antonio Marante Valdes, Ph.D. / University of Central Florida
Adri Olde Daalhuis, Ph.D. / University of Edinburgh
Jeppe Olsen, Ph.D. / Aarhus University, Denmark
Aman Rani, Ph.D. / JHU Applied Physics Laboratory
Moritz Schubotz, Ph.D. / University of Karlsruhe, Germany

Quantum Information Group

Ronald Boisvert, *Acting Leader*, Ph.D. (Computer Science), Purdue University, 1979
Victor Albert, Ph.D. (Physics), Yale University, 2017
Matthew Coudron, Ph.D. (Computer Science), Massachusetts Institute of Technology, 2017
*Shawn Geller, (Physics), University of Colorado, 2024
Thomas Gerrits, Ph.D. (Physics), Radboud University Nijmegen, 2004
*Scott Glancy, Ph.D. (Physics), University of Notre Dame, 2003
*Emanuel Knill, *NIST Fellow*, Ph.D. (Mathematics), University of Colorado at Boulder, 1991
Paulina Kuo, Ph.D. (Physics), Stanford University, 2008
*Alexander Kwiatkowski, Ph.D. (Physics), University of Colorado, 2024
Yi-Kai Liu, Ph.D. (Computer Science), University of California, San Diego, 2007
Lijun Ma, Ph.D. (Precision Instruments and Machinery), Tsinghua University, 2001
Oliver Slattery, *Project Leader*, Ph.D. (Physics), University of Limerick, 2015

NRC Postdoctoral Associates
Anthony Brady, Ph.D. (Physics), Louisiana State University, 2021

Guest Researchers (Name, Degree / Home Institution)
Mehdi Alasti, Ph.D. / GBS Dakota IT
Sesha Challa, Ph.D. / Pusan National University (India)
Riley Dawkins, Ph.D. / Louisiana State University
Nijil Lal Cheriya Koyyottummal, Ph.D. / University of Napoli Federico II
Shon Cook, B.S. / SRI International
Joseph Christesen, Ph.D. / SRI International
Daniel Jones, PhD. / Army Research Laboratory
Navin Lingaraju, Ph.D. / Johns Hopkins University Applied Physics Laboratory
Alan Mink, Ph.D. / Theiss Research
Changhoon Park, Ph.D. / Korea Institute of Science and Technology
Anouar Rahmouni, Ph.D. / University of Maryland, College Park
Yicheng Shi, Ph.D. / National University of Singapore
Jin Su, Ph.D. / Lehigh University
Xiao Tang, Ph.D. / NIST Retired
*James Van Meter, Ph.D. / HRL Laboratories

High Performance Computing and Visualization Group

Judith Terrill, *Leader*, Ph.D. (Information Technology), George Mason University, 1998
William George, Ph.D. (Computer/Computational Science), Clemson University, 1995
Terence Griffin, B.S. (Mathematics), St. Mary's College of Maryland, 1987
Sandy Ressler, M.F.A. (Visual Arts), Rutgers University, 1980
William Sherman, M.S. (Computer Science), University of Illinois, 1989
Simon Su, Ph.D. (Computer Science), University of Houston, 2001
Justyna Zwolak, Ph.D. (Physics), Nicolaus Copernicus University, Poland, 2011

Guest Researchers (Name, Degree / Home Institution)
Donovan Buterakos, Ph.D. / University of Maryland
Steven Satterfield, M.S. / NIST Retired
Dachollom Sambo, Ph.D. / Morgan State University
James Sims, Ph.D. / NIST (retired)
Brian Weber, Ph.D. / Shanghai Institute of Technical Physics

Glossary of Acronyms

1D	one-dimensional
2D	two-dimensional
3D	three-dimensional
AAAI	American Association for Artificial Intelligence
ACM	Association for Computing Machinery
ACMD	NIST/ITL Applied and Computational Mathematics Division
ACS	American Chemical Society
ACTS	Advanced Combinatorial Testing System (software)
ADHE	adaptive histogram equalization
ahG	ad hoc group
AI	artificial intelligence
AIAA	American Institute of Aeronautics and Astronautics
AL	Analytic Methods (DLMF chapter)
AMO	atomic molecular and optical
ANARI	Analytic Rendering Interface for Data Visualization
APRES	Aspects of Postdoctoral Researcher Experience Scale Survey
APC	active polarization compensator
APS	American Physical Society
AQECC	approximate quantum error correction code
AR	augmented reality
arXiv	preprint archive at https://arxiv.org/
AS	autonomous system
ASES	Aspects of Student Experience Survey
ASMS	American Society of Mass Spectrometry
ASTRA	Attosecond TRAnsitions (software)
ASWF	Academy Software Foundation
AVS	American Vacuum Society
BAN	body area network
BATIS	Bootstrapping, Autonomous Testing, and Initialization System
BBP	broad-band pulsed
BCI	brain-computer interface
BEC	Bose-Einstein Condensate
BDD	bounded distance decoding
Bio-FET	biological field effect transistor
BMP	Bateman Manuscript Project
BOF	birds-of-a-feather
Bq	becquerel: absolute activity of radionuclide mixtures
BQP	bounded-error quantum polynomial time
CAD	computer aided design
Caltech	California Institute of Technology
CAR	coincidence-to-accidental
CAVE	CAVE Automatic Virtual Environment
CCM	Combinatorial Coverage Measurement (software)
CENAM	Center for Metrology of Mexico
CHIPS	Creating Helpful Incentives to Produce Semiconductors (Federal program)
CI	configuration interaction
CFSF	Continued Fractions for Special Functions
CLEO	Conference on Lasers and Electro-Optics
CMOS	complementary metal-oxide semiconductor
CMU	Carnegie Mellon University
CNN	convolutional neural network
CS	coordinating server
CSD	charge stability diagram
CT	computed tomography

CT	combinatorial testing
CTL	NIST Communications Technology Laboratory
CV	continuous (quantum) variables
CY	calendar year
DARPA	Defense Advanced Research Projects Agency
DC-QNet	DC area Quantum Network testbed
DER	data extraction rate
DES	distal esophageal spasm
DGR	NIST Domestic Guest Researcher
DLMF	NIST Digital Library of Mathematical Functions
DNA	deoxyribonucleic acid
DNN	deep neural network
DO	dispersive optics
DOC	US Department of Commerce
DOD	US Department of Defense
DOE	US Department of Energy
DOI	digital object identifier
DPC 4D-STEM	differential phase contrast four-dimensional scanning transmission electron microscopy
DPD	dissipative particle dynamics
DQD	double quantum dot
DRL	deep reinforcement learning
DRMF	Digital Repository of Mathematical Formulae
DV	discrete (quantum) variable
DWDM	dense wavelength division multiplexing
E2E	end-to-end
EBSD	electron backscatter diffraction
eCF	Wolfram Computational Knowledge of Continued Fractions Project
EBM	explainable boosting machine
EC	error correction
EL	NIST Engineering Laboratory
ENS	exposure notification system
EVaSR	entropic value at risk
FEM	finite element method
FGR	NIST Foreign Guest Researcher Program
FL	federated learning
FY	fiscal year
GaAs	gallium arsenide
GI	gastro-intenstinal
glTF	standard file format for three-dimensional scenes and models
GNO	green network optimization
GWT	Gabor wavelet transform
HDF	data file format
HEV	high end visualization
HIM	helium ion microscope
HOM	Hong-Ou-Mandel
HPC	high performance computing
HPCVG	ACMD High Performance Computing and Visualization Group
HPFS	high-permittivity flexible substrate
HPO	hyperparameter optimization
Hy	Hylleraas
Hy-CI	Hylleraas-Configuration Interaction technique
ICST	International Conference of Software Testing
IEC	International Electrotechnical Commission
IEEE	Institute of Electronics and Electrical Engineers
IFIP	International Federation for Information Processing
IMS	NIST Innovations in Measurement Science (internal funding program)
iNET	NIST internal web site

IoT	Internet of things
IQP	instantaneous quantum polynomial
ISO	International Standards Organization
ITL	NIST Information Technology Laboratory
IVE	immersive visualization environment
JHU	Johns Hopkins University
JTC	joint technical committee
KIST	Korean Institute of Science and Technology
KLS	Koekoek, Lesky and Swarttouw
KPI	key performance indicator
LaCASt	Java tool to convert math expressions from LaTeX to computer algebra systems
LaTeX	a math-oriented text processing system
LaTeXML	a LaTeX to Math ML converter
LDPC	low-density parity checks
LO	local oscillator
LOD	limit of detection
LoRaSIM	discrete event simulator for LoRaWAN
LoRaWAN	long range wide area networks
LP	NIST Laboratory Programs Office
LSU	Louisiana State University
LWE	learning with errors
MAViS	Modular Autonomous Virtualization System
MBQC	measurement-based quantum computation
MESF	dimensionless measure of brightness
MICS	medical implant communications
ML	machine learning
MLP	multilayer perceptron
MMD	maximum mean discrepancy
MML	NIST Material Measurement Laboratory
MOS	Magnus, Oberhettinger, and Soni
MOT	magneto-optical trap
MRAM	magneto-resistive random-access memory
MSDC	NIST Mass Spectrometry Data Center
MSE	mean-squared error
MSF	Metaverse Standards Forum
MTEX	texture analysis software
NALS	network analysis for Likert-style surveys
nanoHUB	Web portal for nanotechnology research at https://nanohub.org/
NBS	National Bureau of Standards (former name of NIST)
NG-QNET	NIST Gaithersburg Quantum Network
NISQ	noisy intermediate-scale quantum
NIST	National Institute of Standards and Technology
NISTIR	NIST Internal Report
NITRD	Networking and Information Technology Research and Development
NLSS	no low-energy sampleable states
NLTS	no low-energy trivial states
NN	neural network
NP	non-deterministic polynomial time
NRC	National Research Council
NREL	National Renewable Energy Laboratory
NS	network slice
NUM	network utility maximization
OD	object detector
OOF	Object-Oriented Finite Elements (software)
OOF3D	3D version of OOF
OOMMF	Object-Oriented Micromagnetic Modeling Framework (software)
OP	orthogonal polynomials

OP	observation points
OpenXR	Open Extended Reality
OPSF	orthogonal polynomials and special functions
OTDR	optical time-domain reflectometers
OTF	optical transfer function
OU	NIST organizational unit
OUSD	Open USD
PCP	probabilistically checkable proof
PDC	parametric down-conversion
PECASE	Presidential Early Career Award for Science and Engineering
PER	physics education research
pHEMT	pseudomorphic High-Electricity Mobility Transistor
PIE	physics-informed excitation
PML	NIST Physical Measurement Laboratory
PNN	partial convolutional neural network
POA	price of anarchy
POMDP	partially observable Markov decision process
P-OTDR	polarization-sensitive OTDR
PPKTP	periodically poled $KTiOPO_4$
PQC	post-quantum cryptography
PREP	NIST Professional Research Education Program
PRISM	Polycentric Routines for Ionization and Scattering in Molecules
PSB	Pauli spin blockade
PT	project team
QD	quantum dot
QDPD	Quaternion-based Dissipative Particle Dynamics simulation code
QIP	Quantum Information Processing (conference)
QKD	quantum key distribution
QoS	quality of servisse
QRNG	quantum random number generation
QuANET	DARPA Quantum Augmented Network program
QuICS	UMD-NIST Joint Center for Quantum Information and Computer Science
RCP	Research Conduct Policy
RBC	ray-based classification
ReLU	rectifier linear unit
RGB	red-green-blue color system
RS	recommender system
RSA	Rivest-Shamir-Adelman public key cryptographic algorithm
SAR	specific absorption rate
SARS-CoV-2	the virus that causes the respiratory disease COVID-19
SBC	single-board computer
SDO	standards development organization
SEM	scanning electron microscopy
SFWM	spontaneous four-wave mixing
SHAP	Shapley additive explanations
SHIP	NIST Summer High School Internship Program
SIAM	Society for Industrial and Applied Mathematics
SiC	silicon carbide
SIGGRAPH	ACM Special Interest Group on Graphics
SIP	Scientific Integrity Policy
SPDC	spontaneous parametric down conversion
SPH	smooth particle hydrodynamics
SPIE	International Society for Optical Engineering
SPT	symmetry-protected topological order
SRM	standard reference material
SST	separable shape tensors
STEM	science, technology, engineering, and mathematics

SURF	NIST Student Undergraduate Research Fellowship program
SVP	shortest vector problem
SVP	NIST Student Volunteer Program
TDA	topological data analysis
TFLN	thin-film lithium niobate
TN	technical note
TNT	Template Numerical Toolkit
UC	University of California
UCLA	University of California Los Angeles
UHPC	ultra-high-performance concrete
UMD	University of Maryland
UMIACS	University of Maryland Institute for Advanced Computer Studies
UQ	uncertainty quantification
URL	universal resource locator
USC	University of Southern California
USD	universal scene description
UWB	ultra-wideband
VEMOS	Visual Explorer for Metric of Similarity (software)
VR	virtual reality
VTK	visualization software library
W3C	World Wide Web Consortium
XR	extended reality
XSEDE	NSF eXtreme Science and Engineering Discovery Environment
ZP	zona pellucida